The Estimation of Cardiac Power Output Using Multiple Physiological Signals

WANG, Ling

A Thesis Submitted in Partial Fulfillment of the Requirements for the Degree of Doctor of Philosophy in Electronic Engineering

The Chinese University of Hong Kong

September 2010

ProQuest LLC.
789 East Eisenhower Parkway
P.O. Box 1346
Ann Arbor, MI 48106 - 1346

Acknowledgment

I am greatly indebted to my supervisor, Prof. Y. T. Zhang, for his enlightening and insightful advices throughout this study. Warmest thanks to Prof. C. C. Y. Poon for her invaluable suggestions and discussion with me for the models and thesis writing. Special thanks to Dr. Felix Chen for his constrictive suggestions and corrections on my thesis writing. Thanks to Mr. Y. P. Liang in the BME laboratory for his technical help and assistance. I do appreciate my previous colleague Miss. J. Meng for her encouragement and help during the time we spent together. I also appreciate my previous colleague Z. Zhao for her assistance during the experiment and efforts on our paper. Besides, special thanks are given to my team-mate Prof. C. C. Y. Poon, Dr. Mico Wong and Mr. Laurence Chen for our teamwork and collaboration in the 10th "Challenge Cup" competition.

During these four years, my lab-mates, Miss Y. Li, Miss Q. Liu, Mr. Billy Leung, Mr. Stanley Sy, Miss W. B. Gu and Miss Y. B. Liu always showed their warm heart in giving me their hands. A number of them have been involved in many hours of tedious experiments or engaged in the long-time pre-preparations and set up for the experiments. I would like to express my sincere gratitude to them.

Finally, I would like to express my deepest love and appreciations to my parents for their support and care to me all the time.

Abstract

Heart failure is the end stage of many cardiovascular diseases, such as hypertension, coronary heart disease, diabetes mellitus, etc. Around 5.8 million people in the United States have heart failure and about 670,000 people are diagnosed with it each year. In 2010, heart failure will cost the United States $ 30.2 billion, and the cost of healthcare services is a major component of this total. With the resultant burden on health care resources it is imperative that heart failure patients with different risk stages are identified, ideally with objective indicators of cardiac dysfunction, in order that appropriate and effective treatment can be instituted.

Cardiac power output (CPO) is defined as the product of mean arterial blood pressure (MBP) and cardiac output (CO), and CPO measured during peak dynamic exercise (i.e. peak CPO) has been shown as a powerful predictor of death for heart failure patients. However, so far there has been no existing device which directly measures CPO, and CPO is acquired from simultaneous measurement of MBP and CO. Further, simultaneous MBP and CO measurement during dynamic exercise is a challenge for current BP and CO methods. Therefore, there is an urgent need to develop new devices which are fully wearable and unobtrusive for monitoring of CPO during dynamic exercise. Since the core problem in most wearable devices is how to estimate the target cardiovascular parameter, e.g. CPO in this study, through physiological signals measured from body surface, this thesis focus on developing a direct measurement technique of CPO in dynamic exercise using multiple physiological signals measured on body surface, specifically, electrocardiogram (ECG) and photoplehtysmogram (PPG).

Recently, a wearable measurable parameter, pulse arrival time or PAT, has been developed for BP measurement. PAT is the time delay from the R peak of ECG to the systolic foot of PPG. PAT consists of two timing components, the pre-ejection period (PEP) of the heart and pulse transit time (PTT). PTT is related to BP by an arterial elastic model and thus can be used to estimate beat-to-beat BP. However, PTT is difficult to be measured through a wearable device, and thus PAT is usually used as a surrogate of PTT for BP estimation, under the assumption of a constant PEP. However, PEP is not a constant but changing with physiological conditions, which may alter the PAT-BP relationship. Thus, it is important to clarify the PAT-BP relationship and address the feasibility of MBP estimation using PAT during dynamic exercise.

In this thesis, a model based study is conducted to address the above problem. Firstly, we deduced the mathematical expression of PEP as a function of DBP by introducing the arbitrary heart rate into the exponential mathematical description of a pressure-source model. Secondly, an asymmetric T-tube model was modified by introducing a nonlinear pressure-volume relationship where PTT was expressed as a dependent variant of BP. Thirdly, we proposed the mathematical equation between PAT and BP by coupling the modified ventricular and arterial models. Then, the relationships between PAT with systolic blood pressure (SBP), MBP and DBP were simulated under changing heart contractility, preload, heart rate, peripheral resistance, arterial stiffness and a mimic exercise condition. The simulation results indicated significantly high and negative correlations between PAT and SBP and between PAT and MBP whereas the correlation between

DBP and PAT was low.

Next, we developed a novel CO index, namely pulse time reflection ratio (PTRR), expressed in terms of MBP and mean aortic reflection coefficient ($\Gamma(0)$), from the modified asymmetric T-tube model. PTRR was further expressed in terms of PAT and inflection point area (IPA), a surrogate of $\Gamma(0)$ from the shape feature of PPG. The simulation results suggested significantly and positive relationship between PTRR and CO and between IPA and $\Gamma(0)$ during dynamic exercise.

In order to verify the theoretical findings, two experiments were carried out. One was incremental supine bicycle exercise conducted on 19 young healthy subjects and the other was incremental to maximum supine bicycle exercise conducted on 65 subjects, including heart failure patients, cardiovascular patients and healthy elderly. PAT showed significantly high and negative correlation with SBP and MBP, but lower correlation with DBP. PTRR showed significantly high and positive correlation with CO.

Finally, based on the theoretical and experimental verifications, linear prediction models were proposed to estimate MBP from PAT and estimate CO from PTRR. The results showed that PAT can estimate MBP with a standard deviation of 7.42 mmHg, indicating PAT model has the potential to achieve the accuracy required by AMMI standard (mean error within ± 5 mmHg and SD less than 8 mmHg). The results also showed that PTRR can estimate CO with a percent error of 22.57%, showing an accuracy which was considered as clinically acceptable (percent error less than 30%).

To summarize, the original contributions of this thesis are:

1. An explicit mathematical description of PEP in terms of DBP was proposed, which in the first time quantitatively clarified the ventricular and arterial effects on PEP timing.

2. A nonlinear pressure-volume relationship which reflected the natural arterial wall properties was introduced into the asymmetric T-tube arterial model, which effectively and quantitatively described the effect of pulsatile BP on arterial parameters, e.g., compliance, PTT etc.

3. A mathematical relationship between PAT and BP was firstly proposed as a result of the heart-arterial interaction, which simulated a significantly strong and negative relationship between PAT and SBP and between PAT and MBP but a much weaker negative relationship between PAT and DBP during exercise. The hypothesis was supported by the experiment data. To our knowledge, it is the first study describing the quantitative relation of PAT and BP by both model-based study and experimental data.

4. A novel wearable measurable CO parameter, PTRR, was proposed and it successfully showed a significantly high and positive correlation with CO during exercise both in model simulation and in the experiments.

5. Linear prediction models using PAT to estimate MBP and using PTRR to estimate CO were

proposed and evaluated in two exercise experiments conducted on 84 subjects with different ages and cardiovascular diseases. Results showed the proposed method could achieve the accuracy required for medical diagnosis.

6. Taken the findings in 3, 4 and 5 together, this study in the first time provided both the theoretical basis and experimental verifications of developing a wearable and direct measurement technique of CPO in dynamic exercise using multiple physiological signals measured on body surface.

摘要：

心力衰竭，简称心衰，是高血壓、冠心病和糖尿病等多種心血管疾病的終末期。美國有大約580萬心衰患者，而每年，有67萬人被診斷患有心衰。2010年，美國用在心衰上的相關費用預計將達到302億，其中的很大比重將用於心衰患者的醫療監護。為了減輕醫療監護的沈重負擔，迫切需要針對不同危險級別的心衰患者采用相宜的治療監護手段，而首要的，要通過心血管功能參數評定心衰患者的危險級別。

心臟輸出功率定義為平均動脈血壓和心輸出量的乘積。多項研究表明，運動下的極限心臟輸出功率能夠區分心衰患者的危險級別，預測心衰患者的死亡。然而，到目前為止，心臟輸出功率尚未能夠通過一種儀器單獨測量，而需要通過同步的血壓測量和心輸出量測量計算獲得。另一方面，現有的血壓和心輸出量測量設備由於體積龐大，無法實時測量等問題，很難實現運動狀態下的同步精確測量。因此，目前急需開發集成化、穿戴式的新型測量設備，用於直接測量動態心臟輸出功率。對於多數穿戴式測量設備而言，其核心技術在於如何建立待測的心血管參數與穿戴式可測量的各體表生理信號之間的關系。因此，本論文致力於研究一種通過體表可測的各種生理信號，具體的為心電信號和光電容積描記信號，直接估測運動狀態下心臟輸出功率的方法。

近年來，基於脈搏波到達時間（PAT）的穿戴式可測量參數被廣泛應用於血壓估測。PAT 定義為從心電信號R波到光電容積描記信號上升沿起始點之間的時間間隔。它由兩個時間分量組成：心臟等容收縮期（PEP）和脈搏波傳輸時間（PTT）。其中，PTT 可通過動脈彈性模型與血壓建立相關關系，從而用於血壓的逐拍估測。但是，PTT 很難通過穿戴式儀器測量得到，因此，在很多血壓估測場合，PEP 被假定為不隨時間變化的常數，而 PAT 則作為 PTT 的近似值，用於估測血壓。然而，相關研究表明 PEP 並非常數，而會隨實際生理狀態的改變而變化，進而導致 PAT 與血壓關系的改變。因此，弄清 PAT 與血壓的真實關系，進而探討 PAT 在運動狀態下測量平均血壓的可行性研究，顯得尤為重要。

本論文通過建立心血管系統生理模型來探討上述問題。首先，本研究通過引入心率參數，修正了基於指數函數關系表達的左心室血壓源模型的數學公式，推導出了 PEP 與動脈舒張壓之間的顯性數學公式。第二步，本研究在傳統非對稱 T 管動脈模型中導入了符合真實動脈壁力學特性的非線性血壓-容積變化關系，從而將 T 管模型中的 PTT 等常數參量表達為隨血壓變化的函數。第三步，通過修正後的心室模型和動脈模型的動態耦合，建立了血壓和 PAT 之間的定量數學關系，並通過計算機仿真，研究了外周阻力、動脈順應性、心率、心肌收縮力、前負荷的變化，特別是模擬運動狀態中的各參數變化對 PAT 與血壓之間關系的影響。參數化分析的仿真結果顯示：在運動狀態下，PAT 與收縮壓、平均血壓的變化呈現高度負相關關系，而與舒張壓的負相關關系較弱。

下一步，本研究基於非對稱 T 管動脈模型提出了一種新的心輸出量測量參數，定義為傳導時間反射比（PTRR），表征為與平均血壓和主動脈平均反射系數相關的動態參數。進一步的，利用 PAT 與血壓的逆線性關系，PTRR 可被表達為 PAT 和 IPA 的函數。其中，IPA 定義為拐點面積比，是從光電容積描記信號提取的波形特征參數。計算機仿真結果顯示，在模擬運動狀態下，PTRR 與心輸出量之間、IPA 與主動脈平均反射系數之間，均具有顯著的正相關變化趨勢。

為了驗證理論模型的相關結果，我們設計了兩組臨床運動實驗。實驗一為人體仰臥姿態下的漸進式腳踏車運動實驗，實驗對象為 19 名健康年輕成年人。實驗二為人體仰臥姿態下的漸進至最大強度腳踏車運動實驗，實驗對象為包括心衰患者、心血管病患者和健康老年人三個對比組在內的 65 人。在兩組實驗結果中，PAT 與收縮壓、平均血壓的變化呈現高度負相關關系，而與舒張壓的負相關關系較弱。PTRR 與心輸出量呈現高度正相關關系。

最後，基於理論模型和實驗驗證的相關結果，本研究提出了一種線性預測模型以實現利用 PAT 和 PTRR 分別預測運動狀態下的平均血壓和心輸出量。臨床實驗結果顯示，通過 PAT 預測的平均血壓與標準平均血壓值之間的標準差為 7.42 mmHg，達到了 AMMI 血壓測量國際標準（誤差均值在±5 mmHg 之間，標準差小於 8 mmHg）。通過 PTRR 預測的心輸出量與標準心輸出量測量值之間的百分數誤差為 22.57%，達到了公認的臨床精度要求（百分數誤差小於 30%）。

綜上所述，本論文的主要創新貢獻在於：

1. 建立了 PEP 與舒張壓之間的顯性數學公式，首次量化描述了心室和動脈相關參數對 PEP 的影響。

2. 通過引入非線性血壓-容積變化關系，在傳統非對稱 T 管動脈模型中引入了血壓變化對動脈壁相關參數的影響，如動脈順應性，PTT 等，有效建立了動脈模型中血壓和 PTT 的動態變化關系。

3. 建立了新的心臟動脈耦合模型，首次提出了 PAT 和血壓之間的數學關系，並仿真得出：在運動狀態下，PAT 與收縮壓、平均血壓的變化呈現高度負相關關系，而與舒張壓的負相關關系較弱。該結果在隨後的臨床運動實驗中得到了有力驗證。就我們所知，本研究首次從心臟動脈耦合模型和臨床實驗雙重角度定量描述了 PAT 和血壓之間的關系。

4. 本研究提出了一種新型的穿戴式可測量心輸出量參數（PTRR）。該參數在模型仿真結果和相關臨床運動實驗中均與心輸出量呈現顯著的正相關關系。

5. 本研究提出了一種線性預測模型以實現通過 PAT 和 PTRR 分別估測運動狀態下的平均血壓和心輸出量，並設計臨床實驗，在不同年齡段和患病情況的 84 個測試對象上對該方法的準確性進行了評估，結果表明該技術所估測的平均血壓和心輸出量均有望達到臨床診斷所要求的精確度。

6. 總結 3、4、5 部分的工作，本研究通過理論模型研究和臨床實驗驗證，創新性地提出了一種通過穿戴式可測的心電信號和光電容積描記信號直接估測運動狀態下心臟輸出功率的方法，為進一步開發集成化、穿戴式的心臟輸出功率新型測量設備奠定了理論基礎和實驗基礎。

List of Figures

List of Tables

List of Abbreviations

Association for the Advancement of Medical Instrumentation	AAMI
Atrioventricular node	AV node
Blood pressure	BP
Body mass index	BMI
Carbon dioxide	CO_2
Cardiac output	CO
Cardiac power output	CPO
Carotid-femoral PWV	cfPWV
Coronary artery bypass graft surgery	CABG
Correlation coefficient	r
Diastolic blood pressure	DBP
Electrocardiogram	ECG
Exercise cardiac power	ECP
Heart failure	HF
Heart rate	HR
Inflection point area	IPA
Joint Research Center for Biomedical Engineering	JCBME
Left ventricle ejection fraction	LVEF
Mean aortic reflection coefficient	$\Gamma(0)$
Mean blood pressure	MBP
Nitrous oxide	N_2O
Photoplethysmogram	PPG
Physio Flow 05	PF-05
Pre-ejection time	PEP
Pressure contour analysis	PCA
Pulse arrival time	PAT
Pulse pressure	PP
Pulse time reflection ratio	PTRR
Pulse transit time	PTT
Pulse wave velocity	PWV
Root mean squared normalized error	RMSNE
Sinus node	SA node
Standard deviation	SD
Stroke volume	SV
Systolic blood pressure	SBP
The Chinese University of Hong Kong	CUHK
Thoracic electrical bio-impedance	TEB

Contents

Chapter 1

Introduction

1.1 General background

Heart failure progressively occurs when the heart muscle becomes weakened and loses its ability to pump enough blood and oxygen to supply the body needs. Different from other cardiovascular diseases, heart failure is not a single disease, but the end stage of many cardiovascular diseases, such as hypertension, coronary heart disease, diabetes mellitus, etc. [1]. Around 5.8 million people in the United States have heart failure and about 670,000 people are diagnosed with it each year [2]. About one in five people who have heart failure die within one year from diagnosis. Heart failure was a contributing cause of 282,754 deaths in 2006 [2].

An effective indicator to predict the modality of heart failure patients would be invaluable in formulating the management plans in these patients. Many studies published in the 1990s have shown peak oxygen consumption (peak VO_2) to be a significant independent predictor of mortality [3-5]. Based on these studies, American Heart Association consensus reports have recommended that peak VO_2 be used to help determine the timing of heart transplantation in ambulatory patients with chronic heart failure [6]. However, later studies revealed that peak VO_2 can be influenced by non-cardiac factors such as muscle conditioning, motivation, age and gender [7, 8]. Therefore, research groups have been trying to find other variables as predictors of outcome.

Several investigators have shown cardiac work related performance to be prognostically superior to peak VO_2 in the evaluation of patients with congestive heart failure, using indexes such as peak stroke work index [9] and cardiac output response to exercise [10]. However, it must be remembered that heart generates pressure as well as flow. A number of groups have shown the prognostic importance of the pressure generating ability of the heart and have concluded peak exercise blood pressure to be independent predictive of prognosis [11-14]. The incorporation of pressure into exercise haemodyamic assessment is therefore crucial. **Cardiac power output** (CPO) is defined as the product of the cardiac output (CO) and mean aortic blood pressure (MBP). It was first introduced by Tan in 1986 [15] by taking into account both the flow and pressure generating ability of the heart, and can therefore be viewed as a comprehensive indicator of cardiac function. One may anticipate, therefore, that CPO would provide a more accurate prognostic indicator than either of its two components, CO and MBP.

To answer this question, four clinical studies related to this hypothesis were found out from previous literatures and their results are listed in Table 1.1. In Table 1.1, three out of four studies [16, 18, 23] show that CPO is the only independent predictor of mortality on the testing patients when CPO, CO and MBP are all tested as predictors of death in the multivariate analysis. These evidences strongly supported the hypothesis that CPO is a more accurate prognostic indicator than either MBP and CO. While in one study [17], CO reserve was shown to be the only independent predictor of death in the multivariate analysis, although the peak CPO in that study was still

significantly different between the survival and non-survival groups. The possible reason is that that study mainly aimed at investigating the long-term impact of the indicators of cardiac pumping function on cardiac death (8.6±1.0 years' follow up) while in other studies, the short (acute inhospital modality in [16], [18]) to medium (4.8 years follow up in [23]) term predictors of cardiac death were investigated. And the impact of BP varies under short and long term follow up: markedly low BP (eg, in cardiogenic shock or pre-shock) was usually seen in short term cardiac deaths while the impact of BP on long term prognosis is dichotomous, i.e. both markedly low BP and high BP (hypertension) conferred negative impacts on prognosis. Considering the high modality rate of heart failure patients within one year from diagnosis (about one in five), a prognostic indicator more effective in short term outcome would be of much more importance for these patients.

Table 1.1. Comparison amongst performances of CPO, CO and MBP as predictor of modality.

Year	Author	Measured parameters	Patients (no.)	Protocol	Independent predictor of death
2001	Williams et al.[23]	CPO, CO, MBP, VO_2 …	Chronic HF (219)	exercise	peak CPO
2004	Fincke et al. [16]	CPO, CO, MBP, SV, SBP, DBP…	Cardiogenic shock (541)	rest	rest CPO
2005	Williams et al.[17]	CPO, CO, MBP, CPO reserve, CO reserve, VO_2 …	Mild-moderate chronic HF (219)	exercise	CO reserve
2007	Mendoza et al.[18]	CPO, CO, MBP, …	Acute cardiac diseases (349)	rest	rest CPO

CPO: cardiac power output; CO: cardiac output; MBP: mean systematic blood pressure; VO_2: oxygen consumption; SV: stroke volume; SBP: systolic blood pressure; DBP: diastolic blood pressure; CPO reserve: peak CPO- rest CPO; CO reserve: peak CO – rest CO; HF: heart failure.

Another consideration is the necessity to obtain peak CPO. As shown in Table 1, two studies [16, 18] showed that the rest CPO was already an effective predictor of outcomes for cardiogenic shock patients and patients with acute cardiac diseases. In these two studies [16, 18] however, all hemodynamic indicators included in the multivariate analysis were obtained at rest, and they were not compared with performances of their counterparties obtained at peak conditions. In 1990, Tan and Litter [19] measured both CPO at rest and peak CPO under dobutamine stimulation on 28 patients with cardiogenic shock. They found that CPO measured during the basal resting state was only able to indentify unambiguously non-survivors whose cardiac function was most severely compromised but peak CPO clearly separated the cardiac pump function of the survivors and those who died. As shown in Fig.1.1, survivors and non-survivors can be significantly distinguished with a peak CPO of 1 watt, however, there is an obvious overlapping between the values of resting CPO survived and died subjects. This experimental observation was supported by a later study on critically ill patients in intensive care units [20]. On critically ill patients, survivors

were found to have better cardiac reserve (Peak CPO - baseline CPO) with greater increments of CPO in response to lower doses of dobutamine and optimal fluid administration [20].

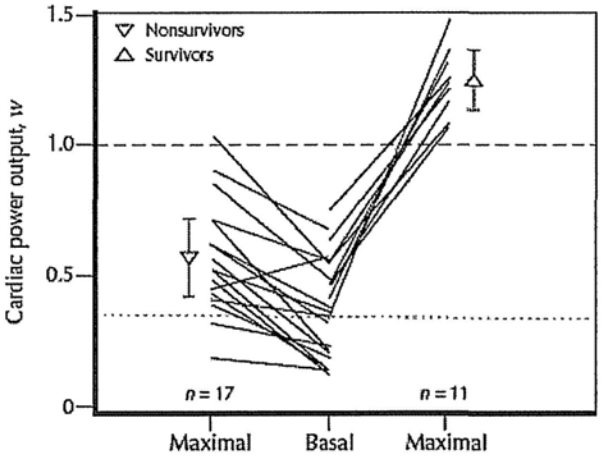

Fig. 1.1 Cardiac power output at baseline resting states and during peak dobutamine stimulation of survivors and nonsurvivors from consecutive patients admitted to a coronary care unit presenting with cardiogenic shock [19].

In the studies above, pharmacological stress such as dobutamine stimulation was utilized to produce the peak CPO. Although dobutamine stimulation causes positive inotropic and chronotropic responses, it tends to reduce preload and therefore tends to result in an underestimation of the peak CPO. Maximal exercise therefore is a better approach to stimulate the peak CPO on patients who are not too ill to participate in a symptom-limited exercise testing [21]. Using maximal exercise test, Roul *et al.* [22] measured invasive hemodynamic parameters at rest, during exercise and exercise peak on 50 chronic heart failure patients and found that peak exercise CPO, exercise LV work indices, and peak exercise VO_2 were the most useful factors for assessing prognosis [22]. However, the golden measurement methods of BP and CO are both invasive and are not preferred during exercise due to numerous concerns including the complexity of the testing, bleeding, pneumothorax, arrhythmias, infection, and catheter dislodgement. Recent studies thus intended to estimate CPO using noninvasive CO and BP measurement methods.

The combination of noninvasive hemodynamic measurements and exercise was firstly employed in the study by Williams et al. [23] on 219 chronic heart failure patients where CO was measured by the noninvasive CO_2 re-breathing method. The patients were followed up for a mean period of 4.64 (4.47-4.82, 95% credit interval) years. When peak and resting CPO, peak MBP, peak and resting CO and peak VO_2 were all tested as potential predictors of outcome, peak CPO was the only independent predictor of mortality in the mutilvariant analysis. Fig. 1.2 shows the Kaplan-Meier survival curves for peak CPO </> 1.96 watts. A total of 38 patients had a peak CPO <1.96 watts and 12 of 38 died in the follow-up study, with a cumulative survival of 89.2% at 1year, 75.7% at 2 years, 67.4% at 3 years and 43.4% at 4 years. Of the remaining 181 patients having a peak CPO > 1.96 watts, cumulative survival was 98.3%, 94.2%, 91.4% and 90.5% at 1, 2, 3, 4 years, respectively. The authors thus concluded that peak CPO can provide a more accurate

prognostic indicator than peak VO_2 along, or either of its two components, CO and MBP. This conclusion is mainly supported by a latter study by Lang et al [24] on 148 chronic heart failure patients.

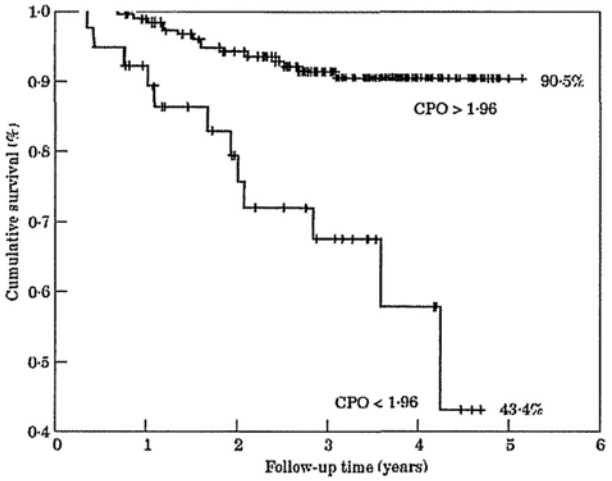

Fig. 1.2 Kaplan-Meier survival curves for peak cardiac power output (CPO) greater or less than 1.96 watts (log rank Chi-square = 21.77, df = 1, $P < 0.00001$) [23].

However, as will be mentioned in detail in later sections 1.2 and 1.3, it is rather difficult to measure cardiac output and blood pressure noninvasively, accurately and simultaneously at peak exercise. For instance, the gas re-breathing CO measuring methods utilized in [23] and [24] suffer from the long response time which makes the methods difficult to seize the peak CO. In addition, the CO_2 re-breathing approach in [23] was further influenced by acidosis which may cause an underestimation of CO by up to 50% at high levels of exercise [24]. The peak mean BP however, is usually calculated according to Eq. 1.1 by SBP and DBP readings from auscultatory cuff sphygmomanometer, where the accurate interpretations of Korotcoff sounds become rather difficult as the exercise test progresses.

Due to a number of problems faced in the direct measurement of CPO, surrogates of CPO which are easier to be acquired were reported and evaluated. Recently, both Cohen-Solal *et al.* [25] and Scharf *et al.* [14] independently used the product of VO_2 and systolic BP as an approximation of CPO, referred as 'circulatory power' [25] or 'exercise cardiac power' (ECP) [26], respectively. However, peak VO_2 itself is also dependent on factors other than CO, such as muscle de-conditioning, motivation, obesity, the age, and gender [27]. These confounding factors may explain why some patients with CHF may have a favorable prognosis despite a low peak VO_2 [28]. Although easier to measure, systolic blood pressures are generally exaggerated in stiffened arterial systems, such as those found in the elderly.

These facts alone serve to illustrate the importance of research on the development of novel techniques and devices for noninvasive BP and CO measurements in order to obtain peak CPO. Further, it would be a great advance if an integrated approach is developed to measure CPO directly, as will be developed in this work. In the following two sections (1.2 and 1.3), current BP

and CO techniques are reviewed with the discussion on the feasibility of applying these methods in the exercise testing. In section 1.4 and 1.5, the objective and structure of this thesis are introduced, where the whole idea of developing an integrated method to measure CPO directly during dynamic exercise is presented.

1.2 Review of present blood pressure measurement

Current blood pressure measurement methods are mainly divided into two categories, the invasive and noninvasive methods. The first category directly measures the blood pressure inside the cardiac chamber or large arteries by inserting catheters inside the body whereas the second category includes indirect methods which read intra-vascular blood pressure using different physical measuring mechanisms.

1.2.1 Invasive approach

The fluid-filled catheter-manometer system may have been regarded as the most dominant approach to monitor blood pressure waveform invasively. By placing a cannula into an artery and meanwhile connecting it to an electronic pressure transducer, the intra-arterial BP can be most accurately measured [30]. This method provides accurate and beat-to-beat measurement of BP waveform, which is regarded as the invasive golden standard. However, it is usually only limited to the intensive unit to very ill patients due to the risk and potential complications of invasive measurement, e.g. thrombosis, infection and bleeding.

1.2.2 Non-invasive cuff sphygmomanometer

In routine clinical practice, the most common device to measure blood pressure is the noninvasive cuff sphygmomanometer. As shown in Fig. 1.3, this instrument consists of an inextensible cuff with an inflatable bag inside, which is connected to rubber squeeze bulb through a needle valve. The cuff is wrapped around the upper arm so that the inflatable bag lies between the cuff and the skin, directly above the artery to be compressed. The artery is occulted by the inflating the bad, by means of the rubber squeeze bulb, to a pressure higher than the arterial systolic pressure. The pressure in the bag is measured by mercury or an aneroid manometer. Pressure is released from the bag at a rate of 2 or 3 mmHg per heart beat by means of a needle valve in the inflating bulb. Using sphygmomanometer with a cuff, blood pressure can be determined by either the auscultatory or the oscillometric method [31].

The most standard manual BP measurement technique is the auscultatory method. It measures BP by the Korotkoff sounds produced by the return of pulsatile blood flow inside the pre-occluded artery. The working principle is as follows: first, the cuff pressure is inflated to a level higher than the systolic blood pressure of the underlying artery, to about 160 mmHg. The blood flow in the artery stops and there are no sounds heard at that moment. Then, this pressure is released at a rate of 2 or 3 mmHg per heart beat. When the cuff pressure is right lower than the systolic blood pressure of the underlying artery, small spurts of blood escape through the cuff and slight tapping sounds (Korotkoff sounds) begin to be heard (see Fig. 1.4). The systolic blood pressure thus can be read from the cuff pressure at the appearance of the Korotkoff sounds, as indicated in Fig. 1.4.

The Korotkoff sounds are heard every heartbeat afterwards and become louder as the cuff pressure continues dropping. When the inflating pressure approaches the diastolic level, the Korotkoff sounds become muffles. As it falls just below the diastolic level, the sounds disappear, and this indicates the diastolic blood pressure [32]. The auscultatory method is simple and thus most widespread in the clinic for routine blood pressure measurement; however, there is still some deficiency and limitations in this method: first, it requires a quiet measuring environment and can not be used under noisy condition; second, professional practitioner has to be trained for operation whose hearing acuity must be good for low frequencies from 20 Hz to 300 Hz. In addition, the accuracy of this method on infants and hypertensive patients is still doubted [32].

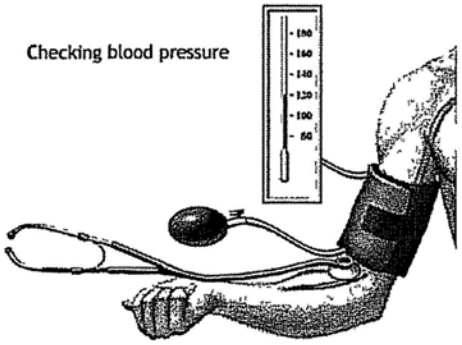

Fig. 1.3 Illustration showing the noninvasive cuff sphygmomanometer [33].

The measurement of auscultatory method required professional skills to interpret the onset and disappearing of the Korotcoff sounds, and thus is difficult to be made automatic. An alternative BP measurement method which also utilizes cuff sphygmomanometer but is easy to be automatic is the oscillometric method. The first study of oscillometric method is by Marey [34], who used a fluid-filled chamber to surround the arm and observed that as the pressure in the chamber was increased, the pressure perturbations reached a maximum value, and then decreased.

The mechanism of oscillometric method is as follows [35]: the cuff pressure is first raised to above the systolic blood pressure and then stops the blood flow. Although the artery segment under the cuff is occluded, the oscillations of the pulsatile blood pressure at the upstream can be transmitted to the cuff through the adjacent tissues and causes small amplitude oscillations on the cuff pressure. Then, the cuff pressure slowly decreases due to deflation. When it drops just under the systolic blood pressure, blood spurts through the underlying artery segment and the oscillation of cuff pressure becomes significantly larger. As shown in Fig. 1.4, the point where the oscillations significantly augment indicates the systolic blood pressure. The oscillations continue augmenting as the cuff pressure decreases, until reach the maximum, which corresponds to the mean blood pressure. Then, the oscillations decrease again. The diastolic pressure is not identifiable from the cuff pressure oscillations, and instead it is calculated from the proprietary algorithm developed by different manufacturers. As pointed out by Ramsey [36], the most robust measurement of oscillometric method is the mean blood pressure as compared with the systolic and diastolic blood pressure.

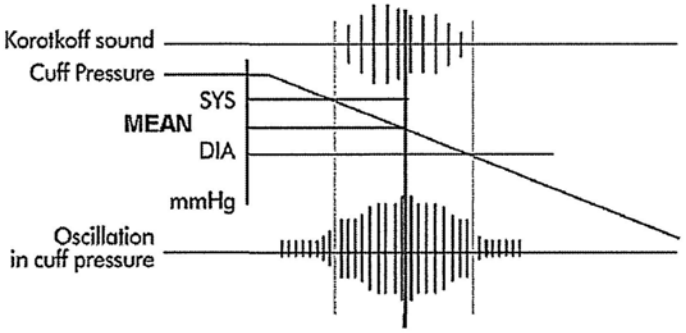

Fig. 1.4 The oscillometric method illustration [37].

The main disadvantage of the sphygmomanometer measurement is that it does not provide blood pressure in beat to beat manner and this makes it unable to trace the rapid changes of blood pressure and thus misses important diagnosis information. In order to interpret the characteristics of the Korotkoff sounds or cuff pressure oscillation, the sphygmomanometer takes several seconds to raise the cuff pressure above the systolic blood pressure and tens of seconds to release the cuff pressure slowly. In total, it takes about 1 min to complete one measurement and thus is unable to catch the rapid blood pressure changes. The spectrum analysis of blood pressure variability with respect to time is also limited in the frequency domain. Further, the occlusion of brachial artery during measurement will block the venous return of the down stream arteries, which will affect the readings of the sequential measurements and cause damage to the local artery.

1.2.3 Non-invasive and continuous approach

There has always been the need of the patients in the intensive care unit for the noninvasive and continuous blood pressure measurement. Two such approaches have been developed to complement the shortcomings of the intermittent blood pressure measurement.

One approach is the tonometry, which is developed by Pressman and Newgard in 1961 [38-39]. The usual measurement site of this method is the radial artery which is superficial under the wrist skin lying on the bone. The artery is then flattened by applying external pressure noninvasively to squeeze the artery against the bone. The basic principle of tonometry is that, when a pressurized vessel is partly collapsed by an external force, the circumferential tension of the arterial wall disappears and the internal and external pressures are equal. Therefore, the applied pressure to maintain the flattened shape indicates the internal arterial blood pressure reading. An array of piezoelectric transducers is used for the pressure reading. The arterial tonometer suffers from relatively high cost when compared with a conventional sphygmomanometer and its accuracy is decreased by wrist movement [32].

The other approach is the volume-clamp method utilized in the "Finapres" blood pressure waveform measurement system. Penaz proposed this method based on the principle of vascular wall unloading [40]. In this method, a small inflatable finger cuff containing an infrared photoplethysmography is applied to one of the subject's finger. The pressure in cuff is first inflated to a pressure equal to the mean pressure in the artery and then is continuously adjusted by a servo control system to maintain the transmural pressure at zero as determined by the maximum

amplitude of photoplethysmographic signal. This method was further developed by Wesseling [41, 42] and successfully commercialized as "Finapres", which delivers a continuous finger arterial pressure waveform. From the finger pressure waveform, systolic, diastolic, mean pressures and pulse rate are estimated beat-by-beat.

There are problems in the two techniques mentioned above. For the tonometer, it requires trained operator to perform the measurement and hence is unsuitable for long-term measurement, even though, it is unstable in practice since the radial artery is easy to slip by movements of wrist beyond the range of the piezoelectric transducers [32]. The volume-clamp method utilizes a vascular-unloading status (maximal arterial diameter) indicated by photoplethysmography to read the intra-vascular blood pressure directly from cuff pressure, which is not always reliable, since the maximal diameter of the local artery is determined both by pressure and local compliance, the latter of which is sensitive to changes of vascular tone [43]. A common problem of tonometry and volum-clamp method is that they measure blood pressure at the peripheral arteries, which not only reflect the central blood pressure information but are influenced by the local factors such as peripheral circulation, perfusion of peripheral arteries, temperature, etc. Therefore, it is necessary to develop a novel blood pressure measurement method which is more convenient and unobtrusive in the practical applications.

1.2.4 Non-invasive, continuous and cuffless approach

The blood pressure estimation method based on pulse wave velocity (PWV) or pulse transit time (PTT) is perhaps one of the most dominant novel techniques under investigation. This technique is developed fundamentally based on the relationship between PWV and the trans-mural blood pressure (BP) on the same arterial segment described by the Moens-Korteweg equation [44] or Bramwell and Hill equation [45]. The **pulse transit time** is defined as the time delay between the onsets of blood pressure pulses at the aorta and the peripheral artery within one heartbeat, as indicated in Fig. 1.5. Many investigators have studied the relationship between PWV and BP using PTT [46-48]. Under different experimental conditions, previous studies have reported a moderate to strong correlation between PTT and BP, depending upon how PTT and BP were measured, the method of recording and changing the blood pressure, and whether the patients displayed differences in blood pressure reactivity.

Strictly speaking, in order to measure PTT, both BP waves at the proximal and peripheral sites should be recorded. However, since the BP pulse, especially the central BP pulse, is too difficult to obtain, in practice, the R-wave of Electrocardiogram (ECG) has been commonly used to initiate PTT and the peripheral pulses like photoplethysmogram (PPG) are used to replace the peripheral BP pulse because they are easy to detect and usually more artifact-free [49]. As explained in detail in latter section 2.1.3, ECG is the potential difference measured on the body surface which reflects the electrical activation of the heart muscle. The R wave of ECG indicates the initialization of ventricular re-polarization which stimulates the ventricular contraction and is often regarded as the start of a cardiac cycle. To distinguish from PTT, the time delay between ECG R wave and the onset of a peripheral pulse is defined as **pulse arrival time** (PAT), which is equal to the summation of ventricular pre-ejection time (PEP) and PTT, as shown in Fig. 1.5.

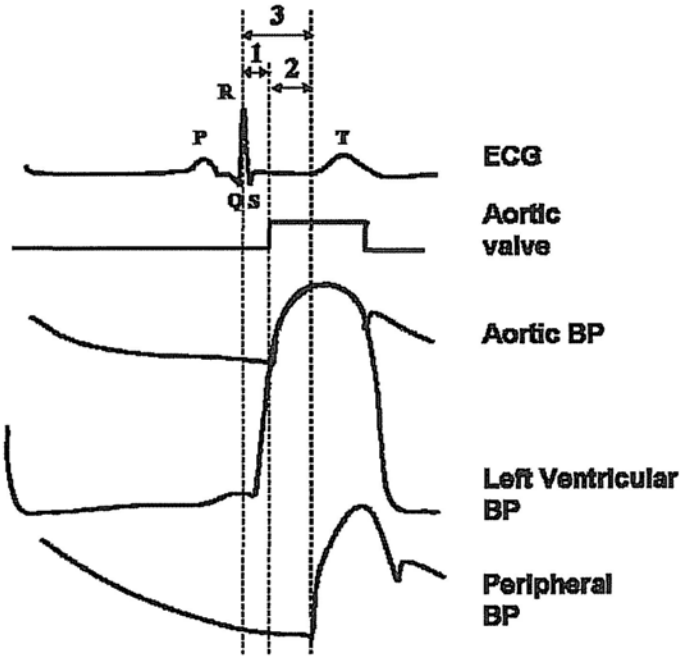

Fig. 1.5 The illustration of pre-ejection period (PEP, "1" in the figure), pulse transit time (PTT, "2" in the figure) and pulse arrival time (PAT, "3" in the figure).

In many applications related to BP estimation, PAT was utilized due to its simplicity and reliability of measurement [46, 49-53]. In these applications, estimation equations are directly derived from arterial elastic models [44, 45] which described the relationship between PTT and BP, and PAT is utilized as a surrogate of PTT assuming PEP is a constant. PAT covaried appreciably with SBP and MBP negatively under a variety of conditions, such as rest, cold pressor test, and paced respiration in both normotensive and hypertensive subjects, whereas it covaried inconsistently with diastolic blood pressure, with both directions [46, 49, 51, 53]. Some studies reported that PTT had higher relationship with BP than PAT [54, 55]; other studies however, especially those related to dynamic exercise, showed that PAT had a high correlation with SBP and MBP, better than that of PTT [56, 57].

In order to explain these conflicting observations, some studies measured the changes of PAT, PTT and PEP together with BP and found that the conflicting observations were mainly due to the inconstant relationship between PEP and BP under different physiological conditions [52, 55, 58, 59]. Based on these observations, Aubert *et al* [60] simulated the relationship between PEP and BP under varying parameters in a ventricle model coupled with a three-element Windkessel model, and meanwhile described the relationship between PTT and BP using the classic Moens-Korteweg equation. They then concluded that the relationship between PAT and blood pressure depended on the relatively dominant contribution of PTT or PEP in PAT. To our best knowledge, this is the first investigation using a theoretical model to describe the relationship between PAT and arterial blood pressure directly, however, there are some limitations: 1) the basic assumptions of the Windkessel model and Moens-Korteweg equation are conflicting, where the first assumes the infinite pulse wave velocity whereas the latter describes the relationship of the finite pulse wave velocity

determined by elastic properties of the artery; 2) although PEP was simulated under conditions with varying physiological parameters, the simulation situations are not practical since not a single physiological parameter can vary alone under the real physiological condition. The interactions among different parameters are ignored and no conclusions have been drawn on the PEP-BP relationship in terms of different physiological conditions (e.g., exercise). Therefore, further theoretical investigations are essentially needed to clarify and conclude the relationship between PAT and arterial blood pressure.

1.3 Review of present cardiac output measurement

Similar to the BP measurement, the cardiac output (CO) measurement methods are also divided into the invasive and non-invasive approaches. In this section, we first introduce the invasive but the accurate method, thermodilution, which is regarded as the golden standard. Then, four established noninvasive approaches, including the ultrasound Doppler, gas-rebreathing, blood pressure contour analysis (PCA) and bio-impedance, are reviewed.

1.3.1 Invasive method

It was not until the early 1970s that Swan and Ganz introduced the balloon-tipped pulmonary artery catheter (Fig. 1.6) into clinical practice which finally allowed the routine measurement of CO at the bedside by thermodilution [61]. As shown in Fig. 1.6, a bolus of sterile solution, i.e. the injectate, that is colder than the patient's blood is injected into the proximal port of a pulmonary artery catheter located in the right artrium (blue line, Fig. 1.6). In the atrium, the injectate mixes with the blood and passes through the tricuspid valve into the right ventricle. A thermistor within the catheter senses the change in blood temperature as the blood passes the catheter tip located in the pulmonary artery. A curve that shows the change in temperature over time is then converted into a measurement of cardiac output. CO is inversely proportional to the area under the curve [62].

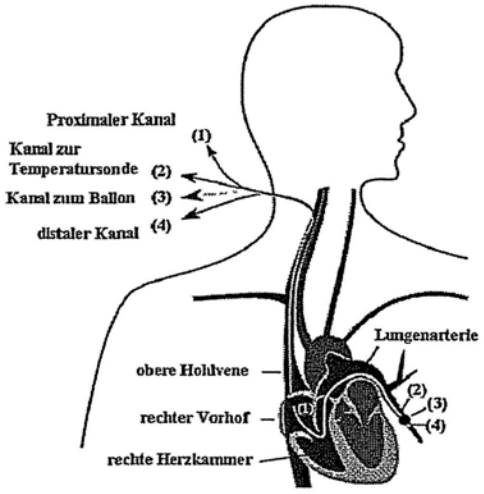

Fig. 1.6 Diagram of invasive CO measurement with Swan-Ganz catheter [63].

Measurements of CO by pulmonary artery catheter thermodilution provide CO values with high accuracy, even through, errors can be induced by indicator loss [64], and structural cardiac abnormalities [65]. Besides, greater limitations of the pulmonary artery catheter perhaps are the highly invasive operating procedures and the risk of damage to cardiac valves with prolonged use. Other complications include catheter knotting, pulmonary artery rupture and pulmonary embolism [66]. Use of this device is now declining in favor of less invasive and noninvasive technologies.

1.3.2 Non-invasive methods

Doppler ultrasound

The change in the observed frequency of a sound wave when the source of the signal is moving in relation to the observer is known as Doppler shift. The measurement of the Doppler shift of transmitted ultrasound waves has been used to calculate aortic blood velocity and to estimate CO. The oesophageal Doppler technique involves the measurement of blood velocity in the descending thoracic aorta using an ultrasound probe placed in the lower oesophagus, and the estimation of aortic cross-sectional area by utilizing an M mode ultrasound or directly deriving a value of total cardiac output from a nomogram using aortic blood velocity, height, weight and age [67]. The principal advantage of oesophageal Doppler technique is speed and ease of use, and the method has proved ideal for intra-operative use. The major limitation of this technique is that the probe is not well tolerated by conscious patients and its use is generally confined to anaesthetised or sedated patients.

Supra-sternal Doppler is essentially a noninvasive alternative to the oesophageal Doppler technique, by using a non-invasive ultrasound probe positioned in the jugular notch and measuring blood velocity in the ascending aorta. Stroke volume and cardiac output are calculated using a measurement of cross-sectional area of the aortic outflow tract. Since measuring from the aortic root, the technique is not affected by changes in distribution of cardiac output between the upper and lower body. Cardiac output measurements by the supra-sternal Doppler method were similar to those taken with pulmonary artery catheter thermodilution in clinical studies [68-69]. The portable and non-invasive nature of this technology is a major advantage; however, it may be very difficult to identify the aortic root in some subjects due to the anatomy and position. Consequently, this technique may have greater inter-observer variability than other methods. Because measurements are taken in the supine position, they may be poorly tolerated by breathless patients.

Another technique using Dopper ultrasound is the trans-oesophageal echocardiography. The use of this technique allows real time imaging of the left ventricular outflow tract. Stroke volume may be calculated by measurement of the blood velocity profile using the Doppler technique and then measuring aortic valve area. Studies suggest that measurements taken using this technique are similar to those taken using pulmonary artery catheter thermodilution [70-71]. However, accuracy is highly dependent on both the quality of echocardiographic views and operator skill.

Gas re-breathing

Non-invasive rebreathing methods to assess cardiac output are based on the principle that

exchange rates of physiological or non-physiological gases can be determined from analysis of alveolar gas exchange. Based on this assumption, it is possible to calculate pulmonary capillary blood flow [72]. Popular rebreathing methods today include the inert gas (nitrous oxide, N_2O) method and carbon dioxide (CO_2). The indirect estimation of mixed venous partial pressure of carbon dioxide using the CO_2 rebreathing method can be made using either the exponential method described by Defares [73] or using the equilibrium method described by Collier [74]. The equilibrium method appears more valid for measurement of cardiac output at rest, while during high intensity exercise, the exponential method is recommended as there is a greater potential for unpleasant side effects and as the equilibrium method requires inhalation of higher CO_2 concentration [75]. The inert gas (N_2O) rebreathing method was recently validated against direct Fick and thermodilution methods [76-77]. Good reliability of inert gas rebreathing method was also reported [76-77].

Blood pressure pulse contour analysis

Otto Frank first suggested calculating cardiac output by analysis of the arterial pressure waveform in 1899 [78], where cardiac output was calculated from mean arterial pressure and total peripheral resistance analyzed from the time constant of diastolic aortic pressure decay and arterial compliance, estimated by measuring aortic pulse wave velocity. In 1970, Kochoukos et al. described a more accurate method of stroke volume estimation involving measurement of the area under the systolic portion of the arterial pressure waveform (Fig. 1.7) [79]. This work was developed by Wesseling et al., who devised an algorithm of calculating stroke volume from aortic impedance and the change in arterial pressure during systole [80-81]. Although the method suggested by Wesseling may provide a reliable estimate of changes in cardiac output [82–83], accuracy may be influenced by changes in total peripheral resistance [84]. Perhaps the most important difficulty with arterial waveform analysis is that aortic impedance is dependent on both cardiac output and aortic compliance. Consequently, it is only possibly reliable to estimate changes in stroke volume rather than absolute values. Such systems must therefore be calibrated before use.

An alternative method of arterial waveform analysis is to apply the physical principle of conservation of mass to calculate changes in pulse power. Ejection of blood into the aorta during systole causes fluctuations in blood pressure around a mean value. Using a mathematical technique termed auto-correlation, analysis of these fluctuations allows determination of changes in stroke volume with each cardiac cycle [85]. The pulse power method is calibrated intermittently by the lithium indicator dilution to provide updated cardiac output data [86]. In lithium indicator dilution method, lithium is detected following intravenous injection by an external lithium ion sensitive electrode attached to a standard arterial catheter. Cardiac output is calculated using a modified Stewart-Hamilton equation. Comparisons of pulse power analysis to intermittent determinations of cardiac output by thermodilution and lithium dilution suggest this method of continuous cardiac output measurement is reliable [87-89]. Compared to pulmonary artery catheter thermodilution, this combined technique is less invasive, allowing use for longer periods of time in a wider range of patients. Limitations include potential interference between nondepolarising muscle relaxants and lithium ion sensitive electrode which may results in baseline

placed on the upper and lower thorax. TEB value negatively proportional to the volume of thoracic fluids such that increasing fluid in the thorax results in less TEB. Therefore, the inverse of TEB, and thus changes in CO, are reflected as a change in total bio-impedance or fluid conductivity. SV is thus calculated according to the famous Kubicek' equation using resistivity of blood, distance between the electrodes, basic chest impedance Z_0, and features extracted from the impedance signal. Kubicek' equation was later modified by Bernstein to account for the non-cylindrical shape of the chest, which might result in an erroneous determination of the CO [97].

Many investigators found there is a significant correlation between cardiac output measured with impedance cardiography and that measured with other methods. Clinical trials of TEB have been shown to be reliable in young healthy volunteers, but in critically ill or surgical patients, the results have been inconsistent [98-100]. A meta-analysis of TEB Meta-analysis of studies in cardiac patients using the different TEB methods shows correlation coefficients of 0.77 (0.71 – 0.82) when compared with thermodilution [101]. There are several limitations in TEB techniques. Firstly, such techniques are affected by tissue fluid volume and changes in the volume of pulmonary and venous blood induced by respiration. Secondly, any alteration in the position or contact of the electrodes will thus affect these measurements. Thirdly, any acute change in tissue water, such as the development of pulmonary edema or pleural effusions or chest wall edema, will alter bioimpedance readings and affect CO measurements.

A new generation of TEB device, Physio Flow 05 (PF-05, Manatec Biomedical, Macheren, France) overcomes some of the initial limitations of the first generation TEB devices by improved algorithms. This device utilizes an improved algorithm that excludes the basal thoracic impedance Z_0 and the distance between electrodes to ensure that the CO readings are robust to electrode positions, skin thickness and perspiration [102-103]. Several validation studies have shown that PF-05 agrees well with direct Fick's method in exercise tests [102, 104, 105]. This device is later utilized as the reference CO method in the dynamic exercise experiments involved in this work.

1.3.3 Feasibility of non-invasive cardiac output measurements during exercise

The requirements for a CO measuring method used in dynamic exercise are quite high: first of all, the measurement should be noninvasive to reduce the risk and discomfort of the patients; secondly, in order to indicate quick CO changes, it should be continuous and with short response time; thirdly, it is preferred to be automatic and inexpensive; last but not least, the ambulatory or wearable devices are required during exercise.

As mentioned above, Doppler ultrasound approach measures beat to beat CO, whereas it has to be operated by a professional practitioner and is unsuitable for long-term monitoring. The gas re-breathing method requires long response time before a measurement can be made and this influences its ability to track rapid hemodynamic changes. Impedance cardiography and the model flow method (BP pulse contour analysis) are both automatic and continuous. However, the measuring equipments are complicated and relatively expensive.

To develop a CO technique potentially applicable in ambulatory settings, a comparably unobtrusive alternative is to analyze the pulse contour of photoplethysmogram (PPG). PPG is a

drift in calibration and the measurement error occasionally caused by irregular cardiac rhythms or damping of the arterial waveform.

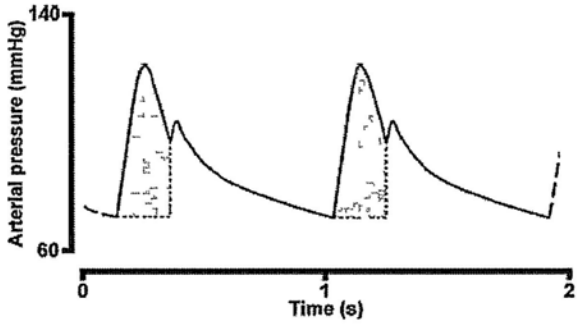

Fig. 1.7 Stroke volume estimated from systolic portion (shaded) of arterial waveform [79].

Another combined technology is the trans-pulmonary thermodilution and arterial waveform analysis. In trans-pulmonary thermodilution, a cold saline indicator is injected via a central venous catheter and measurement of the temperature of arterial blood is performed using a thermistor-tipped catheter sited in the femoral or brachial artery. Cardiac output is then calculated using a modified Stewart-Hamilton equation allowing calibration of continuous cardiac output data by a pulse contour analysis method. The combined technology correlates well with measurements made by pulmonary artery catheter thermodilution [91, 92]. An important limitation is the requirement for a specific thermistor-tipped arterial catheter to allow thermodilution measurements. In most cases this necessitates the insertion of a new arterial catheter to facilitate cardiac output measurement by this technique.

A recently developed cardiac output monitoring technology FloTrac involves arterial waveform analysis utilizing a proprietary algorithm to calculate CO without calibration. At present, limited information is available about this technology, although published data suggest that further development is necessary before the device can be recommended for clinical use [93].

As mentioned in section 1.2.3 above, non-invasive measurements of arterial pressure may be performed using the volume-clamp method with a small pressure cuff placed on the finger. An aortic flow waveform is constructed by simulating a non-linear three element model of the aortic input impedance as described by Wesseling et al. [94]. Integration of the computed aortic flow waveform allows the calculation of stroke volume and thus cardiac output. This method does not appear to correlate well with bolus thermodilution using the pulmonary artery catheter [95]. However, the method does have a useful role in research and outpatient medical practice.

Thoracic electrical bio-impedance (TEB)

First proposed by Kubicek in 1966 [96], TEB is based on the theory that the thorax is a cylinder that is perfused with a fluid (blood) of a specific resistivity. Thoracic bio-impedance is the electrical impedance to high frequency low amplitude current that is transmitted from electrodes

function impact upon the long-term prognosis of patients with chronic heart failure, *Am. Heart. J.*, vol. 150, pp. 983, 2005.

[18] D. D. Mendoza, H. A. Cooper and J. A. Panza, Cardiac power output predicts mortality across a broad spectrum of patients with acute cardiac disease, Am. Heart J., vol. 153, pp. 366-370, 2007.

[19] L. B. Tan and W. A. Littler, Measurement of cardiac reserve in cardiogenic shock: implications for prognosis and management, *Br Heart J*, vol. 64, pp. 121–128, 1990.

[20] A. C., Timmins, M. Hayes, E. Yau, J. D. Watson and C. J. Hinds, The relationship between cardiac reserve and survival in critically ill patients receiving treatment aimed at achieving supranormal oxygen delivery and consumption, Postgrad. Med. J., vol. 68, pp. S34–S40, 1992.

[21] L. B. Tan, R. J. I. Bain and W. A. Littler, Assessing cardiac pumping capability by exercise testing and inotropic stimulation, *Br. Heart J.*, vol. 62, pp. 20–25, 1989.

[22] G. Roul, M. E. Moulichon, P. Bareiss, et al., Prognostic factors of chronic heart failure in NYHA class II or II: value of invasive exercise haemodynamic data, *Eur. Heart J.*, vol. 16, pp. 1387–1398, 1995.

[23] S. G. Williams, G. A. Cooke, D. J. Wright, et al., Peak cardiac power output: a powerful prognostic indicator in chronic heart failure, vol. 22, *Eur. Heart J.*, pp 1496–1503, 2001.

[24] C. C. Lang, P. Karlin, J. Haythe, et al., Peak cardiac power output, measured noninvasively, is a powerful predictor of outcome in chronic heart failure, *Circ. Heart Fail.*, vol. 2, pp. 33-38, 2009.

[25] A. Cohen-Solal, J. Y. Tabet, D. Logeart, et al., A non-invasively determined surrogate of cardiac power ('circulatory power') at peak exercise is a powerful prognostic factor in chronic heart failure, *Eur Heart*, vol. 23, pp. 806–814, 2002.

[26] C. Scharf, T. Merz, W. Kiowski, et al., Noninvasive assessment of cardiac pumping capacity during exercise predicts prognosis in patients with congestive heart failure, Chest, vol. 122, pp. 1333–1339, 2002.

[27] J. R. Wilson, G. Rayos, T. K. Yeoh, P. Gothard, Dissociation between peak exercise oxygen consumption and hemodynamic dysfunction in potential heart transplant candidates, *J. Am. Coll. Cardiol.*, vol. 26, pp. 429–435, 1995.

[28] D. B. Chomsky, C. C. Lang, G. H. Rayos, et al., Haemodynamic exercise testing: A valuable tool in the selection of transplantation candidates, *Circulation*, vol. 94, pp. 3176–3183,1996.

[29] L. W. Stevenson, A. E. Steimle, G. Fonarow, et al., Improvement in exercise capacity of candidates awaiting heart transplantation, *J. Am. Coll. Cardiol.*, vol. 25, pp. 163–170, 1995.

[30] J. K.-J. Li, Hemodynamic measurements and clinical monitoring, in *The Arterial Circulation: Physical Principles and Clinical Applications*. Totowa, NJ: Human Press, 2000, pp. 129-159.

[31] R. B. Northrop, *Noninvasive Instrumentation and Measurement in Medical Diagnosis*, Boca Raton, CRC Press, 2002.

[32] J. G. Webster, J. W. C. Jr., M. R. Neuman, et al., Medical Instrumentation: application and design, 3rd ed., New York: Wiley, 1998, pp. 317-320.

[33] Available at: http://onunddy-generalhealth.blogspot.com/2009_06_01_archive.html

[34] E. J. Marey, Pression et Vitesse du Sang, Physiologie Experimentale, vol. 2, pp. 307-343, 1876.

executive summary (update 2005): the task force for the diagnosis and treatment of chronic heart failure of the European Society of Cardiology, *European Society of Cardiology*, 2005.

[2] D. Lloyd-Jones, R. J. Adams, T. M. Brown, et al. Heart Disease and Stroke Statistics—2010 Update. A Report from the American Heart Association Statistics Committee and Stroke Statistics Subcommittee, *Circulation*, vol. 121, pp: e1-e170, 2010.

[3] D. M. Mancini, H. Eisen, W. Kussmaul, et al., Value of peak exercise oxygen consumption for optimal timing of cardiac transplantation in ambulatory patients with heart failure, *Circulation*, vol. 83, pp. 778–786, 1991.

[4] J. Parameshwar, J. Keegan, J. Sparrow, et al., Predictors of prognosis in severe chronic heart failure, *Am Heart J*, vol. 123, pp. 421–426, 1992.

[5] J. Myers and L. Gullestad, The role of exercise testing and gas exchange measurement in the prognostic assessment of patients with heart failure, *Curr Opin Cardiol*, vol. 13, pp. 145-155, 1998.

[6] M. R. Costanzo, S. Augustine, R. Bourge et al., Selection and treatment of candidates for heart transplantation. A statement for health professionals from the Committee on Heart Failure and Cardiac Transplantation of the Council on Clinical Cardiology, American Heart Association, Circulation, vol. 92, pp. 3593-612, 1995.

[7] J. L. Fleg and E. G. Lakata, Role of muscle loss in age-associated reduction in VO_{2max}, *J Appl Physiol*, vol. 65, pp. 1147-1151, 1988.

[8] J. R. Wilson, G. Rayos, T. K. Yeoh, et al., Dissociation between peak exercise oxygen consumption and haemodynamic dysfunction in potential heart transplant candidates, *J Am Coll Cardiol*, vol. 26, pp. 429–435, 1995.

[9] B. P. Griffin, P. K. Shah, J. Ferguson, et al., Incremental prognostic value of exercise haemodynamic variables in chronic congestive heart failure secondary to coronary artery disease or dilated cardiomyopathy, *Am J Cardiol*, vol. 67, pp. 848–853, 1991.

[10] D. B. Chomsky, C. C. Lang, G. H. Rayos, et al., Haemodynamic exercise testing: A valuable tool in the selection of transplantation candidates, *Circulation*, vol. 94, pp. 3176–3183,1996.

[11] T. L. Kelly, R. Cremo, C. Nielsen, et al., Prediction of outcome in late-stage cardiomyopathy. Am Heart J, vol. 119, pp. 1111–1121, 1990.

[12] J. K. Ghali, S. Kadakia, A. Bhatt, et al., Survival of heart failure patients with preserved versus impaired systolic function: the prognostic implication of blood pressure, *Am Heart J*, vol. 123, pp. 993–997, 1992.

[13] P. De Groote, A. Millaire, E. Decolouix, et al., Kinetics of oxygen consumption during and after exercise in patients with dilated cardiomyopathy, *J Am Coll Cardiol*, vol. 28, pp. 168–175, 1996.

[14] Osada N, Chaitman BR, Miller LW et al. Cardiopulmonary exercise testing indentifies low risk patients with heart failure and severely impaired exercise considered for heart transplantation, *J Am Coll Cardiol*, vol. 31, pp. 577–582, 1998.

[15] L. B. Tan, Cardiac pumping capability and prognosis in heart failure, *Lancet*, vol. 2, pp. 1360–1363, 1986.

[16] R. Fincke, J. S. Hochman, A. M. Lowe, et al., Cardiac power is the strongest hemodynamic correlate of mortality in cardiogenic shock: a report from the SHOCK trial registry, *J Am Coll Cardiol*, vol. 44, pp. 340-348, 2004.

[17] S. G. Williams, M. Jackson, G. A. Cooke, et al., How do different indicators of cardiac pump

blood volume signal acquirable by wearable optoelectronic sensors from body terminals such as finger and ear. PPG is found to contain information about changes of CO, e.g. in patients undergoing mechanical ventilation, indices derived from PPG were sensitive markers of CO fluctuations induced by hypovolemia or volume expansion [106, 107]. McCombie et al [108] proposed a blind system identification method to reconstruct aortic blood flow curve from two PPGs. In their results, qualitative aortic flow information was obtained, but no quantitative CO values were reported. Awad et al [109] utilized a multi-linear regression model to estimate CO from ear PPG width and heart rate (HR) in patients undergoing coronary artery bypass graft surgery (CABG). The estimated bias was small; the precision however was too large to be clinically acceptable. Recently, our group tried an approach based on the Windkessel model to estimate CO from finger PPG [110]. The results on young healthy subjects were promising, with bias and precision both within the clinical acceptable limit. However, since the Windkessel model is a lumped model assuming infinite pulse wave velocity, it disregards the strong effect of wave reflections on beat-to-beat CO and brings inherent errors into the estimation.

In this thesis, a modified asymmetric T-tube model is later developed to propose a novel CO parameter extracted from ECG and PPG signals. The most significant advantage of this technique is that it considers the wave reflection phenomenon and assesses the strength of wave reflection at the aortic root from shape features of the PPG signal. In addition, an integrated approach for cardiac power output (CPO) estimation can be developed from the combination this novel CO parameter plus PAT, a BP index also from ECG and PPG and utilized to provide CPO beat to beat during dynamic exercise.

1.4 Motivation and objective of this thesis

The main objective of this thesis is to develop a model-based, integrated method for noninvasive and continuous estimation of CPO, especially for measuring peak CPO during exercise. The whole work is implemented by four main steps:

The first step is to build a model-based mathematical explicit equation between the PAT and BP by modeling approach. Since PAT is the summation pre-ejection period (PEP) and the pulse transit time (PTT), in order to interpret such a relationship, explicit expressions of both PEP and PTT with arterial blood pressure are required. PEP is mainly determined by the cardiac function and thus is discussed by modeling the left ventricular isovolumic pressure as a function of time, volume together with its after load (aortic blood pressure). PTT is involved in a wave transmission model where the pulse wave velocity (PWV) is related to the BP by including the arterial elastic property and nonlinear pressure-volume relationship. Then, mathematical equation between PAT and BP is proposed by coupling the ventricular and arterial models.

In the second step, based on the theoretical equations built in step 1, the impacts of different cardiac and arterial factors, e.g. heart contractility, preload, heart rate, peripheral resistance, arterial stiffness on the relationship between PAT and MBP are simulated and discussed. To specifically investigate the case of exercise, simulations are conducted with varying model parameters mimicking the physiological changes induced by dynamic exercise. The effect of

exercise on relationship between PAT and MBP is discussed and concluded.

In the third step, a novel CO index, namely pulse time reflection ratio (PTRR), is derived from the proposed model and expressed in terms of MBP and mean aortic reflection coefficient ($\Gamma(0)$). The CO index was further expressed in terms of PAT and inflection point area (IPA), a surrogate of $\Gamma(0)$ from the shape feature of PPG. IPA is the ratio of the area after the inflection point on the PPG waveform to the area of the whole curve and it was proposed based on the hypothesis that the diastolic part of the PPG curve was mainly composed of reflective waves and the systolic PPG wave mainly consisted of the forward wave. The impacts of different cardiac and arterial factors, e.g. heart contractility, preload, heart rate, peripheral resistance, arterial stiffness on the relationship between PTRR and CO and between IPA and $\Gamma(0)$ are simulated and discussed.

In the forth step, in order to validate the novel estimation approaches, two experiments are carried out, one on young healthy people and the other on three groups subjects, including normal elderly, cardiovascular and heart failure patients. In both experiments, supine bicycle exercise is conducted, with a three-step exercise in the first experiment and a symptom-limited maximal exercise in the second experiment. Linear prediction models are proposed to estimate MBP from PAT and estimate CO from PTRR and the corresponding estimation errors are presented and evaluated. The effects of physical characteristics of the subject, such as the age, gender and disease effect are discussed and concluded. Finally, potential source of errors and possible limitations of the proposed methods are also discussed.

1.5 Organization of this thesis

The whole thesis is composed of six chapters. The first chapter is a general introduction including the definition of cardiac power output (CPO), the significance of the peak CPO estimation, reviews on the current measurement techniques, as well as the motivation and organization of this thesis. In the second chapter, the fundamental knowledge related to this work is reviewed, including the basis of cardiovascular physiology, bio-fluid mechanics, and photoplethysmography. Chapter 3 and 4 involve the modeling and development of novel estimation techniques of BP and CO, respectively. In chapter 3, a heart-arterial coupling model is built to investigate the relationship between PAT and BP. The mathematical equation between PAT and BP is firstly proposed and the relationship between PAT and BP under different physiological conditions, especially under a mimic dynamic exercise condition, are simulated and discussed. Chapter 4 introduces the deductions of a novel CO parameter from model proposed in chapter 3. And then, similar to that in chapter 3, the relationship between this CO parameter and CO under different physiological conditions, especially under a mimic dynamic exercise condition, are simulated and discussed. Chapter 5 illustrates the experimental validation, which includes the protocol design, data analysis, results and discussions. Finally, chapter 6 summarizes the contributions of this thesis, highlights the most important conclusions, and points out the future work.

Reference

[1] K. Swedberg, et al., Guidelines for the diagnosis and treatment of chronic heart failure:

[35] L. A. Geddes, *Cardiovascular Devices and Their Application*, New York: Wiley, 1984.

[36] M. Ramsey, Blood pressure monitoring: automated oscillometric devices, J. Clin. Monit., vol. 7, pp.56-67, 1991.

[37] Available at:
www.jawon.com/.../oscillometric-method.html

[38] G. Pressman and P. Newgard, A transducer for continuous external measurement of arterial blood pressure, *IEEE Trans. on Biomed. Eng.*, vol. 10, pp. 73-81, 1961.

[39] G. M. Drezewiecki, J. Melbin, and A. Noordergraaf, Arterial tonometry: review and analysis, *J. Biomech.*, vol. 16, pp. 141-152, 1983.

[40] J. Peñáz, Photo-electric measurement of blood pressure, volume and flow in the finger, *Digest of the 10th Int. Conf. on Medical and Biolog. Eng*, pp. 104, 1973.

[41] N. T. Smith, K. H. Wesseling, and B. de Wit, Evaluation of two prototype devices producing non-invasive, pulsatile, calibrated blood pressure measurement form a finger, *J. Clin. Monit.*, vol. 1, pp. 17-29, 1985.

[42] K. H. Wesseling, B. de Wit, G. M. A. van der Hoeven, et al., Physiocal, calibrating finger vascular physiology for Finapres, *Homeostasis*, vol. 36, pp. 76–82, 1995.

[43] W. J. Kaspari and R. A. Stern, Apparatus and method for noninvasive blood pressure measurement, *U. S. Patent*, no. 5,533,511, 1996.

[44] J. W. Remington, The physiology of the aorta and major arteries, *Handb. Physiol.*, Chapter 24, pp. 799-838, 1961.

[45] W. W. Nichols and M. F. O'Rourke, *McDonald's blood flow in arteries: theoretical, experimental and clinical principles*. London: Arnold; New York: Oxford University Press, 1998.

[46] J. D. Lane, L. Greenstadt, D. Shapiro, et al., Pulse transit time and blood pressure: an intensive analysis, *Psychophysiology*, vol. 20, pp. 45-49, 1983.

[47] R. Asmar, A. Benetos, J. topouchian, et al., Assessment of arterial distensibility by automatic pulse wave velocity measurement: validation and clinical application studies, *Hypertension*, vol. 26, pp. 485-490, 1995.

[48] J. D. Pruett, J. D. Bourland and L. A. Geddes, Measurement of pulse-wave velocity using a beat-sampling technique, *Ann. Biomed. Eng*, vol. 16, pp. 341-347, 1988.

[49] P. A. Obrist, K. C. Light, J. A. McCubbin, et al., Pulse transit time: relationship to blood pressure and myocardial performance, *Psychophysiology*, vol. 16, pp. 292-301, 1979.

[50] G. V. Marie, C. R. Lo, J. Van Jones, et al., The relationship between arterial blood pressure and pulse transit time during dynamic and static exercise, *Psychophysiology*, vol. 21, pp. 521-527, 1984.

[51] A. Steptoe, Pulse wave velocity and blood pressure changes: calibration and applications, *Psychophysiology*, vol. 13, pp. 488-493, 1976.

[52] W. Zong, G. B. Moody and R. G. Mark, Effects of vasoactive drugs on the relationship between ECG-pulse wave delay time and arterial blood pressure in ICU patients, Computer in Cardiology, vol. 25, pp. 673-676, 1998.

[53] R. A. Allen, J. A. Schneider, D. M. Davidson et al., The covariation of blood pressure and pulse transit time in hypertensive patients, *Psychophysiology*, vol. 28, no. 3, pp. 301-306, 1981.

[54] L. A. Geddes, M. H. Voelz, C. F. Babbs, et al., Pulse transit time as an indicator of arterial

blood pressure, *Psychophysiology*, vol. 18, pp. 71-74, 1981.

[55] M. H. Pollak and P. A. Obrist, Aortic-radial pulse transit time and ECG Q-wave to radial pulse wave interval as indices of beat-by-beat blood pressure change, *Psychophysiology*, vol. 20, pp. 21-28, 1983.

[56] M. Wong and Y. T. Zhang, The effects of pre-ejection period on the blood pressure estimation using pulse transit time, 5th Int. Summer School and Sym. on Medical Device and Biosensors, ISSS-MDBS 2008, Hong Kong, China, pp. 254-255, 2008.

[57] J. Muehlsteff, X. L. Aubert and M. Schuett, Cuffless estimation of systolic blood pressure for short effort bicycle tests: The prominent role of the pre-ejection period, *Proc. of the 28th IEEE International Engineering in Medicine and Biology Conference, EMBC 2006*, New York, USA, pp. 5088-5092.

[58] R. Ochiai, J. Takeda, H. Hosaka, et al., The relationship between modified pulse wave transit time and cardiovascular changes in isoflurane anesthetized dogs. *J. Clin. Mon. and Computing*, vol. 15, pp. 493-501, 1999.

[59] R. A. Payne, C. N. Symeonides, D. J. Webb, et al., Pulse transit time measured from the ECG: an unreliable marker of beat-to-beat blood pressure. *J. Appl. Physiol.*, vol. 100, pp. 136-141, 2006.

[60] X. L. Aubert and J. Muehlsteff, A model-based study of the influence of vaso-active drugs on pulse delays measured from the electrocardiogram, Computers in Cardiology, vol. 34, pp. 382-386, 2007.

[61] W. Ganz, R. Donoso, H. S. Marcus, J. S. Forrester and H. J. Swan, "A new technique for measurement of cardiac output by thermodilution in man," *Am J Cardiol.*, vol. 27, pp. 392-396, Apr. 1971.

[62] A. Gawlinski, Measuring cardiac output: intermittent bolus thermodilution method, Crit. Care Nurse, vol. 20, pp. 118-120, 122-124, 2000.

[63] Available at:
http://commons.wikimedia.org/wiki/File:Pulmonary_artery_catheter_german.jpg

[64] H. U. Wessel, M. Paul, G. James, et al., Limitations of thermal dilution curves for cardiac output determinations, *Journal of Applied Physiology*, vol. 30, pp. 643–652, 1971.

[65] T. Nishikawa and S. Dohi, Errors in the measurement of cardiac output by thermodilution, Canadian Journal of Anaesthesia, vol. 40, pp. 142–153, 1993.

[66] C. M. Gomez and M. G. Palazzo, Pulmonary artery catheterization in anaesthesia and intensive care, *British Journal of Anaesthesia*, vol. 81, pp. 945–956, 1998.

[67] B. P. Cholley and M. Singer, Esophageal Doppler: noninvasive cardiac output monitor, *Echocardiography*, vol. 20, pp. 763–769, 2003.

[68] K. Knobloch, A. Lichtenberg, M. Winterhalter, et al., Non-invasive cardiac output determination by two-dimensional independent Doppler during and after cardiac surgery, Annals of Thoracic Surgery, vol. 80, pp. 1479–1483, 2005.

[69] R. Chand, Y. Mehta, N. Trehan, Cardiac output estimation with a new Doppler device after off-pump coronary artery bypass surgery, *Journal of Cardiothoracic and Vascular Anesthesia*, vol. 20, pp. 315–319, 2006.

[70] M. S. Feinberg, W. Hopkins, V. Davila-Roman, et al., Multiplane transesophageal echocardiographic Doppler imaging accurately determines cardiac output measurements in critically ill patients, *Chest*, vol. 107, pp. 769–773, 1995.

[71] A. Descorps-Declere, N. Smail, B. Vigue, et al, Transgastric, pulsed Doppler echocardiographic determination of cardiac output, *Intensive Care Medicine*, vol. 22, pp. 34–38, 1996.

[72] M. A. Sackner, The respiratory system. In: Fishman AP (ed) *Handbook of physiology*. American Physiological Society, Bethesda, pp. 233–255, 1987.

[73] J. G. Defares, Determination of $PvCO_2$ from exponential CO_2 rise during rebreathing, *J. Appl. Physiol.*, vol. 13, pp. 159–164, 1958.

[74] C. R. Collier, Determination of mixed venous CO_2 tensions by rebreathing, *J. Appl. Physiol.*, vol. 9, pp. 25–29, 1956.

[75] L. Vanhees, J. Defoor, D. Schepers, et al., Comparison of cardiac output measured by two automated methods of CO_2 rebreathing, *Med. Sci. Sports Exerc.*, vol. 32, pp. 1028–1034, 2000.

[76] P. Agostoni, G. Cattadori, A. Apostolo, et al., Noninvasive measurement of cardiac output during exercise by inert gas rebreathing technique: a new tool for heart failure evaluation, *J. Am. Coll. Cardiol.*, vol. 46, pp. 1779–1781, 2005.

[77] P. Christensen, P. Clemensen, P. K. Anderson, et al., Thermodilution versus inert gas rebreathing for estimation of effective pulmonary blood flow, *Crit. Care Med.*, vol. 28, pp. 51–56, 2000.

[78] O. Frank, Die Grundform des arteriellen Pulses. Erste Abhandlung. Mathematische Analyse. *Zeitschrift fur Biologie*, vol. 37, pp. 485–526, 1899.

[79] N. T. Kouchoukos, L. C. Sheppard and D. A. McDonald, Estimation of stroke volume in the dog by a pulse contour method, *Circulation Research*, vol. 26, pp. 611–23, 1970.

[80] K. H. Wesseling, B. deWitt, A. P. Weber, et al., A simple device for the continuous measurement of cardiac output, *Advanced Cardiovascular Physiology*, vol. 5, pp. 1–52, 1983.

[81] J. Jansen, K. Wesseling, J. Settels, et al., Continuous cardiac output monitoring by pulse contour during cardiac surgery, *European Heart Journal*, vol. 11, pp. 26–32, 1990.

[82] O. Goedje, K. Hoeke, M. Lichtwarck-Aschoff, et al., Continuous cardiac output by femoral arterial thermodilution calibrated pulse contour analysis: comparison with pulmonary arterial thermodilution, *Critical Care Medicine*, vol. 27, pp. 2407–2412, 1999.

[83] C. Zollner, M. Haller, M. Weis, et al., Beat-to-beat measurement of cardiac output by intravascular pulse contour analysis: a prospective criterion standard study in patients after cardiac surgery, *Journal of Cardiothoracic and Vascular Anesthesia*, vol. 14, pp. 125-129, 2000.

[84] G. Rodig, C. Prasser, C. Keyl, et al., Continuous cardiac output measurement: pulse contour analysis vs thermodilution technique in cardiac surgical patients, *British Journal of Anaesthesia*, vol. 82, pp. 525–530, 1999.

[85] A. Rhodes and R. Sunderland, Arterial pulse power analysis: The LiDCOTMplus System. In: Pinsky M, Payen D, eds. *Functional Haemodynamic Monitoring* Berlin: Springer-Verlag, pp. 183–192, 2005.

[86] R. A. Linton, D. M. Band and K. M. Haire, A new method of measuring cardiac output in man using lithium dilution, *British Journal of Anaesthesia*, vol. 71, pp. 262–266, 1993.

[87] R. M. Pearse, K. Ikram and J. Barry, Equipment review: an appraisal of the LiDCO plus method of measuring cardiac output, *Critical Care*, vol. 8, pp. 190–195, 2004.

[88] T. T. Hamilton, L. M. Huber and M. E. Jessen, PulseCO: a less-invasive method to monitor

cardiac output from arterial pressure after cardiac surgery, *Annals of Thoracic Surgery*, vol. 74, pp. S1408–S1412, 2002.

[89] N. W. Linton and R. A.. Linton, Estimation of changes in cardiac output from the arterial blood pressure waveform in the upper limb, *British Journal of Anaesthesia*, vol. 86, pp. 486–496, 2001.

[90] L. Heller, et al., Continuous intra-operative cardiac output determination with arterial pulse wave analysis (PulseCOTM) is valid and precise, *Anesthesia and Analgesia*, vol. 93, pp. SCA1–112, 2002.

[91] S. G. Sakka, K. Reinhart and A. Meier-Hellmann, Comparison of pulmonary artery and arterial thermodilution cardiac output in critically ill patients, vol. 25, *Intensive Care Medicine*, pp. 843–846, 1999.

[92] O. Godje, M. Peyerl, T. Seebauer et al., Reproducibility of double indicator dilution measurements of intrathoracic blood volume compartments, extravascular lung water, and liver function, *Chest*, vol. 113, pp. 1070–1077, 1998.

[93] J. Mayer, J. Boldt, T, Schollhorn, et al., Semi-invasive monitoring of cardiac output by a new device using arterial pressure waveform analysis: a comparison with intermittent pulmonary artery thermodilution in patients undergoing cardiac surgery, *British Journal of Anaesthesia*, vol. 98, pp. 176–182, 2007.

[94] K. Wesseling, J. Jansen, J. Settels, et al., Computation of aortic flow from pressure in humans using a nonlinear, three-element model, *Journal of Applied Physiology*, vol. 74, pp. 2566–2573, 1993.

[95] J. J. Remmen, W. R. Aengevaeren, F. W. Verheugt, et al., Finapres arterial pulse wave analysis with Modelflow is not a reliable non-invasive method for assessment of cardiac output, *Clinical Science (London)*, vol. 103, pp. 143–149, 2002.

[96] W. G. Kubicek, J. N. Karnegis, R. P. Patterson, et al., Development and evaluation of an impedance cardiac output system, *Aerosp. Med.*, vol. 37, pp. 1208–1212, 1966.

[97] D. P. Bernstein, A new stroke volume equation for thoracic electrical bioimpedance: theory and rationale, *Crit. Care Med.*, vol. 14, pp. 904–909, 1986.

[98] A. C. Jr Perrino, A. Lippman, C. Ariyan et al., Intraoperative cardiac output monitoring: comparison of impedance cardiography and thermodilution, *J. Cardiothorac. Vasc. Anesth.*, vol. 8, pp. 24–29, 1994.

[99] Barin E, Haryadi DG, Schookin SI, Westenskow DR, Zubenko VG, Beliaev KR, Morozov AA. Evaluation of a thoracic bioimpedance cardiac output monitor during cardiac catheterization. *Crit Care Med* 2000;28:698–70.

[100] M. Imhoff, J. H. Lehner, J. H. Lohlein, Noninvasive whole-body electrical bioimpedance cardiac output and invasive thermodilution cardiac output in high-risk surgical patients, *Crit. Care Med.*, vol. 28, 2812–2818, 2000.

[101] E. Raaijmakers, T. H. Faes, J. C. Sholten, et al., A meta-analysis of published studies concerning the validity of thoracic impedance cardiography, *Ann N Y Acad Sci*, vol. 873, pp. 121–127, 1999.

[102] R. Richard, E. Lonsdorfer-Wolf, A. Charloux, et al., Non-invasive cardiac output evaluation during a maximal progressive exercise test, using a new impedance cardiograph device, *Eur. J. Appl. Physiol.*, vol. 85, pp. 202-207, 2001.

[103] K. H. Tan, F. O. Lai and N. C. Hwang, Measurement of cardiac output using Physio

Flow® with different positions of electrode placement, *Singapore Med. J.*, vol. 47, pp. 967-970, 2006.

[104] A. Charloux, E. Lonsdorfer-Wolf, R. Richard, et al., A new impedance cardiograph device for the non-invasive evaluation of cardiac output at rest and during exercise: comparison with the "direct" Fick method, *Eur. J. Appl. Physiol.*, vol. 82, pp. 313-320, 2000.

[105] N. Tordi, L. Mourot, B. Matusheski, et al., Measurements of cardiac output during constant exercises: comparison of two non-invasive techniques, *Int. J. Sports Med.*, vol. 25, pp. 145-149, 2004.

[106] G. Natalini, A. Rosano, M. Taranto, et al., Arterial versus plethysmographic dynamic indices to test responsiveness for testing fluid administration in hypotensive patients: a clinical trial, *Anesth. Analg.*, vol. 103, pp. 1478-1484, 2006.

[107] M. Shamir, L. A. Eidelman, Y. Floman, et al., Pulse oximetry plethysmographic waveform during changes in blood volume, *Br J Anaesth.*, vol. 82, pp. 178-181, 1999.

[108] D. McCombie, H. Asada and A. Reisner, Identification of vascular dynamics and estimation of the cardiac output waveform from wearable PPG sensors, *Conf. Proc. 27th IEEE Engineering in Medicine and Biology Society (EMBS),* Shanghai, China, pp 3490-3493, 2005.

[109] A. A. Awad, R. G. Stout, M. A. Ghobashy, et al., Analysis of the ear pulse oximeter waveform, *J. Clin. Monit. Comput.*, vol. 20, pp. 175-184, 2006.

[110] L. Wang, E. Pickwell-MacPherson, Y. P. Liang, et al., Noninvasive cardiac output estimation using a novel photoplethysmogram index, *Conf. Proc. 31th IEEE Engineering in Medicine and Biology Society (EMBS)*, Hilton Minneapolis, USA, pp. 1746-1749, 2009.

Chapter 2

Basis of Cardiovascular Physiology, Bio-fluid Mechanics and Photoplethysmogram

The aim of this thesis is to address the feasibility of estimating CPO using multiple physiological signals measured from the body surface, specifically, from electrocardiogram (ECG) and photoplethysmogram (PPG). In this chapter, we provide a necessary background for this work. The CPO is the product of heart ejection (CO) and after load (MBP), and is determined by both the cardiac and arterial functions and their mechanical interaction. Thus, we start from introducing the cardiac physiology, from the heart anatomy to its electrical activities and the mechanical actions, and then we introduce the vascular physiology, including the arterial properties, bio-fluid mechanics inside the arteries and pulse wave propagation. The mechanism of ECG is interpreted in the section for electrical activities of the heart. The mechanism of PPG is introduced in the last section of this chapter.

2.1 Cardiology physiology

2.1.1 Heart anatomy

The heart is the active source of the cardiovascular system. As shown in Fig. 2.1 (a), it is located inside the left chest between the lungs behind the sternum and above the diaphragm. The wall of the heart is composed of cardiac muscle, called **myocardium**, whose structure is similar to

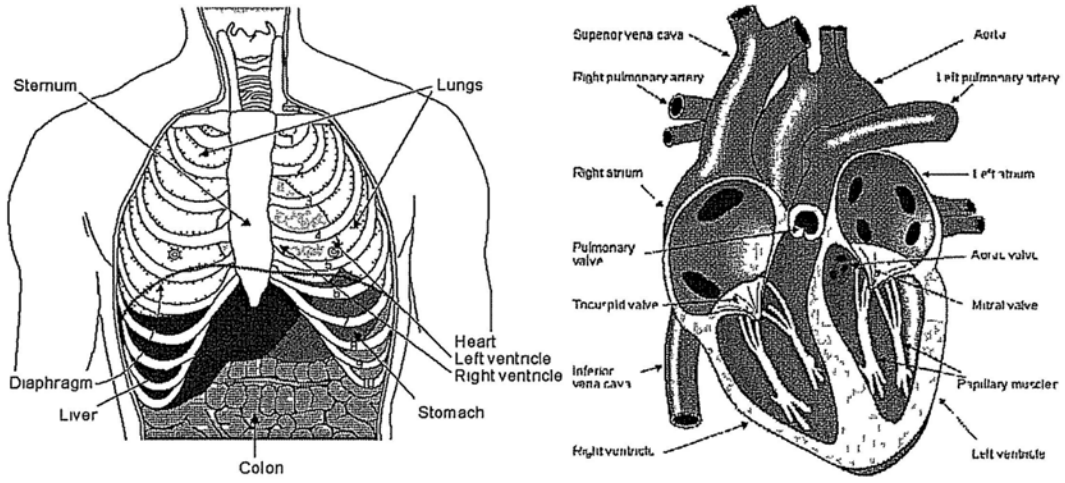

(a) **(b)**

Fig. 2.1 (a) The location of the heart in the left chest [1] and (b) the anatomy of the heart and associated vessels [1].

the skeletal muscle. The heart is separated into the left and right side by the **septum**, and there are two chambers at either side of the heart. At either side, the upper chamber connected to a vein is called the **atrium** and the lower chamber connected to an artery is called the **ventricle**. Hence, there are four chambers in the heart: left, right atria and left, right ventricles, as indicated in Fig.

2.1 (b). At the boundaries between different heart chambers, there are four valves: the **tricuspid valve** between the right atrium and ventricle, the **mitral valve** between the left atrium and ventricle, the **pulmonary valve** between the right ventricle and the pulmonary artery and the **aortic valve** between the left ventricle and aorta [1].

2.1.2 Electric activation and conduction of the heart

The heart muscle cell, namely **myocyte**, is the excitable cell which has the ability to conduct an action potential, when adequately stimulated. Fig. 2.2 shows the activation of the action potential on the membrane of a myocyte. It is worth noting that the duration of the cardiac muscle cell is about 300 ms, two orders of magnitude longer than that in either nerve cell or skeletal muscle.

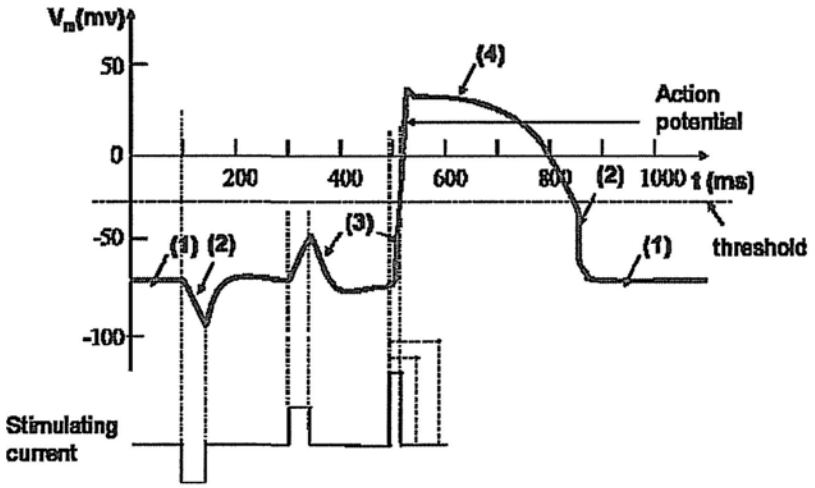

Fig. 2.2 Activation of action potential on the cardiac cell membrane. V_m: transmembrane current; t: time; (1): resting potential; (2): hyperpolarization; (3): depolarization; (4) the plateau phase; (5) repolarization.

The heart pumping is electrically activated by a group of specialized muscle cells called **sinus node (SA node)** and is at a rate of about 70 *beats* min^{-1} for normal human being at rest. Sinus node located in the right atrium at the superior vena cava and is a group of self-excitatory, pacemaker cells which automatically and periodically generate action potentials. Once an action potential is produced at SA node, its wave rapidly sweeps throughout the atria and makes the atria contract. When this electrical wave reaches the atrium-ventricle boundary, it is delayed by passing through the **atrioventricular node** (AV node) whose intrinsic frequency is 50 *beats* min^{-1}, which produces adequate time delay between the atrial and ventricular contraction. Once the AV node is activated, the activation wave propagates to the entire ventricle rapidly by a conduction system composed of bundles and makes the ventricle contract. Fig. 2.3 shows the shape and propagation time delay of action potentials triggered on heart muscles at different locations and their contributions to the shape feature of the electrocardiographic signal [2].

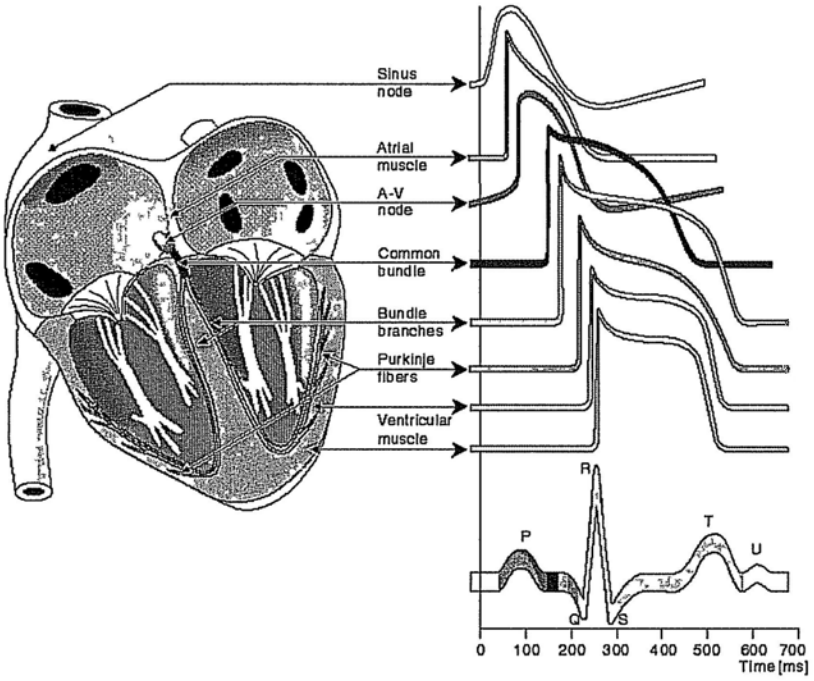

Fig. 2.3 Activation and conduction of activation in the heart and genesis of electrocardiogram [1].

2.1.3 Genesis of electrocardiogram

The sequence of action potential events from the SA node at right atrium to the distal ventricular muscle forms a heart electric vector with time-varying magnitude and direction (see Fig. 2.4 a, the arrow across the heart), which induces potential differences at different locations on the body surface, which can be recorded as **electrocardiogram (ECG)** [3]. Fig 2.4 (a) shows an instant of the heart electrical vector and the measurement of electrocardiogram using classic three-lead electrocardiogram system. In the three-lead electrocardiogram system, three electrodes were attached on the surfaces of the left arm (*LA*), right arm (*RA*) and left leg (*LL*), and lead *I, II* and *III* are defined as the potential difference between *LA* and *RA*, between *LL* and *RA*, and between *LL* and *LA*, respectively. These three basic leads make up a frontal-plane ECG of the time-varying heart vector and the characteristic points on the measured lead curves have important physiological meanings. Fig. 2.3 and Fig 2.4 (b) show a typical ECG curve measured from lead II, where *P* wave is produced by arterial depolarization, *QRS* complex is primarily produced by ventricular depolarization and *T* wave results from the ventricular re-polarization [3].

In the clinical electrocardiography, besides the three-lead system, there are the standard clinical ECG (12 leads) system and the monitoring ECG (1 or 2 lead) system. The standard clinical ECG is composed of 12 leads, 6 leads on the frontal plane and 6 leads on the transverse plane. From 12 leads system, entire information of the time-varying heart vector can be obtained and utilized to diagnosis the cardiac diseases. In the monitoring ECG system, the electrocardiographic signal is usually only utilized to extract the QRS wave, where R point indicates the starting point of a cardiac cycle and heart rate can be calculated from the R-R intervals.

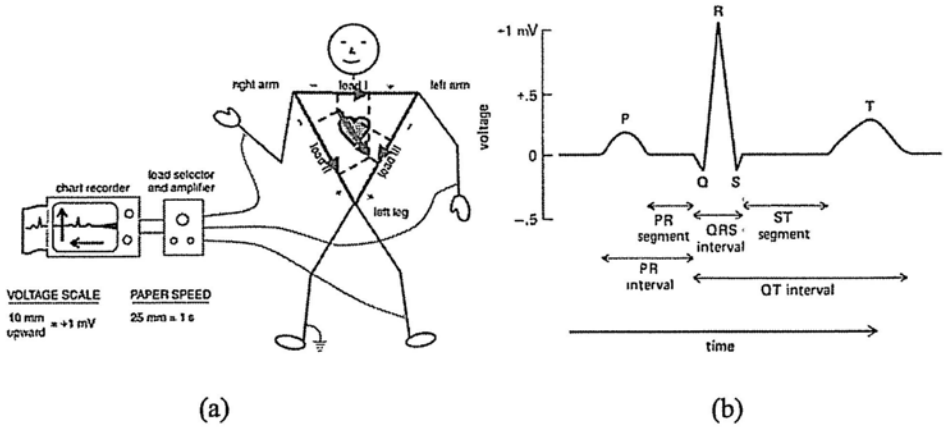

(a) (b)

Fig. 2.4 (a) Three-lead ECG measurement system [2] and (b) typical ECG wave from lead II [2].

2.1.4 Mechanical activation of the heart

Associated with the electrical activation of the heart is its mechanical activation. A whole cardiac cycle is defined as a complete sequence of contraction and relaxation of the heart. The mechanical function of the heart can be described by the pressure, volume and flow changes that occur in it during one cardiac cycle. Fig. 2.5 illustrates a whole cardiac cycle happening in the left heart by relating the pressure, volume, flow and electrocardiographic information.

The diastolic phase of left heart begins when the mitral valve opens and the blood stored in the left atrium flows into the left ventricle and the pressure inside the left ventricle increases slowly. At the end of the diastolic phase, the left atrium contract is induced by the depolarization of the heart muscle, which is shown as the *P* wave on *ECG* wave. The contraction of the left atrium further increases the volume and pressure in the left ventricle.

When the electrical activation passes through the AV node, the rapid sweeping of activation wave makes the left ventricular muscle contract, which starts the systolic phase and corresponds to the *QRS* complex on the electrocardiogram. The left ventricular pressure sharply increases as the muscle contracts and immediately closes the mitral valve. After that, it comes to the isovolumic contraction phase of the left ventricle, since the pressure in left ventricle increases while the volume keeps at a constant. When the pressure of the left ventricle exceeds the pressure at the root of aorta, the aortic valve opens and blood is ejected from the left ventricle to the systematic arterial system. Normally, the time period from the *R* wave of electrocardiogram to the aortic valve open is defined as the **pre-ejection period (PEP)**. Pre-ejection period indicates the length of left ventricular isovolumic contraction. After the aortic valve opens, left ventricular pressure keeps rising due to the shortening of the ventricular muscle, and aortic blood pressure follows the rise of ventricular pressure by the force of ejected blood until these two pressures reaches the maximum, which is the systolic blood pressure. After systolic blood pressure, the left ventricular muscle contraction begins to wane, the muscle shortening and ejection continues, but at a lower rate. The aortic blood pressure falls since the blood stored at the aortic root during the early ejection began to flow out into the peripheral.

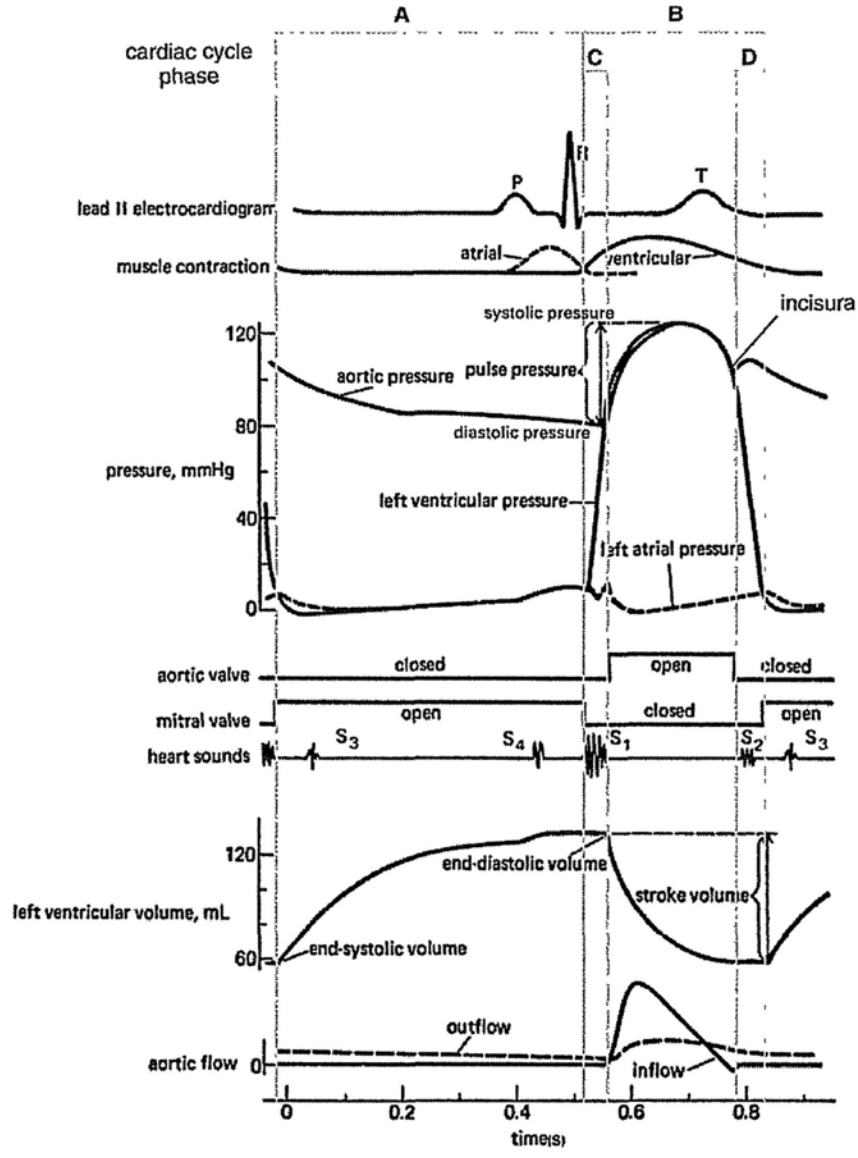

Fig. 2.5 Cardiac cycle of left heart. Cardiac cycle phases: A: diastole; B: systole; C: isovolumetric contraction; D: isovolumetric relaxation [2].

Eventually, the contraction strength of left ventricle falls to a point when the blood in the aorta begins to flow back. The aortic valve suddenly closes, which induces an incisura on the aortic blood pressure curve due to the returned flow. Hence, the time delay from the diastolic blood pressure of the previous beat to the incisura of the current beat on the aortic blood pressure curve can be used to indicate the ejection time of the left ventricle. After the aortic valve closes, the pressure in the left ventricle rapidly decreases due to the relaxation of the ventricular muscle. When the left ventricular pressure falls below the pressure in the left atrium, the mitral valve opens and a new cardiac cycle begins [2].

2.1.5 Pressure-volume and tension-length relationships in one cardiac cycle

Since wall of ventricular chamber is composed of myocardium, the ventricular pressure-volume

relationship is closely related to the tension-length relationship of the cardiac muscle. Fig. 2.6 shows the changes of pressure-volume relationship in the left ventricle (A) and the corresponding changes of tension-length relationship of the surrounding muscle (B) within a cardiac cycle.

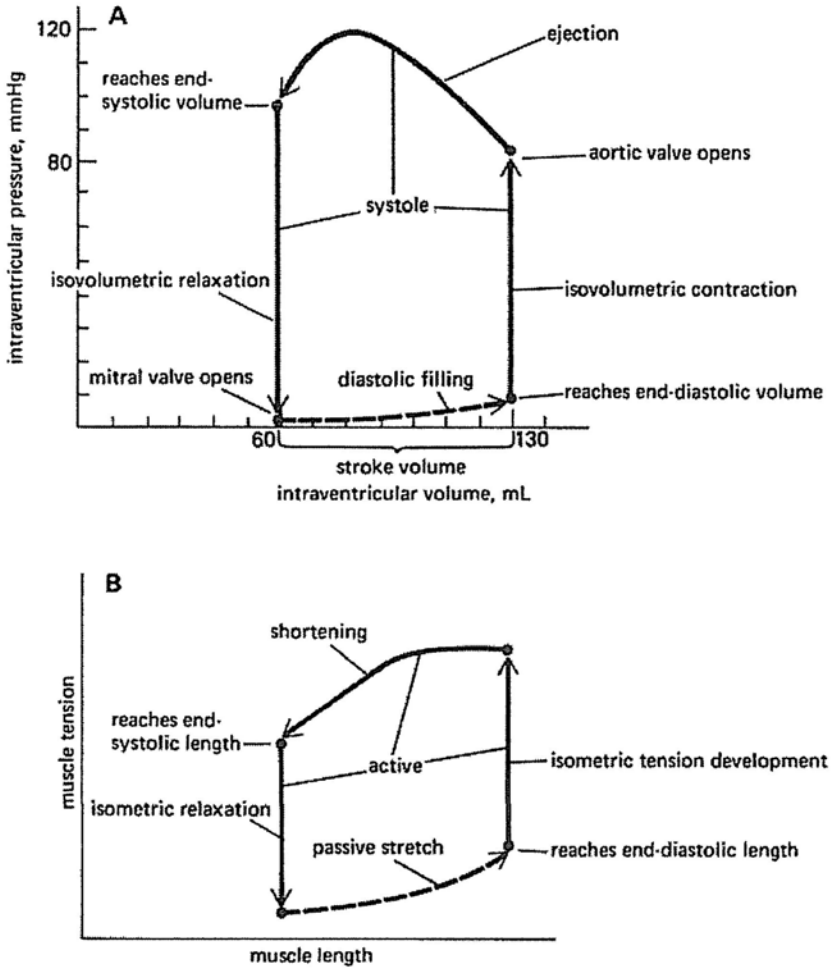

Fig. 2.6 A Ventricular pressure-volume cycle and B corresponding cardiac muscle length-tension cycle [2].

After mitral valve opens, the diastolic filling increases the left ventricular volume, which lengthens and increases the tension of the cardiac muscle and thus raises the intra-ventricular pressure. The intra-ventricular pressure at the end of the diastolic filling phase, the **end-diastolic ventricular pressure**, is the regarded as **preload** to ventricular contraction, since it determines the end-diastolic volume and the length of the cardiac muscle cell which is passively stretched.

During systolic phase, the cardiac muscle develops sharp and strong tension with a constant length during the isovolumic contraction phase. As a result, the intra-ventricular pressure increases rapidly until the aortic valve opens. The aortic blood pressure is regarded as the ventricular **after load** since it sets a threshold for the increase of cardiac muscle tension before it is shortened in the ejection phase.

During the whole ejection phase, the cardiac muscle keeps shortening, which reduces the ventricular volume and ejects the blood out of the ventricle. The amount of blood ejected during the systolic ejection, the **stroke volume**, is determined both by the maximum length of cardiac muscle shortening and the after load of ventricular ejection, the aortic blood pressure. The tension of cardiac muscle however keeps at the relative high value at the early ejection, which increases the ventricular and aortic pressure to a maximum point, the systolic pressure, and then decrease, which decreases the ventricular and aortic pressure. Once shortening ceases and the output valve closes, the cardiac muscle cells relax isometrically. Ventricular wall tension and intraventricular pressure fall in unison during isovolumetric relaxation [2].

2.2 Arterial function

2.2.1 Types of artery and arterial elastic property

The main function of artery system is to distribute the blood ejected by the heart to the tissue throughout the body. The structure of arterial wall is anisotropic, multi-storey and nonlinearly elastic, which makes its material properties highly nonlinear [4]. In general, the overall mechanical properties of the arterial wall are determined by how different compositions of collagen, elastin and protein are linked. The general rule is that when the elastin ratio is higher than the collagen ratio, the elastic modulus decreases and distensibility increases, and vice versa. The elasticity and resistance vary dynamically from big arteries, e.g. aorta, to small arteries and arterioles. The big arteries are mainly elastic, with pulsatile blood pressure and flow inside, while the small arteries are muscular arteries which mainly determine the peripheral resistance of the arterial system. The function of the large, elastic arteries is to carry blood from central to peripheral, while the muscular arteries control the distribution of blood to regions of the body by muscular contraction and dilation [4].

The elastic properties of the arterial wall are often characterized by a parameter called **compliance** (C), which describes how much the volume changes (ΔV) can be produced by a given change in transmural pressure

$$C = \frac{\Delta V}{\Delta P}. \tag{2.1}$$

Transmural pressure P is the difference between internal and external pressures, and is mainly influenced by the changes of internal pressure, since the external pressure is approximately a constant under normal conditions.

Another parameter to characterize the elastic properties of the artery is named the **distensibility** (D), and it is defined as

$$D = \frac{\Delta V}{V \times \Delta P}, \tag{2.2}$$

where V is the diastolic volume at the end of diastole. Compared with compliance, distensibility accounts for the relative changes of blood volume per given change of pressure.

The elastic characteristics of the artery can also be evaluated by elastic modulus, which gives the relationship between stress and strain. The elastic modulus in longitudinal direction is called

Young's module E, which is defined as

$$E = \frac{\Delta P}{\frac{\Delta d}{d}}\ , \tag{2.3}$$

where d is the mean arterial diameter during the cardiac cycle and Δd is the maximal change in arterial diameter during the cardiac cycle. Thus E is inversely related to compliance, which is the ratio of ΔV to ΔP.

2.2.2 Fluid mechanics

The arterial blood pressure and flow waves are highly pulsatile, and their relationship was derived by Womersley in 1955 [5, 6] from the equation of motion of a liquid as

$$\frac{\partial^2 \varpi}{\partial r^2} + \frac{1}{r}\frac{\partial \varpi}{\partial r} - \frac{1}{\nu}\frac{\partial \varpi}{\partial t} = -\frac{1}{\mu}\frac{\partial P}{\partial z}, \tag{2.4}$$

where P is the pusatile blood pressure, ϖ is the velocity of blood, z is the axial distance along the tube, $\frac{\partial P}{\partial z}$ is the pressure gradient with axial distance, r is the radial distance from axis, μ is the blood viscosity.

If the pressure difference is taken over a distance L as the pressure gradient and represent it by a simple harmonic motion, then

$$\frac{P_1 - P_2}{L} = \frac{\partial P}{\partial z} = A^* e^{i\omega t}, \tag{2.5}$$

and the solution for the velocity, ϖ, of the blood flow at a distance (y=r/R) from the axis is

$$\varpi = \frac{A^*}{i\omega\rho}\left(1 - \frac{J_0\left(\alpha y i^{3/2}\right)}{J_0\left(\alpha i^{3/2}\right)}\right)e^{i\omega t}, \tag{2.6}$$

since

$$\alpha^2 = \frac{R^2\omega\rho}{\mu} = \frac{R^2\omega}{\nu}. \tag{2.7}$$

To obtain the volume flow Q (unit, cm^3/s) it is necessary to integrate the velocity across the lumen of the tube:

$$Q = \frac{\pi R^2 A^*}{i\omega\rho}\left(1 - \frac{2J_1\left(\alpha i^{3/2}\right)}{\alpha i^{3/2} J_0\left(\alpha i^{3/2}\right)}\right)e^{i\omega t}, \tag{2.8}$$

where J_0 and J_1 are Bessel functions of order zero and one respectively. The expression was termed $\left[1 - F_{10}\right]$ by Womersley. The physical interpretation of the equation is, however, easier if the function $\left[1 - F_{10}\right]$ is expressed in modulus ($M_{10}^{'}$) and phase (ε_{10}) form, so that

$$\left[1 - F_{10}\right] = M_{10}^{'} e^{i\varepsilon_{10}}, \tag{2.9}$$

thus

$$Q = \frac{\pi R^4 A^*}{i\mu} \frac{M_{10}^{'}}{\alpha^2} e^{i\varepsilon_{10}} e^{i\omega t}, \tag{2.10}$$

and the corresponding term for the average velocity across the tube is

$$\overline{V} = \frac{Q}{\pi R^2} = \frac{A^* R^2}{i\mu} \frac{M_{10}^{'}}{\alpha^2} e^{i\varepsilon_{10}} e^{i\omega t}. \tag{2.11}$$

Analog to the terms in electricity, an alternating pressure gradient is treated as analogous with an alternating voltage and the alternating flow is analog to the current. It was suggested by McDonald in 1955 that the term 'impedance' should be used when considering 'dynamic' pulsatile flow and pressure in arteries, and that the term 'resistance' should be confined to the 'static', or mean flow, terms [7]. From Eq.(2.10), the longitudinal impedance, defined as the impedance per unit length L of the tube and is thus given by

$$\begin{aligned} Z_L &= \frac{A^* e^{i\omega t}}{\overline{V}} = \frac{i\mu}{R^2} \frac{\alpha^2}{M_{10}^{'}} e^{-i\varepsilon_{10}} \\ &= \frac{\mu\alpha^2}{R^2 M_{10}^{'}} \sin\varepsilon_{10} + \frac{i\mu\alpha^2}{R^2 M_{10}^{'}} \cos\varepsilon_{10} \end{aligned} \tag{2.12}$$

The electrical complex impedance analogous to flow in a rigid tube is written as

$$Z = R + i\omega L, \tag{2.13}$$

where R is resistance and L is the inductance; hence the real part of Eq.(2.12) may be called the resistance and the imaginary part may be called the inductive term of reactance. Thus

$$\mathrm{Re}\,sis\tan ce = \frac{\mu\alpha^2}{R^2 M_{10}^{'}} \sin\varepsilon_{10} \tag{2.14}$$

and

$$\mathrm{Re}\,ac\tan ce = \frac{\mu\alpha^2}{R^2 M_{10}^{'}} \cos\varepsilon_{10}. \tag{2.15}$$

Expanding the term α^2 ($= R^2\omega\rho/\mu$), it yields

$$\mathrm{Re}\,sis\tan ce = \frac{\omega\rho}{M_{10}^{'}} \sin\varepsilon_{10} \tag{2.16}$$

and

$$\mathrm{Re}\,ac\tan ce = \frac{\omega\rho}{M_{10}^{'}} \cos\varepsilon_{10}, \tag{2.17}$$

so that

$$Induc\tan ce = \frac{\rho}{M_{10}^{'}} \cos\varepsilon_{10}. \tag{2.18}$$

When considering a conducting system along which the wave of oscillatory flow is propagated, there is the relationship between the characteristic impedance Z_0 and the velocity of propagation c

(apparent pulse wave velocity, see section 2.2.4) as

$$Z_0 = \frac{cZ_L}{i\omega}; \tag{2.19}$$

so that from Eq.(2.12), after expanding α^2, there is

$$Z_0 = \frac{\rho c}{M_{10}'} e^{-i\varepsilon_{10}}. \tag{2.20}$$

The characteristic impedance is defined as the ratio of oscillatory pressure to flow at the input of a tube in which no reflected waves return to the origin. The term 'input impedance' is used to express the ratio of oscillatory pressure to flow at the input to any region of the circulation and is modified by reflected waves. Arterial input impedance is useful description of the properties of the vasculature [7].

2.2.3 Pulse wave propagation

When blood is pumped from the heart to the artery, it expands the elastic artery and produces a pressure pulse wave. This pressure pulse wave transmitted along the big arteries at a certain speed, which is called the **pulse wave velocity** (PWV). The pulse wave velocity can be characterized by the **pulse transit time (PTT)**, which is the time used for a blood pressure pulse to travel through an artery segment, as illustrated in Fig. 2.7. The transmitting, forward wave on an artery reflects when there is impedance mismatching in the arterial network, e.g. bifurcations, tapering of the artery etc [8]. Theoretically speaking, wave reflection happens at any point of impedance mismatching, while experiment observations have shown that major reflections happen at the arterioles level where the arterial resistance rapidly rises as the sharp reduction of arterial radius.

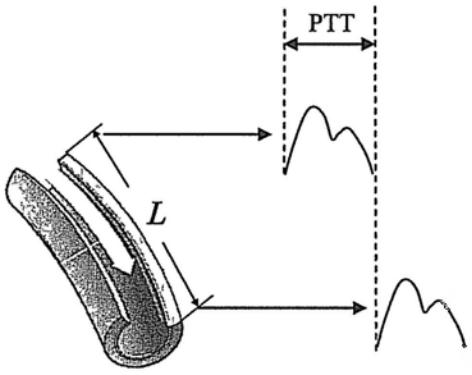

Fig. 2.7 Pulse transit time on an arterial segment [2].

PWV depends on the physical properties of the arterial vessel, such as its stiffness (or elasticity) and geometric dimensions, such as vessel size as well as blood density [9]. Since fluid is contained in a system of elastic conduits, energy propagation occurs predominantly along the arterial wall and not through the incompressible blood [10]. The material properties of the arterial wall, its thickness, and the lumen diameter thus become the major determinants of the pulse wave velocity. Moens [11] determined empirically and Korteweg [12] derived theoretically an expression (known as the Moens-Kortweg equation) which describes the relationship between the velocity of a

pressure pulse and the elastic modulus of a thin-walled elastic tube with ideal incompressible and inviscous fluid

$$c = \sqrt{\frac{Eh}{2r\rho}}, \tag{2.21}$$

where c is the pulse wave velocity, h is the wall thickness, r is the lumen radius, ρ is the density of the fluid within the lumen, and E is Young's modulus of the tube material. In 1922, Bramwell and Hill derived an expression of PWV which throws much light upon the mechanics of the circulation (known as Bramwell-Hill equation) [13]

$$c = \sqrt{\frac{V}{\rho \frac{dV}{dP}}} = \sqrt{\frac{V}{\rho C}}. \tag{2.22}$$

In the Bramwell-Hill equation, if the pressure-volume relationship of a blood vessel is known, *PWV*, as well as its reciprocal *PTT*, can be expressed as a function of transmural pressure, and a varying parameter within an cardiac cycle.

2.2.4 Clinical significance of pulse wave velocity

From Eq.(2.4) and (2.5), it is clear that PWV is a good indicator of the elasticity and compliance of the artery, generally, the arterial stiffness. Further, PWV is superior to other indicators of arterial stiffness like elasticity and compliance due to the ease and noninvasiveness of its measurement procedures where PWV is calculated from the surface distance and pulse transit time between two blood pressure waves on the same arterial segment [14, 15]. The golden standard arterial stiffness index is the **carotid-femoral PWV (*cfPWV*)**, defined as the mean pulse wave velocity from the carotid to femoral artery [14]. In clinic, various disease processes are known to change the stiffness of the arteries (*cfPWV*). There have been many investigations which relate the effects of aging and vascular diseases to vessel pathology and distensibility based on the studies of PWV [16-19]. For instance, atherosclerosis causes the arterial wall to become thicker and harder, and narrows the arterial lumen. The resultant decreasing in arterial distensibility hence causes PWV to increase [20]. PWV is now well accepted as a useful index of arterial stiffness, which can be measured both accurately and reproducibly [21]. In recent years, a number of papers have been published on the diagnosis of cardiovascular diseases and mortality risk prediction using PWV [22-25]. One potential problem is that PWV may be influenced by the transmural blood pressure and the changes of vascular tone induced by neural activities, which may bring errors to the arterial stiffness measurement using PWV [26].

2.2.5 Measurement of pulse wave velocity

Any pulse wave velocity measured from experiment in fact represents the velocity of the wave relative to the blood, plus the velocity of the blood in the artery. Since the pressure wave travels at a rate more than 10 times of that of flow, the measured PWV can be regarded as an acceptable approximation of the true transmitting rate of pressure wave. The method that has been most commonly used in measuring PWV is to measure the pulse transit time between the points at the same position on two blood pressure waves on the same arterial segment (see A and A' in Fig. 2.7).

However, it is found that in the frequency domain, the phase delay between two sequent blood pressure waves varies as frequency increases [27, 28]. This indicates that the pulse wave velocity may change from point to point on the blood pressure waveform. This is mainly due to the wave reflections in the arterial network. This frequency-dependent pulse wave velocity is called the apparent PWV. The appearance of apparent PWV implies that the experimentally measured PWV from PTT may vary with the value of the theoretically derived PWV represented by Eq.(2.4) and Eq.(2.5). Later studies revealed that the averaged apparent PWV at high frequencies approximately equals to the theoretically derived PWV and such a high-frequency apparent PWV can be experimentally measured from the foot, or upstroke, of the two sequential blood pressure waves over a distance on an artery, since the upstroke point is the steep rise of wave front at the early systole and is assumed to be not influenced by the reflected waves [29]. For superficial arteries such as the carotid artery and femoral artery, passage of the pressure wave can be picked up by externally applied pressure sensors.

The clinical standard measurement of *cfPWV* is based on aforementioned foot-to-foot pulse transit time method. By acquiring two blood pressure pulses, one at the carotid artery and the other at the femoral artery, through sensors on the body surface, *cfPWV* is estimated from dividing the surface distance between two measurement sites (L) by the carotid-femoral pulse transit time, which is the time delay between the upstrokes of carotid and femoral blood pressure pulses [14]. An alternative noninvasive method to obtain the pulse transit time is through an easy optical means called photoplethysmography (PPG), invented by Hertzman in 1930s [30, 31]. The application of PPG on PWV measurement can date back to 1971 [32] and later on the work by Weinman *et al* [33] who claimed an overall superiority of optical techniques relative to mechanical techniques. Pulse wave velocity measurement by PPG was suggested as a convenient method for routine clinical use. In a recent validity study, pulse wave velocity measured by a photoplethysmographic method was found to be comparable to those obtained from invasive intra-arterial pressure wave [34].

2.3 Photoplethysmography

In 1937, Hertzman and Spielman [31] first produced the term "photoplethysmograph" which is the combination of "photo" meaning the optical means, "plethysmos" meaning increase, and "graph" meaning write, to define a new optical signal acquired from a device that "takes advantage of the fact that the absorption of light by a transilluminated tissue varies with its blood contents". This is theoretically related to the Lambert-Beer law (Fig. 2.8), which relates light absorption to optical density. Nowadays, the PPG technology has been used in a wide range of commercially available medical devices for measuring oxygen saturation [35], blood pressure and cardiac output ('Finapres', mentioned in Chapter 1) [36], assessing autonomic function [37] and also detecting peripheral vascular disease [38]. Besides, there are hot research topics which utilize the PPG pulse wave analysis to reveal important cardiovascular information, such as the respiratory rate [39], the presence and stages of the peripheral arterial disease [40], arterial stiffness [14], etc.

There are mainly two measuring arrangements for photoplethysmogram, the reflection and transmission mode. Fig. 2.8 (a) shows an early photoplethysmographic device for measuring light transmission through the finger. The working principle is as follows: a small light source (B in Fig. 2.8(a)) and a photodetector (S in Fig. 2.8(a)) are applied to the skin. The emitted light is

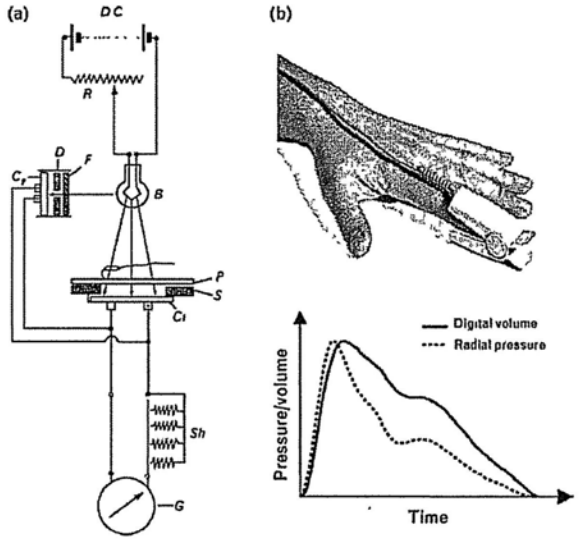

Fig. 2.8 (a) An early photoplethysmograph device for measuring light transmission through the finger [31] and (b) a modern photoplethysmograph incorporating a light-emitting diode and sensor within a finger clip. A typical waveform (solid line) is shown, together with a radial pressure waveform (obtained using a tonometer) in the same individual [41].

scattered in the tissue and partly absorbed. Part of the scattered light emerges again through the skin and is detected by the photo detector. Photo detector can be placed either beside or opposite the light source. The light transmission mode shown in Fig. 2.8 (a) is only possible for body terminal locations, such as the earlobe and fingers. A more widespread arrangement is the reflection mode where the light emitter and detector are placed side by side, this design hence can be used at any position of the body. The principles of reflection and transmission modes are very similar [42].

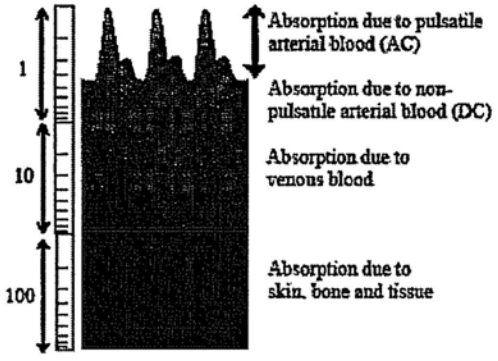

Fig. 2.9 Breakdown of the components of the detected photoplethysmographic signal [43].

As shown in Fig. 2.9, the PPG signal is basically composed of two parts with distinct physiological meanings, a steady component (DC), which is related to the changes of blood volume in the non-pulsatile component of the tissue and often referred to as the total "blood volume", and a pulsatile component (AC) at the same frequency as the heart rate, which is related

to changing arterial blood volume and often referred to as the "pulse volume" [44]. AC component is very small compared with its DC counterpart. Their amplitudes depend on the skin structure, blood flow in the vascular bed and the skin temperatures [45]. Under normal conditions, the blood volume changes in the capillary bed and veins are neglectable, since the blood volume changes has been greatly damped by the high-resistance and low-compliance arterioles and capillary bed. In addition, simultaneous measurement of the AC and the DC components provides more information on the vascular changes of the skin than that can be obtained by either component separately [46].

The physiological meaning of the pulstile PPG signal obtained by the transmission mode can be easily interpreted by the Lambert-Beer law, that is, the changes of the PPG amplitude is caused by the variations in absorption. Since the light absorption of the blood is higher than its surrounding tissue, when there is a light passing through, the light absorption changes significantly with the blood volume changes inside the artery and hence in anti-phase with the transmitted signal detected by the photo detector.

The physiological relevance of the reflection mode PPG signal, however, is more complicated due to the reflection induced by erythrocytes. Studies have shown that the reflective PPG measured from a rigid tube with pulsatile blood flow is proportional to the flow rate [47]. Besides, when it comes to the artery, the movement of the arterial wall can also play a role. In an experiment conducted by Weinman *et al* [48], the transducers were embedded in agar blocks over a single carotid artery and the reflective PPGs were obtained by placing the transducers at different measurement locations. The authors observed that sometimes the systolic rise of blood volume inside the artery caused rise in the reflective PPG [48]. This may be due to the enhanced reflection induced by increasing flow rate and arterial wall movement. However, the observations varied with different arterial beds where the measurements were carried out. Experimental results conducted on peripheral skin areas such as finger and ear lobe suggested that the reflective PPG changed in phase with the transmission PPG, which is inverse to the blood volume fluctuations [49]. The main reason for this phenomenon is that the erythrocytes have reflecting as well as absorbing properties. A relative predominance from one to the other may be influenced by the optical density of the embedding tissue. The blood volume rise will cause an increase of reflective PPG due to the orienting erythrocytes and the expanding of arterial wall. However, this increase will become insignificant if the reflections from the embedding tissue are strong. Therefore, the pulsation of the reflection PPG is dominated by the absorbing properties of erythrocytes, which is in anti-phase with blood volume variations. As a result, the optical characteristics of the surrounding tissue plays an essential role in the predominance of absorption or reflection influence of the erythrocyte on reflective PPG, and thus determines the main physiological interpretation of this signal, i.e. in phase or anti-phase with blood volume pulsations. As mentioned before, in peripheral measurement sites as fingers and ear lobes, reflective PPG reveals similar information as the transmission PPG.

2.4 Summary

In this chapter, fundamental knowledge of cardiovascular physiology, bio-fluid mechanics and

photoplethymogram is described. It provides a necessary background on the cardiac and vascular functions which influences cardiac power output and the physiological mechanisms underline the electrocardiogram and photoplethysmogram measured on the body surface. The knowledge introduced in this chapter provides basis for further investigations and analysis on building a model based-approach for the estimation of cardiac power output using physiological signals measured on the body surface in chapter 3 and 4..

Reference

[1] Bioelectromagnetism, Available at: http://www.bem.fi/book/00/tx.htm

[2] David E. Mohrman and Lois Jane Heller, *Cardiovascular Physiology*, 6th ed: McGraw-Hill Companies, Inc., 2006. Available at: http://www.accessmedicine.com/resourceTOC.aspx?resourceID=64

[3] J. G. Webster, J. W. C. Jr., M. R. Neuman, et al., *Medical Instrumentation: application and design*, 3rd ed., New York: Wiley, 1998, pp. 317-320.

[4] W. W. Nichols and M. F. O'Rourke, McDonald's blood flow in arteries: theoretical, experimental and clinical principles, 5th ed., London: Hodder Arnold, 2005, pp. 11-67.

[5] J. R. Womersley, Oscillatory flow in arteries: effect of radial variation in viscosity on rate of flow, *Journal of Physiology*, vol. 127, pp. 38P-39P, 1955.

[6] J. R. Womersley, Method for the calculation of velocity, rate of flow and viscous drag in arteries when the pressure gradient is known, *Journal of Physiology*, vol. 127, pp. 553-563, 1955.

[7] D. A. McDonald, The relation of the pulsatile pressure to flow in arteries, Journal of Physiology, vol. 127, pp. 533-552, 1955.

[8] D. B. Doublin and A. A Rovick, Influence of vascular smooth muscle on contractile mechanics and elasticity of arteries, *American Journal of Physiology*, vol. 217, pp. 1644-1651, 1969.

[9] R. Carola, J. P. Harley and C. R Noback, *Human Anatomy & Physiology*, McGraw-Hill publishing company, USA, 1990.

[10] A. P. Avolio, *Pulse wave velocity and hypertension*, in M. Safar ed., *Arterial and Venous Systems in Essential Hypertension*, Boston, Mass: Martinus-Nijhoff, pp. 133-152, 1991.

[11] A. I. Moens, *Die Pulscurve* (E. J. Brill, Leiden), pp. 87-95, 1878.

[12] D. J. Korteweg, Uber die Fortpflanzungsgeschwindigkeit des Schalles in elastischen Rohren, *Ann. Phys. Chem.*, vol. 5, pp. 525-542, 1878.

[13] J. C. Bramwell and A. V. Hill, The velocity of the pulse wave in man. *Proceedings of the Society for Experimental Biology and Medicine*, vol. 93, pp. 298-306, 1922.

[14] S. Laurent, J. Cockcroft, L. Van Bortel, et al., Expert consensus document on arterial stiffness: methodological issues and clinical applications, *Eur. Heart J.*, vol. 27, pp. 2588-2605, 2006.

[15] T. Weber, M. Ammer, M. Rammer, et al., Noninvasive determination of carotid-femoral pulse wave velocity depends critically on assessment of travel distance: a comparison with invasive measurement, *J. Hypertens.*, vol. 27, pp. 1624-1630, 2009.

[16] M. F. O'Rourke, W. W. Nichols, M. E. Safar, Pulse waveform analysis and arterial stiffness: realism can replace evangelism and scepticism. *J Hypertens*, vol. 22, pp. 1633–1634, 2004.

[17] S. Laurent, P. Boutouyrie, P. Lacolley, Structural and genetic bases of arterial stiffness, *Hypertension*, vol. 45, pp. 1050–1055, 2005.

[18] P. Boutouyrie, C. Bussy, D. Hayoz, et al., Local pulse pressure and regression of arterial wall hypertrophy during long term antihypertensive treatment, *Circulation*, vol. 101, pp. 2601–2606, 2000.

[19] M. T. Schram, R. M. Henry, R. A. van Dijk, et al., Increased central artery stiffness in impaired glucose metabolism and type 2 diabetes: the Hoorn Study, *Hypertension*, vol. 43, pp. 176–181, 2004.

[20] R. Ross, Atherosclerosis an inflammatory disease, *New England Journal of Medicine*, vol. 340, pp. 115-126, 1999.

[21] E. D. Lehmann, Non-invasive measurements of aortic stiffness: methodological considerations, *Path. Biol.*, vol. 47, pp. 716-730, 1999.

[22] J. Blacher, R. Asmar, S.. Djane, et al., Aortic pulse wave as a marker of cardiovascular risk in hypertensive patients, *Hypertension*, vol. 33, pp. 1111-1117, 1999.

[23] S. Laurent, P. Boutouyrie, R. Asmar, et al., Aortic stiffness is an independent predictor of all-cause and cardiovascular mortality in hypertensive patients, *Hypertension*, vol. 37, pp. 1236-1240, 2001.

[24] N. M. van Popele, D. E. Grobbee, M. L. Bots, et al., Association between arterial stiffness and atherosclerosis, *Stroke*, vol. 32, pp. 454-457, 2001.

[25] J. Mclaughlin, M. McNeill, B. Braun, et al., Piezoelectric sensor determination of arterial pulse wave velocity, Physiol. Meas., vol. 24, pp. 693-702, 2003.

[26] L. Wang, C. C. Y. Poon and Y. T. Zhang, "The Age Effects on the Waveform of Photoplethysmogram at a Specific Range of Arterial Blood Pressure," in Proc. of the 6th International School and Symposium on Medical Devices and Biosensors (MDBS2009), in conjunction with the 4th International School and Symposium on Biomedical and Health Engineering (BHE2009), Shenzhen, China, Dec. 26 - 28,2009.

[27] M. G. Taylor, An approach to the analysis of the arterial pulse wave: I. Oscillations in an attenuating line. *Physics in Medicine and Biology*, vol. 1, pp. 258-269.

[28] M. G. Taylor, An approach to the analysis of the arterial pulse wave: II. Fluid oscillations in an elastic tube. *Physics in Medicine and Biology*, vol. 1, pp. 321-329.

[29] D. A. McDonald, Regional pulse-wave velocity in the arterial tree, *Journal of Applied Physiology*, vol. 24, pp. 73-78, 1968.

[30] A. B. Hertzman, Photoelectric plethysmography of the finger and toes in man, *Proceedings of the Society of Experimental Biology and Medicine*, vol. 37, pp. 529-534, 1937.

[31] A. B. Hertzman and C. R. Spielman, Observations on the finger volume pulse recorded photoelectrically, *Am. J. Physiol.*, vol. 119, pp. 334-335, 1937.

[32] J. Weinman and D. Sapoznikov, Equipment for continuous measurements of pulse wave velocity, *Med. and Biol. Eng.*, vol. 9, pp. 125-138, 1971.

[33] J. Weinman, A. Hayat and G. Raviv, Reflection photoplethysmography of arterial blood volume pulses, *Med. Biol. Eng. Comput.*, vol. 15, pp. 22-31, 1977.

[34] S. Loukogeorgakis, R. Dawson, N. Phillips, et al., Validation of a device to measure arterial pulse wave velocity by a photoplethysmographic method, *Physiological Measurement*, vol. 23, pp. 581-596, 2002.

[35] I. Yoshiya, Y. Shimada and K. Tanaka, Spectrophotometric monitoring of arterial oxygen

saturation in the fingertip, *Med. Biol. Eng. Comput.*, vol. 18, pp. 27–32, 1980.

[36] K. H. Wesseling, B. de Wit, G. M. A. van der Hoeven, et al., Physiocal, calibrating finger vascular physiology for Finapres, *Homeostasis*, vol. 36, pp. 76–82, 1995.

[37] W. B. Murray and P. A. Foster, The peripheral pulse wave: information overlooked, *J. Clin. Mon.*, vol. 12, pp. 365–377, 1996.

[38] C. Laurent, B. Jonsson, M. Vegfors, et al., Non-invasive measurement of systolic blood pressure on the arm utilising photoplethysmography: development of the methodology, *Med. Biol. Eng. Comput*, vol. 43, pp. 131–135, 2005.

[39] L. Nilsson, A. Johansson and S. Kalman, Monitoring of respiratory rate in postoperative care using a new photoplethysmographic technique, *J. Clin. Monit. Comput.*, vol. 16, pp. 309–315, 2000.

[40] A. Gunarathne, J. V. Patel, E. A. Hughes, et al., Measurement of stiffness index by digital volume pulse analysis technique: clinical utility in cardiovascular disease risk stratification, *Am. J. Hyperens.*, vol. 21, pp. 866-872, 2008.

[41] R. P. Kelly, C. Hayward, J. Ganis, et al., Noninvasive registration of the arterial pressure pulsewave for measuring high-fidelity applanation tonometry, *J Vasc. Med. Biol.*, vol. 1, pp. 142–149, 1989.

[42] Y. Mendelson and V. D. Ochs, Noninvasive pulse oximetry utilizing skin reflectance photoplethysmography, *IEEE Trans. on Biomedical Engineering*, vol. 35, pp. 798-805, 1988.

[43] V. P. Crabtree and P. R. Smith, Physiological models of the human vasculature and photoplethysmography, *1st Electronic Systems and Control Division Research Miniconference*, pp. 57-60, Leicestershire, UK, 25th September 2003.

[44] L. S. D'Agrosa and A. B. Hertzman, Opacity pulse of individual minute arteries, *J. Applied Physiology*, vol. 23, pp. 613-620, 1967.

[45] A. A. R. Kamal, J. B. Harness, G. Irving, et al., Skin photoplethysmography-a review, *Computer methods and Programs in Biomedicine*, vol. 28, pp. 257-269, 1989.

[46] A. B. Hertzman and J. B. Dillon, Reaction of large and small arteries in man to vasoconstrictor stimuli, *Am. J. Physiol.*, vol. 130, pp. 56-68, 1942.

[47] K. R. Visser, R. Lamberts, H. H. M. Korsten, et al., Observations on blood flow related electrical impedance changes in rigid tubes, *Prugers. Arch.*, vol. 366, pp. 289-291, 1976.

[48] J. Weinman, A. Hayat and G. Ravi, Reflection photoplethysmography of arterial blood volume pulses, *Med. Biol. Eng. Comput.*, vol. 15, pp. 22-31, 1977.

[49] J. A. Nijboer, J. C. Dorlas and J. F. Mahieu, Photoelectric plethysmography-some fundamental aspects of the reflection and transmission method, *Clin. Phys. Physiol. Meas.*, vol. 2, no. 3, pp. 205-215, 1981.

Chapter 3

A Model-based Study on the Relationship between Pulse Arrival Time and Arterial Blood Pressure

In this chapter, models of left ventricle and systematic arterial system are developed to deduce the mathematical equation which relates pulse arrival time to arterial blood pressure. Ventricular-arterial coupling based on the modified models is then utilized to simulate the relationship between pulse arrival time and arterial blood pressure when changing different cardiac and arterial functions, e.g. heart rate, contractility, peripheral resistance etc. This is then followed by a further simulation to mimic the dynamic exercise condition by simultaneously changing related model parameters. In addition, the relationship between pulse arrival time and arterial blood pressure under exercise condition is revealed and concluded. Main investigations include: 1) an explicit equation which relates pre-ejection period to arterial diastolic blood pressure is deduced based on an recently proposed pressure source ventricular model [1-4]; 2) a nonlinear pressure-volume relationship [5] is introduced into the classic linear asymmetric T-Tube model [6] [7] so as to make characteristic impedance, tube compliance and pulse transit time changing variables with arterial blood pressure in the T-tube model; 3) the theoretical equation which relates pulse arrival time to arterial blood pressure is built based on 1) and 2), and the relationship between pulse arrival time and systolic, diastolic and mean blood pressure is simulated, discussed and concluded under variant cardiovascular conditions, especially under a mimic condition for dynamic exercise. Relative contributions of pre-ejection period and pulse transit time to the relationship between arterial blood pressure and pulse arrival time are discussed and concluded.

3.1 Ventricular modeling and the relationship between pre-ejection period and diastolic blood pressure

This section models the underlying mechanism that determines the relationship between pre-ejection period and aortic blood pressure. The pre-ejection period is the time length of ventricular isovolumic contraction, defined as the time delay from the start of ventricular contraction and aortic valve opening. The open/close status of aortic valve is controlled by the interaction of forces on its both sides, i.e. the left ventricular pressure and the aortic blood pressure. The time length of pre-ejection period hence is determined by how fast the left ventricular pressure rises during the isovolumic contraction meanwhile how fast the aortic blood pressure drops during diastole. At the time of aortic valve opening, the pressure inside the left ventricular chamber equals to the pressure in the aorta, i.e. diastolic blood pressure, if ejection resistance is ignored. Making use of this relationship, we deduced the mathematical equation between the pre-ejection period and the diastolic aortic blood pressure from a pressure-source model originally proposed by Mulier [1] [2] which describes the left ventricular pressure as a function of ventricular volume and time. This equation is later combined with the equation which relates pulse transit time to arterial blood pressure in the latter section to build the mathematical relationship between pulse arrival time and arterial blood pressure.

3.1.1 Review of current left ventricular models

The pumping left ventricle is classically modeled as an elastic bag which becomes stiffer during contraction, and the ventricular compliance is defined as:

$$C_v = \frac{dV_v}{dP_v}, \tag{3.1}$$

which is estimated by the linear relationship as:

$$C_v = \frac{V_v}{P_v}, \tag{3.2}$$

where "*d*" indicates derivative, and V_v and P_v are the ventricular volume and pressure, respectively. In the early study, the ventricular compliance was modeled as a step function which had a higher value during diastole and a lower value during systole [8]. Some researchers also utilized the reciprocal of compliance, i.e. elastance, to describe the ventricular-volume relationship and such elastance was further extended to be a continuous function of time by De fares *et al* in 1963 [9].

In the early 1970s, Suga and co-workers designed a series of experiments to measure instantaneous ventricular pressure and volume changes simultaneously in the isolated dog heart under varying pre-load (end-diastole ventricular volume), after-load (arterial blood pressure), heart rate and heart contractile conditions [10] [11] . They defined a time-varying elastance (*E(t)*) model shown as Eq.(3.3) and found that 1) *E(t)* does not change with different end-diastole ventricular volumes and loading conditions; 2) the shape of normalized *E(t)* with respect to its maximum value, E_{max}, and the time corresponding to E_{max}, t_{max}, is invariant with all fore mentioned changing conditions (see Fig. 3.1 C). *E(t)* is described by:

$$E(t) = \frac{P_v(t)}{V_v(t) - V_d}, \tag{3.3}$$

where V_d is the ventricular volume when ventricular pressure equals to zero. The concept of time-varying elastance defined in Eq.(3.3) is illustrated in Fig. 3.1 [12]. Since *E(t)* is indifferent with changing end-diastolic volume and after load, the 'isochronic' points at time point T_i, $i=1,2,\ldots$, from different pressure-volume loops form a linear curve (see Fig. 3.1 A) whose slope corresponds to the value of $E(T_i)$ on the time varying elastance curve (see Fig. 3.1 B) and intercept equals to V_d. According to Eq.(3.3), 'isochronic' curves at different time points in an cardiac cycle are with different slopes (elastance) but should converge into the point of V_d on the volume axis, as shown on Fig. 3.1 A.

The time-varying elastance model is perhaps the most popular mathematical description of the pulsatile left ventricle and has been utilized in many applications related to cardiovascular modeling. The popularity of this model is due to: 1) the single time-varying elastance function is able to represent many important features of the left ventricular pumping; 2) the unique shape of normalized *E(t)* which is invariant with different loadings and heart rates makes this model easy to be adopted to applications related to variant physiological and pathological conditions.

However, this widely embraced model is subject to limitations and discrepancies in describing

either the isovolumic contraction or ejection behaviors of the left ventricle. During isovolumic contraction, the time-varying elastance model assumes that there is a linear relationship between the end-diastole ventricular volume and the isovolumic ventricular pressure, whereas in contract to the nonlinear behavior for higher ventricular volume as measured by Palladino *et al* [13]. During ejection, the experimental data of other studies reveals that the ventricular pressure at early ejection decreases more than that expected from the time-varying elastance model due to reduced ventricular volume along, namely deactivation [14], and raises to a higher value at late systole than the isovolumetric pressure at the same volume, namly hyperactivation [15]. The deactivation was then later modeled into the time-varying elastance concept by introducing a passive resistive term or inductive term [16]. This modified model, however, failed to predict the timing of peak isovolumetric pressure accurately [17]. These observations is mainly due to the fact that time-varying elastance is proposed based on the experimental measurements of ventricular blood pressure and volume changes within the entire cardiac cycle, which includes both the isovolumic and ejection phases. This model thus does not separate the ventricular effect from vascular effect on the measured pressure-volume relationship and hence is difficult to gain insight into the properties of the ventricle.

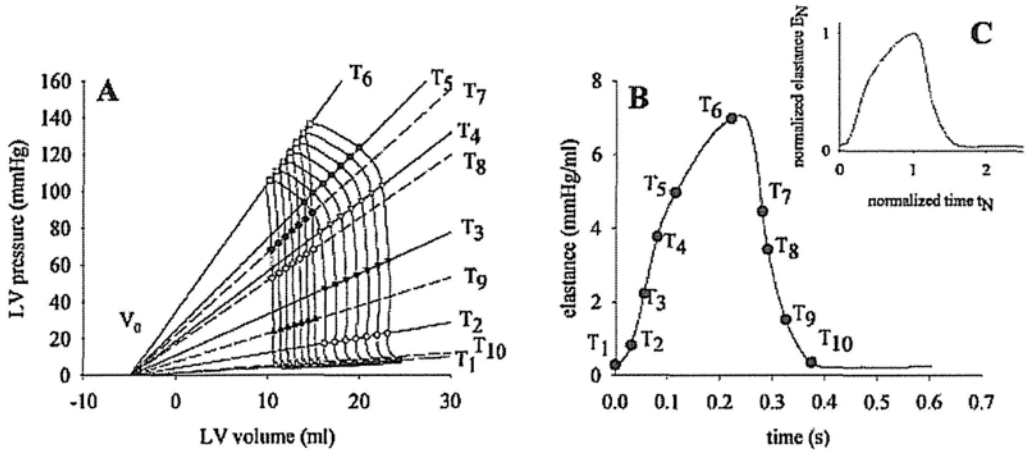

Fig. 3.1 Time-varying elastance concept as elaborated by Suga and Sagawa [10-12]. The symbols in panel A indicate 'isochronic' points on the different PV-loops, occurring at the moment during the cardiac cycle. These points line up and, stepping through the cardiac cycle (T_1, T_2, ...), the slope of the line (the elastance, panel B) varies in a cyclic way, while the intercept with the volume axis remains constant (V_0). The elastance curve can be normalized with respect to both its amplitude and the time at which the amplitude occurs (panel C).

An alternative analytical description of left ventricle is proposed by Mulier in 1994 [1] who modeled the ventricular pressure as a function of time and volume contained. This model is named the pressure-source model and is based on the Frank mechanism: "The peak developed pressure of the isovolumically contracting ventricle increases with end-diastolic pressure to an upper physiological limit." Different from the time-varying elastance model with combined the effects from ventricular and vascular sides in its concept, Mulier started from building an isovolumic ventricular pressure model purely based on the ventricular properties extracted from experimental

observations on an isolated heart of dog [1]. The influence of vascular loading is later introduced into the model by adding an ejection effect term [2]. By doing so, the ventricular and vascular effects are separated and described by individual mathematical formulas. Mulier developed the mathematical description from experiments on dog hearts with a fixed heart frequency equal to 1 Hz [1]. He showed that:

$$p_v(V_v,t) = a(V_v - b)^2 + (cV_v - d)f(t), \tag{3.4}$$

where parameter a relates to ventricular elastance during relaxation, b represents ventricular volume for zeros diastolic pressure, c and d relate to the volume-dependent and volume-independent components of developed pressure, respectively, 't' respects time and $f(t)$ is a continuous function, termed the activation function. This function f generates a bell-shaped curve that varies between 0 and 1. The activation function f is described by:

$$g(t) = \begin{cases} \left(1 - e^{-(t/\tau_c)\alpha}\right) & ,0 \le t \le t_b \\ \left(1 - e^{-(t/\tau_c)\alpha}\right)e^{-((t-t_b)/\tau_r)\alpha} & ,t_b < t < t_h \end{cases}, \tag{3.5}$$

where $f(t) = g(t)/g(t_p)$, and t_p represents time for peak ventricular pressure and τ_c, τ_r, α are ventricular parameters. The parameters τ_c and τ_r represent contraction (increase in pressure) and relaxation (pressure decreases), respectively. The parameter α describes the overall rate of onset of these processes and t_b denotes the time when the relaxation process starts. It is worth noting here that the Eq. (3.5) successfully separates the contraction and relaxation of phase of ventricular muscle, which is important later in the deduction of an explicit mathematical expression between pre-ejection period and aortic blood pressure in section 3.1.2. The heart period is represented by t_h.

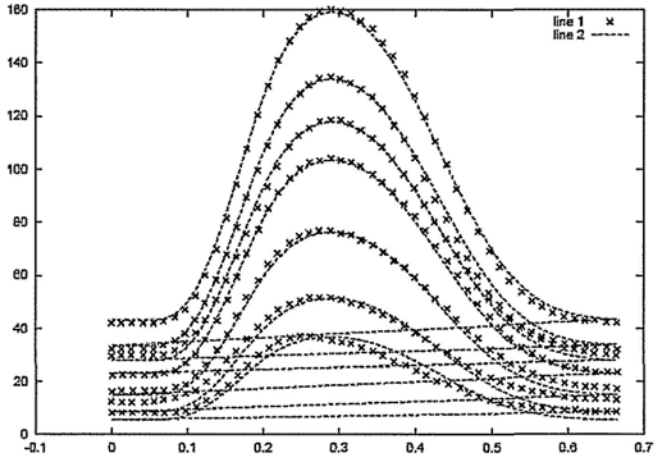

Fig. 3.2 Measured isovolumic ventricular pressure for seven different volumes in dog hearts (×) taken from [1]. Superimposed is the best fit using Eq.(3.4) and Eq.(3.5) (dashed). The nearly horizontal lines are included solely to indicate that all seven curves are fitted using the same parameters.

Fig. 3.2 compares measured isovolumic ventricular pressure in Mulier's experiments with the model computed pressure using Eq.(3.4) and Eq.(3.5) [1]. Table 3.1 depicts the parameter values

and corresponding correlation coefficients R^2 between the computed and measured results in [1]. The parameters in Eq.(3.4) and Eq.(3.5) are unchanging with varying end-diastole ventricular volume at a certain heart rate. Notice that the parameter t_b is calculated from the others parameters in Table 3.1 since $f'(t_p) = 0$ implies

$$t_b = t_p \left\{ 1 - \left(\frac{\tau_r}{\tau_c} \right)^{\alpha/(\alpha-1)} \left[\frac{e^{-(t_p/\tau_c)^\alpha}}{1 - e^{-(t_p/\tau_c)^\alpha}} \right]^{1/(\alpha-1)} \right\}. \tag{3.6}$$

Table 3.1 Best-fit parameter values for Eq. (3.5) to measured isovolumic pressures [1].

Parameter	All seven curves
τ_c	*0.13561 s*
τ_r	*0.20441 s*
α	*2.68440*
t_p	*0.23705 s*
R^2	*0.99753*

R^2 is the correlation coefficient for all seven curves in Fig. 3.2 [1].

However, with several revealing discrepancies, the isovolumic pressure model does not offer a full description of the ventricular performance of an ejecting beat. Therefore, the ejection effect was introduced by Danielsen *et al* [2] by modifying the activation function f

$$p_v(V_v, t) = a(V_v - b)^2 + (cV_v - d)F(t, Q_v), \tag{3.7}$$

where Q_v represents the ventricular outflow and $F(t, Q_v)$ is given by:

$$F(t, Q_v) = f(t) - k_1 Q_v(t) + k_2 Q_v^2(t - \tau), \quad \tau = \kappa t. \tag{3.8}$$

The positive parameters k_1 and k_2 represent the strength of deactivation and hyperactivation, respectively, while τ is a time-varying time delay. The term $k_2 Q_v^2(t-\tau)$ represents hyperactivation and becomes active τ later in time than the deactivatioin which is represented by the term $k_1 Q_v(t)$. The parameter κ ($0<\kappa<1$) relates to the change in the rate of formation of new bonds with time. It has been demonstrated that the simulation results obtained from the model with ejection effect (Eq. 3.7) covered most of the features of the human ventricle during normal and altered vascular conditions [2].

The above pressure-source model is proposed under a constant heart rate (60 beats/min), limiting the model from many applications with arbitrary heart rates. In an experiment on dogs in 1993, Regen et al found that peak isovolumic pressure was elevated and the pressure curve becomes narrower when heart rate increased [18]. Fig. 3.3 presented the measured isovolumic ventricular pressure in dog hearts for different heart rate [18]. It is also showed that the measured isovolumic ventricular pressure curves are almost identical when normalized with respect to time and peak

isovolumic pressure [18].

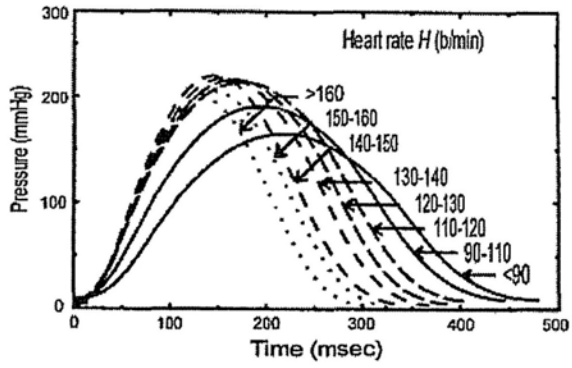

Fig. 3.3 Measured isovolumic ventricular pressure in dog hearts for different heart rates [18].

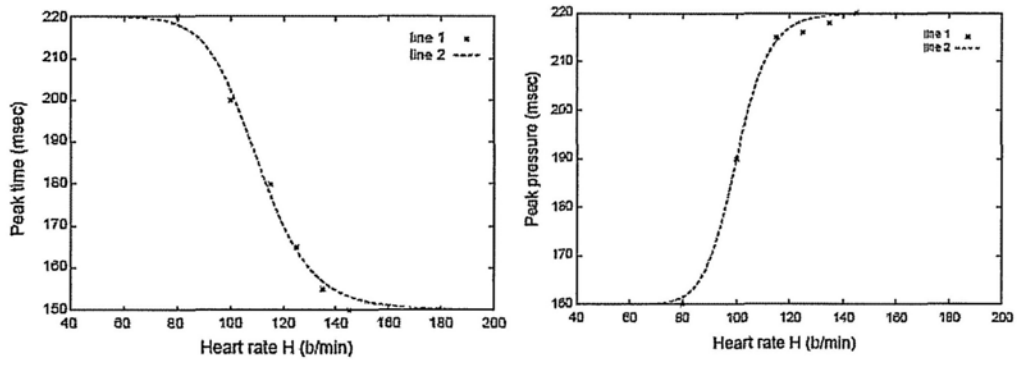

(a) (b)

Fig. 3.4 Experimental data extracted from Fig. 3.3 showing (a) time for peak time t_p as a decreasing sigmoidal function in heart rate and (b) peak pressure p_p as an increasing sigmoidal function in heart rate [4].

Based on this fact, Ottensen and Danielsen modified the isovolumic pressure-source model to include changes in HR by scaling time and peak values of the activation function f [4]. As plotted in Fig. 3.4, the experimental data extracted from Fig. 3.3 show that the time for peak time t_p is a decreasing sigmoidal function in heart rate, and peak pressure p_p an increasing sigmoidal function in heart rate [4]. The relationship between the time for peak pressure t_p and hear rate H is formulated by the Hill function as:

$$t_p(H) = t_{p,\min} + \left[\frac{\theta^\nu}{H^\nu + \theta^\nu}\right]\left(t_{p,\max} - t_{p,\min}\right), \tag{3.9}$$

where θ represents the median and ν the steepness of the relation, respectively, $t_{p,min}$ and $t_{p,max}$ denote the minimum and maximum values, respectively [4]. Similarly, the relationship between the peak ventricular pressure p_p and HR is described by the Hill function as

$$p_p(H) = p_{p,\min} + \left[\frac{H^\eta}{H^\eta + \varphi^\eta}\right]\left(p_{p,\max} - p_{p,\min}\right), \tag{3.10}$$

where ϕ is the median, η represents the steepness of the relationship and $p_{p,min}$ and $p_{p,max}$ represent the minimum and maximum values, respectively [4].

Then, Ottesen and Danielsen discussed a number of activation functions *g(t)*, altered Eq.(3.5) by the simplest polynomial form of action function, and altered the action function *g(t)* by introducing the relationship between *HR* and t_p (Eq.(3.9)) and that between *HR* and p_p (Eq.(3.10)) as follows:

$$g(t) = \begin{cases} (t-\alpha)^n(\beta(H)-t)^m, & \alpha \le t \le \beta(H) \\ 0, & \beta(H) \le t \le t_h \end{cases}, \tag{3.11}$$

where $f(t,H) = \dfrac{p_p(H)g(t)}{g(t_p)}$, α, $\beta(H)$, n and m are ventricular parameters, and t_h and H are the heart period and frequency, respectively. The parameter t_p fulfills g'(t_p) = 0. Thus, $\beta(H) = \dfrac{n+m}{n}t_p(H) - \dfrac{\alpha m}{n}$ and $g(t_p) = n^n m^m[(\beta-\alpha)/(m+n)]^{m+n}$.

3.1.2 Modeling the relationship between pre-ejection period and aortic blood pressure

Since the objective of this chapter is to build the relationship between pulse arrival time and arterial blood pressure, it is necessary to express the pre-ejection time explicitly in the deduced mathematical equation. In Eq.(3.11), a unique higher order polynomial is utilized to describe *g(t)* in both the isovolumic contraction and ejection phases, which makes the variable *t* difficult to be expressed explicitly in terms of ventricular pressure. Hence, we start our deduction from the activation function form described by Eq.(3.5), which gives a simpler form of *g(t)* in isovolumetric contraction phase. We rewrite Eq.(3.5) as follows:

$$g(t) = \begin{cases} \left(1 - e^{-(t/\tau_c)\alpha}\right) & ,0 \le t \le t_b \\ \left(1 - e^{-(t/\tau_c)\alpha}\right)e^{-((t-t_b)/\tau_r)\alpha} & ,t_b < t < t_h \end{cases}. \tag{3.5}$$

Since pre-ejection period is the time length of isovolumic contraction, there exists PEP < t_b. Thus from Eq.(3.5) we get:

$$g(PEP) = 1 - e^{-(PEP/\tau_c)\alpha}. \tag{3.12}$$

Using Tayler Series to represent $e^{-(t/\tau_c)^\alpha}$ at t=0, we get $e^{-(t/\tau_c)^\alpha} = 1 - \left(\dfrac{t}{\tau_c}\right)^\alpha$, and Eq.(3.12) changes to be:

$$g(t)=\left(\frac{t}{\tau_c}\right)^{\alpha}, \tag{3.13}$$

where α is a positive integer. Substituting Eq.(3.13) into Eq.(3.4) and expressing PEP explicitly, we get:

$$PEP=\tau_c\cdot\left(\frac{DBP-P_{v,d}}{A}\right)^{\frac{1}{\alpha}}, \tag{3.14}$$

where $P_{v,d}=a(V_v-b)^2$ and $A=\dfrac{(cV_{v,d}-d)}{g(t_p)}$.

Since Eq.(3.5) is proposed under a constant heart rate (60 beats/min), arbitrary heart rate needs to be added. We follow the idea proposed by Ottesen and Danielsen [4] by using the relationships between heart rate and the time for peak pressure t_p (Eq.(3.9)) and peak pressure p_p (Eq.(3.10)):

$$t_p(H)=t_{p,\min}+\left[\frac{\theta^{\nu}}{H^{\nu}+\theta^{\nu}}\right]\left(t_{p,\max}-t_{p,\min}\right) \tag{3.9}$$

and

$$p_p(H)=p_{p,\min}+\left[\frac{H^{\eta}}{H^{\eta}+\varphi^{\eta}}\right]\left(p_{p,\max}-p_{p,\min}\right). \tag{3.10}$$

Different from the polynomial form where the shape of $g(t)$ is purely determined by t_p, p_p and β, the shape of $g(t)$ described by Eq.(3.5) is determined by t_p, p_p, t_b, τ_c and τ_r. Therefore, effect of changing heart rate needs to be expressed in terms of $\tau_c(H)$, $\tau_r(H)$ and $t_b(H)$ together with $t_p(H)$ and $p_p(H)$.

Since τ_c and τ_r are time constants indicating the increasing and decreasing speed of isovolumic pressure, if we calculate the ratio between τ_c and t_p, τ_r and t_p at heart rate frequency equals to 1 Hz (60 beats/min), these two ratios should not change at different heart rates if the corresponding normalized isovolumetric curves are identical with respect to t_p. The ratio between τ_c and t_p (*r_tauc*), τ_r and t_p (*r_taur*) at heart rate frequency equals to 1 Hz can be calculated from parameter values listed in Table 3.1. Then we get

$$\tau_c(H)=r\_tauc\cdot t_p(H) \tag{3.15}$$

and

$$\tau_r(H)=r\_taur\cdot t_p(H), \tag{3.16}$$

where *r_tauc* = 0.57207 and *r_taur* = 0.86231. Substituting Eq.(3.15) and (3.16) into Eq.(3.6), we get:

$$t_b(H) = t_p(H)\left\{1-\left(\frac{\tau_r(H)}{\tau_c(H)}\right)^{\alpha/(\alpha-1)}\left[\frac{e^{-\left(t_p(H)/\tau_c(H)\right)^{\alpha}}}{1-e^{-\left(t_p(H)/\tau_c(H)\right)^{\alpha}}}\right]^{1/(\alpha-1)}\right\} . \quad \textbf{(3.17)}$$

Substituting Eq.(3.15), (3.16) and (3.17) into Eq. (3.7), (3.8) and (3.5), it yields:

$$p_v(V_v,t,H) = a(V_v-b)^2 + (cV_v-d)F(t,Q_v,H), \quad \textbf{(3.18)}$$

$$F(t,Q_v,H) = f(t,H) - k_1Q_v(t) + k_2Q_v^2(t-\tau), \ \tau = \kappa t, \quad \textbf{(3.19)}$$

and

$$g(t,H) = \begin{cases} \left(1-e^{-(t/\tau_c(H))\alpha}\right) & ,0 \le t \le t_b(H) \\ \left(1-e^{-(t/\tau_c(H))\alpha}\right)e^{-((t-t_b(H))/\tau_r(H))\alpha} & ,t_b(H) < t < t_h \end{cases} . \quad \textbf{(3.20)}$$

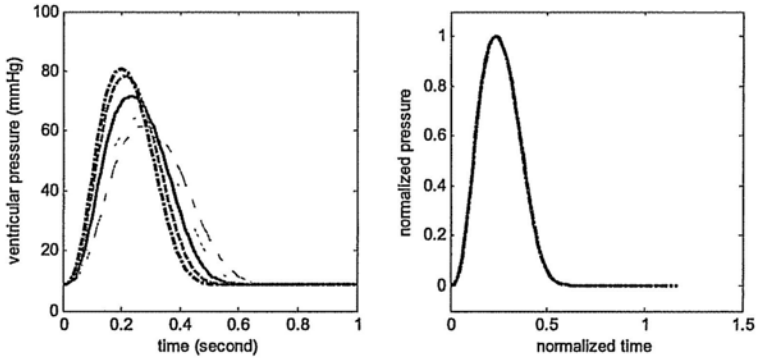

(a) (b)

Fig. 3.5. (a) Calculated left ventricular pressure curves using Eq.(3.18)-(3.20) under different heart rates and (b) and normalized curves of the pressure curves in (a) with respect to t_p and p_p. In (a), the heart rates of the curves are: 42 beats min^{-1} (dash dot, thin curve), 54 beats min^{-1} (dash, thin curve), 60 beats min^{-1} (solid, thick curve), 66 beats min^{-1} (dash, thick curve), 72 beats min^{-1} (dash dot, thick curve).

Fig 3.5 (a) shows the left ventricular pressure curves under different heart rates calculated from Eq.(3.18)-(3.20), and 3.5(b) shows the corresponding normalized curves with respect to p_p and t_p. The overlapping of the normalized curves in 3.5(b) validates the effectiveness of Eq. (3.18)-(3.20) to correctly describe the phenomenon reported by Regen et al. 1993 [18]. Combining the relationship of t_p, p_p, t_b, τ_c and τ_r with heart rate and Eq. 3.14, we get:

$$PEP = \tau_c(H)\cdot\left(\frac{DBP - P_{v,d}}{A(H)}\right)^{\frac{1}{\alpha}}, \quad \textbf{(3.21)}$$

where

$$A(H) = \frac{P_p(H) \cdot (cV_{v,d} - d)}{g(t_p(H))} \tag{3.22}$$

and

$$g(t_p(H)) = \left(1 - e^{-\left(t_p(H)/\tau_c(H)\right)\alpha}\right) e^{-\left(\left(t_p(H) - t_b(H)\right)/\tau_r(H)\right)\alpha} \tag{3.23}$$

Eq.(3.21) is an explicit mathematical description of PEP in terms of DBP, which models the ventricular and arterial effects on PEP timing.

3.2 Arterial modeling and the relationship between pulse transit time and arterial blood pressure

Systematic arterial system is coupled to the left ventricle pump as its after-load. The arterial system has been modeled in mainly three ways: lumped models [20, 22], tube models [8, 41, 80] and anatomically based distributed models [24, 25]. In this section, a short review is first given interpreting the main model concepts and mathematical descriptions of these three types of models with comments on the main advantages and disadvantages. Then, the main idea of the asymmetric T-tube model is introduced followed by the detailed mathematical descriptions of this model both in frequency and time domain. Next, we modify the asymmetric T-tube model by introducing a nonlinear pressure-volume relationship and express characteristic impedance, tube compliance and pulse transit time in the model as functions of changing arterial blood pressure. Combined this result with PEP-DBP relationship (Eq.(3.21)- (3.23)) deduced in section 3.1, the mathematical equation which relates pulse arrival time to arterial blood pressure is formulated.

3.2.1 Current models of arterial system

The lumped model, windkessel, is first qualitatively described by Stephen Hales in 1733 [19]. "Windekessel" is a German word which means fire engines with an air chamber (see Fig. 3.6 (a)). As envisioned by Hales, the arterial system works analogous to the Windkessel in a cardiac cycle: during systole the heart injects blood into the arterial system, distending the large arteries; during diastole the arteries recoil, propelling the blood continuously through the small arteries. Otto Frank [20] first quantified the Windkessel concept on the basis of conservation of mass in 1899 and represented the arterial system by a two-element Windkessel model, as shown in Fig 3.6 (b). In Fig 3.6 (b), P_{in} and Q_{in} represent the blood pressure and volume at the aortic root, respectively. C_w is the total arterial compliance and R_w is the total peripheral resistance. In a two-element Windkessel, there is:

$$Q_{in} = C_w \frac{dP_{in}}{dt} + \frac{P_{in}}{R_w}, \tag{3.24}$$

where the term compliance (C_w) is commonly used to describe the change in volume stored (V) per change in input pressure (P_{in}), and R_w is calculated from the average pressure ($\overline{P}_{in}$) per

average flow ($\overline{Q}$):

$$C_w = \frac{dV}{dP_{in}} \tag{3.25}$$

and

$$R_w = \frac{\overline{P_{in}}}{\overline{Q}}. \tag{3.26}$$

The two-element Windkessel predicts that in diastole, when the aortic valve is closed, pressure will decay exponentially with a characteristic decay time R_wC_w

$$P_{dia} = P_{es}e^{-t/R_wC_w}, \tag{3.27}$$

where P_{dia} is the diastolic blood pressure and P_{es} is the blood pressure at end systole.

The two-element Windkessel model describes the whole arterial system in terms of a pressure-flow relation at its entrance, by two parameters that have physiological meanings. However, it was later founded that in systole the relation between pressure and flow was poorly predicted by the two-element Windkessel, and in frequency domain, the high frequencies of the input impedance predicted by the two-element Windkessel is inconsistent with the experimental results of aortic input impedance in mammals [21]. In order to overcome this shortcoming, the characteristic impedance of aorta which equals to the input impedance modulus at higher frequencies is added as the third element into the Windkessel model [22], which is shown in Fig. 3.6 (c). Compared with the two-element model, three-element Windkessel is able to predict the main features of the input impedance in both the lower and higher frequency ranges and thus is utilized widely to mimic the systematic arterial function.

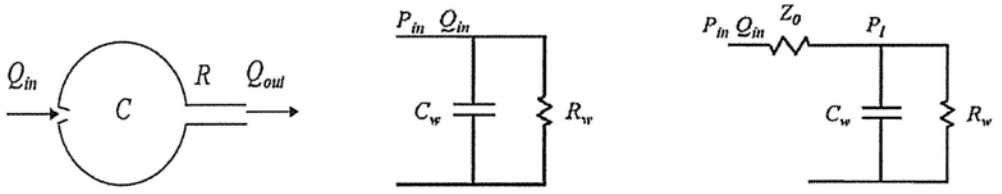

(a) (b) (c)

Fig. 3.6. (a) Conceptual representation of windkessel. C: compliance of large arteries; R: total resistance of small arteries; Q_{in} and Q_{out}: flow into and out of arterial tree. (b) Two-element Windkessel model. P_{in}: input pressure at aortic root; C_w and R_w: total arteiral compliance and total peripheral resistance, respectively. (c) Three-element Windkessel model. Z_0: characteristic impedance; P_I: pressure on the total arterial compliance.

Due to its simplicity and the capability of revealing some gross features of arterial hemodynamics, Windkessel models have been widely utilized in the ventricular-arterial coupling applications [23] [24]. However, the lumped model assumes infinite pulse wave velocity along the arteries. This is

unrealistic and ignores the important wave transmission and reflection phenomenon which substantially influences ventricular-arterial coupling conditions. For example, wave transmission characteristics of the arterial load can affect left-ventricular pumping depending on the timing and strength of related waves as they return to the aortic root from the periphery.

On the other hand, the distributed models consider the finite pulse wave velocity on the arterial segments and regard the arterial system as a network of elastic tubes [24, 25]. Fig 3.7 (a) shows a distributed model composed of 55 anatomically based arterial segments [25]. Hemodynamic condition in each segment is described by a group of partial differential equations based on conservation of mass and balance of momentum, and the blood pressure and flow is then obtained by solving these partial differential equations. Compared with the Windkessel model, the distributed models are much more realistic and reveal more information of the peripheral circulation. However, the mathematical descriptions are extremely complex and cost a large amount of calculation time, which does not lead distributed itself to easy simulation. Moreover, not only are there insufficient data on localized vascular properties to serve as inputs to the model, but it is also difficult to evaluate the effect of alterations in one or more of these elements on the impedance of the entire system.

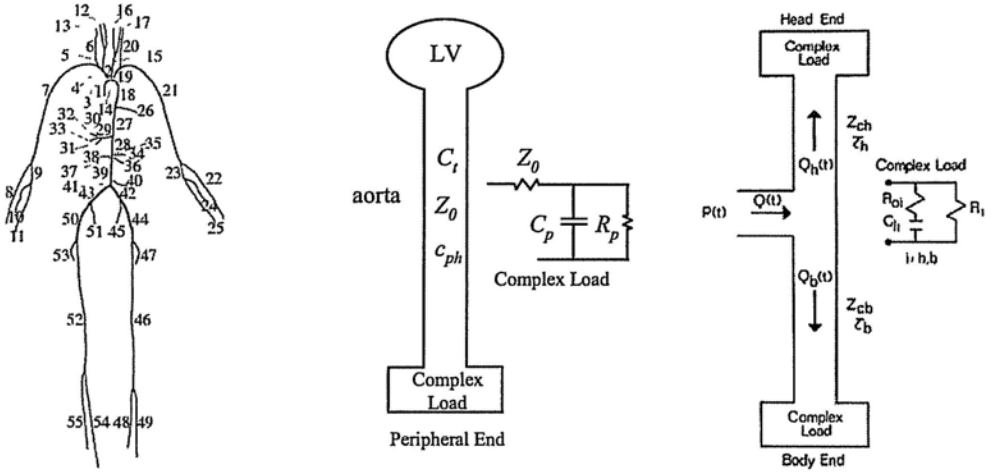

Fig. 3.7. (a) A distributed arterial model composed of 55 arterial segments [25], (b) the single tube model and (c) the asymmetric T-tube model in [29]. C_t: tube compliance; Z_0: tube characteristic impedance; c_{ph}: phase pulse wave velcocity; $P(t)$: aortic blood pressure; $Q(t)$, $Q_h(t)$, $Q_b(t)$: blood flow in the aorta, upper body and lower body tube, respectively; Z_{ch}, Z_{cb}: characteristic impedance in the upper and lower body tube, respectively; τ_{ch}, τ_{cb}: pulse transit time in the upper and lower body tube, respectively; R_{0i}, R_i, C_{li}: terminal resistance, peripheral resistance and terminal compliance at *ith* branch , i= h, b.

The tube model combines the ideas of the lumped and distributed arterial models [26-29]. In the tube models, arterial system is represented by elastic tubes ended with the complex loads (see Fig. 3.7 (b) and (c)). The elastic tube considers the wave transmission in the big, elastic artery and the complex load is represented by a lumped model, e.g. three-element Windkessel model. Arterial

pulses transmit on the elastic tubes while reflect at the junctions of the tube and its complex load. Tube and its load are coupled in the way that the load impedance equals to the characteristic impedance of the tube at high frequencies. There are mainly two types of tube models: a single tube model [27] (see Fig. 3.7 (b)) and an asymmetric T-tube model [26, 28-29] (see Fig. 3.7 (c)). The former assumes that the systemic arterial tree, as seen from the heart, can be represented by a uniform tube with a single effective reflection site [27] [30]. The latter assumes the presence of two functionally discrete reflection sites, one for the upper body and the other for the lower body [26]. Based on data where this diastolic oscillation was not evident, a good representation of the arterial pressure-flow relationships was achieved using a single tube model [30]. This model, however, is not suitable to describe the arterial system when a diastolic oscillation in pressure is evident [26]. In this case, the asymmetric T-tube may be more appropriate.

To summarize, compared the pure lumped and distributed models, the tube model is a good trade-off between the precision and complexity of arterial model and is capable of describing the wave transmission and reflection phenomenon. Compared with the single tube model, the asymmetric T-tube model is more realistic to the anatomical structure of the systematic arterial system and provides better prediction of arterial pressure wave characteristics during diastole. Hence, this model is adopted in this work to represent the arterial load to the fore mentioned pressure-source ventricular model.

3.2.2 Asymmetric T-tube model

The asymmetric T-tube model was first conceptually proposed by McDonald in 1960s [26] when he tried to explain the positions of the multiple maxima and minima in the observed ascending aortic impedance spectra which is difficult to be explained by the single tube model. As shown in Fig. 3.7 (c), the asymmetric T-tube model consists of two elastic tubes of differing lengths, one being the result of all arterial terminations in the upper part of the body, and the other the result of all terminations in the lower part of the body. Due to this design, differing relative lengths of the upper and lower extremities in species with differing body shapes could be conceptualized as different lengths of the tubes, thereby accounting for the different impedance patterns. This notion was later utilized by O'Rourke and co-workers as a conceptual one to explain arterial impedance patterns and pressure and flow wave shapes in a variety of animals and in humans [31]. Furthermore, variant mathematical descriptions can be built under the same model concept by using different assumptions on the tube properties and complex load structures, which make this model easy to be adapted to widespread applications [28-29, 32-33].

The asymmetric T-tube model adopted in this work is the version proposed by Burattini and Campbell in 1989 [28]. This version assumes that the transmission paths have no frictional losses and are terminated with complex impedances. Validation work has shown the ability of this model to accurately reproduce pressure and flow waves in the ascending aorta and proximal descending aorta [28]. Furthermore, this model is rather suitable for ventricular-arterial coupling since the time domain interpretations have already been developed and validated [29].

The electrical analog of the asymmetric T-tube model proposed in [28] is shown in Fig. 3.8. The model parameters are described in the legend. The short and long tube lengths d_1 and d_2,

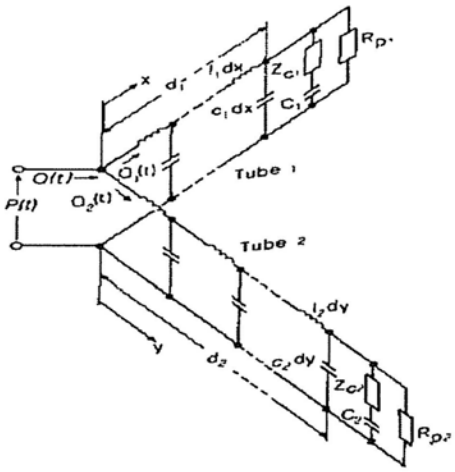

Fig. 3.8. Electrical analogue of the asymmetric T-tube model proposed in [28]. Tube 1 and tube 2 represent upper and lower body circulation, respectively. Their characteristic impedances are Z_{c1}, and Z_{c2}, respectively. Load compliances are C_1, and C_2, respectively. Distributed compliances are c_1 and c_2 and distributed inertances are l_1 and l_2. Tube lengths are d_1 and d_2. Peripheral resistances of upper and lower circulations are R_{p1} and R_{p2}, respectively. Total peripheral resistance is given by the parallel of these two. $Q(t)$ is ascending aortic flow and $P(f)$ is ascending aortic pressure. $Q_1(t)$ and $Q_2(t)$ are flows to the upper and lower body, respectively. Their sum equals $Q(t)$.

respectively, representing the distances to the effective reflection sites located in the upper and lower body circulations. The sum

$$C_t = C_1 + C_2 + (c_1 d_1) + (c_2 d_2) \tag{3.28}$$

represents total compliance of the systemic arterial bed. Total peripheral resistance (ratio of mean ascending aortic pressure $\overline{P}$ to cardiac output $\overline{Q}$) is

$$R_p = R_{p1} R_{p2} / \left(R_{p1} + R_{p2}\right) = \overline{P} / \overline{Q}. \tag{3.29}$$

Characteristic impedance of each tube is a real constant since these tubes have no frictional losses ($Z_{ci} = \sqrt{\left(l_i / c_i\right)}$). For high frequencies the individual tube load reduces to the parallel of characteristic impedance and peripheral resistance. Since Z_{ci} is small with respect to R_{pi}, the resulting equivalent resistance is close to Z_{ci}. Regional wave reflection is therefore negligible at these frequencies and the impedance as seen at the input of the parallel tubes (joining with ascending aorta) can be approximated by the parallel of Z_{c1} and Z_{c2}.

In the frequency domain (ω) the input impedance of individual tubes assumes the following expression:

$$Z_i(jw) = Z_{ci} \frac{Z_{Li}(jw) + Z_{ci} \tanh(\gamma_i d_i)}{Z_{ci} + Z_{Li}(jw) \tanh(\gamma_i d_i)}, \quad i = 1, 2, \tag{3.30}$$

where γ_i is the propagation constant and Z_{Li} is the load impedance. This quantity is complex and,

in general, can be written as follows:

$$\gamma_i = \alpha_i + j\beta_i, \tag{3.31}$$

where α_i is the attenuation constant (equal to zero for a frictionless tube), and β_i is the phase constant. The latter is related to the velocity of propagation of a sinusoidal wave in the tube (phase velocity, c_{ph}) by the following equation:

$$\beta_i = \omega / c_{phi} = \omega\sqrt{(l_i c_i)}. \tag{3.32}$$

The load impedance has the following expression:

$$Z_{Li}(jw) = R_{pi}(1 + j\omega C_i Z_{ci}) / [1 + j\omega C_i (R_{pi} + Z_{ci})], \quad i = 1, 2. \tag{3.33}$$

The impedance, as seen from the entrance of the model (ascending aorta input impedance), results in

$$Z_a(jw) = 1/[1/Z_1(j\omega) + 1/Z_2(j\omega)]. \tag{3.34}$$

In order to merge the asymmetric T-tube model easily to time-domain characterizations of the left ventricular for the study of left ventricular-arterial interaction, Campbell *et al* 1990 formulated the asymmetric T-tube model in the domain as follows [29]:

$$Q(t) = \frac{1}{Z_c} P(t) - \frac{1}{R_{01}} x_1(t - T_1) + \frac{1}{R_{02}} x_2(t - T_2) \tag{3.35}$$

and

$$\frac{dx_i(t)}{dt} = -\alpha_i x_i(t) + \beta_i \left[2P(t - T_i) - \frac{Z_{ci}}{R_{0i}} x_i(t - 2T_i) \right], \quad i = 1, 2, \tag{3.36}$$

where

$$\alpha_i = \frac{1}{2R_{0i}C_{li}} \left[\frac{2R_{0i} + R_{pi}}{R_{0i} + R_{pi}} \right], \quad i = 1, 2 \tag{3.37}$$

and

$$\beta_i = \frac{1}{2R_{0i}C_{li}}, \quad i = 1, 2, \tag{3.38}$$

where $x_1(t)$, $x_2(t)$ are state variables representing the pressures across C_{l1} and C_{l2} (for locations of C_{l1} and C_{l2}, see Fig. 3.8), respectively, and T_1, T_2 are the pulse transit times for the pressure wave to transmit from aortic arch to the upper and lower body effective terminals, respectively. And there exists:

$$c_i d_i = \frac{T_i}{Z_{ci}}, \quad i = 1, 2. \tag{3.39}$$

Campbell *et al* validated the above formulations (Eq.(3.35)-(3.39)) by comparing the pressure and flow waveforms predicted by Eq.(3.35)-(3.39) with the measured data from anesthetized open-chest dogs under different vasoactive states [29]. The results showed that the T-tube model

fitted the data well in all formulations and in all vasoactive states [29]. Fig. 3.12 in later section 3.3.1 depicts the measured and predicted aortic blood pressure and flow waveforms from one dog for basal, vasoconstricted and vasodilated states.

When it comes to the application in this work where the relationship between pulse transit time and arterial blood pressure is investigated, the above model shows a significant shortcoming: the tube parameters (characteristic impedance Z_{ci}, tube compliance c_i and pulse transit time T_i) do not change inherently with arterial blood pressure. This is in contrast to the experimental observations that these parameters changed when arterial blood pressure altered [34-36]. Hence, a relationship between tube parameters and arterial blood pressure has to be embedded into the model formulations, which is discussed in section 3.2.3.

3.2.3 Pressure-volume relationship in elastic artery

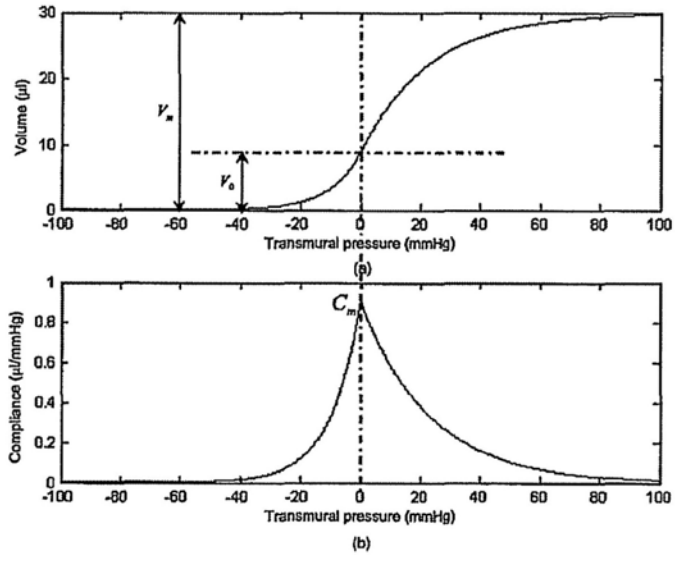

Fig. 3.9. Exponential model of (a) transmural pressure versus volume relationship and (b) corresponding compliance curve [37-38].

The biomechanical properties of the arterial wall under variant blood pressure can be described by a nonlinear (S-shape) arterial pressure-volume relationship as shown in Fig. 3.9 (a) [37]. In Fig. 3.9 (a), the x axis is the transmural pressure P_t, which is defined as:

$$P_t = P_i - P_o, \tag{3.40}$$

where P_i is the intra-arterial blood pressure and P_o is the extra-arterial pressure. We assumes P_o as zero and there exists $P_t = P_i$. Further, since the arterial blood pressure in our application is assumed within the physiological range, i.e 50~250 mmHg, we only consider the curve segment where P_o>0 in Fig. 3.9(a).

In 1982, Hardy and Collins proposed a generalized equation of pressure-volume relationship [37] and showed that the equation fitted the previously published atrial, ventricular, venoeous and

arterial data measured on animals and human being. The equation describes the pressure-volume relationship as follows:

$$k(V_m - V) = \frac{dV}{dP_t} \quad , \tag{3.41}$$

where k is a constant, having dimensions of compliance, characterizing the elastic property of the vessel wall and surrounding tissue while V_m is a limiting value of the vessel volume. Explicit expression of volume V with respect to transmural pressure P_t can be obtained by integration and rearrangement of Eq.(3.41)

$$V = V_m(1 - K_0 e^{-kP_t}), \tag{3.42}$$

where

$$K_0 = \frac{V_m - V_0}{V_m} e^{-kP_0}, \tag{3.43}$$

with V_0, P_0 being the values of V and P, respectively, at an arbitrary point on the pressure-volume curve. If this arbitrary point is at $P_t=0$, there is

$$V = V_m - (V_m - V_0) e^{-\frac{C_m}{V_m - V_0} P_t} \quad , \tag{3.44}$$

where C_m is the maximum compliance at $P_t=0$, as indicated in Fig. 3.9 (b). Taking the derivative of P_t on both sides of the Eq. (3.44), we get

$$C = \frac{dV}{dP_t} = C_m e^{-\frac{C_m}{V_m - V_0} P_t} . \tag{3.45}$$

From Bramwel-Hill equation [36], we have

$$PWV = \sqrt{\frac{V}{\rho \frac{dV}{dP_t}}} \quad , \tag{3.46}$$

where ρ is the density of blood, equal to 1050 $kg\ m^{-3}$. Substituting Eq.(3.44)-(3.45) into Eq.(3.46), and let $PWV = \frac{L}{PTT}$, we have

$$PTT = L \cdot \left(\frac{V_m}{\rho C_m} e^{\frac{C_m}{V_m - V_0} P_t} - \frac{V_m - V_0}{\rho C_m} \right)^{-\frac{1}{2}} , \tag{3.47}$$

where L is the length of pulse travelling. Since the arterial characteristic compliance (Z_c) per unit length is defined as

$$Z_c = \sqrt{\frac{\rho dP_t}{AdA}} . \tag{3.48}$$

Substituting Eq.(3.44)-(3.45) into Eq.(3.48), it yields

$$Z_c = \left(\frac{C_m V_m}{\rho} e^{-\frac{C_m}{V_m - V_0} P_t} - \frac{C_m (V_m - V_0)}{\rho} e^{-\frac{2C_m}{V_m - V_0} P_t} \right)^{-\frac{1}{2}} . \quad (3.49)$$

Eq.(3.45), (3.47) and (3.49) represent arterial tube compliance, characteristic impedance and pulse transit time as functions of arterial blood pressure. Then the question comes to whether these functions can be substituted into the asymmetric tube model (Eq.(3.35)-(3.39)), which can only be done after the confirmation of the physiological relevance of the tube model parameters. Burattini and Campbell in 1993 [39] found that, on anesthetized, open-chest dogs, the predicted parameters of the body tube branch fitted well with the measured data on the descending aorta in the chest and abdominal regions: 1) predicted pressure wave shape at the termination of the body tube fitted well with the pressure waves measured in the abdominal aorta near the origin of renal arteries; 2) calculated body tube length (l_2, averaged 30.3±2.8 cm) approximates the measured length from the aortic arch to the region of renal arteries (averaged 30.6±3.0 cm); 3) the calculated body tube compliance is comparable to the published data [40] and can be interpreted as the descending thoracic aortic compliance. These observations were supported by a later study conducted also on dogs by Shroff et al in 1995 [41] where the physiological relevance of both the higher and lower tube parameters were tested and validated by introducing local balloon inflation and vasoactive drugs. Recently, Hahn and his colleagues [42] compared the pulse transit time estimated from the asymmetric T-tube model and the measured data on five swine subjects from aortic root to radial artery and the results showed the measured aortic-radial pulse transit time can be accurately estimated by the estimated data if the estimated PTT is calibrated by a constant bias. They also pointed out that the bias was probably due to the shorter length of effective tube compared with the measured real arterial segment. Fig. 3.10 shows the data from swine subject #1 in their experiment. It is clear that the PTT estimated from the tube model is able to trace the change of real PTT measured on site, with an approximate constant bias.

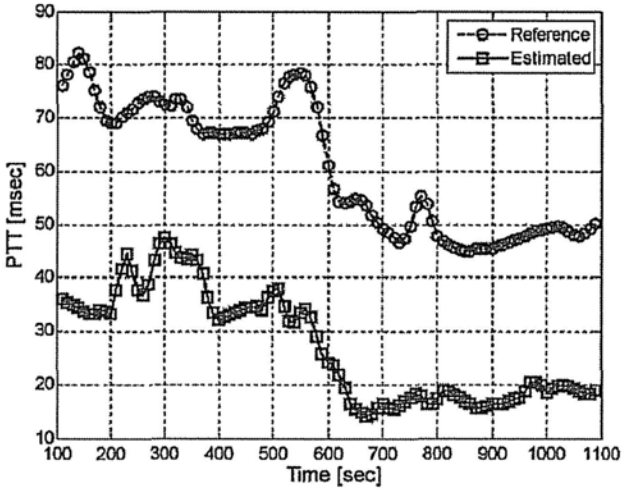

Fig. 3.10. A comparison of PTT measured from aortic root to radial artery (reference) and PTT estimated from asymmetric T-tube model (estimated) on swine subject #1 in [42]. The physiological condition undergoes a dynamic transient between 500s and 700s. The bias between the red and blue time series is about 40 ms.

According to the observations of studies mentioned above, we assumed that the tube parameters in the asymmetric T-tube model can represent the real physiological data measured in situ. Therefore, Eq.(3.45), (3.47) and (3.49) can be substituted into the time-domain formulations of the T-tube model (Eq.(3.35)-(3.38)), which yields:

$$Q(t,P)=\frac{Z_{c1}(P_t)Z_{c2}(P)}{Z_{c1}(P_t)+Z_{c2}(P)}Q(t)$$
$$-\frac{1}{R_{01}(P)}x_1\left(t-T_1(P)\right)+\frac{1}{R_{02}(P)}x_2\left(t-T_2(P)\right) \quad \textbf{(3.50)}$$

and

$$\frac{dx_i(t,P)}{dt}=-\alpha_i(P)x_i(t)$$
$$+\beta_i(P)\left[2P(t-T_i(P))-\frac{Z_{ci}(P)}{R_{0i}(P)}x_i\left(t-2T_i(P)\right)\right] \quad \textbf{(3.51)}$$

where

$$PTT_i(P)=T_i(P)+\Delta T_i$$
$$=l_i\cdot\left(\frac{V_m}{\rho C_m}e^{\frac{C_m}{V_m-V_0}P}-\frac{V_m-V_0}{\rho C_m}\right)^{-\frac{1}{2}}+\Delta T_i \quad \textbf{(3.52)}$$
$$i=1,2,$$

$$Z_{ci}(P)=\left(\frac{C_mV_m}{\rho}e^{-\frac{C_m}{V_m-V_0}P}-\frac{C_m\left(V_m-V_0\right)}{\rho}e^{-\frac{2C_m}{V_m-V_0}P}\right)^{-\frac{1}{2}}, \quad \textbf{(3.53)}$$

$$R_{0i}(P)=\frac{R_{pi}Z_{ci}(P)}{R_{pi}-Z_{ci}(P)}, \quad \textbf{(3.54)}$$

$$\alpha_i(P)=\frac{1}{2R_{0i}(P)C_{li}}\left[\frac{2R_{0i}(P)+R_{pi}}{R_{0i}(P)+R_{pi}}\right], \quad \textbf{(3.55)}$$

and

$$\beta_i(P) = \frac{1}{2R_{0i}(P)C_{li}}, \tag{3.56}$$

where ΔT_i is constant, representing the bias between the measured and estimated pulse transit time.

We combine Eq.(3.52) with Eq.(3.21) and it yields the equation which relates pulse arrival time to arterial blood pressure:

$$PAT_i(P) = l \cdot \left(\frac{V_m}{\rho C_m} e^{\frac{C_m}{V_m - V_0} P} - \frac{V_m - V_0}{\rho C_m} \right)^{-\frac{1}{2}} + \tau_c(H) \cdot \left(\frac{DBP - P_{v,d}}{A(H)} \right)^{\frac{1}{\alpha}} + \Delta T_i \tag{3.57}$$

It is clearly shown in Eq.(3.57) that the relationship between pulse arrival time and arterial blood pressure is determined by both vascular and cardiac functions. In order to investigate the influence of different cardiac and vascular parameters to such a relationship, heart-arterial interaction is studied and related simulation results were shown in the next sections. In addition, we are particularly interested in revealing the mechanism under the correlation between PAT measured on the finger (upper body PAT) and SBP, DBP, MBP during dynamic exercise, since our experimental data indicated that PAT measured on the finger showed excellent linear correlations with SBP and MBP during our exercise experiments but failed to correlate strongly with DBP (for detail, see the experimental results in Chapter 5). We are also interested in revealing the roles played by PEP and PTT on the change of PAT under different physiological conditions.

3.2.4 Modeling heart-arterial interaction

In this section, we couple the pressure source model represented by Eq.(3.18)-(3.20) with the modified asymmetric T-tube model represented by Eq.(3.50-3.56) to study the heart-arterial interaction. The mechanical interactions between the left ventricle and the vascular system are idealized with the following assumptions: 1) aortic pressure ($P(t)$) is equals to the left ventricular pressure (p_v) during ejection; 2) aortic valve is closed when the flow rate into the aorta from the left ventricle is equal to zero.

The arterial flow follows the interaction between the heart and the arterial system. Ventricular volume (V_v) and outflow Q_v (equals to $Q(t,P)$ in Eq.(3.50)) are related as:

$$\frac{dV_v}{dt} = -Q_v . \tag{3.58}$$

The combined model can be solved numerically with an iteration scheme. An iteration loop starts at the onset of ventricule isovolumic contraction ($t=0$). As the ventricular contracts isovolumically,

the time course of p_v is given by Eq.(3.18), and p_v rises until an initially assumed valve for DBP is reached. Then, the aortic valve opens and the heart starts to eject. At each further time step, aortic flow (Q_v) is determined such that the increase in aortic pressure ($P(t)$) relative to diastolic blood pressure (DBP) matches the increase in p_v. The end of left ventricular ejection is reached when Q_v become negative, and it is further assumed that $Q_v=0$ in diastole. At the end of the first iteration is obtained and a new cycle calculated. The iteration continues until the difference in DBP between two successive iteration loops is less than 1%. The model has been programmed in Matlab 7.1 (The Mathworks, Inc.).

3.3 Simulation

3.3.1 Validation of the model

The model was tested by using available data from previous experiments on the anesthetized open-chest dogs reported in other literatures [29]. Table 3.2 listed values of all the cardiac and vascular parameters utilized in the validation. The parameters of pressure-source model are obtained from Mulier's [1] and Danielsen's [2-4] studies. For the modified asymmetric T-tube model, the parameters V_0, V_m and C_m are estimated from the dog's data reported in [40]. Tube effective lengths l_1 and l_1 are obtained from the dog's data summarized by Burattini and Campbell [43]. Parameters which characterize the load characteristics were separately assigned according to different vasoactive states, according to the group-averaged data reported in [29]. Other parameters in the T-tube model are variables determined by the instantaneous arterial blood pressure. We made use of the parameters listed in Table 3.2 to test if the new model is able to reproduce the mean blood pressure and flow data reported in [29] and also demonstrate the basic features of blood pressure and flow waveforms at different vasoactive states.

Table 3.3 shows the comparison of measured mean blood pressure and flow data reported in [29] and those estimated by the new model. The close agreement between measured and estimated data indicated that the new model is able to mimic the real hemodynamic conditions in dogs. Fig. 3.11 demonstrates the aortic blood pressure and flow waveforms simulated by the new model under different vasoactive states. This figure reveals several similar observations as reported by Campbell et al: a) due to enhanced wave reflections, the peak pressure occurred from early systole in basal state to late systolic in vasoconstricted state; b) due to reduced wave reflections the pronounced diastolic wave in basal state becomes less pronounced in vasodilated state. Fig. 3.12 shows the aortic blood pressure and flow waveforms measured from one dog in [29]. The simulated waveforms in Fig. 3.11 and waveforms on dog (Fig. 3.12) are close both in wave shapes and magnitudes of SBP, DBP and peak flow under different vasoactive states.

Table 3.2 Parameters of modified asymmetric T-tube model and modified pressure source model.

Pressure-source model (Eq. (3.18)-(3.20))					
Parameter	value	unit	Parameter	Value	Unit
a	*0.007*	*mmHg/ml*^{2}	$t_{p,min}$	*0.1859*	*s*
b	*5*	*Ml*	$t_{p,max}$	*0.2799*	*s*
c	*3.2*	*mmHg/ml*	$p_{p,min}$	*0.842*	
d	*1*	*mmHg*	$p_{p,max}$	*1.372*	
α	*3*		φ	*1.66*	
k_1	*4.0×10*$^{-4}$	*s ml*$^{-1}$	ν	*9.9*	
k_2	*1.5×10*$^{-6}$	*s ml*$^{-1}$	θ	*1.83*	
κ	*0.45*		η	*17.5*	
r_tauc	0.57207		*r_taur*	0.86231	
Modified asymmetric T-tube model (Eq.(3.50-3.56))					
Parameter	value	unit	Parameter	Value	Unit
ρ	*1050*	*kg · m*$^{-3}$	V_m	3.0	*ml*
V_0	0.1	*ml*	C_m	0.015	*ml · mmHg*$^{-1}$
l_1	*12*	*cm*	l_2	*30*	*cm*
ΔT_1	60	*ms*	ΔT_2	0	*ms*
Basal					
C_{l1}	*9.50×10*$^{-5}$	*ml · mmHg*$^{-1}$	R_{p1}	*94.8*	*mmHg · s · ml*$^{-1}$
C_{l2}	*1.76×10*$^{-4}$	*ml · mmHg*$^{-1}$	R_{p2}	*45.4*	*mmHg · s · ml*$^{-1}$
Vasoconstriction					
C_{l1}	*6.62×10*$^{-5}$	*ml · mmHg*$^{-1}$	R_{p1}	*138.1*	*mmHg · s · ml*$^{-1}$
C_{l2}	*0.91×10*$^{-4}$	*ml · mmHg*$^{-1}$	R_{p2}	*86.8*	*mmHg · s · ml*$^{-1}$
Vasodilation					
C_{l1}	*12.9×10*$^{-5}$	*ml · mmHg*$^{-1}$	R_{p1}	*81.2*	*mmHg · s · ml*$^{-1}$
C_{l2}	*3.04×10*$^{-4}$	*ml · mmHg*$^{-1}$	R_{p2}	*27.6*	*mmHg · s · ml*$^{-1}$

The values with italic style are those obtained from literatures. For detailed explanation, please refer to the text.

Table 3.3 Hemodynamic data reported in [29] and those estimated by the proposed model.

Vasoactive status	$\overline{P}$			$\overline{Q}$		
	$\overline{P_{meas}}$ (mmHg)	$\overline{P_{est}}$ (mmHg)	Error (%)	$\overline{Q}_{meas}$ (l · min^{-1})	$\overline{Q}_{est}$ (l · min^{-1})	Error (%)
Vasoconstricted	*135.7*	136.5	0.59	*2.62*	2.52	-3.82
Basal	*85.1*	85.4	0.04	*2.83*	2.74	-3.18
Vasodilated	*51.6*	53.1	2.91	*2.53*	2.52	-0.40

The values with italic style are those reported in [29].

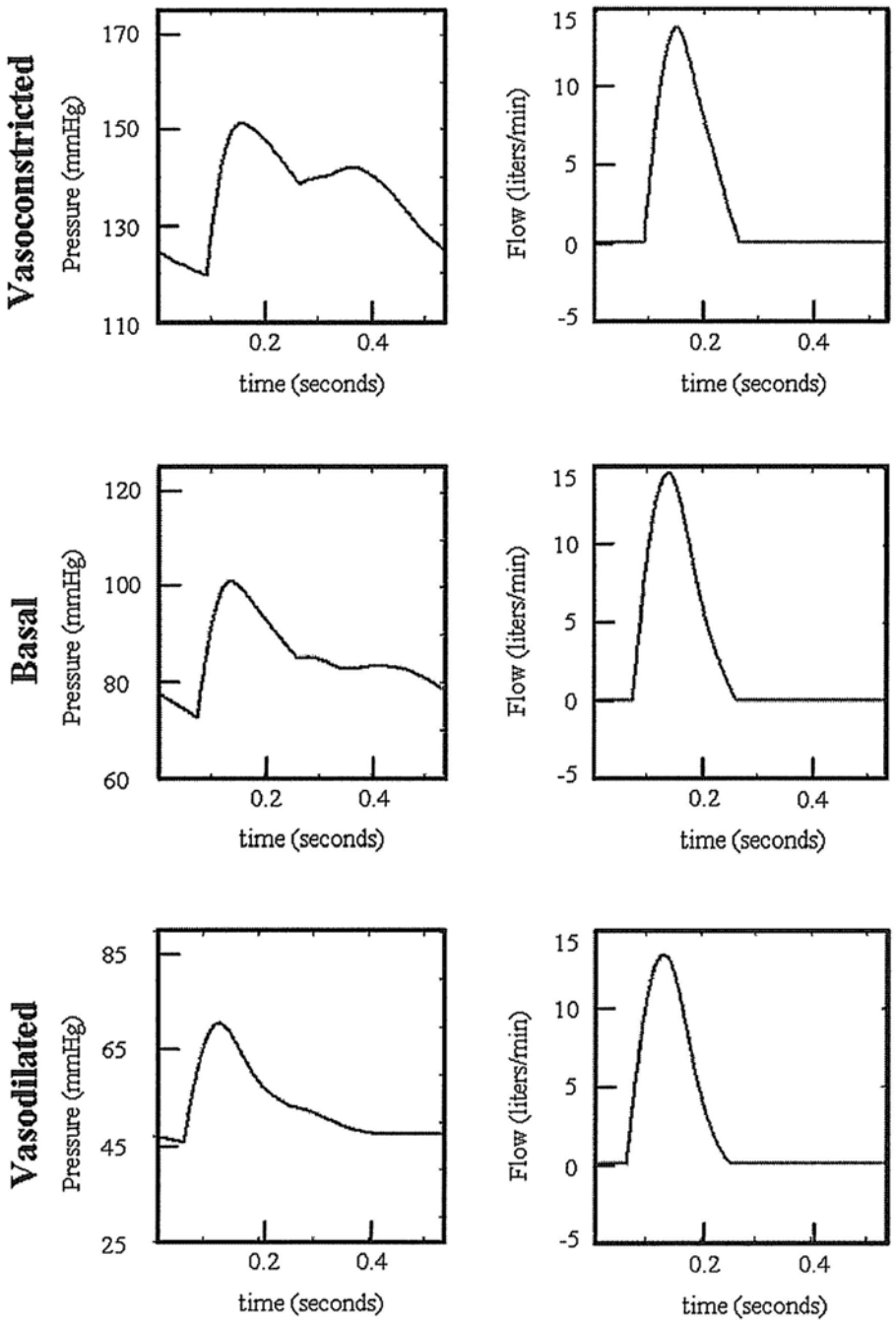

Fig. 3.11 Simulated aortic blood pressure (left column) and blood flow (right column) from the proposed model by using group-averaged T-tube parameters reported in [29] and selected ventricular parameters in this work.

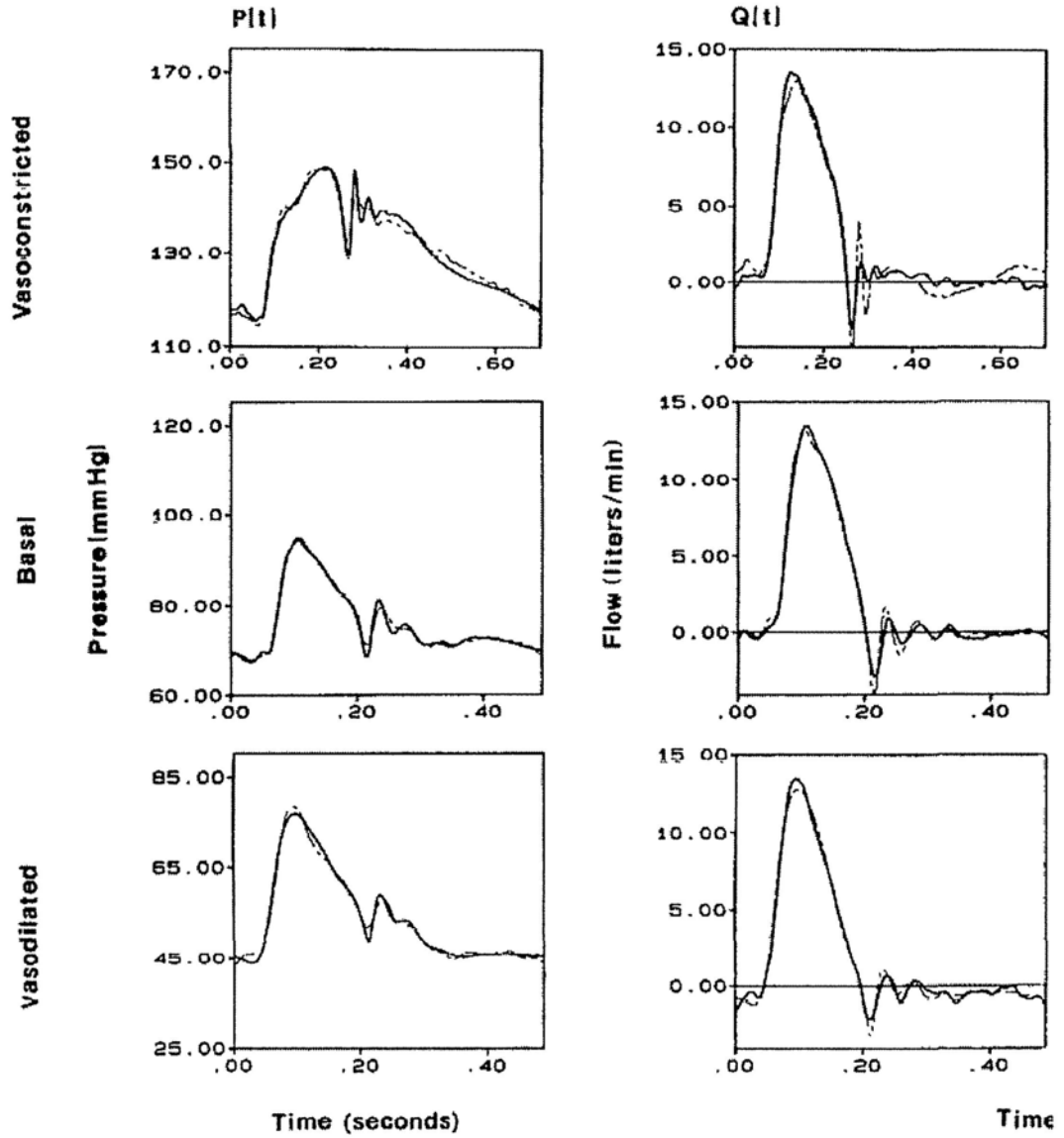

Fig. 3.12 Comparison of aortic blood pressure (left column) and blood flow (right column) waveforms measured from one dog (solid line) at different vasoactive states [29] and those simulated by the asymmetric T-tube model (dashed line) proposed in [29].

3.3.2 Effect of changing heart contractility (c)

The heart contractility (c) changes from 1 to 5 with a step of 0.1, while the parameters for HR, pre-load of the ventricle (end-diastole V_{vd}), upper and lower terminal peripheral resistance (R_{p1} and R_{p2}) and arterial stiffness (C_m) were kept unchanged. The effects of variations in heart contractility on various hemodynamic parameters are shown in Fig. 3.13. Systolic blood pressure (SBP), diastolic blood pressure (DBP), mean blood pressure (MBP) are defined as the highest value, end value and mean value of the aortic blood pressure wave at each cardiac cycle. Pulse pressure (PP) equals SBP minus DBP. Pre-ejection time (PEP) is the time delay from the start of ventricular contraction ($t=0$ in each cardiac cycle) to the time when aortic valve opens, and finger PTT equals to ΔT_1 plus the pulse transit time (T_1) calculated from the upper tube. Finger PAT is the summation of PEP and finger PTT. Stroke volume (SV) is the summation of left ventricular flow Q_v in a cardiac cycle and cardiac output (CO) is the product of SV and HR.

The increase of heart contractility enhanced the cardiac function, which is reflected by the rising stroke volume, cardiac output. Since aortic compliance is unchanging, the pulse pressure increases. The after-loads, SBP, DBP and MBP, are also augmented, under the same vascular states. Finger PAT, finger PTT and PEP are all decreasing with enhanced heart contractility.

Computational results show that finger PAT, finger PTT and PEP all have a significant negative correlation with SBP, DBP and MBP, respectively (r =-0.99, $p<0.01$, for all above). Fig. 3.14 demonstrates the changes in finger PAT in relations to SBP, DBP and MBP under changing heart contractility.

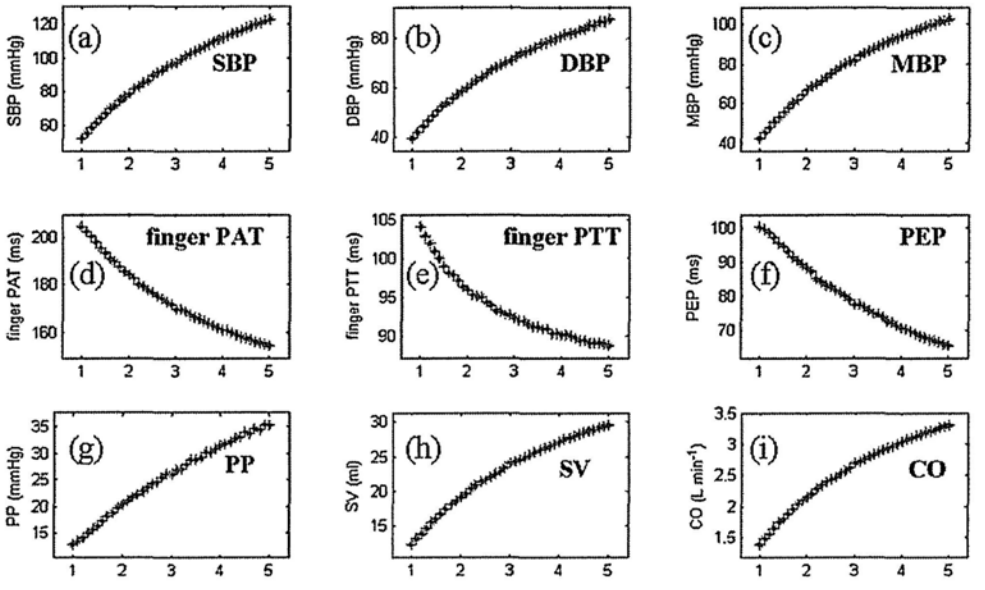

Fig. 3.13 Effects of changing heart contractility on hemodynamic characteristics (a) SBP, (b) DBP, (c) MBP, (d) finger PAT, (e) finger PTT, (f) PEP, (g) PP, (h) SV and (i) CO.

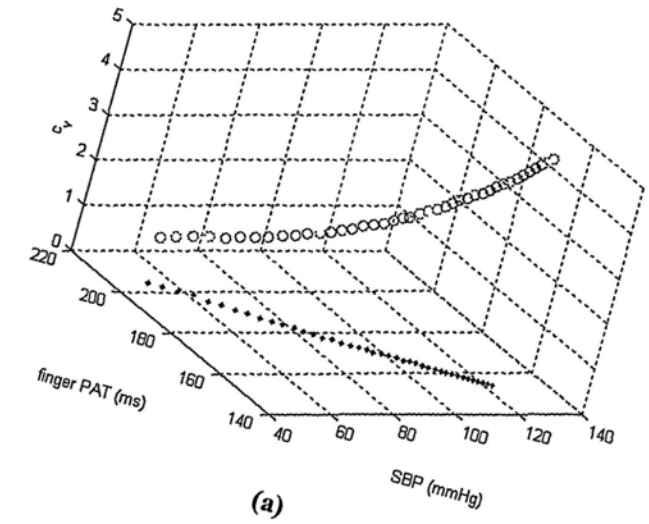

(a)

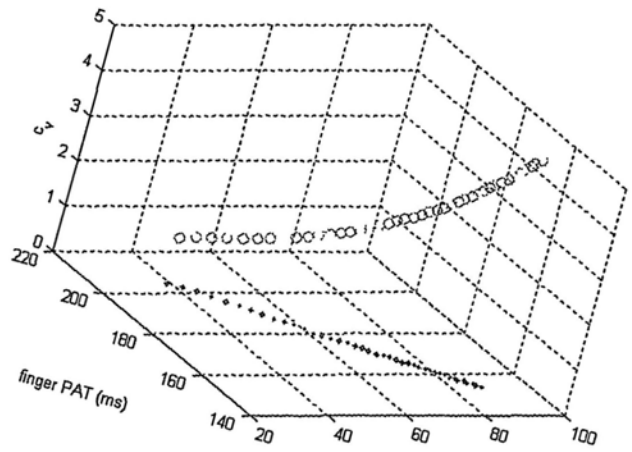

(b)

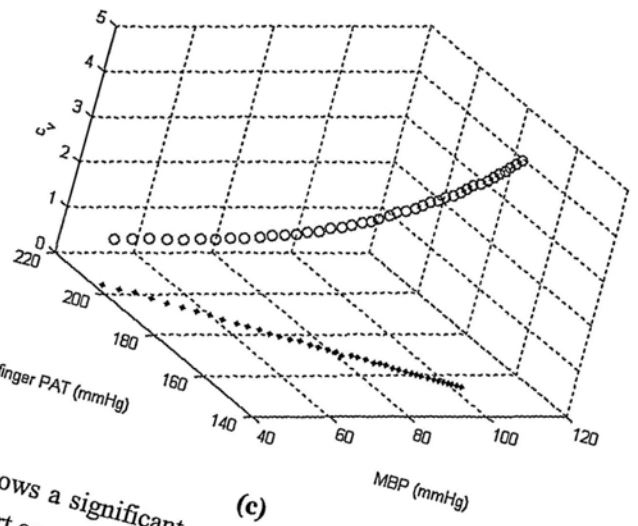

(c)

Fig. 3.14 Finger PAT shows a significant negative correlation with (a) SBP, (b) DBP and (c) MBP under changing heart contractility.

3.3.3 Effect of changing ventricular preload (V_{vd})

The end diastolic volume (V_{vd}) changes from 20 ml to 50 ml, with a step of 1 ml, while the parameters HR, heart contractility, upper and lower terminal peripheral resistance (R_{p1} and R_{p2}) and arterial stiffness (C_m) were kept unchanged. The effects of variations in ventricular preload on various hemodynamic parameters are shown in Fig. 3.15. The increase of pre-load brings similar changes to the model output variables as that of the enhancing heart contractility. The only exception is the pre-ejection, which decreased much less than that during increasing heart contractility.

Computational results show that finger PAT, finger PTT and PEP have significant negative correlations with SBP, DBP and MBP (r =-0.99, p<0.01, *for all*). Fig. 3.16 demonstrates the changes in finger PAT in relations to SBP, DBP and MBP with changing ventricular preload.

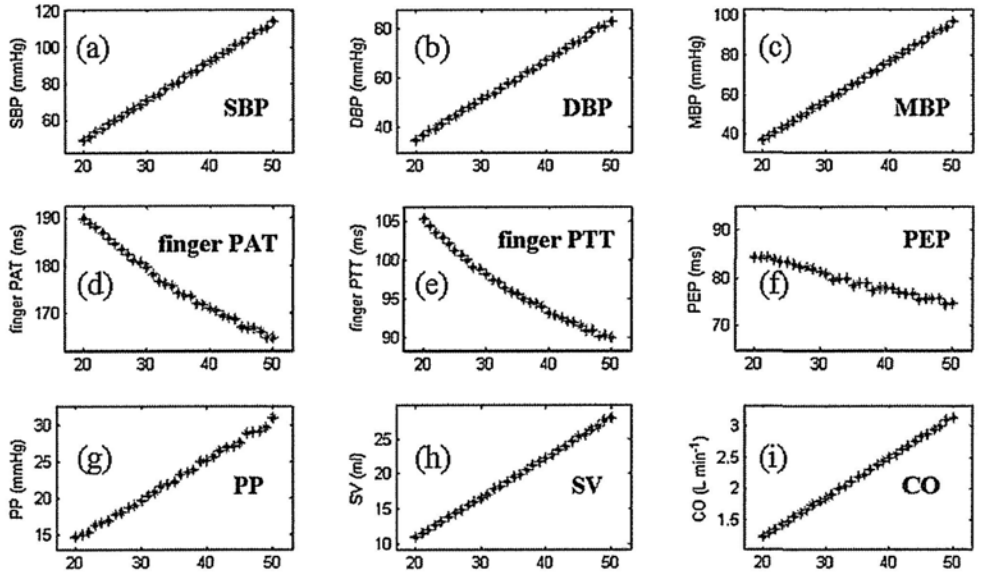

Fig. 3.15 Effects of changing ventricular preload on hemodynamic characteristics (a) SBP, (b) DBP, (c) MBP, (d) finger PAT, (e) finger PTT, (f) PEP, (g) PP, (h) SV and (i) CO.

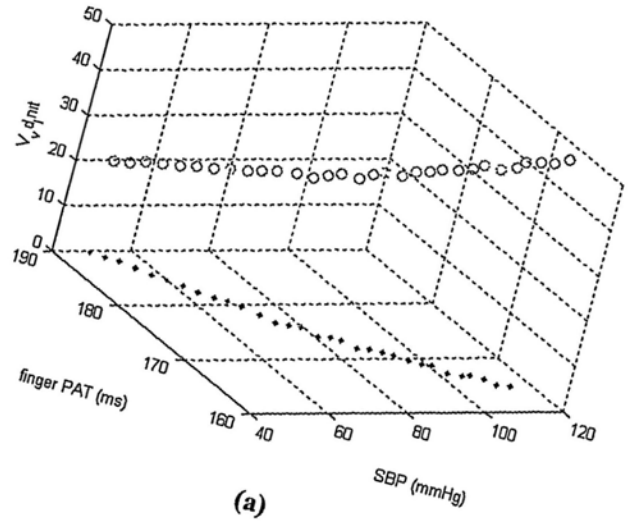

(a)

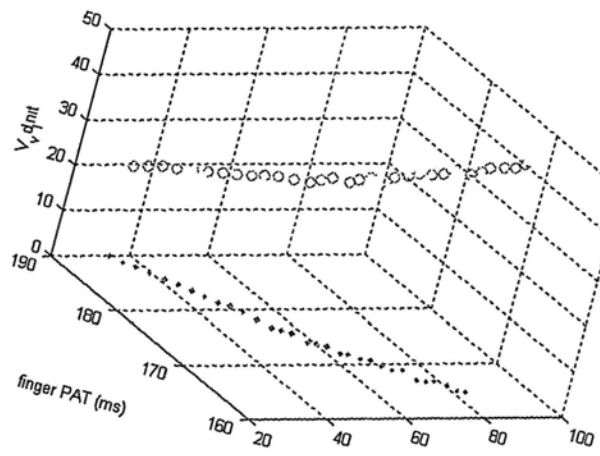

(b)

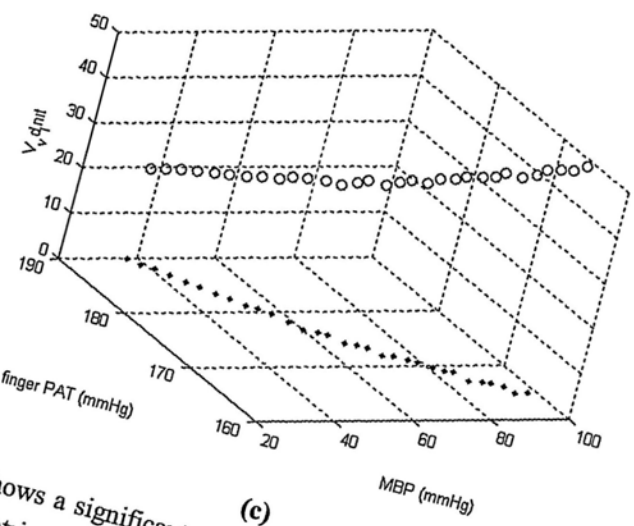

(c)

Fig. 3.16 Finger PAT shows a significant negative correlation with (a) SBP, (b) DBP and (c) MBP under changing ventricular preload.

3.3.4 Effect of changing lower (R_b) and upper (R_h) body peripheral resistances

The total peripheral resistance of the asymmetric T-tube model can be changed by varying either upper or lower tube peripheral resistance. Since finger PTT is measured on the upper branch, we separately change the upper and lower peripheral resistances to see the possible differences effects if any. First, the lower peripheral resistance (R_{p2}) was changed from 1 mmHg · s · ml^{-1} to 5 mmHg · s · ml^{-1} with a step of 0.1 mmHg · s · ml^{-1}, while other parameters including HR, heart contractility, pre-load of the ventricle (end-diastole V_v), arterial stiffness (C_m) and upper terminal peripheral resistance (R_{p1}) were kept unchanged. The effects of variations in lower peripheral resistance on various hemodynamic parameters are shown in Fig. 3.17.

Under the same cardiac function, the increased peripheral resistance elevated the SBP, DBP and MBP. However, PP decrease, which is consistent with the decreasing of stroke volume and cardiac output. The finger PTT and PEP show different changing trends with elevated peripheral resistance. Since PEP increased more than the drop of finger PTT, it dominate the changes of finger PAT.

Computational results show that both finger PAT and PEP has significant positive correlations with SBP, DBP and MBP ($r = 0.99$, $p<0.01$), meanwhile, finger PTT has significant negative correlations with SBP, DBP and MBP ($r = -0.99$, $p<0.01$). Fig. 3.18 demonstrates the changes in finger PAT in relations to SBP, DBP and MBP.

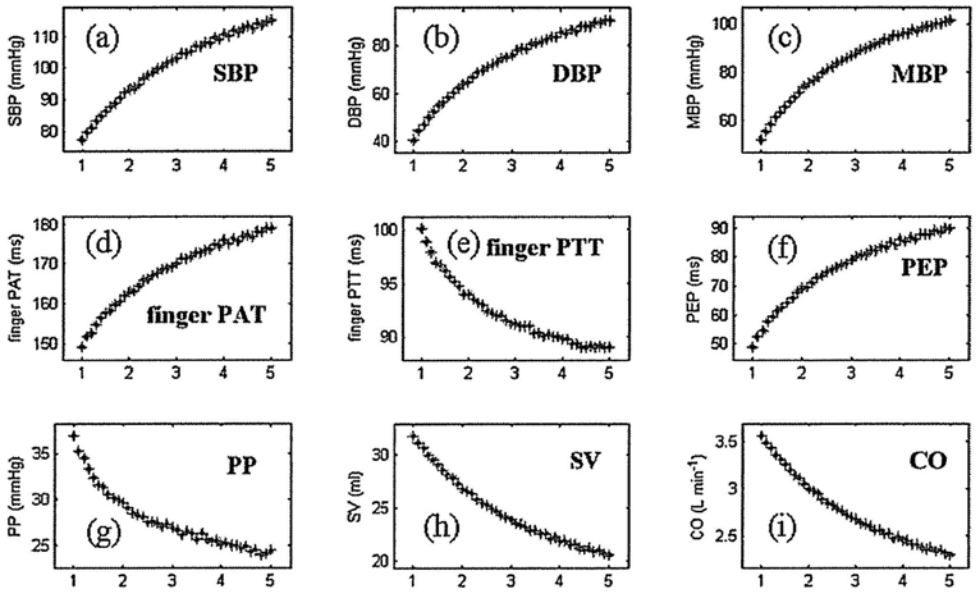

Fig. 3.17 Effects of changing lower body peripheral resistance on hemodynamic characteristics (a) SBP, (b) DBP, (c) MBP, (d) finger PAT, (e) finger PTT, (f) PEP, (g) PP, (h) SV and (i) CO.

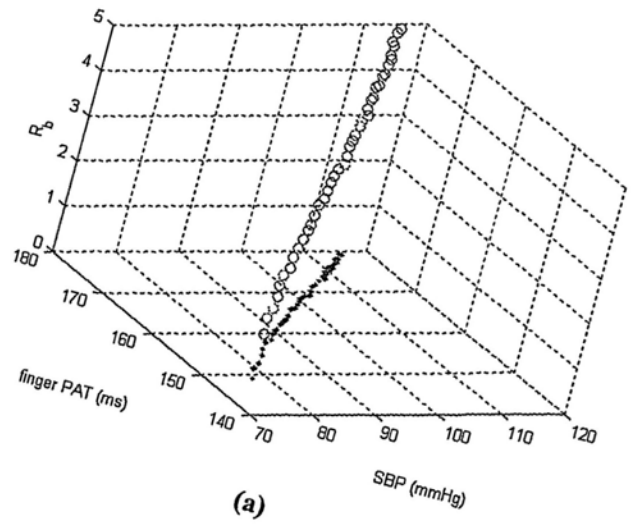

(a)

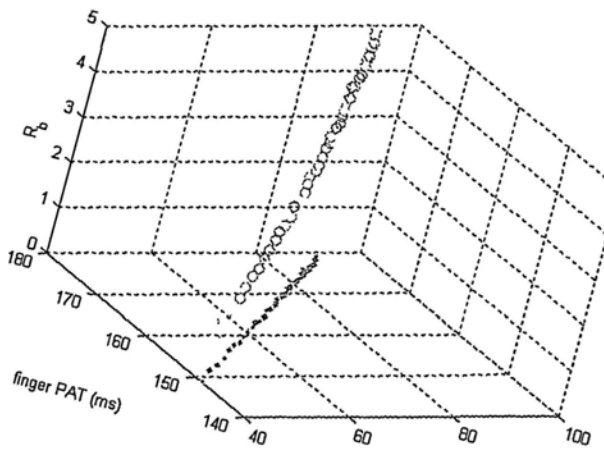

(b)

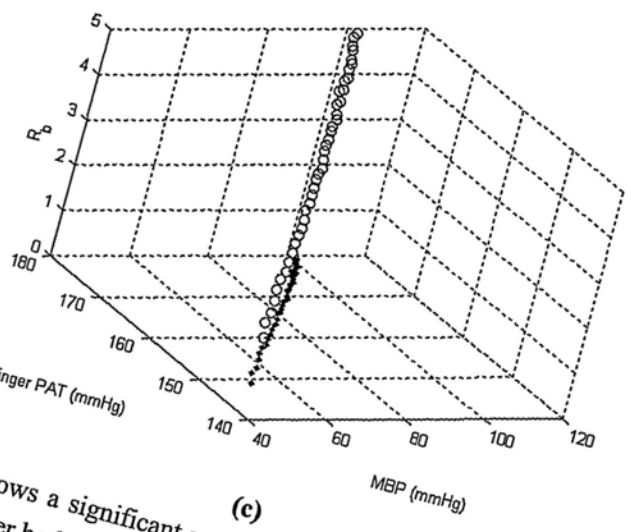

(c)

Fig. 3.18 Finger PAT shows a significant positive correlation with (a) SBP, (b) DBP and (c) MBP under changing lower body peripheral resistance.

Second, the upper body peripheral resistance (R_{p1}) was changed from 2 mmHg · s · ml^{-1} to 10 mmHg · s · ml^{-1} with a step of 0.2 mmHg · s · ml^{-1}, while other parameters including HR, heart contractility, pre-load of the ventricle (end-diastole V_{vd}), arterial stiffness (C_m) and lower terminal peripheral resistance (R_{p2}) were kept unchanged. The effects of variations in lower peripheral resistance on various hemodynamic parameters are shown in Fig. 3.19. The changes of model output variable induced by increased R_{p1} have qualitative similarity to the changes induced by R_{p2}, except for the pulse pressure, which is almost unchanging. The changes of SV, CO, SBP and PEP are almost the same as that induced by R_{p2}. The quantitative changes of other parameters, however, are much smaller than that induced by R_{p2}. For example, the drop of DBP is just half of that induced by R_{p2}.

Computational results show that both finger PAT and PEP have significant positive correlations with SBP, DBP and MBP ($r = 0.99$, $p<0.01$), meanwhile, finger PTT has significant negative correlations with SBP, DBP and MBP ($r = -0.99$, $p<0.01$). Fig. 3.20 demonstrates the changes in finger PAT in relations to SBP, DBP and MBP.

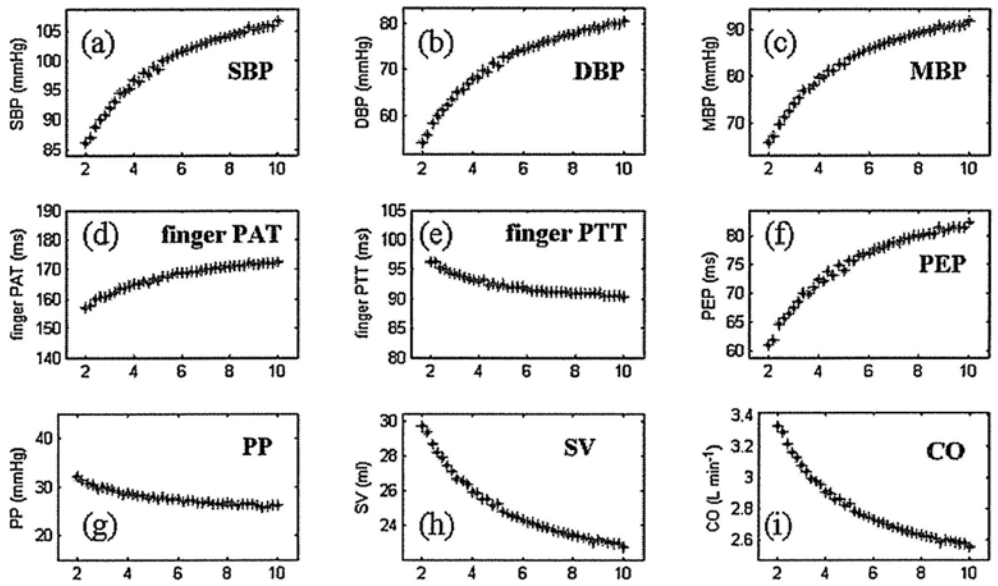

Fig. 3.19 Effects of changing upper body peripheral resistance on hemodynamic characteristics (a) SBP, (b) DBP, (c) MBP, (d) finger PAT, (e) finger PTT, (f) PEP, (g) PP, (h) SV and (i) CO.

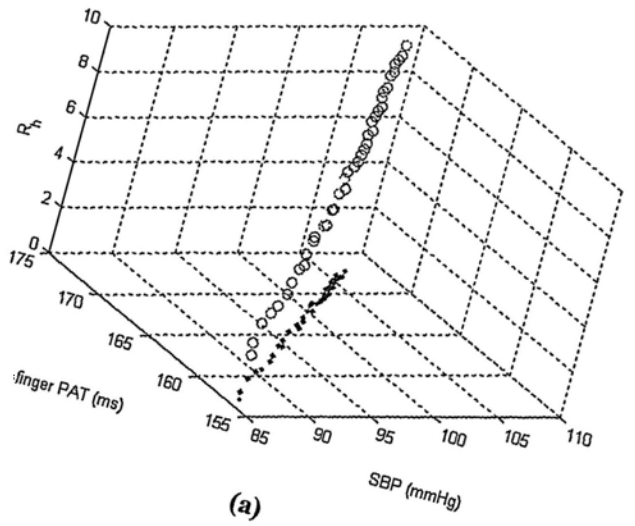

(a)

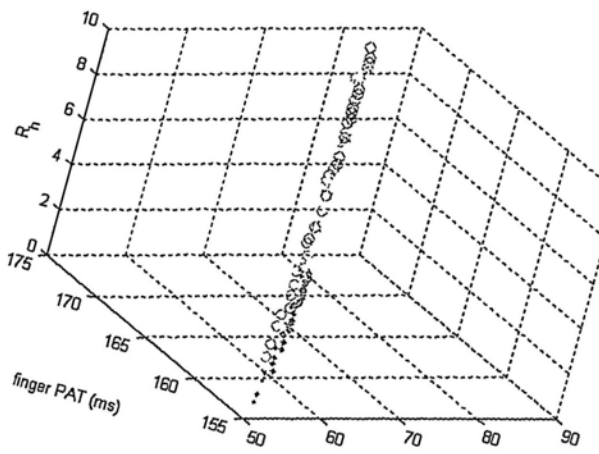

(b)

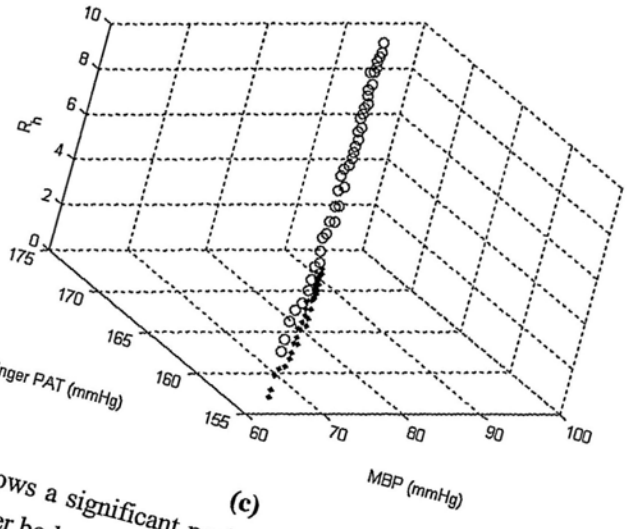

(c)

Fig. 3.20 Finger PAT shows a significant positive correlation with (a) SBP, (b) DBP and (c) MBP under changing upper body peripheral resistance.

3.3.5 Effect of changing heart rate (HR)

HR changes from 60 beats min^{-1} to 200 beats min^{-1}, with a step of 5 beats min^{-1}, while the other parameters heart contractility, preload, upper and lower terminal peripheral resistance (R_{p1} and R_{p2}) and arterial stiffness (C_m) were kept unchanged. The effects of variations in HR on various hemodynamic parameters are shown in Fig. 3.21. The SBP and DBP increase phase in phase with rising of heart rate, which make pulse pressure nearly a constant. Finger PTT decreases with heart rate increases, while the changes of PEP fluctuate with heart rate changing. The trend of PAT changes is roughly decreasing whereas with fluctuation similar to that of PEP. Stroke volume curve roughly decreases with increasing heart rate, where a small increase happens at the middle of the curve. Cardiac output increases as heart rate increases.

Computational results show that finger PAT, finger PTT and PEP have significant negative correlations with SBP, DBP and MBP ($p<0.01$ for finger PAT and PTT, $p<0.05$ for PEP). The correlation coefficients between finger PTT and BP values are -0.99. The correlation coefficients for finger PAT are: finger PAT versus SBP (r = -0.89); finger PAT versus DBP (r = -0.87); finger PAT versus MBP (r = -0.87). The correlation coefficients for PEP are: PEP versus SBP (r = -0.46); PEP versus DBP (r = -0.41); finger PAT versus MBP (r = -0.42). Fig. 3.22 demonstrates the changes in finger PAT in relations to SBP, DBP and MBP under changing heart rate.

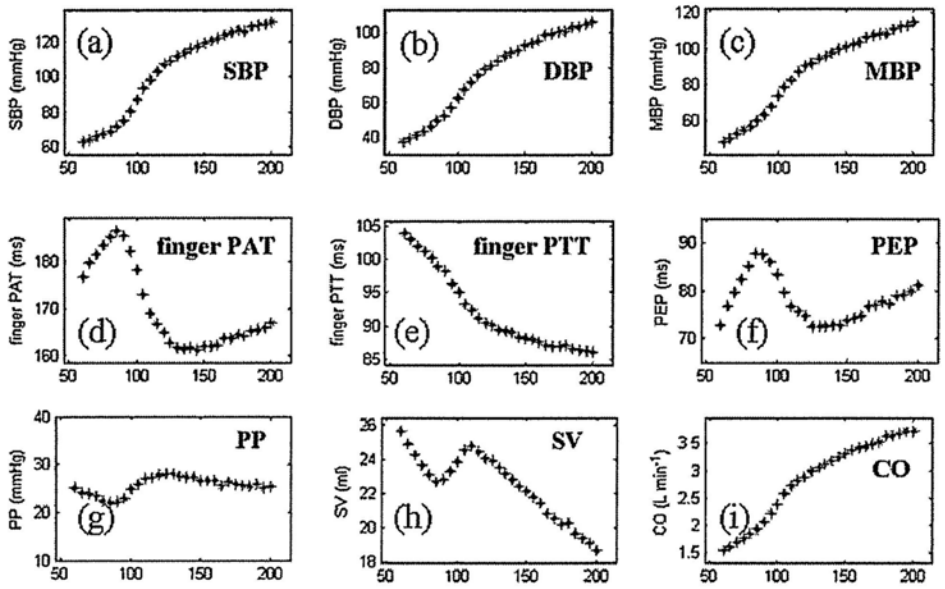

Fig. 3.21 Effects of changing heart rate on hemodynamic characteristics (a) SBP, (b) DBP, (c) MBP, (d) finger PAT, (e) finger PTT, (f) PEP, (g) PP, (h) SV and (i) CO.

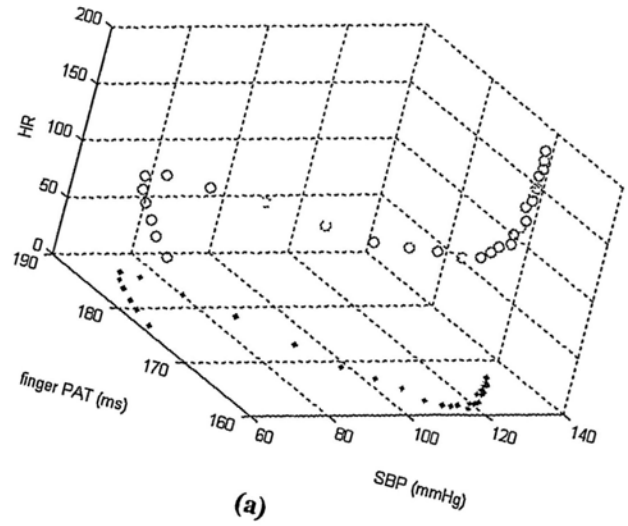

(a)

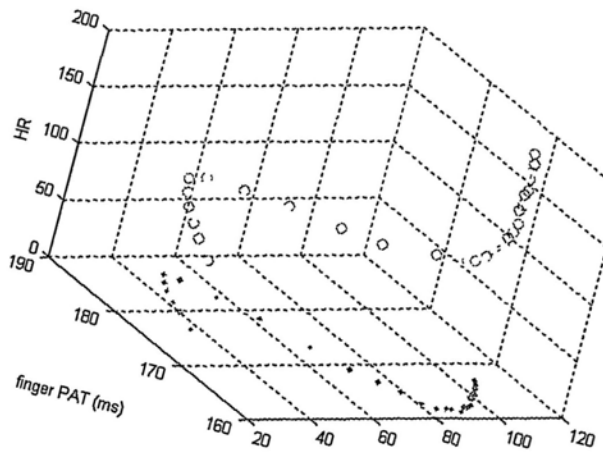

(b)

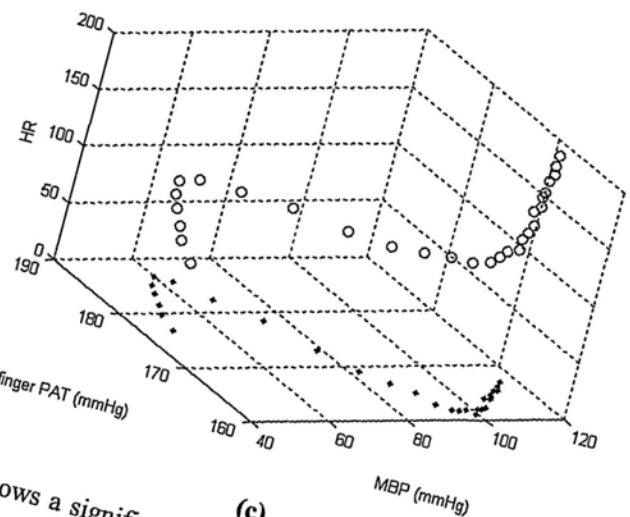

(c)

Fig. 3.22 Finger PAT shows a significant negative correlation with (a) SBP, (b) DBP and (c) MBP under changing heart rate.

3.3.6 Effect of changing arterial compliance (C_m)

Maximal tube compliance changes from 0.005 to 0.05 ml $mmHg^{-1}$, with a step of 0.001 ml $mmHg^{-1}$, while the other parameters heart contractility, preload, upper and lower terminal peripheral resistance (R_{p1} and R_{p2}) and heart rate were kept unchanged. The effects of variations in C_m on various hemodynamic parameters are shown in Fig. 3.23. The variation of maximal tube compliance does not result in wide changes in most of the model output variables, expect for the pulse pressure, which decreases by a certain amount due an increase in DBP and decrease in SBP with changes of C_m

As shown in Fig. 3.23, magnitude of the finger PAT changes is within a small range and the changing trend is dominated by the rise of PEP at the beginning and dominated by the falling down of finger PTT at the middle to the end, which results in an insignificant correlation coefficient between finger PAT with DBP, SBP and MBP. Finger PTT shows a significant, negative correlation with DBP (r = -0.81, $p<0.01$) and MBP (r = -0.89, $p<0.01$) whereas a significant, positive correlation with SBP (r = 0.66, $p<0.01$). PEP shows a significant, positive correlation with DBP (r = 0.99, $p<0.01$) and MBP (r = 0.97, $p<0.01$) whereas a significant, negative correlation with SBP (r = -0.86, $p<0.01$). Fig. 3.24 demonstrates the changes in finger PAT in relations to SBP, DBP and MBP under changing maximum tube compliance.

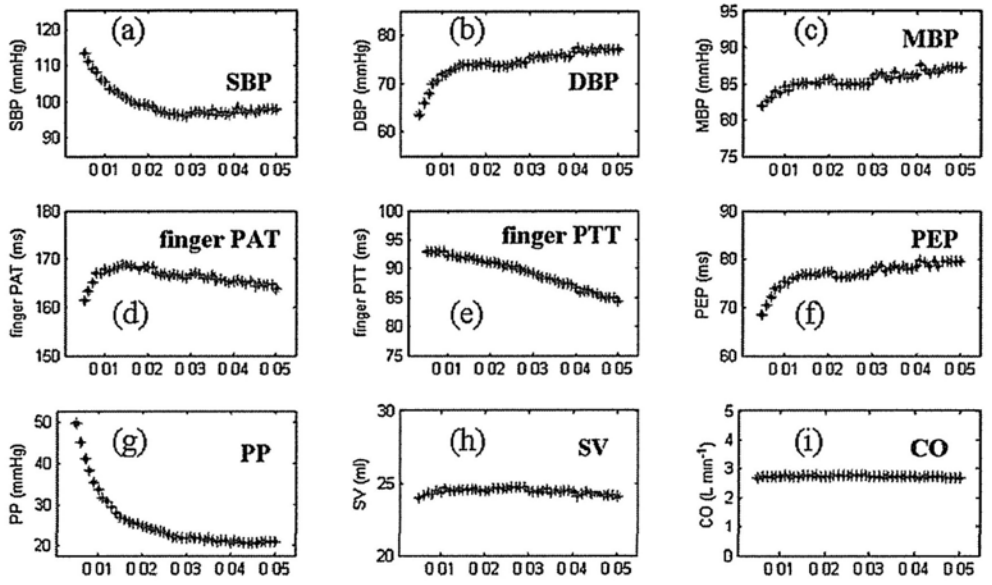

Fig. 3.23 Effects of changing arterial compliance on hemodynamic characteristics (a) SBP, (b) DBP, (c) MBP, (d) finger PAT, (e) finger PTT, (f) PEP, (g) PP, (h) SV and (i) CO.

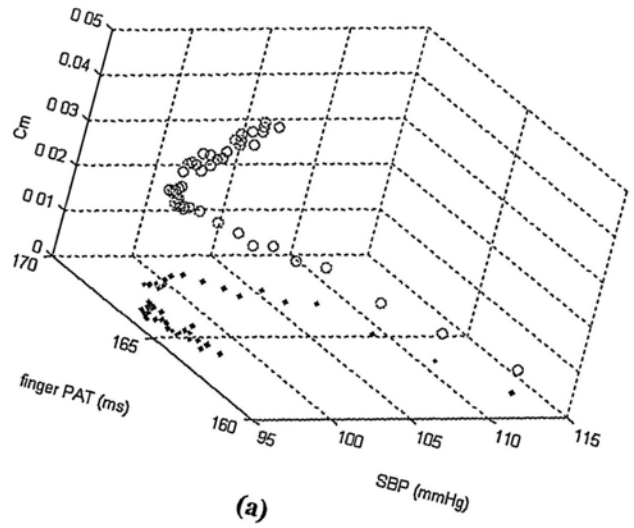

(a)

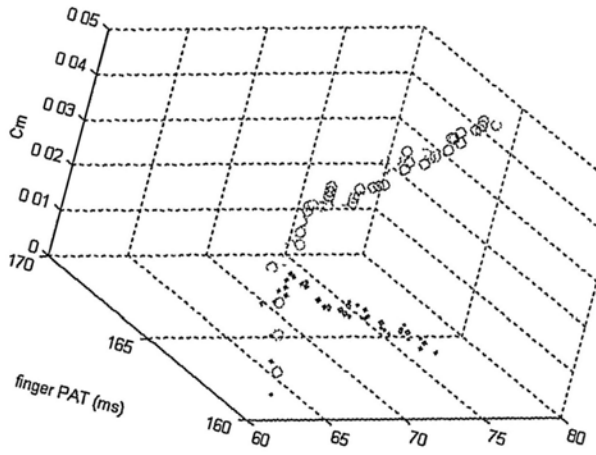

(b)

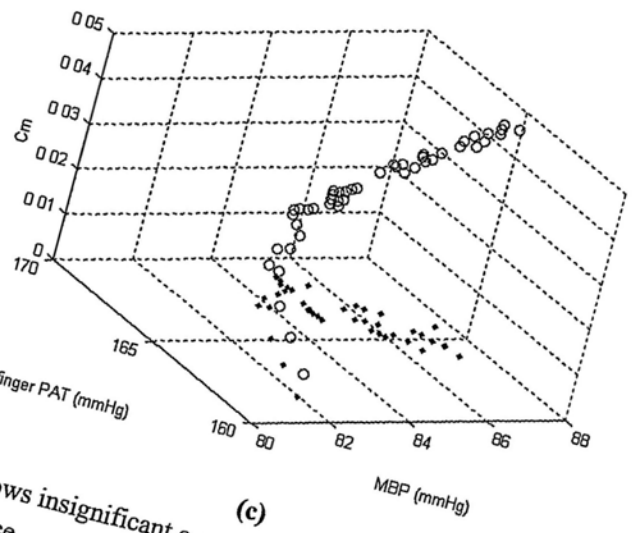

(c)

Fig. 3.24 Finger PAT shows insignificant correlation with (a) SBP, (b) DBP and (c) MBP under maximum tube compliance.

3.3.7 Simulation on mimic exercise condition

In this section, model parameters were changed in a trend to mimic the condition of dynamic exercise. Dynamic exercise increases HR from a resting level of 65-75 beats min^{-1} to individual maximum HR (around 200 beats min^{-1} for at age 20 years, but falling by around 1 beat/min per year). During exercise, two factors inducing more venous return increase the end-diastolic ventricular volume (V_{vd}). One is the increased negative pressure inside the thorax during inspiration that results from larger tidal volume. The other is external compression of veins in the moving limbs by muscle contraction (muscle pumping) and in the abdomen by abdominal wall muscle activity during expiration. The heart contractility (c) is enhanced by the presence of sympathetic activation, meanwhile, the smooth muscle in the proximal aorta receives a sympathetic innervation and contraction of these muscle cells reduces aortic compliance (C_m). In the peripheral, due to the sharp increase of metabolic level of the skeletal muscle, the local blood flow can increase by 10-20 folds compared with the values at rest, which results in the peripheral vessel dilation and a reduction of peripheral resistance.

According the exercise cardiology mentioned above, we change the model parameters as follows:
HR: from 110 to 200 $beats\ min^{-1}$, with a step of 4.5 $beats\ min^{-1}$;
V_{vd}: from 40 to 60 ml, with a step of 1 ml;
Contractility (c): from 3 to 6, with a step of 0.15;
C_m: from 0.015 to 0.007 $ml\ mmHg^{-1}$, with a step of -0.0004 $ml\ mmHg^{-1}$;
R_h: 6 to 2 $mmHg \cdot s \cdot ml^{-1}$, with a step of -0.2 $mmHg \cdot s \cdot ml^{-1}$;
R_b: 3 to 1 $mmHg \cdot s \cdot ml^{-1}$, with a step of -0.1 $mmHg \cdot s \cdot ml^{-1}$;

The effects of dynamic exercise on various hemodynamic parameters are shown in Fig. 3.25. In Fig. 3.25, the x axis demonstrates the exercise levels indicated by changes of model parameters according to their trends mentioned above. Stroke volume and cardiac output increases significantly with higher exercise level. SBP also increases sharply, while DBP increases at the lower exercise level and decreases at the higher levels. MBP also rises by a large amount whereas drops a little at the very high exercise levels. PEP decreased obviously, while the change of finger PTT is not much. Finger PAT decreases as exercise level increases.

Finger PAT shows significantly high and negative correlations with SBP (r = -0.99, $p<0.01$) and MBP (r = -0.93, $p<0.01$) whereas a moderate correlation with DBP (r = -0.65, $p<0.01$). Finger PTT only shows moderate correlation with DBP during dynamic exercise (r = -0.65, $p<0.01$). PEP shows similar correlations to BP values to the situation of finger PAT: PEP versus SBP (r = -0.97, $p<0.01$); PEP versus MBP (r = -0.90, $p<0.01$); PEP versus DBP (r = -0.59, $p<0.01$). Different from the case of PEP and finger PAT, finger PTT shows a significantly high, negative correlation with DBP (r = -0.97, $p<0.01$). The correlations of PTT to MBP and SBP are r = -0.95, $p<0.01$ and r = -0.80, $p<0.01$, respectively.

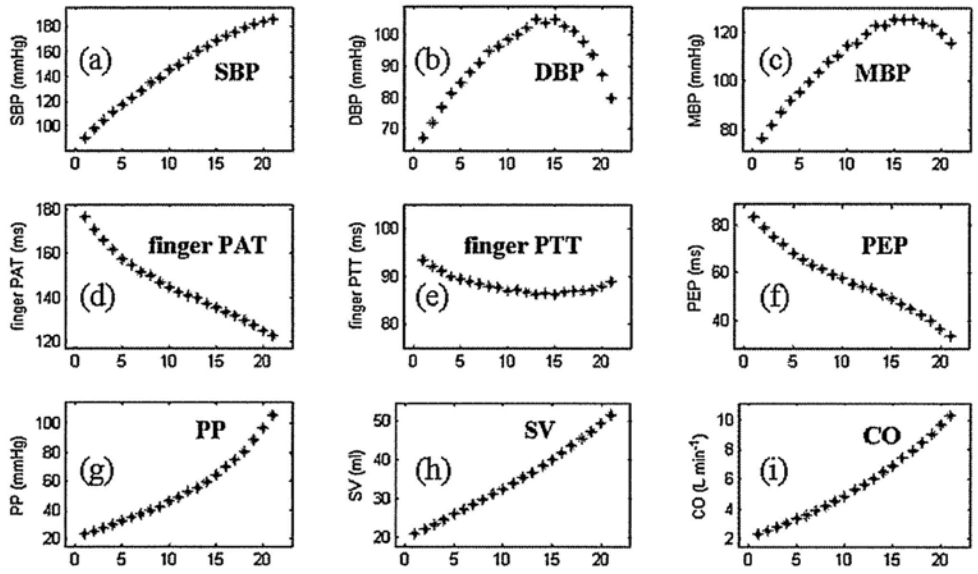

Fig. 3.25 Effects of dynamic exercise on hemodynamic characteristics (a) SBP, (b) DBP, (c) MBP, (d) finger PAT, (e) finger PTT, (f) PEP, (g) PP, (h) SV and (i) CO.

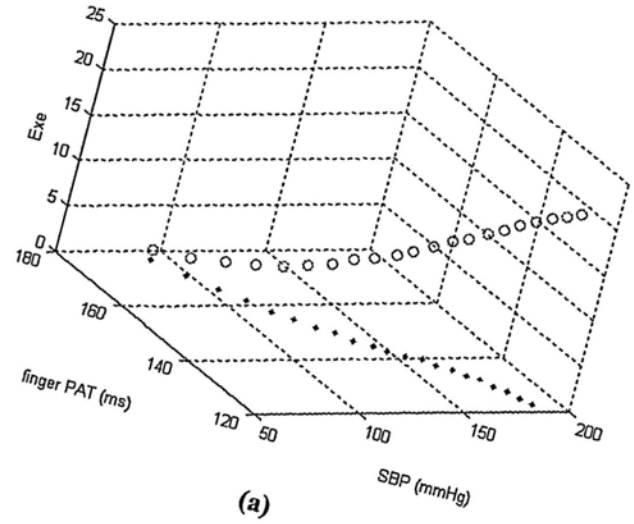

(a)

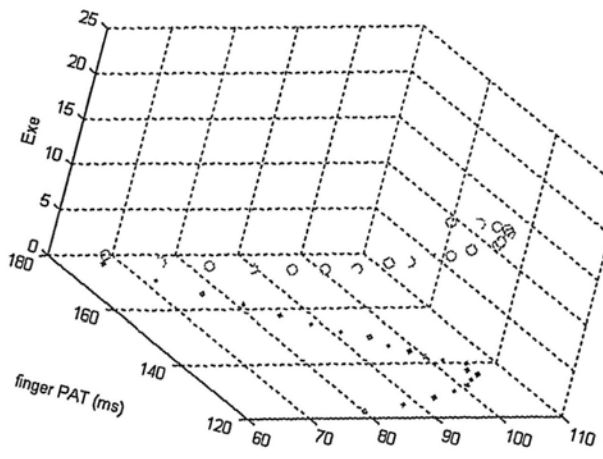

(b)

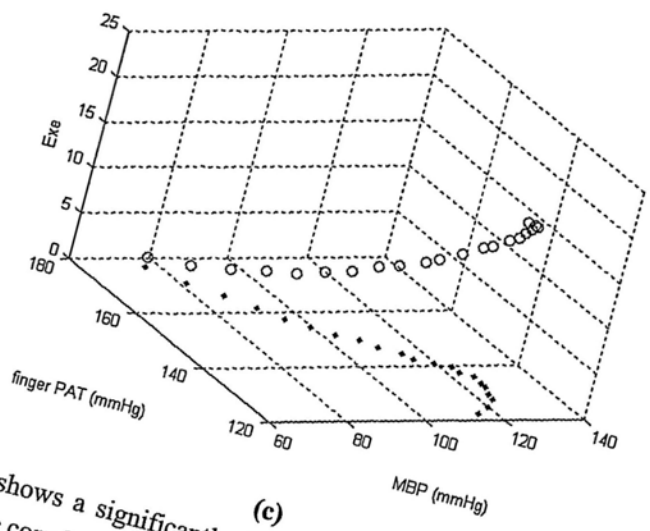

(c)

Fig. 3.26 Finger PAT shows a significantly high and negative correlation with (a) SBP, (b) DBP and lower negative correlation with (c) MBP under mimic exercise condition.

3.4 Discussion

In the previous sessions, mechanical events of the cardiac cycle are described by using a modified electrical model of heart-arterial system proposed in this study. We validated the current model using the reported real animal data in [29]. The results show that the mean blood pressure and blood flow data estimated from the proposed model agree well with the reported real animal data. And the blood pressure and flow curved simulated by the proposed model are visually comparable to the reported measured curves in [29]. Thus we claimed that the new model is validated. However, such a model validation method may be limited in several aspects. First of all, some data useful for model validation may be not included in the experimental data reported in the literature. For example, a parameter namely the normalized root-mean-square error, e*, was calculated in [29] to report the accuracy of their model to predict real pressure and flow data. e* is calculated by: $e^* = \frac{1}{n}\sqrt{\sum_{i=1}^{n} e(i)^2}$, where n is the number of data points and i represents the *ith* point. *e(i)* is the normalized residual error calculated from $e(i) = \frac{V(i) - \hat{V}(i)}{\overline{V}}$, where *V(i)* and $\hat{V}(i)$ are the respective sampled values of the measured and model-generated waveforms of the output variable, either *P(t)* or *Q (t)* in [29]. Therefore, a direct and quantitative comparison on the accuracy of their model and our model is available only if the e* of our model can be calculated. However, this is impossible, since in that case, we have to know the values of sampled *P(t) and Q(t)* curves measured in [29] but these data were not reported. Another limitation is the lack of knowledge on the accuracy of the measured data. The accuracy of the measured data may be influenced by many error sources such as device errors, wrong operations, interruptions during experiments, etc. And this may induce errors if the simulation results are compared with the measured data and cause the model validation unreliable, which is unknown to us since we are not involved in the real data collection.

After model validation, functional relationships are explored among the parameters identifying the cardiac and vascular aspects of model and the experimentally observed quantities such as pressure, flow, ejection time and so on. We discuss the significant functional relations between the characteristics of the cardiovascular system and the hemodynamic parameters and give a reasonable interpretation of the simulation results by interpreting the underlining mechanisms and related these results to the experimental observations. The cardiovascular conditions we are going to discuss are:

1. The effect of changing heart contractility;
2. The effect of changing preload;
3. The effect of changing upper and lower body peripheral resistance;
4. the effect of changing heart rate;
5. the effect of changing maximum tube compliance (arterial stiffness);
6. the effect of dynamic exercise

The effect of changing heart contractility

Enhanced heart contractility increases the active tension of the heart muscle, which speeds up the rising of isovolumic ventricular pressure and reduces the pre-ejection time. During ejection, the heart muscle with higher contractility ejects more blood into the arterial system, which increases the stroke volume and cardiac output. Since peripheral resistance and arterial compliance are unchanging, the increased stroke volume further elevates the pulse pressure and the entire blood pressure waveform. According to Eq.(3.52), the elevated blood pressure waveform reduced the corresponding pulse transit time.

Table 3.4 Changes in cardiovascular and timing parameters on dogs reported in [44].

	Systolic pressure (mmHg)	Mean pressure (mmHg)	HR (bpm)	CO (l/min)	CVP (mmHg)	PWTT (msec)	PEP (msec)	m-PWTT (msec)
Control	127.5 ± 34.2	93.8 ± 28.4	126.3 ± 11.8	1.79 ± 0.54	4.3 ± 3.5	74.2 ± 16.1	71.7 ± 11.1	145.9 ± 20.5
Isoflurane	90.7 ± 20.7[a]	61.6 ± 16.1[a]	118.2 ± 13.0[b]	1.20 ± 0.40[a]	5.4 ± 3.8	87.8 ± 13.7[a]	66.5 ± 10.0[b]	154.3 ± 17.4[a]
Control	154.5 ± 15.3	120.1 ± 14.4	128.0 ± 10.8	1.65 ± 0.36	5.2 ± 4.4	59.0 ± 9.3	86.7 ± 16.6	145.7 ± 13.4
Nitroglycerine	127.7 ± 27.8[a]	94.7 ± 23.9[a]	140.3 ± 10.6[a]	1.95 ± 0.82	2.7 ± 2.7	70.9 ± 11.2[a]	68.8 ± 18.6[a]	139.7 ± 17.0[a]
Control	129.6 ± 10.8	112.9 ± 11.7	126.6 ± 12.0	1.62 ± 0.52	4.1 ± 2.5	65.1 ± 8.3	86.4 ± 16.8	151.6 ± 56.7
Hypovolemia	79.7 ± 13.9[a]	65.3 ± 12.1[a]	127.2 ± 19.4	0.75 ± 0.22[a]	0.9 ± 2.1[a]	75.7 ± 8.2[a]	86.4 ± 11.7	162.1 ± 15.0[a]
Control	168.6 ± 34.9	127.2 ± 22.5	123.9 ± 20.7	1.75 ± 0.33	4.3 ± 3.0	63.6 ± 12.4	68.9 ± 16.6	132.5 ± 15.9
Dobutamine	226.3 ± 39.6[a]	154.6 ± 23.3[a]	139.3 ± 43.3	3.33 ± 1.46[a]	5.4 ± 3.9	52.7 ± 8.7[a]	42.6 ± 5.9[a]	95.2 ± 9.6[a]
Control	159.6 ± 24.4	122.3 ± 15.9	127.0 ± 8.2	1.78 ± 0.43	4.0 ± 3.8	62.1 ± 8.4	80.3 ± 10.8	142.4 ± 7.7
Phenylephrine	190.3 ± 29.9[a]	151.3 ± 21.0[a]	112.3 ± 15.2[a]	1.22 ± 0.28[a]	8.1 ± 4.6[a]	50.2 ± 5.8[a]	97.9 ± 9.9[a]	148.1 ± 10.6[a]

PWTT: PTT; m-PWTT: PAT; CVP: central venous pressure.

As a result, in our simulation results, PEP changes phase to phase with PTT and all the timing components (PEP, PTT, PAT) show a negative correlation with blood pressure. This is consistent with the experimental observations in [44], where the timing components (PTT, PEP and PAT) were measured on dogs and their correlations with blood pressure were studied under hypotension and hypertension induced by drug interventions. Table 3.4 shows the changes of cardiovascular and timing parameters reported in [44], and Table 3.5 and Table 3.6 demonstrate the correlations between systolic pressure and timing components and those between mean pressure and timing components in [44], respectively. It is clearly shown in Table 3.4-3.6 that when changes in blood pressure is due to the myocardial contractility, i.e. after dobutamine influsion, PEP changes phase in phase with PTT and all timing components show a consistent and negtative correlation with systolic and mean blood pressure.

Table 3.5 Correlation between SBP and timing components on dogs reported in [44].

	PWTT		PEP		m-PWTT	
	Slope	r^2	Slope	r^2	Slope	r^2
Isoflurane	−0.412 ± 0.160	0.964	0.192 ± 0.072	0.806	−0.287 ± 0.124	0.840
Nitroglycerine	−1.314 ± 1.718	0.927	1.126 ± 1.270	0.966	0.378 ± 0.652	0.910
Hypovolemia	−0.229 ± 0.184	0.830	−0.078 ± 0.318	0.801	−0.295 ± 0.269	0.874
Dobutamine	−0.263 ± 0.145	0.861	−0.627 ± 0.295	0.919	−0.797 ± 0.254	0.928
Phenylephrine	−0.496 ± 0.368	0.954	0.825 ± 0.560	0.947	0.431 ± 0.459	0.717

PWTT: PTT; m-PWTT: PAT.

Table 3.6 Correlation between mean pressure and timing components on dogs reported in [44].

	PWTT		PEP		m-PWTT	
	Slope	r^2	Slope	r^2	Slope	r^2
Isoflurane	-0.505 ± 0.319	0.961	0.228 ± 0.116	0.826	-0.353 ± 0.221	0.836
Nitroglycerine	-0.797 ± 0.747	0.925	0.814 ± 0.350	0.974	0.282 ± 0.457	0.917
Hypovolemia	-0.272 ± 0.219	0.818	-0.114 ± 0.400	0.820	-0.367 ± 0.368	0.890
Dobutamine	-0.670 ± 0.508	0.853	-2.130 ± 1.957	0.810	-2.501 ± 1.842	0.903
Phenylephrine	-0.517 ± 0.380	0.959	0.838 ± 0.548	0.958	0.420 ± 0.443	0.725

PWTT: PTT; m-PWTT: PAT.

The effect of changing preload

According to the Frank-Starling mechanism of the heart, more filling of blood into the ventricle during diastole results in more stroke volume and cardiac output. Simulation results in Fig. 3.15 show that SV and CO increase with rising end-diastolic ventricular volume (EDV), which is consistent with Frank-Starling law. Results also show that the change of PEP with changing EDV is small (less than 10 ms), which agrees well with the previous experimental observations reported in [45]. As shown in Table 3.7, PEP changes from 74 ± 16 ms (PEEP=0 cm H_2O) and 83 ± 18 ms (PEEP=15 cm H_2O) at baseline to 73 ± 18 ms (PEEP=0 cm H_2O) and 83 ± 14 ms (PEEP=15 cm H_2O), respectively, when EDV was increased by arterial volume loading, and 82 ± 11 ms (PEEP=0 cm H_2O) and 92 ± 16 ms (PEEP=15 cm H_2O), respectively, when EDV was decreased with haemodilution blood. And no significant changes of PEP are seen from Table 3.7 under altering EDV. Since the changes of PEP is small, finger PTT dominates the changes of finger PAT and finger PAT decreases as pre-load increases.

Table 3.7 Hemodynamic data and cardiac preload variables reported in [45].

	Baseline		Volume loading		Haemorrhage	
	PEEP 0	PEEP 15	PEEP 0	PEEP 15	PEEP 0	PEEP 15
HR (bpm)	102 (17)	98 (28)	89 (14)[b]	92 (15)	92 (15)	93 (22)
MAP (mmHg)	62.6 (8.0)	44.1 (9.4)	80.0 (19.0)	67.8 (18.0)	45.1 (11.3)[c]	34.2 (10.8)
GEDV (ml)	366 (77)	289 (68)[a]	436 (96)	389 (110)	308 (95)[c]	262 (63)
ITBV (ml)	657 (115)	–	729 (241)	–	452 (93)[b,c]	–
TBV (ml)	1970 (364)	–	2131 (488)	–	1488 (570)[b,c]	–
CO ($l\ min^{-1}$)	1.8 (0.8)	1.2 (0.4)[a]	1.8 (0.3)	1.4 (0.4)	1.3 (0.4)[c]	0.7 (0.3)
SV (ml)	18.0 (8.1)	12.9 (7.1)	20.7 (4.0)	15.2 (4.4)	14.3 (5.1)[d]	8.4 (4.5)
PEP (ms)	74 (16)	83 (18)	73 (18)	83 (14)[a]	82 (11)	92 (16)[a]
AWPmean (mbar)	8 (3)	22 (4)[a]	8 (3)	20 (2)[a]	8 (2)	20 (2)[a]

PEEP: positive end-expiratory airway pressure (cm H_2O); HR: heart rate: MAP: mean arterial pressure; GEDV global end-diastolic volume, ITBV: intrathoracic blood volume; TBV: total blood volume: CO: cardiac output; SV stroke volume; PEP: pre-ejection period; AWPmean: mean airway pressure. All mean $\pm$ SD.
[a] $p < 0.05$. PEEP versus no PEEP at the same volaemic state.
[b] $p < 0.05$. versus no PEEP at baseline.
[c] $p < 0.05$. versus no PEEP after volume loading.
[d] $p < 0.001$. versus no PEEP after volume loading.

To conclude, variation in cardiac functions induced phase to phase changes of PEP and PTT,

which is inversely correlated with altered arterial blood pressure. As a result, PAT is an effective indicator of arterial blood pressure under such conditions.

The effect of changing upper and lower body peripheral resistance

The increase of lower peripheral resistance indicates the vasoconstriction in the lower body, which elevates arterial blood pressure. As a result, DBP, SBP and MBP rise with increase of R_{p2}. The augmented arterial blood pressure elevates the afterload to ventricular ejection, which decrease the stroke volume and cardiac output, as well as the pulse pressure, with a constant arterial compliance. Since DBP is the threshold for aortic valve opening, the increase of DBP lengthens the ventricular isovolumic contraction period, i.e. PEP. Meanwhile, the increase of arterial blood pressure causes a decrease of the finger PTT.

When the upper body peripheral resistance increases, both SBP and DBP are elevated; however, the increase of DBP is just half of that induced by lower body peripheral resistance while the increase extent of SBP is almost the same for changes of both lower and upper body peripheral resistances. One possible reason is the early arrival of upper body reflection wave. The augmented reflective wave from the upper body may arrive at the aortic root at systole, mainly elevates the systolic blood pressure, and contributes less to the diastolic blood pressure.

Table 3.8 Effect of increase in peripheral resistance only and decreases in total arterial compliance only on aortic and left ventricular pressure and on aortic flow reported in [46].

	Increase in R_p (208% ± 13) without change in capacitance (%)	Decrease in C (21% ± 4) without change in peripheral resistance (%)
RCT	208 ± 13	21 ± 4
SP	87 ± 6	62 ± 5
P_{ao}		
P_s	124 ± 4	115 ± 4
P_d	138 ± 7	52 ± 9
$\bar{P}$	133 ± 6	78 ± 3
P_{lv}		
P_s	124 ± 4	113 ± 3
$\bar{P}$	130 ± 7	116 ± 7
I_{ao}		
I_p	74 ± 2	66 ± 9
SV	66 ± 3	79 ± 5
$\bar{I}$	66 ± 3	79 ± 5

All changes are given as percent changes ± SE compared with the control situation. Six isolated hearts were studied. RCT = time constant of system, SP = steady power, P_{ao} = aortic pressure, P_s = systolic pressure, P_d = diastolic pressure, $\bar{P}$ = mean pressure, P_{lv} = left ventricular pressure, I_{ao} = aortic flow, I_p = peak flow, SV = stroke volume, and $\bar{I}$ = mean flow.

Changing peripheral resistance can be regarded as one representative form of the impact of altering afterload to the heart. And the simulation results obtained in this study are confirmed by the finding of previous experimental studies on isolated hearts. Utilizing a hydraulic model, Elzinga and Westerhof [46] varied the resistance and compliance independently while maintaining

the characteristic impedance constant in isolated feline left hearts. As shown in Table 3.8, they found that SBP and DBP increased when the peripheral resistance was elevated. Sunagawa et al [47] studied the heart-arteiral interaction by loading the isolated canine ventricles with computer simulated arterial input impedance which could precisely control the afterload. They found that, with the increase in resistance, PP decreased.

Further, with the parameters set in our simulation, the extent of PEP increasing is more than that of finger PTT decreasing, PAT thus shows a similar changing trend with PEP. This is also consistent with the experimental results obtained on dogs in [44]. As shown in Table 3.3-3.5, PEP and PTT change anti-phase with each other under either the vasodilation (decreasing R_p) caused by nitroglycerine infusion or the vasoconstriction (increasing R_p) by phenylephrine infusion; meanwhile, under these two conditions, PEP dominates the changes of PAT, which agrees with our simulation observations. The authors in [44] further indicated that PEP took as much as 68% of the PAT on dogs and hence was the major factor of PAT changes.

The effect of changing maximum tube compliance

When C_m increases, the aorta becomes more compliant; as a result, the same heart ejection produces less pressure rise inside the aorta. That's why the pulse pressure and systolic blood pressure decreases. In the diastole, larger compliance results in more stored blood during systolic, which slows the damping of the arterial blood pressure during diastole, resulting in a higher diastolic blood pressure and mean blood pressure. Since varying arterial compliance is another representative form of changing afterload, the previous experimental studies on isolated hearts [46, 47] also investigated the effect of arterial compliance on the cardiac function and they agree well with the simulation results in this study. As shown in Table 3.8, a decrease of arterial compliance caused an increase in systolic pressure and a decrease in diastolic and mean sortic pressure, which is consistent with our simulation results where SBP drops and DBP and MBP elevate under increasing arterial compliance. In [47], PP increased with rising arterial stiffness, which agrees with the simulation results that PP decreases with rising arterial compliance (decreasing arterial stiffness).

An increasing mean blood pressure induces a decreasing of finger PTT, while the increasing diastolic blood pressure sets a higher threshold for the ventricular pressure to open the aortic valve, which lengthens PEP. Hence, C_m causes inverse changes of PEP and finger PTT. However, it is worth noting that the changes of hemodynamic variables induced by variations of C_m are small, the correlations between PAT and arterial blood pressure are insignificant.

In Fig. 3.23, it shows that all investigated hemodynamic parameters except for pulse pressure change little with changing arterial compliances. Take stroke volume (SV) for example: compared with its sharp decrease with rising peripheral resistance, SV increases just a small amount with enhanced arterial compliance. This result agrees with the experimental observations which indicated that SV was far more sensitive to the change of peripheral resistance than that of the arterial compliance. Sunagawa et al [47] found that SV was decreased by about 5% under 50% decrease in arterial compliance and increased by about 3% under 100% increase in arterial

compliance. Elzinga and Westerhof [46] showed that SV decreased about 66% with a 4.8-fold increase in resistance, whereas it decreased only 27% when the compliance was tremendously decreased to one-twelfth. Ishide et al [48] have shown in a study in isolated canine left ventricles that SV decreased about 73% with a 6.3-fold increase in the resistance whereas it increased only 46% with a 30-fold increase in the compliance. These observations indicate that SV is far more sensitive to changes in the resistance than changes in compliance. This is quite consistent with our observations, even from a quantitative point of view (noting that peripheral resistance mentioned in these studies is total peripheral resistance, R_p, which is calculated from the upper, R_{p1}, and lower body , R_{p2} , peripheral resistances by: $R_p = \frac{R_{p1} \cdot R_{p2}}{(R_{p1} + R_{p2})}$).

The effect of changing heart rate

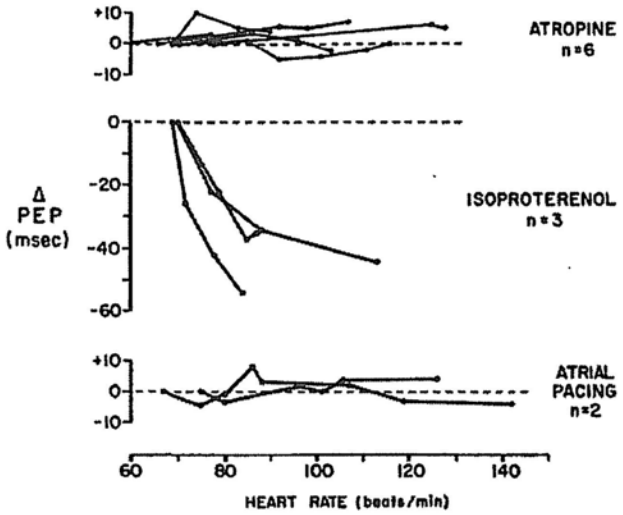

Fig. 3.27 Effects on PEP period of cardioacceleration by atropine, isoproterenol, and right atrial pacing reported in [49]. Each curve presents data from a normal subject. Three of the six subjects who received atropine (top panel) were restudied on another day with graded infusions of isoproterenol (middle panel).

When HR increases, heart period decreases, this will reduce the ventricular diastolic time and diastolic ventricular volume, then further decrease the heart ejection in each heart beat, i.e. stroke volume. However, since heart ejection frequency is sharply increased, the cardiac output increases, resulting in corresponding increasing in systolic blood pressure. When heart period decreases, the length of diastolic period decreases accordingly, which make the arterial blood pressure drop less during diastole and increases the diastolic blood pressure. The increases of both SBP and DBP cause a consistent decrease of PTT with heart rate. The increase in diastolic blood pressure elongates pre-ejection time; however, increased heart rate changes the activation function of ventricular pressure by increasing the peak pressure (p_p) and shortening the peak time (t_p), which results in a drop of PEP. As a result, PEP neither significantly increases nor significantly decreases

with changing heart rate, showing a combined impact of the above two opposite factors. This phenomenon have been previously confirmed in many experimental observations where the measured PEP was shown to be insensitive to change of heart rate. Fig. 3.27 shows the changing trends of PEP with increasing heart rate on normal human beings before and after drug and cardiac interventions (atropine, isoproterenol and atrial pacing) [49]: PEP is almost unchanging with interventions which only increase heart rate, e.g. atropine and atrial pacing, while, PEP drops significantly under infusion of isoproterenol, a drug which increases the heart contractility and decreases the diastolic blood pressure. In another study conducted on 26 normal volunteers, Dennis et al [50] also observed that PEP was almost constant with the increase of heart rate from mean 73.94±1.97 to 103.61±2.72 L min^{-1}, by either intravenous atropine administration or rapid right atrial pacing. Table 3.9 shows the experimental data reported in their study [50].

Table 3.9 systolic time intervals and heart rate before and after tachycardia reported in [50].

			I: Basal						*II: After tachycardia*					
Case No.	*Sex*	*Age (y)*	*HR min*	*QS_2 (ms)*	*LVET (ms)*	*PEP (ms)*	*PEP/ LVET*	*PEP_I/ $LVET_I$*	*HR min*	*QS_2 (ms)*	*LVET (ms)*	*PEP (ms)*	*PEP/ LVET*	*PEP_I/ $LVET_I$*
1	F	21	61·2	416·0	303·8	112·2	0·369	0·340	92·3	381·0	265·3	115·7	0·436	0·369
2	M	36	56·5	452·4	347·5	104·9	0·301	0·287	63·4	445·1	338·1	107·0	0·316	0·296
3	F	20	81·0	388·3	276·5	111·8	0·404	0·355	127·6	331·5	224·8	106·7	0·474	0·367
4	F	20	79·0	381·4	283·0	94·8	0·334	0·308	130·1	331·1	239·1	92·0	0·384	0·322
5	M	25	83·9	374·5	266·0	108·5	0·407	0·347	107·3	324·5	224·0	100·5	0·448	0·352
6	M	19	59·5	415·3	307·5	107·8	0·350	0·322	96·8	340·0	243·5	96·5	0·396	0·331
7	M	17	72·4	381·2	281·7	99·5	0·353	0·317	113·2	341·5	231·1	110·4	0·477	0·367
8	M	24	62·5	365·6	276·7	88·9	0·321	0·297	96·7	344·2	260·0	84·2	0·323	0·289
9	A	22	77·1	397·7	287·7	110·0	0·382	0·342	107·1	373·9	249·7	124·2	0·497	0·386
10	A	22	71·2	417·5	301·4	116·1	0·385	0·342	93·0	384·5	262·8	121·7	0·463	0·377
11	A	37	82·9	379·0	275·3	103·7	0·376	0·335	109·0	338·8	232·6	106·2	0·456	0·368
12	F	38	68·7	391·4	276·5	114·9	0·415	0·361	107·1	324·2	219·0	105·2	0·480	0·379
13	F	23	75·3	387·8	287·8	100·5	0·349	0·319	87·3	380·7	285·0	95·1	0·332	0·306
14	F	24	70·6	385·4	278·7	106·7	0·382	0·344	103·6	365·0	263·0	102·0	0·387	0·334
15	M	38	77·0	388·5	284·5	104·0	0·365	0·324	114·7	324·0	229·5	94·5	0·411	0·411
16	F	30	91·0	411·4	316·0	95·4	0·301	0·285	109·0	379·1	286·2	92·9	0·324	0·296
17	F	22	82·6	393·3	298·2	95·1	0·318	0·297	104·7	348·1	263·8	84·3	0·319	0·292
18	F	29	66·6	432·0	317·3	114·7	0·361	0·333	105·2	374·5	257·2	117·3	0·456	0·374
19	M	17	88·0	358·6	252·4	104·2	0·412	0·346	124·2	321·7	214·2	107·5	0·501	0·369
20	M	30	69·3	424·2	297·0	127·2	0·428	0·373	86·2	410·0	278·5	132·0	0·473	0·391
21	M	31	80·3	373·4	272·8	100·6	0·368	0·328	101·6	358·1	256·1	102·0	0·398	0·332
22	M	30	79·1	395·8	277·0	118·8	0·428	0·365	93·7	386·3	256·5	129·8	0·506	0·402
23	M	30	64·2	418·5	308·3	110·2	0·357	0·325	100·0	364·5	246·0	118·5	0·481	0·385
24	M (P)	30	93·7	361·5	259·5	102·0	0·393	0·333	111·1	344·0	243·3	100·7	0·414	0·335
25	M	34	67·7	418·5	298·7	119·8	0·401	0·354	100·0	371·4	243·0	128·4	0·528	0·407
26	M (P)	38	61·2	413·5	299·4	114·1	0·381	0·343	109·0	348·6	245·7	102·9	0·418	0·339
Mean		27·1	73·94	397·0	289·66	107·16	0·370	0·331	103·61	359·08	252·23	106·85	0·426	0·349
SEM			±1·97	±2·72 (548·29) ±3·20	±3·99 (412·41) ±3·09	±1·75 (136·73) ±1·61	±0·0071	±0·0047	±2·72	±5·79 (572·71) ±3·2	±5·09 (424·23) ±2·84	±3·26 (148·28) ±2·56	±0·0143	±0·007
Significance														

Abbreviations: HR: Heart rate; (P): right atrial pacing.
In parentheses: Corrected values for heart rate according to Weissler's regression equations.

The effect of dynamic exercise

During dynamic exercise, due to increased preload, heart contractility and decreased peripheral resistance, the stroke volume and cardiac output increase as increasing exercise level. Generalized sympathetic nervous system activation elevates SBP, due to a variety of factors. First, increased cardiac muscle contractility reduces end-systolic ventricular volume and increases stroke volume. Second, the smooth muscle in the proximal aorta receives a sympathetic innervation and contraction of these muscle cells reduces aortic compliance. This stiffening allows all of the energy of ejection to be used in pressure generation. Finally, sympathetic vasoconstrictor drive to vein stiffens these and mobilizes blood normally stores in the venous reservoir back into active

circulation, aiding cardiac filling and further increasing stroke volume.

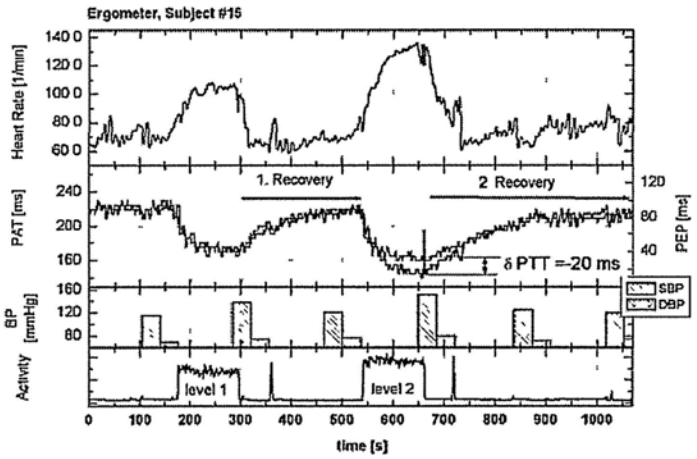

(a)

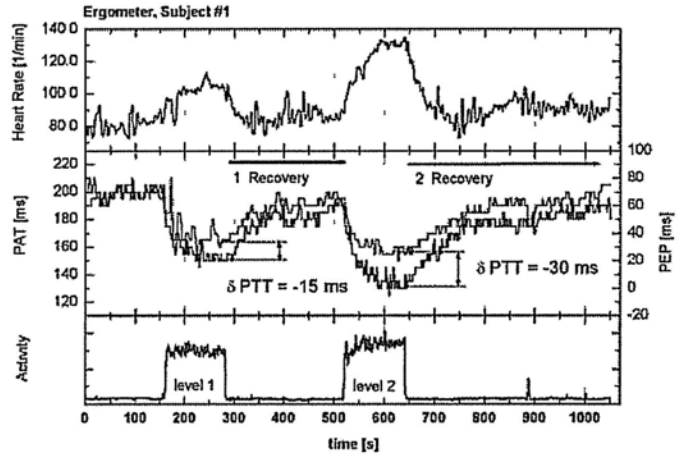

(b)

Fig. 3.28 Bicycle test of (a) a 25 years old male and (b) a 34 years old male. 1st: HR (t); 2nd: PAT (t) and the PEP (t), the PEP evolution follows closely the PAT; 3rd: (a) SBP and DBP measurement or (b) the subject's activity during the different phases; 4th: (a) the subject's activity during the different phases.

There are two main influencing factors of DBP. One is heart rate, since DBP respresents the lowest value of which pressure falls in the arteries before the next systolic ejection and must be influenced the period over which the pressure can fall, which determined by the heart rate. The other factor is the total peripheral resistance which determined the rate at which intra-arterial pressure falls after systolic ejection ceases. In Fig. 3.25, DBP first increase and then decrease in the dynamic exercise, which reflex the combination effects of the increasing heart rate and peripheral resistance. The resting MBP is more determined by DBP than SBP, whereas, during exercise, it has been pointed out that the contribution of DBP and SBP to MBP is almost half to half. MBP therefore shows a roughly increasing curve during dynamic exercise, with slightly damping when DBP drops a lot.

The changes of PEP during exercise is mainly determined by the cardiac functions, PEP hence shows a significant, consistent decrease due to the sharp increase of pre-load and heart contractility. The increase of DBP at lower exercise levels and decrease of DBP at the higher exercise levels changes the shape of the decreasing PEP curve, making it concave (slow decreasing) at the early exercise and convex (rapid decreasing) at the late exercise. PEP shows significantly high and negative correlation with SBP (r = -0.97, $p<0.01$) and MBP (r = -0.90, $p<0.01$) and moderate and negative correlation with DBP (r = -0.59, $p<0.01$).

The simulation results show that PAT has highest correlation with SBP amongst all timing components (PAT, PEP and PTT). This agrees with the previous experimental data obtained in exercise studies. Wong et al [51] measured the arterial blood pressure and timing components on 22 normotensive participants in post-exercise recovery and found that PAT showed the highest negative correlation with SBP (mean r=-0.81) as compared with that of PEP (mean r=-0.61) and PTT (mean r=-0.25). The simulation results further show that the changes of PAT during exercise is dominated by changing PEP due to enhanced heart function, while the magnitude of PTT changing is small (less than 10 ms). This result is strongly supported by the experimental observations in a bicycle exercise study conducted by Muehlsteff et al [52]. Fig. 3.28 shows two typical examples of changes of PAT and PEP as well as blood pressure and heart rate in their study. It is clearly from Fig. 3.28 that the change of PAT during exercise is mostly induced by changing PEP, while the change of PTT is relatively small.

3.5 Conclusion

In this chapter, we deduce the theoretical equation which relates PAT with arterial blood pressure and simulate such a relationship under different physiological conditions, especially under mimicking dynamic exercise condition, by introducing a nonlinear pressure-volume relationship into the asymmetric T-tube model and coupling it to a pressure-source ventricular model with arbitrary heart rate. The simulation results indicated that PAT had consistent, negative correlations with SBP, DBP and MBP under variation of heart contractility, preload and heart rate. When there are changes of peripheral resistance and maximal tube compliance, PEP and PTT changes inversely, resulting in uncertain changes of PAT. Under dynamic exercise, due to the combined effects of PEP and PTT, PAT shows significantly high and negative correlation with SBP and MBP. PTT is a good indicator of DBP during dynamic exercise whereas PAT is not. The linear negative relationship between MBP and PAT during exercise provides basis for developing a dynamic MBP estimation method using PAT. Further, the proposed model in this chapter is further developed in the next chapter to propose a novel wearable measurable parameter of cardiac output.

Reference

[1] J. P. Mulier, "Ventricular pressure as a function of volume and flow," 1994, Univ. Leuven, Belgium.

[2] M. Danielsen and J. T. Ottesen, "Describing the pumping heart as a pressure source," *J. Theor. Biol.*, vol. 212, pp. 71–81, 2001.

[3] J. L. Palladino, J. P. Mulier, and A. Noordergraaf, "An alternative to time-varying elastance

descriptions of the heart," in *Proc. 18th Annu. Int. Conf. IEEE EMBS*, 1996, pp. 1713–1714.

[4] J. T. Ottesen and M. Danielsen, "Modeling ventricular contraction with heart rate changes," *J. Theor. Biol.*, vol. 222, pp. 337–346, 2003.

[5] H. H. Hardy and R. E. Collins, On the pressure-volume relationship in circulatory elements, *Med. Biol. Eng. Comput.*, vol. 20, pp. 565-570, 1982.

[6] R. Burattini and K. B. Campbell, Modified asymmetric T-tube model to infer arterial wave reflection at the aortic root, *IEEE Trans Biomed Eng*, vol. 36, pp. 805–814, 1989.

[7] K. B. Campbell, R. Burattini, D. L. Bell, et al., Time-domain formulation of asymmetric T-tube model of arterial system, *Am J Physiol Heart Circ Physiol*, vol. 258, pp. H1761–H1774, 1990.

[8] H. Warner, The use of an analog computer for analysis of control mechanisms in the circulation, *Proceeding IRE*, vol. 47, pp. 1913-1916, 1959.

[9] J. G. Defares, H. H. Hara, J. J. Osborn, et al., Theoretical analysis and computer simulation of the circulation with special reference to the Starling properties of the ventricle. In: *Circulatory Analog Computers*, ed. by Noordergraaf, A., Jager, G. N. &Westerhof, N., North Holland Publ., Amsterdam. pp. 91, 1963.

[10] H. Suga, K. Sagawa and A. A. Shoukas, Load independence of the instantaneous pressure-volume ratio of the canine left ventricle and effects of epinephrine and heart rate on the ratio, *Circ. Res.*, vo. 32, pp. 314-322, 1973.

[11] H. Suga and K. Sagawa, Instantaneous pressure-volume relationships and their ratio in the excised, supported canine left ventricle, *Circ. Res.*, vol. 35, pp. 117-126, 1974.

[12] P. Segers, N. Stergiopulos, N. Westerhof, et al., Systemic and pulmonary hemodynamics assessed with a lumped-parameter heart-arterial interaction model, *Journal of Engineering Mathematics*, vol. 47, pp. 185-199, 2003.

[13] J. L. Palladino and A. Noordergraaf, The changing view of the heart through the centuries, *Stud. Health Technol. Inform.*, vol. 71, pp. 3-11, 2000.

[14] W. C. Hunter, J. S. Janicki, K. T. Weber, et al., systolic mechanical properties of the left ventricle, Effects of volume and contractile state, *Circ. Res.*, vol. 52, pp. 319-327, 1983.

[15] W. C. Hunter, End-systolic pressure as a balance between opposing effects of ejection, Circ. Res., vol. 64, pp. 265-275, 1989.

[16] S. G. Shroff, J. S. Janicki and K. T. Weber, Evidence and quantitation of left ventricular systolic resistance, *AM. J. Physiol.-Heart and Circulatory Physiology*, vol. 249, pp. H358-H370, 1985.

[17] W. C. Litter and G. L. Freeman, Description of LV pressure-volume relations by time-varying elastance and source resistance, *AM. J. Physiol.-Heart and Circulatory Physiology*, vol. 253, pp. H83-H90, 1987.

[18] D. M. Regen, W. C. Howe, L. H. Peterson, et al., Characteristics of single isovolumic left-ventricular pressure waves of dog hearts in situ, *Heart Vessels*, vol. 8, pp. 136-148, 1993.

[19] S. Hales, *Statical Essays: Containing Haemostaticks.* vol. II. London, UK: Innys and Manby, 1733.

[20] O. Frank, Die Grundform des arteriellen Pulses, *Z. Biol.*, vol. 37, pp. 483–526, 1899. [Translated by K. Sagawa, R. K. Lie and J. Schaefer. *J. Mol. Cell Cardiol.*, vol. 22, pp. 253–277, 1990.

[21] N. Stergiopulos, J.-J. Meister, and N. Westerhof, Evaluation of methods for the estimation of total arterial compliance, *Am. J. Physiol.- Heart Circ. Physiol*, vol. 268, pp. H1540–H1548, 1995.

[22] N. Westerhof, G. Elzinga and P. Sipkema, An artificial arterial system for pumping hearts, *J. Appl. Physiol.*, vol. 31, pp. 776-781, 1971.

[23] X. Y. Zhang, E. MacPherson and Y. T. Zhang, Relations between the timing of the second heart sound and aortic blood pressure, *IEEE. Trans. Biomed. Eng.*, vol. 55, pp. 1291-1297, 2008.

[24] M. Karamanoglu, D. E. Gallagher, A. P. Avolio, et al., Pressure wave propagation in a multibranched model of the human upper limb, *Am. J. Physiol.- Heart Circ. Physiol.* 269, H1363-H1369, 1995.

[25] J. Alastruey, K. H. Parker, J. Peiró, et al., Analysing the pattern of pulse waves in arterial networks: a time-domain study, *J. Eng. Math.*, vol. 64, pp. 331-351, 2009.

[26] M. F. O'Rourke., Pressure and flow waves in the systemic arteries and the anatomical design of the arterial system, *J. Appl. Physiol.,* vol. 23. pp. 139-149. 1967.

[27] R. Burattini., An arterial tree input impedance model: Analysis in the frequencies domain, *Biomechanics,* vol. 10, pp. 20-29, 1981.

[28] R. Burattini and K. B. Campbell, Modified asymmetric T-tube model to infer arterial wave reflection at the aortic root, *IEEE Trans. Biomed. Eng.*, vol. 36, pp. 805-814, 1989.

[29] K. B. Campbell, R. Burattini, D. L. Bell, et al., Time-domain formulation of asymmetric T-tube model of arterial system, *Am. J. Physiol.- Heart Circ. Physiol.*, vol. 258, pp. H1761-H1774, 1990.

[30] R. Burattini and S. Di Carlo, Effective length of the arterial circulation determined in the dog by aid of a model of the systemic input impedance, *IEEE Trans. Biomed. Eng.*, vol. 35, pp. 53-61, 1988.

[31] M. F. O'Rourke and A. P. Avolio, Pulsatile flow and pressure in human systemic arteries: studies in man and in a multi-branched model of human systemic arterial tree, *Circ. Res.*, vol. 46, pp. 363-372, 1980.

[32] Z. R. Liu, S. Feng and F. C. P. Yin, Impedance of arterial system simulated by viscoelstic t tubes terminated in windkessels, *Am. J. Physiol.- Heart Circ. Physiol.*, vol. 256, pp. H1087-H1099, 1989.

[33] K. C. Chang and T. S. Kuo, Exponentially tapered t-tube model in the characterization of arterial non-uniformity, *J. theor. Biol.*, vol. 183, pp. 35-46, 1996.

[34] D. N. Stone and J. P. L. Dujardin, Pressure dependence of the canine aortic characteristic impedance and the effects of alternations in smooth muscle activity. Med. Biol. Eng. Comput. vol. 23, pp. 324-328, 1985.

[35] J. K. Li, T. Cui and G. M. Drzewiecki, A nonlinear model of the arterial system incorporating a pressure-dependent compliance, *IEEE Trans. Biomed. Eng.*, vol. 37, pp. 673-678, 1990.

[36] J. C. Bramwell and A. V. Hill, The velocity of the pulse wave in man, *Proceedings of the Society for Experimental Biology and Medicine*, vol. 93, pp. 298-306, 1922.

[37] H. H. Hardy and R. E. Collins, On the pressure-volume relationship in circulatory elements, *Med. Biol. Eng. Comput.*, vol. 20, pp. 565-570, 1982.

[38] F. K. Forster and D. Turney, Oscillometric determination of diastolic, mean and systolic blood pressure-a numerical model, *J. Biomech. Eng.*, vol. 108, pp. 359-364, 1986.

[39] R. Burattini and K. B. Campell, Effective distributed compliance of the canine descending aorta estimated by modified T-tube model, *Am. J. Physiol.- Heart Circ. Physiol.*, vol. 264, pp. H1977-H1987, 1993.

[40] D. J. Patel, F. M. De Freitas, J. C. Greenfield, et al., Relationship of radius to pressure along the aorta in living dogs, *Am. J. Physiol.- Heart Circ. Physiol.*, vol. 18, pp. 1111-1117, 1963.

[41] S. G. Shroff, D. S. Berger, C Korcarz, et al., Physiological relevance of T-tube model parameters with emphasis on arterial compliances, *Am. J. Physiol.- Heart Circ. Physiol.*, vol. 269, pp. H365-H374, 1995.

[42] Jin-Oh Hahn, A. T. Reisner, H. H. Asada, Estimation of pulse transit time using two diametric blood pressure waveform measurements, *Med. Eng. Phys.*, E-pub ahead of print, 2010.

[43] R. Burattini and K. B. Campbell, Comparative analysis of aortic impedance and wave reflection in ferrets and dogs, *Am. J. Physiol.- Heart Circ. Physiol.*, vol. 282, pp. H244-H255, 2002.

[44] R. Ochiai, J. Takeda, H. Hosada, et al., The relationship between modified pulse wave transit time and cardiovascular changes in isoflurane anesthetized dogs, *J. Clin. Monit. Comput.*, vol. 15, pp. 493-501, 1999.

[45] J. C. Kubitz, G. I. Kemming, G. Schultheib, et al., The influence of cardiac preload and positive end-expiratory pressure on the pre-ejection period, *Physiological Measurement*, vol. 26, pp. 1033-8, 2005.

[46] G. Elzinga and N. Westerhof, Pressure and flow generated by the left ventricle against different impedances, *Circ. Res*, vol. 32, pp. 178-186, 1973.

[47] K. Sunagawa, W. L. Maughan and K. Sagawa, Stroke volume effect of changing arterial input impedance over selected frequency ranges, *Am J Physiol Heart Circ Physiol*, vol. 248, pp. H477-484, 1985.

[48] N. Ishide, Y. Shimiza, Y. Maruyama, et al., Effects of changes in the aortic input impedance on systolic pressure-ejected volume relationships in the isolated supported canine left ventricle, *Cardiovas. Res.*, Vol. 14, pp. 229-243, 1980.

[49] W. S. Harris, C. D. Schoenfeld and A. M. Weissler, Effects of adrenergic receptor activation and blockade on the systolic preejection period, heart rate and arterial pressure in man, *J. Clin. Invest.*, vol. 46, pp. 1704-1714, 1967.

[50] D. V. Cokkinos, E. T. Heimonas, J. N. Demopoulos, et al., Influence of heart rate increase on uncorrected pre-ejection period/left ventricular ejection time (PEP/LVET) ratio in normal individuals, *Br. Heart J.*, vol. 38, pp. 683-688, 1976.

[51] M. Y. Wong, E. Pickwell-Macpherson, Y. T. Zhang, et al., The effects of pre-ejection period on post-exercise systolic blood pressure estimation using the pulse arrival time technique, *Eur. J. Appl. Physiol.*, Sep. 8 2010.

[52] X. Y. Zhang, E. MacPherson, Y. T. Zhang, Relations between the timing of the second heart sound and aortic blood pressure, IEEE Trans Biomed Eng, vol. 55, pp. 1291-1297, 2008.

[53] J. P. Matonick and J. K.-J. Li, Pressure-dependent and frequency domain characteristics of the systemic arterial system, Cardiovascular Engineering, vol. 1, pp. 21-29, 2001.

Chapter 4

A Novel Approach for Cardiac Output Estimation Using Electrocardiogram and Photoplethysmogram

In this Chapter, we aim at developing a novel estimating method of cardiac output using electrocardiogram and photoplethysmogram. Using the wave reflection theory, a novel CO index, is derived from the asymmetric T-tube model which has been discussed in Chapter 3. Then, two assumptions are made: 1) PAT is used as a surrogate to trace MBP changes; 2) IPA, a shape feature parameter of aortic blood pressure waveform or PPG, is used to trace the changes of mean aortic reflection coefficient ($\Gamma(0)$). Then, the CO index is represented in terms of PAT and IPA, namely pulse time reflection ratio (PTRR). The relationship between the PTRR and CO is simulated under different physiological conditions, especially in the exercise condition, by changing the corresponding parameters in the T-tube model. The tracing ability of PTRR to CO is finally discussed and concluded.

4.1 Derivation of a novel cardiac output index from asymmetric T-tube model

According to the wave reflection theory [1] [2], the blood pressure (P_{ao}) and blood flow (Q_{ao}) at the root of the aorta can be expressed as a sum of forward and reflected waves in the frequency domain [3] as follows:

$$P_{ao,z}(\omega) = P_{f,z}(\omega) + P_{r,z}(\omega) \tag{4.1}$$

and

$$Q_{ao,z}(\omega) = Q_{f,z}(\omega) + Q_{r,z}(\omega) = \frac{1}{Z_c}\left(P_{f,z}(\omega) - P_{r,z}(\omega)\right), \tag{4.2}$$

where "*f*' indicates forward wave, '*r*' indicates reflected wave, '*z*' indicates the distance from the measuring site to the entrance of aorta, and Z_c is the aortic characteristic impedance. Since the two tubes in the model are assumed as frictionless, Z_c can be regarded as a real constant. It is worth noting that in our nonlinear asymmetric T-tube model, Z_c is a function of pressure but not a constant. In the later Section of this Chapter, we will discuss the error induced by a constant Z_c in the calculation of CO.

The global reflection coefficient of the arterial system can be defined as the ratio of the reflected and forward waves at the entrance of aorta:

$$\Gamma(\omega) = \frac{P_{r,z=0}(\omega)}{P_{f,z=0}(\omega)}. \tag{4.3}$$

Then, input impedance can be calculated as:

$$Z_{in}(\omega) = \frac{P_{ao,z=0}(\omega)}{Q_{ao,z=0}(\omega)} = Z_c \frac{1+\Gamma(w)}{1-\Gamma(w)}. \tag{4.4}$$

When ω approaches zero, Eq.(4.4) becomes

$$Z_{in}(0) = \frac{P_{ao,z=0}(0)}{Q_{ao,z=0}(0)} = \frac{\overline{P_{ao,z=0}}}{\overline{Q_{ao,z=0}}}, \tag{4.5}$$

where $\overline{P_{ao,z=0}}$ and $\overline{Q_{ao,z=0}}$ are the mean blood pressure and flow at the aortic entrance. CO equals to $\overline{Q_{ao,z=0}} \times Time$, where Time = 1 min = 60 s. Therefore, substituting Eq.(4.4) into Eq.(4.5) yields:

$$CO = Time \times \overline{Q_{ao,z=0}} = \frac{\overline{P_{ao,z=0}}\left(1-\Gamma(0)\right)}{Z_c\left(1+\Gamma(0)\right)}, \tag{4.6}$$

where Z_c is a constant.

According to the conclusions obtained in Chapter 3, there is a linear relationship between PAT and MBP during exercise. Hence, during exercise, the relation between PAT and MBP is modeled as:

$$MBP = A \cdot PAT + B, \tag{4.7}$$

where A and B are constants. Here, we further assume that, the inflection point area (IPA), an index derived from the aortic blood pressure wave (for definition, please see Fig. 4.1), can be used to estimate mean reflection coefficient ($\Gamma(0)$), hence there is

$$\Gamma(0) = C \cdot IPA + D, \tag{4.8}$$

where C and D are constants. Then, CO can be expressed as:

$$CO = \frac{PTRR}{Z_c}, \tag{4.9}$$

where

$$PTRR = \frac{(A \cdot PAT + B) \cdot \left[1-\left(C \cdot IPA + D\right)\right]}{1+\left(C \cdot IPA + D\right)}. \tag{4.10}$$

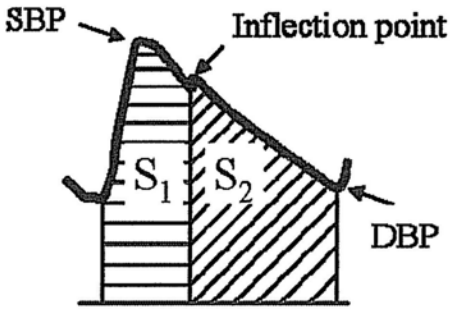

Fig. 4.1 The aortic blood pressure curve in a cardiac cycle. SBP is the highest point, DBP is the ending point and inflection point is the incisura on the curve produced by the closure of the aortic valve. S_1 and S_2 are the areas under the curve during systole and diastole, respectively, and IPA is defined as $S_2/(S_1+S_2)$.

4.2 The relationship between IPA and mean aortic reflection coefficient (Γ(0))

As mentioned before, Γ(0) is the mean correlation coefficient. By definition, it equals to the area ratio of the reflective waves to the forward wave on the blood pressure curve measured at the aortic root. However, the forward and reflective blood pressure waves at time domain is difficult to be obtained from only a single aortic blood pressure curve [4]. Normally, the aortic blood flow or blood velocity curve is needed for decomposition [5, 6]. We therefore proposed IPA, a shape feature which we assume to be closely related to reflection coefficient. Fig. 4.1 gives the definition of IPA, i.e. the ratio of the area after the inflection point on the blood pressure curve to the area of the whole curve within a cardiac cycle. Since the inflection point is the incisura which separates the systolic and diastolic phases on the blood pressure wave, this hypothesis is based on the fact that the diastolic part of the blood pressure curve is mainly composed of reflective waves and the systolic blood pressure wave mainly consists of the forward wave. In order to verify the hypothesis, we simulate the asymmetric T-tube model and analyze the relationship between IPA and Γ(0) under variant physiological conditions by altering the model parameters.

Fig. 4.2 gives the relationship between IPA and Γ(0) under different physiological conditions. The changing trend of each parameter in Fig. 4.2 A-F is the same as the changing trend used in the simulation Section in Chapter 3 (See Simulation in Section 3.3). It is shown in Fig. 4.2 F that there is a positive, high and significant correlation coefficient between IPA and Γ(0) during dynamic exercise (r>0.98, p<0.01).

For individual parameter, the changes of peripheral resistance and arterial stiffness (maximal arterial compliance) both induce a significantly positive and linear relationship between IPA and Γ(0) (r>0.98, p<0.01). When peripheral resistance increases, it will enhance the reflections at the peripheral terminals, and then augment Γ(0) at the aortic root. Since the enhanced reflective waves mainly arrive at the aorta during diastole, the elevated reflection level also raises IPA. When C_m increases, the aorta becomes more compliant, and hence produces less pressure at the same heart ejection. As a result, the forward wave which is produced by the heart ejection decreases and Γ(0) increases. At the same time, the more compliant aorta produced less after load to the ventricular ejection, which results in more rapid blood ejection during systole and shortens the ejection phase, as shown in Fig. 4.3 A. Under the same heart rate, a shorter systolic phase gives rise to a longer diastolic phase, and as a result, the IPA increases.

It is interesting to see from Fig. 4.2 A and B that the enhancement of cardiac function caused by different cardiac factors induces entirely different effects. Either the rising of heart contractility (A) or the increasing of pre-load (B, end-diastolic ventricular volume, V_d), increases Γ(0). However, the IPA increases with heart contractility but decreases with preload. This conflicting phenomenon may be explained by the different changes of T_p and T_{eject} under these two conditions, as illustrated in Fig. 4.3. T_p is the time period from the start of ejection to the peak blood pressure in systole and T_{eject} is the ejection duration. When heart contractility increases, it only enhances the heart muscle tensile. During ejection, the enhanced muscles produces more contracting forces, ejects the blood more rapidly and makes the peak pressure appear earlier (reduced T_p). The ejection time also decreases due to the rapid ejection. As a result, the systolic portion is shortened while the diastolic

portion is elongated, which increases IPA. However, when preload increases, it predominately increases the end-diastolic volume inside the ventricle, meanwhile, it increases the muscle tension by more passive stretching of the muscle cell. During ejection, since there is much more ventricular volume for ejection out of the ventricle, T_p is elongated. Although T_p is meanwhile shortened by the enhanced heart contraction forces, the elongation induced by more volume is the predominant factor. T_{eject} is significantly elongated, due to the same reason for longer T_p The increase of T_{eject} includes more part of reflective waves into the systolic phase, enhances the systolic curve and weakens the diastolic curve. This makes the IPA decrease.

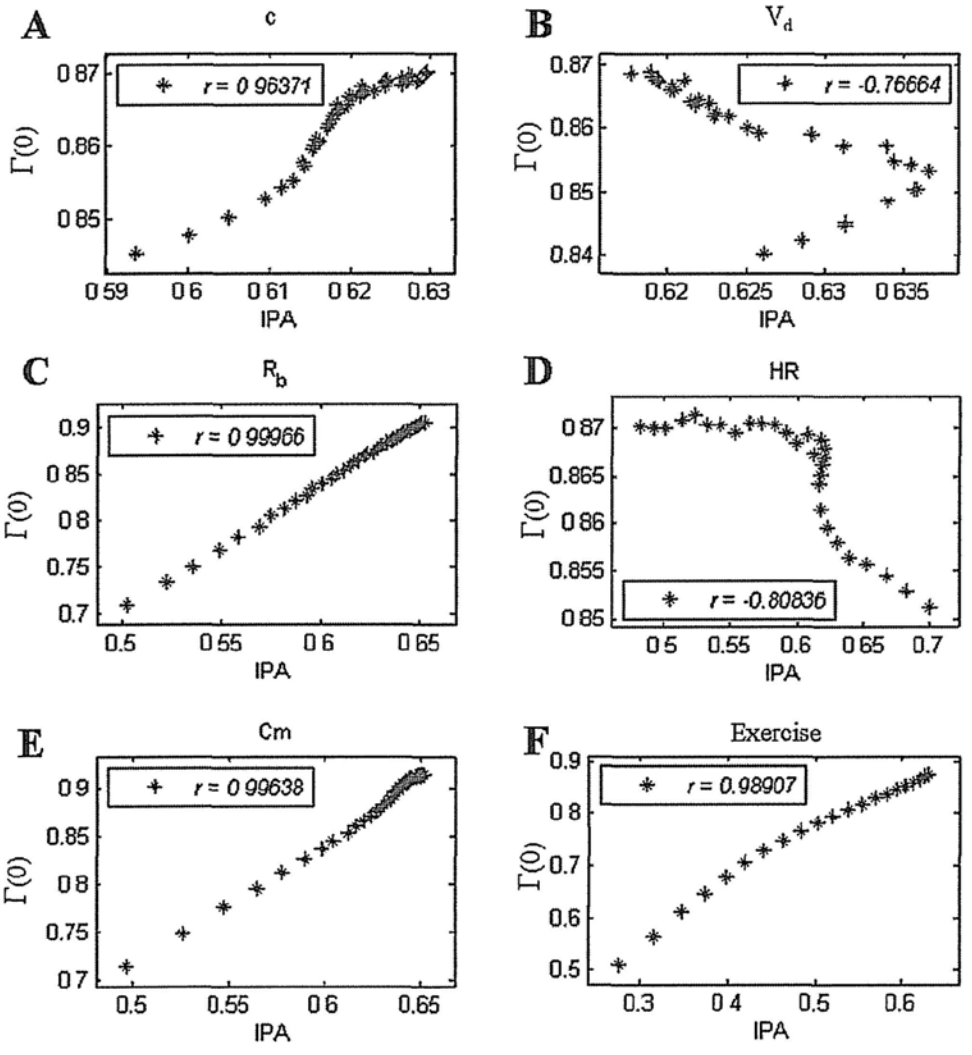

Fig. 4.2 The relationship between IPA and Γ(0) at changing A. heart contractility, B. end-diastolic volume, C. peripheral resistance, D. heart rate, E. maximal arterial compliance and F. mimicking exercise condition. In A-F, r is the correlation coefficient between IPA and Γ(0) (p<0.01).

Γ(0) increases as heart rate increases. Fig. 4.3 shows the changing trends of absolute T_{eject}, T_p (G and H, respectively) and relative T_{eject}, T_p (I and J, respectively) under changing heart rate.

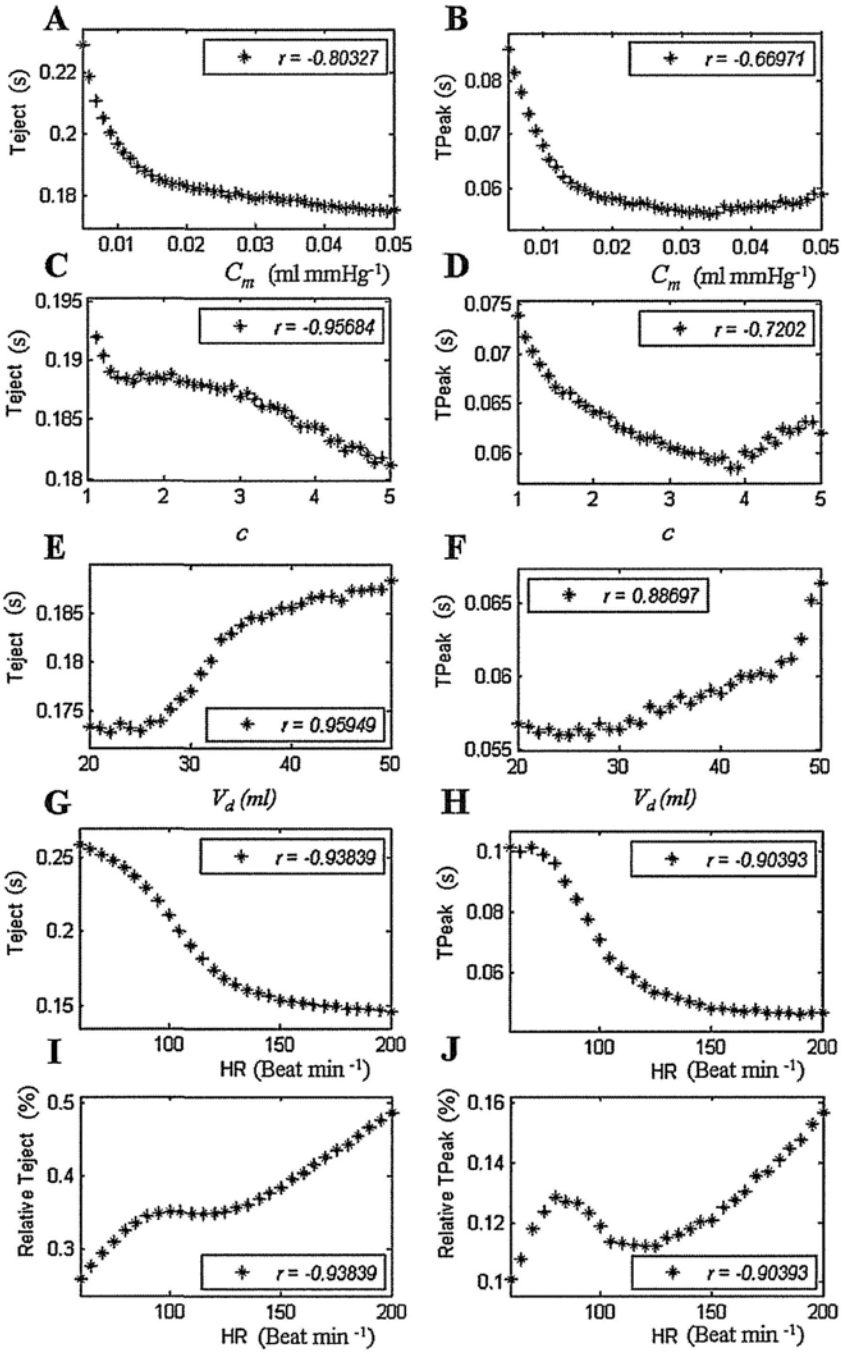

Fig. 4.3 Changing trends of ejection time under A changing C_m, C changing heart contractility, E changing preload and G changing heart rate. B, D, F H are changing trends of peak time under changing C_m, heart contractility, preload and heart rate, respectively. I and J are changing trends of relative ejection time and peak time with changing heart rate, respectively. In A-J, r is the correlation coefficient (p<0.01) between variable indicated in the x axis and the variable indicated in the x axis.

Relative T_{eject} and T_p are defined as absolute T_{eject} and T_p divided by the heart period (time length of a cardiac cycle). It is clear that although the absolute T_{eject} and T_p are decreasing, and the relative T_{eject} and T_p are increasing, which indicates an increase of systolic portion on the blood

pressure curve. As a result, IPA decreases. Hence, there is a negative relationship between Γ(0) and IPA.

To summarize, there is a positive high and significant relationship between IPA and Γ(0) under changing heart contractility, peripheral resistance and arterial stiffness. There is a negative and significant correlation between IPA and Γ(0) under changing preload and HR. Furthermore, Fig. 4.2 shows comparison of the changing magnitudes of Γ(0) induced by different model parameters. It is obvious that Γ(0) is most sensitive to the changes of the peripheral resistance and arterial stiffness and the changes of Γ(0) magnitude induced by these two factors are about 10 times of those induced by other factors. This is why under dynamic exercise, IPA shows a highly positive and significant correlation with Γ(0), in spite of the negative influence induced by other parameters.

4.3 The relationship between PTRR and cardiac output

In this Section, we discuss the relationship between PTRR and CO. In Section 4.1, two assumptions were made in the deduction of PTRR: one was the linear relationship between PAT and MBP and the other was the relationship between IPA and Γ(0). In order to separately discuss the effects of assumption 1) and 2) on the estimation performance of PTRR, we define three more indices. First, we rewrite the definition of PTRR as

$$CO = \frac{PTRR}{Z_c}, \tag{4.9}$$

where

$$PTRR = \frac{(A \cdot PAT + B) \cdot [1 - (C \cdot IPA + D)]}{1 + (C \cdot IPA + D)}. \tag{4.10}$$

Then, we define:

$$PTRR_{PAT} = \frac{(A \cdot PAT + B) \cdot [1 - \Gamma(0)]}{1 + \Gamma(0)}, \tag{4.11}$$

$$PTRR_{IPA} = \frac{MBP \cdot [1 - (C \cdot IPA + D)]}{1 + (C \cdot IPA + D)}, \tag{4.12}$$

and

$$PTRR^{\#} = \frac{-PAT \cdot (1 - IPA)}{(1 + IPA)}. \tag{4.13}$$

From Eq.(4.13), there is

$$CO = E \cdot PTRR^{\#} + F, \tag{4.14}$$

where E, F are constants which can be obtained from calibration. $PTRR_{PAT}$ is defined by only introducing assumption 1) into Eq.(4.6) and $PTRR_{IPA}$ by only introducing assumption 2) into Eq.(4.6). $PTRR^{\#}$ is defined here since it is superior to PTRR sometimes due to simpler calibration required. During CO estimation, $PTRR^{\#}$ needs only two reference CO values to calculate E and F in Eq.(4.14), while PTRR needs two reference CO values plus two BP values to calculate A, B, C, D in Eq.(4.10). Under circumstances where BP measurement is not available, $PTRR^{\#}$ can still be used to estimate CO while PTRR can not.

Table 4.1 Parameters and precision of the linear regression between the reference and estimated CO.

Fig 4.4	Slope	Intercept ($L\ min^{-1}$)	SD of Residuals ($L\ min^{-1}$)
Heart contractility (c)			
A1	0.9996	0.0011	0.0201
B1	0.9932	0.0156	0.0330
C1	0.9909	0.0213	0.0459
D1	1	0	0.0555
Preload (V_d)			
A2	0.9993	0.0014	0.0751
B2	0.9456	0.1050	0.0442
C2	0.9421	0.1116	0.0971
D2	1	0	0.2527
Heart rate (HR)			
A3	0.9974	0.0072	0.3581
B3	0.9662	0.0858	0.0790
C3	0.8817	0.3208	0.3969
D3	1	0	0.4670
Peripheral resistance (R)			
A4	0.9850	0.0414	0.0143
B4	0.9782	0.0605	0.0232
C4	0.9704	0.0822	0.0209
D4	1	0	0.0296
Arterial stiffness (C_m)			
A5	0.1253	2.3767	0.0138
B5	-0.0598	2.8804	0.0138
C5	-0.0650	2.8945	0.0136
D5	1	0	0.0146
Exercise condition (*Exercise*)			
A6	0.9155	0.4358	0.3463
B6	0.9713	0.1314	0.4202
C6	0.9402	0.2895	0.0801
D6	1	0	0.4615

SD: standard deviation.

Fig. 4.4 shows the results of linear regression analysis between reference CO (model output) and estimated CO using $PTRR_{PAT}$, $PTRR_{IPA}$, PTRR and $PTRR^{\#}$, respectively, during changes of heart contractility (c), preload (V_d), heart rate (HR), peripheral resistance (R), arterial stiffness (C_m) and under exercise condition (*Exercise*). Similar to that in Section 4.2, the changing trend of each parameter in the Fig. 4.4 A1-D6 is the same as the changing trend used in the simulation Section in Chapter 3 (see Simulation in Section 3.3). Table 4.1 gives the corresponding parameters in the regression function between reference and estimated CO in each plot in Fig. 4.4. The values of

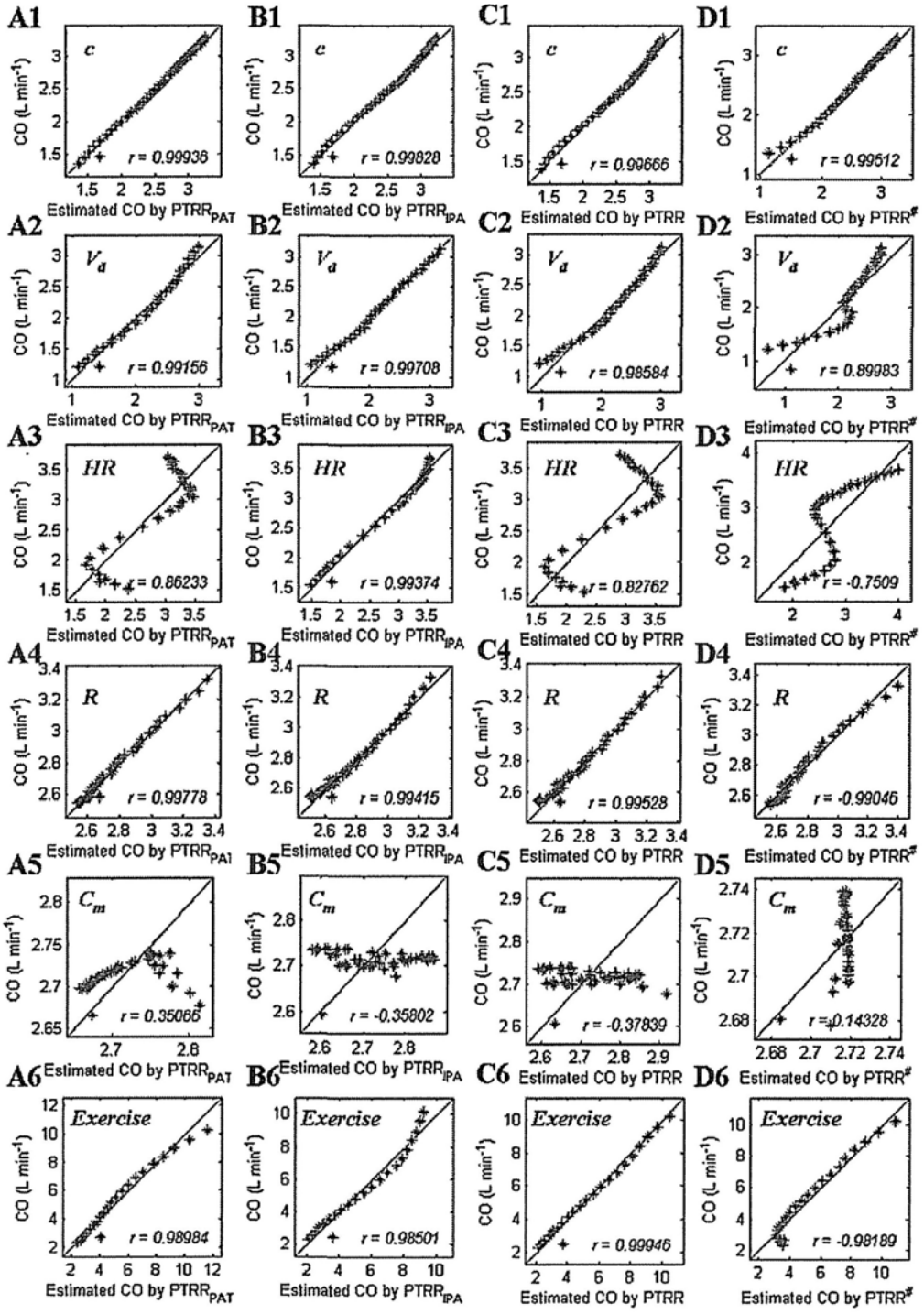

Fig. 4.4 Reference CO and CO estimated from $PTRR_{PAT}$ (A1-A6), $PTRR_{IPA}$ (B1-B6), PTRR (C1-C6) and $PTRR^{\#}$ (D1-D6) during changes of heart contractility (c, A1-D1), preload (V_d, A2-D2), heart rate (HR, A3-D3), peripheral resistance (R, A4-D4), arterial stiffness (C_m, A5-D5) and exercise condition (*Exercise*, A6-D6). In each plot, x axis is the estimated CO and y axis is the reference CO. The black solid line is the equality line. r is the correlation coefficient between parameters (PTRR,$PTRR_{PAT}$, $PTRR_{IPA}$, and $PTRR^{\#}$) and CO. For the definitions of PTRR, $PTRR_{PAT}$, $PTRR_{IPA}$, and $PTRR^{\#}$, please refer to Eq.(4.10)-(4.14).

constant A, B, C, D, E and F are listed in Table 4.2.

It shows that all parameters are able to trace the changes of CO at a high precision during changing heart contractility, peripheral resistance, and during exercise. $PTRR_{PAT}$, $PTRR_{IPA}$ and PTRR show high and significant linear correlations with the changes of preload, while the relationship between $PTRR^{\#}$ and V_d is less linear and the correlation coefficient is lower. When heart rate changes, it seems that only $PTRR_{IPA}$ gives an acceptable estimation of CO, while the performances of the other three factors are worse. All parameters failed to give a reasonable estimation for CO during changing arterial stiffness.

Table 4.2 The values of constants in Eq.(4.10)-(4.14).

Parameter	**Fig. 4.4**	**A**	**B**	**C**	**D**	**E**	**F**
c	A1-D1	-1.20	289.08	0.81	0.36	0.12	7.61
V_d	A2-D2	-2.34	479.78	-1.04	1.51	0.44	20.07
HR	A3-D3	-2.20	464.24	-0.09	0.92	-0.08	-0.63
R	A4-D4	1.66	-195.11	1.64	-0.15	-0.23	-6.35
C_m	A5-D5	-0.08	99.30	1.36	0.03	0.0005	2.74
Exercise	A6-D6	-0.90	240.83	0.96	0.28	-0.25	-6.67

The correlations between the reference CO and CO estimated from $PTRR_{PAT}$, $PTRR_{IPA}$ and PTRR are indifferently high during changing heart contractility (A1-C1), preload (A2-C2) and peripheral resistance (A4-C4). This indicates that both PAT and IPA perform well and they contribute approximately equally to the estimating performance of PTRR under these conditions. Further, the results indicate that PTRR can be effectively replaced by $PTRR^{\#}$ for estimating CO under changing contractility and peripheral resistance, in order to solve the problems if there are only reference CO measurements available for calibration.

Generally, the estimating performances of all parameters are acceptable under exercise. However, it is worth noting that PTRR performs best during exercise condition (see Fig. 4.4). The estimating curve obtained from $PTRR_{PAT}$ is a bit convex and there is an overestimation at high CO level. This is due to the overestimation of PAT on MBP during higher exercise level where the rising of MBP is reduced by the drop of DBP induced by sharply decreasing of peripheral resistance whereas the changing trend of PAT is little influenced by this phenomenon. In contrast, the estimating curve obtained from $PTRR_{IPA}$ is a bit concave and there is an underestimation at high CO level. From visual comparison among Fig. 4.4 B1 to B6, this curve feature may result from the nonlinearity introduced by changing heart rate, since the curve under exercise is quite similar to that obtained under changing heart rate. The convex curve feature induced by PAT and the concave curve feature induced by IPA compensate each other when calculating PTRR by Eq.(4.10), making PTRR a better CO index during exercise. $PTRR^{\#}$ also traces CO well, especially at higher exercise level, at lower CO level however, the estimation precision of $PTRR^{\#}$ does not seem as good as that of PTRR.

In summary, there is a linear relationship between PTRR and CO during changing heart contractility, preload, peripheral resistance and under exercise. PTRR$^{\#}$ can be used as a simpler surrogate of PTRR during changing heart contractility, peripheral resistance and under exercise.

Further it has been reported that the PPG waveform can follow the changes of aortic blood pressure waveform under different physiological conditions [4] [5]. Since aortic blood pressure is very difficult and invasive to be obtained, we utilized IPA derived from PPG wave shape features as a surrogate of IPA discussed here in the later implementation of PTRR in Chapter 5.

4.4 Effect of constant characteristic impedance (Z_c)

In Eq.(4.9), CO equals to PTRR divided by Z_c. In our asymmetric T-tube model, Z_c is a function of arterial blood pressure and varies with time. However, in the practical application, it is difficult to obtain the value of Z_c simultaneously. Since previous experimental results have reported that Z_c is almost unchanging during dynamic exercise [9], we try to address the feasibility of using a constant Z_c in the calculation of PTRR in Eq.(4.9). If this approximate can result in an acceptable estimation of CO, CO can be estimated from PTRR beat to beat.

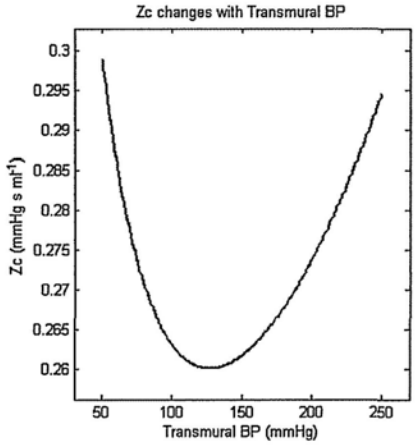

Fig. 4.5 The curve of Z_c with changing transmural BP when V_m = 3 ml, V_0 = 0.1 ml and C_m = 0.015 $ml\ mmHg^{-1}$ in Eq.(3.49).

The relationship between Z_c and MBP is described by Eq.(3.49) in Chapter 3 and visually illustrated in Fig. 4.5. We rewrite Eq.(3.49) as follows:

$$Z_c = \left(\frac{C_m V_m}{\rho} e^{-\frac{C_m}{V_m - V_0} P_t} - \frac{C_m (V_m - V_0)}{\rho} e^{-\frac{2C_m}{V_m - V_0} P_t} \right)^{-\frac{1}{2}}. \qquad (3.49)$$

As noted by Stone and Dujardin [10], the relationship between Z_c and arterial blood pressure is typically parabolic, with the minimum in the physiological range of transmural pressure. Therefore, a change in transmural pressure can yield an increase, a decrease, or no change in characteristic impedance depending on the location of the basal operating point [11], the bottom

of the parabolic curve, as shown in Fig. 4.5.

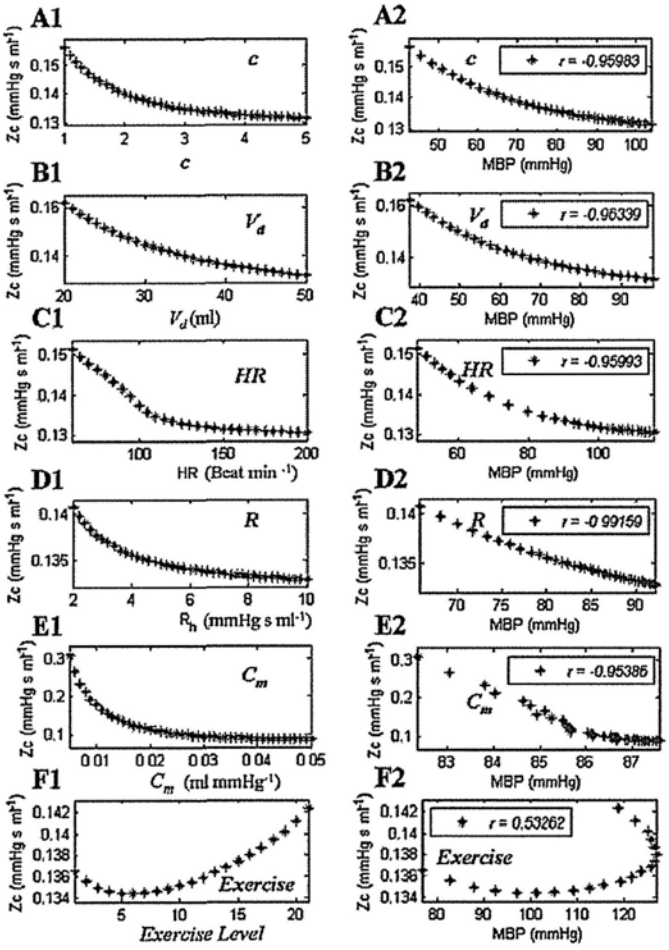

Fig. 4.6 The changing trends of Z_c (A1-F1) and the relationship between Z_c and MBP (A2-F2) during changes of heart contractility (c, A1 and A2), preload (V_d, B1 and B2), heart rate (HR, C1 and C2), peripheral resistance (R, D1 and D2), arterial stiffness (C_m, E1 and E2) and exercise condition (*Exercise*, F1 and F2). r in A2-F2 are the correlation coefficients between Z_c and MBP under different physiological conditions, where $p<0.01$.

Fig. 4.6 shows the changing trends of Z_c (A1-F1) and the relationship between Z_c and MBP (A2-F2) under different physiological conditions. The changing trend of each parameter in the Fig. 4.6 is the same as that used in the simulation Section in Chapter 3 (see Simulation in Section 3.3). It is obvious that Z_c decreases with the increase of blood pressure under all conditions except for the dynamic exercise, indicating that the ranges of transmural blood pressure mainly locate at the left of the basal operating point in Fig. 4.5. During exercise, Z_c changes little, and further, its changing trend looks like the bottom of a parabolic curve. This is mainly due to the combining effects of the changing physiological parameters on the changes of Z_c. During exercise, the rising heart contractility, preload, heart rate decreases Z_c while the decreasing peripheral resistance and arterial compliance increase Z_c. Since Z_c is much more sensitive to the changes of arterial compliance as compared with other factors (see Fig. 4.6), the changing curve of Z_c generally

shows a rising trend.

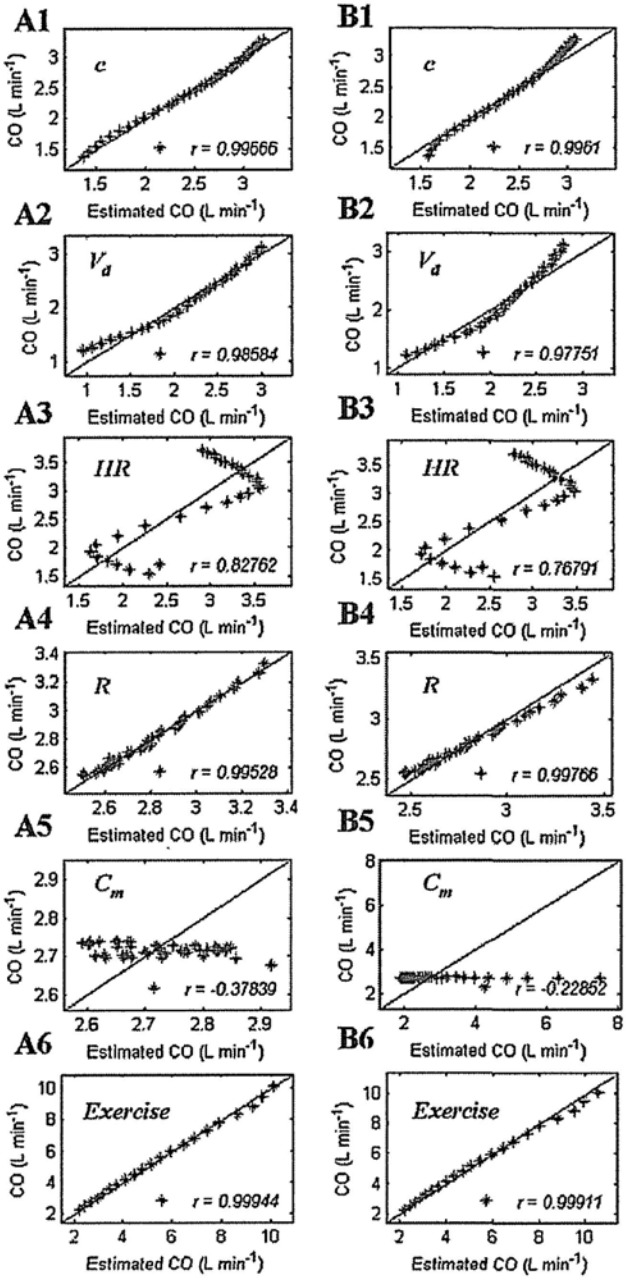

Fig. 4.7 Reference CO and CO estimated from PTRR with variant Z_c (A1-A6) and PTRR with constant Z_c (B1-B6) during changes of heart contractility (c, A1 and B1), preload (V_d, A2 and B2), heart rate (HR, A3 and B3), peripheral resistance (R, A4 and B4), arterial stiffness (C_m, A5 and B5) and exercise condition (*Exercise*, A6 and B6). In each plot, x axis is the estimated CO and y axis is the reference CO. The black solid line is the equality line. r is the correlation coefficient between parameters and CO.

From Fig. 4.6, it is obvious that the changing magnitude of Z_c during exercise is small, which is consistent with previous experimental observations [11]. Then, we address the feasibility of using

a constant Z_c in the calculation of PTRR. Fig. 4.7 gives the visual comparisons between the estimated CO obtained from PTRR with a variant Z_c (A1-A6) and those from PTRR with a constant Z_c (B1-B6). The corresponding quantitative precisions are demonstrated in Table 4.2. Both visual and quantitative data indicate that a constant Z_c does not lead to big errors into the estimation of CO.

Table 4.3 Parameters and precision of the linear regression between the reference and estimated CO using PTRR with variant and constant Z_c.

Variable	Fig. 4.6	Slope	Intercept ($L\ min^{-1}$)	SD of Residuals ($L\ min^{-1}$)
c	A1	0.9909	0.0213	0.0459
	B1	1.1934	-0.4632	0.0496
V_d	A2	0.9421	0.1116	0.0971
	B2	1.1486	-0.2961	0.1221
HR	A3	0.8817	0.3208	0.3969
	B3	0.9519	0.1472	0.4530
R	A4	0.9704	0.0822	0.0209
	B4	0.8106	0.5235	0.0147
C_m	A5	-0.0650	2.8945	0.0136
	B5	-0.0028	2.7249	0.0143
Exercise	A6	0.9402	0.2895	0.0801
	B6	0.9172	0.3923	0.1015

SD: standard deviation.

4.5 Conclusions

In this Chapter, we firstly derived a novel CO index, namely PTRR from our asymmetric T-tube model proposed in Chapter 3. Next, simulation results on the relationship between IPA and $\Gamma(0)$ show that $\Gamma(0)$ is mostly sensitive to the changes of peripheral resistance and arterial stiffness, and changing of these two factors induces a significantly positive and high correlation between IPA and $\Gamma(0)$ during exercise. Further simulations on the estimating performances of PTRR indicate that PTRR is able to trace CO changes with a high precision under changing contractility, preload, peripheral resistance and during exercise. The convex effect from PAT and concave effect from IPA on estimated CO during exercise compensate each other in the calculation of PTRR, making PTRR a better surrogate of CO than introducing PAT or IPA along. What's more, a simpler form of PTRR, $PTRR^{\#}$, can be used as an acceptable surrogate of PTRR during changing heart contractility, peripheral resistance and during exercise. Finally, we addressed the feasibility of using constant characteristic impedance (Z_c) in the PTRR. The simulation results demonstrate that Z_c keeps almost unchanged during exercise and CO estimated by PTRR with constant Z_c approximately achieves a similar precision level those estimated by PTRR with variant Z_c.

Reference

[1] N. Westerhof, P. Sipkema, G. C. Van Den Bos, et al., Forward and backward waves in the arterial system, *Cardiovasc. Res.*, vol. 6, pp. 648-656, 1972.

[2] C. M. Quick, D. S. Berger and A. Noordergraaf, Apparent arterial compliance, *Am J Physiol.*, vol. 274, pp. H1393-H1403, 1998.

[3] W. W. Nichols and M. F. O'Rourke, McDonald's Blood Flow in Arteries, 5th ed., London: Hodder Arnold, 2005.

[4] N. Stergiopulos, B. E. Westerhof and N. Westerhof, Physical basis of pressure transfer from periphery to aorta: a model-based study, *Am. J. Physiol.*, vol. 274, pp. H1386-H1392, 1998.

[5] N. Westerhof, P. Sipkema, C. G. van den Bos, et al., Forward and backward waves in the arterial system, *Cardiovasc. Res.*, vol. 6, pp. 648–656, 1972.

[6] J. P. Murgo, N. Westerhof, J. P. Giolma, et al., Aortic input impedance in normal man: relationship to pressure wave forms, *Circulation*, vol. 62, pp. 105–116, 1980.

[7] P. J. Chowienczyk, R. P. Kelly, H. MacCallum, et al., Photoplethysmographic assessment of pulse wave reflection: blunted response to endothelium-dependent beta2-adrenergic vasodilation in type II diabetes mellitus, *J. Am. Coll. Cardiol.*, vol. 34, pp. 2007-2014, 1999.

[8] K. Takazawa, N. Tanaka, M. Fujita, et al., Assessment of vasoactive agents and vascular aging by the second derivative of photoplethysmogram waveform, *Hypertension*, vol. 32, pp. 365-70, 1998.

[9] J. P. Murgo, N. Westerhof, J. P. Giolma, et al., Effects of exercise on aortic input impedance and pressure wave forms in normal humans, *Circ. Res.*, vol. 48, pp. 334-343, 1981.

[10] D. N. Stone and J. P. L. Dujardin, Pressure dependence of the canine aortic characteristic impedance and the effects of alternations in smooth muscle activity, *Med. Biol. Eng. Comput.*, vol. 23, pp. 324-328, 1985.

[11] S. G. Shroff, D. S. Berger, C Korcarz, et al., Physiological relevance of T-tube model parameters with emphasis on arterial compliances, *Am. J. Physiol.- Heart Circ. Physiol.*, vol. 269, pp. H365-H374, 1995.

Chapter 5

Estimation of Cardiac Power Output in Dynamic Exercise

In this chapter, we focus on the experimental validation of our work. Two experiments were carried out, one on young, healthy subjects (Experiment I) and the other on three subject groups, healthy elderly, cardiovascular patients and heart failure patients (Experiment II). Both experiments are supine bicycle exercise. Experiment I was held on campus and Experiment II conducted in the hospital. The protocols for two experiments are quite similar, just with differences on some special medical measurements for the patients in the hospital. Therefore, data from two experiments are pooled in the later analysis. The data analysis is mainly composed of two parts, MBP analysis and CO analysis. This is mainly due to the lack of standard to evaluate the accuracy of a novel cardiac power output (CPO) measuring method. For BP and CO, there are either existing standard or at least judging criteria which are widely accepted for evaluating the accuracy of measurements.

Since two PPGs were measured during the experiment, one from the ear and one from the finger, two PATs, PAT_{ear} and PAT_{finger} are calculated. In order to verify the theoretical findings in chapter 3, the relationships between PAT to SBP, MBP and DBP were tested and compared. An approximate of PTT on the brachial artery, namely PTT_{bra}, is obtained by subtracting PAT_{ear} from PAT_{finger}, and the correlations of PTT_{bra} to SBP, MBP and DBP were tested and compared with those of PAT. In the later results of linear correlation analysis, PAT_{finger} showed the highest correlation with MBP, it was therefore utilized in the MBP estimation. We utilized two calibration methods to calculate parameter A and B in Eq.(4.7), the best-fit and mean calibration, which will be explained in detail in section 5.1.3. The estimating accuracy of MBP analysis is evaluated by the American National Standard for Electronic or Automated Sphygmomanometers developed by Association for the Advancement of Medical Instrumentation (AAMI Standard).

In CO analysis, since Z_c is unavailable, $PTRR^{\#}$ is calculated from ECG and finger PPG from Eq. (4.13) and utilized to estimate CO. Another surrogate of PTRR, $PTRR^{*}$ is proposed and the performance of $PTRR^{\#}$ and $PTRR^{*}$ in CO estimation are compared. The accuracy of CO estimation is evaluated by the criteria proposed by Critchley and Critchley [1]. In both BP and CO analysis, effects of age, gender and diseases are discussed. Finally, the main experimental observations were discussed and concluded.

5.1 Material and methods

5.1.1 Subjects and experiment protocol

The two experiments were approved by the Clinical Research Ethics Committee, and subjects were informed of the experiment and asked to sign the authorization forms before they participated in the study. In experiment I, 19 university students were enrolled on campus and in experiment II, 65 unselected outpatients were enrolled in the cardiology department of the Prince's Wales Hospital. The patients were then divided into three subject populations according to their

diagnosis decisions. 15 elderly, healthy subjects were subject to the normal control group, 20 patients with at least one cardiovascular disease belonged to the disease control group and 30 heart failure patients were included in the heart failure group. To be consistent with the subject groups in experiment II, the 19 young, healthy subjects enrolled in experiment I was named the normal healthy group. Table 5.1 summarizes the physical parameters, such as the gender, age, body mass index (BMI), and the hemodynamic parameters measured at baseline, such as HR, SBP, DBP and CO of all subject groups. And Table 5.2 lists the diagnosis and medication information related to the patients in the disease control and heart failure groups. In Table 5.2, patients with systolic HF (heart failure) were those with LVEF (left ventricle ejection fraction) less than 50% and patients with diastolic HF are those with LVEF larger than 50%.

Table 5.1 Physical and hemodynamic parameters of all subject populations.

Parameters	Normal Healthy	Normal Control	Disease Control	Heart Failure
No. of subjects	19	15	20	30
Gender (M/F)	9/10	11/4	11/9	27/3
Age (years)	27±4	55 ± 9	60 ± 12	60 ± 10
BMI	21.7±2.1	23.52 ± 3.23	23.06 ± 2.14	27.68 ± 4.84
HR (beats min^{-1})	69±6	73 ± 12	72 ± 14	74 ± 14
SBP (mmHg)	113±12	141 ± 18	136 ± 25	142 ± 14
DBP (mmHg)	62±6	91 ± 7	79 ± 11	85 ± 9
CO (L min^{-1})	5.5±1.0	5.5 ± 1.2	5.1 ± 1.6	5.7 ± 1.8

M= male, F= female, BMI=body mass index, "±": mean ± standard deviation.

Table 5.2 Diagnosis and medication information related to patients.

Information on Diagnosis			Information on Medications		
Diagnosis	DC Group (n)	HF Group (n)	Medications	DC Group (n)	HF Group (n)
Systolic HF	0	9	B-blockers	6	26
Diastolic HF	0	14	CCB	7	10
CAD	2	2	Nitrates	1	6
Hypertension	10	16	Diuretrics	1	16
DM	8	9	Lipid-Lowering	6	14
MI	1	1	ACEI/ARB	7	22
IHD	1	12	Aspirin	4	4
Hyperlipidemia	5	8	ASA	6	15
			TNG	1	5

DC: disease control; HF: heart failure; n: no. of subjects; CAD: coronary artery disease; DM: diabetes mellitus; MI: myocardial infarction; IHD: ischemic heart disease; CCB: calicium channel blockers; ACEI: non-sulfhydryl-containing inhibitors; ARB: angiotensin receptor blocker; ASA: acetylsalicylic acid; TNG: nitroglycerin.

The experiment was conducted at least one hour after meal in the morning or afternoon in a

standard shielding room in the Joint Research Center for Biomedical Engineering (JCBME) at the Chinese University of Hong Kong (CUHK) (Experiment I), or in a standard patient room at the cardiology department of the Prince's Wales Hospital (Experiment II). The room temperature was kept at 25°C during the experiment.

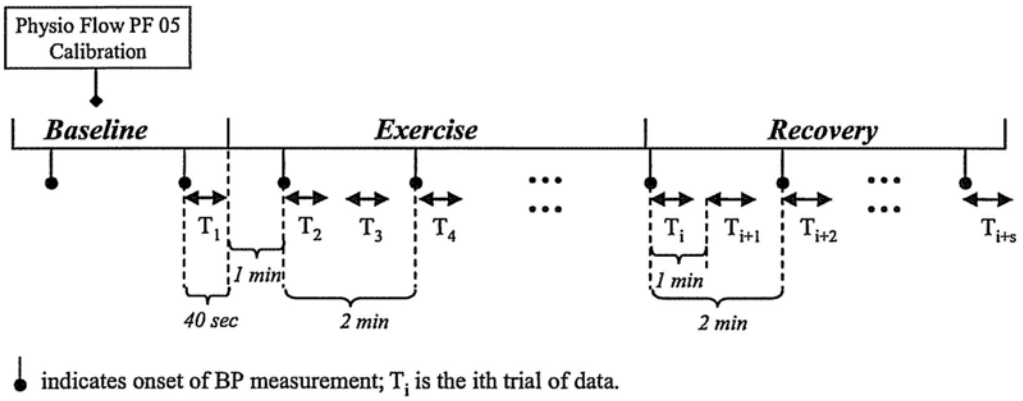

Fig. 5.1 Main experiment phases and procedures.

Fig. 5.1 is the flow chart of the experiment indicating three experimental phases and the most important procedures. Upon arrival, the subject was asked to lie supine on the bicycle ergometer (Lode, Groningen, Netherland) for ten minutes to reach his/her baseline condition. BP was then measured on the right arm either only by a registered nurse using a mercury BP meter (Riester, Germany) (experiment I) or by both the nurse and the automatic auscultatory BP machine (Suntech, USA) (experiment II). SBP and DBP were then inputted into the impedance cardiographic device (Physio Flow PF-05, Macheren, France) to calculate the baseline CO (CO calibration). Continuous and simultaneous ECG, PPG and CO signals were recorded thereafter, until the end of the experiment. Then, subject was asked to rest on bed for another 40 seconds for signal recording at rest with a simultaneous BP measurement. Then, the bed was tilted towards the left hand side of the subject by 20° - 30° (see Fig. 5.2), and the subject started to ride the bicycle. In experiment I, the subject was asked to ride the bicycle for 6 minutes. The riding load was increased every two minutes. In experiment II, the subject started to ride the bicycle at 25W, and then the riding load was increased by 25W every two minutes until it reached the tolerant limit of the testing subject (usually 75~100W), and then the load was kept at this tolerant limit until the testing subject reached his/her target heart rate ($85\% \times (220 - Age)$). For those very old subjects (Age>80) or heart failure patients whose heart rate could not reach the target heart rate even at their exhausting condition, we encouraged them to keep riding to ensure their heart rate as close to the target heart rate as possible. In both experiments, in the exercise phase, BP was first measured one minute after the start of exercise and then measured every two minutes later, until the end of exercise (see Fig. 5.1). In experiment II, the subject was asked to stop riding one minute after BP had been measured at his/her maximal heart rate. After exercise, the subject was asked to lie still on bed to collect data of recovery phase. In experiment I, the recovery phase lasted for 6 min. In experiment II, the recovery phase lasted until CO dropped back to the baseline level or at most for 15 min (blood test after exercise should be done within 15 min after stop of exercise). In both experiments, in the recovery phase, BP was firstly measured immediately after the stop of exercise

reflection mode LED emitter (850 nm, SFH-4250Z, Osram) and detector (850-880 nm, SFH-320 FA-3/4, Osram) embedded. The acquisition devices were connected to a small portable procession unit, where the PPGs were filtered (band-pass filter: 0.35-16 Hz) and amplified (20× dc gain). Then, the analog output of ECG, CO and two PPGs were connected to an analog to digital converter (Dataq D1-720, USA), converted to digital signals (see Fig. 5.2), sampled at 1000 Hz, and then stored in a desktop for offline analysis.

5.1.2 Measuring devices of blood pressure and cardiac output

Fig. 5.4 shows the measuring devices for BP and CO. The BP measurement device is a standard auscultatory cuff sphygmomanometer (Riester, Germany). During experiment, SBP and DBP were measured from the right arm by a registered nurse and MBP is calculated from SBP and DBP by Eq.(1.1):

$$MBP = \frac{2}{3} DBP + \frac{1}{3} SBP . \tag{1.1}$$

The same nurse was utilized in the two experiments.

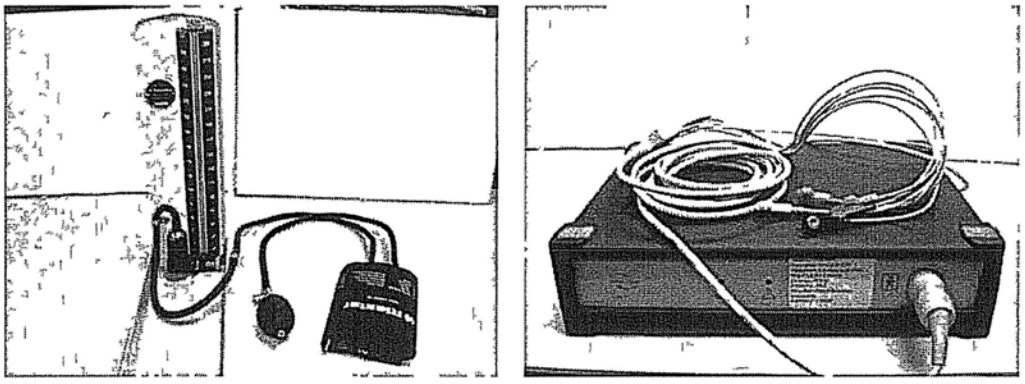

(a) **(b)**

Fig. 5.4. The (a) BP and (b) CO measurement device in the experiment.

The impedance cardiographic device used for reference CO measurement was Physio Flow PF-05 (Manatec Biomedical, Macheren, France). It is automatic and non-invasive, suitable for exercise testing. Moreover, this device utilizes an improved algorithm that excludes the basal thoracic impedance Z_0 and the distance between electrodes (L) to ensure that the CO readings are robust to electrode positions, skin thickness and perspiration [2] [3]. Several validation studies have shown that PF-05 agrees well with direct Fick's method in exercise tests, especially on healthy subjects [2, 4, 5].

The device calculates CO by:

$$CO = HR \times SVi \times BSA , \tag{5.1}$$

where HR is the heart rate ($beats\ min^{-1}$), calculated from R-R interval of the measured ECG signal; BSA is the body surface area (m^2), calculated by the Haycock formula ($BSA = 0.024265 \times BM^{0.5378} \times H^{0.3964}$), where BM is body mass in *kg* and H is the height in *cm*;

and then every two minutes later, until the end of the experiment (see Fig. 5.1). As shown in Fig. 5.1, signal trials (T_i) each of 40s were collected, cut from the onset of each BP measurement and from in between of two sequent BP measurements. In experiment I, 13 trials were collected, including 1 trial measured at baseline, 6 trials during exercise and 6 trials during recovery. In experiment II, for each subject, 1 trial was collected at baseline, while the numbers of trials collected in the exercise and recovery phases were different, depending on the exercise and recovery time of each specific subject.

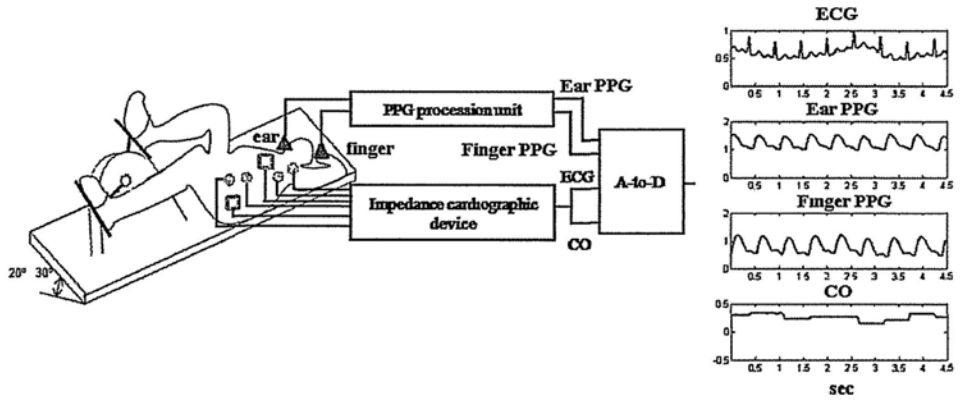

Fig. 5.2 The experiment setup, signal procession and recording block diagrams. The four impedance electrodes (cycles) and two ECG electrodes (squares) are attached on the chest. PPG acquisition devices (triangles) is placed on the right ear lobe and left index finger. Signals are simultaneously acquired, filtered, pass through an A-to-D converter, and are finally displayed and saved in a desktop.

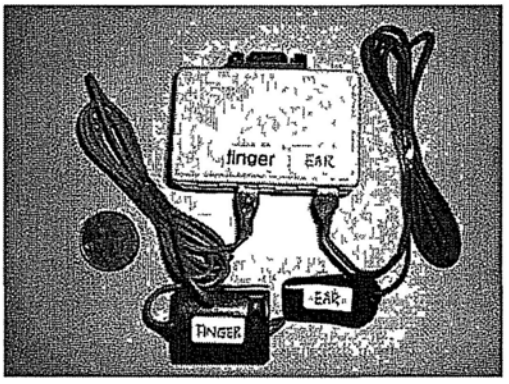

Fig. 5.3 The in-house made PPG acquisition devices and the procession unit (the square box).

The equipment configuration was shown in Fig. 5.2. ECG and CO were acquired through six electrodes attached on the chest and connected to the impedance cardiographic device, which will be described in detail in section 5.1.2. PPG was acquired by the in-house designed acquisition devices (MPAS, JCBME lab, CUHK, Hong Kong, shown in Fig. 5.3) on the right ear lobe and on the left index finger of the subject. The PPG acquisition devices were ear or finger clips with

SVi is the SV index ($ml\ m^{-2}$) , calculated by SV divided by BSA. SVi is calculated by:

$$SVi = SVi_{cal} \times \sqrt[3]{CTI/CTI_{cal} \times TFIT_{cal}/TFIT} \quad , \tag{5.2}$$

where CTI is the contractility index and equals to the largest rate of variation of the impedance signal (dZ/dt_{max}); TFIT (ms) is the thoracic flow inversion time, measured as the time interval between the first zero value following the beginning of the cardiac cycle (beginning of QRS in ECG) and the first nadir after the peak of the ejection velocity (dZ/dt_{max}); 'cal' indicates that the parameters are measured during the calibration phase.

In the algorithm of Physio Flow PF-05, a calibration procedure is critical for the following CO measurements. It is a period of 30 heart beats, when the subject is in his/her baseline condition. The SVi_{cal} is calculated from the largest impedance variation during systole (Z_{max} - Z_{min}), CTI and W (TFIT) (TFIT weighted by measured pulse pressure (PP)), by the formula as follows:

$$SVi_{cal} = k \times \left[(dZ/dt_{\max})/(Z_{\max} - Z_{\min})\right] \times W(TFIT_{cal}) , \tag{5.3}$$

where k is a constant.

The PF-05 provides four analog signals: ECG, impedance (Z), SV and CO. They are internally rolling averaged to ensure signal stability. Hence, averaged CO of each trial (40 s) was calculated for comparison.

5.1.3 Data analysis

Calibration methods

In the BP analysis, estimated BP was obtained from PAT using Eq.(4.7):

$$MBP = A \cdot PAT + B \quad . \tag{4.7}$$

We utilized two calibration methods to obtain constant A and B. First, the best-fit method based on the least square error algorithm was utilized. This method was used so as to test the best possible performance of BP estimation using a linear PAT model. The second method was the mean calibration approach, which utilized the initial value and mean value in a BP sequence to calibrate A and B. The mean value was utilized here, because calibration with any single reference and estimated BP would bias the subsequent evaluation results [6, 7].

In CO analysis, since Z_c was unavailable, two surrogates of PTRR were utilized for CO estimation. One was $PTRR^{\#}$ defined by in chapter 4 by Eq.(4.13):

$$PTRR^{\#} = \frac{-PAT \cdot (1 - IPA)}{(1 + IPA)} \quad , \tag{4.13}$$

and the other surrogate $PTRR^{*}$ was defined as:

$$PTRR^{*} = \frac{(A \cdot PAT + B) \cdot [1 - IPA)]}{1 + IPA} \quad , \tag{5.4}$$

where A and B are constants in Eq.(4.7), obtained from mean calibration through BP analysis. The purpose of introducing $PTRR^{*}$ is to test the necessity of BP measurement in CO estimation. Both

PTRR$^{\#}$ and PTRR* are assumed to be proportional to CO:

$$CO = C \cdot PTRR^{\#} \tag{5.5}$$

and

$$CO = D \cdot PTRR^{*}, \tag{5.6}$$

where C, D are constants. Similar to the BP analysis, the calibration factor C in Eq.(5.5) and D in Eq.(5.6) were calculated from the mean reference CO, a strategy proposed in [6]. In [6], a statistical index called root mean squared normalized error (RMSNE) was used to represent the estimation accuracy based on mean calibration, defined as:

$$RMSNE = \sqrt{\mu^2 + \sigma^2}, \tag{5.7}$$

where μ and σ are the bias and standard deviation of the percentage differences between reference and estimated CO which is calculated by $\frac{x_{1,i} - x_{2,i}}{x_{1,i}}$, where $x_{1,i}$ and $x_{2,i}$ are the *ith* trial of the reference CO and estimated CO, respectively. In the later analysis, RMSNE was also calculated in the result section to evaluate the accuracy of the estimated results.

Statistic Analysis

The data analysis was separated into two parts, MBP analysis and CO analysis. In each part, the results were represented in terms of mean ± standard deviation (SD). Linear regression analysis was first used to indicate the intra-subject correlations. Then, the estimated results were presented. For MBP estimation, the agreements between the reference and testing methods were evaluated by the AMMI standard, that is: the accuracy of the testing method was regarded as acceptable if the mean of estimated errors was less than 5 mmHg and SD of estimated errors was less than 8 mmHg. In the CO estimation, both the absolute and relative estimated errors were evaluated to discuss the agreements on the test and reference CO methods. As outlined in [8], relative errors were introduced in order to eliminate the potential influence of calibration on the agreement between two methods due to the between-patient variability in CO. And the relative errors were suggested [8] to be calculated as the differences between the intra-subject relative changes of CO and CO index with respect to their values at the calibration point, i.e., mean in this study. For example, CO relative changes of 50% and 150% in the result section would, respectively, indicate 50% decrease and 50% increase of CO with respect to its mean.

To interpret the tracing ability of estimated values to reference values, the plot of regression analysis was utilized, and the regression equation was calculated. To specifically discuss the level of agreement on two methods, Bland-Altman plot was utilized [9]. Bias and precision were defined as mean and 1.96 times of standard deviation of the estimated errors, respectively. Limit of agreements was expressed as (bias - precision, bias + precision). Percent error was calculated by dividing precision by mean of reference. The CO method was considered clinically acceptable, if the percent error was below 30%, as proposed in [1]. Differences among subject groups were evaluated by either group student t-test or one-way ANOVA with Bonferroni post hoc analyses, depending on the no. of subject groups considered. All statistical analysis was computed using Matlab 7.0. A p value < 0.05 was considered significant, unless indicated otherwise.

5.2 Results

5.2.1 General description

In total, 1833 trials from 84 subjects were collected, including 84 trials at rest, 1108 trials during

exercise and 641 trials during recovery. 88 trials were removed due to the noises caused by motions and respirations during exercise. Another 36 trials can not be analyzed, including 27 trials removed due to the poor quality of the impedance signal, 7 trials withdrawn due to bad quality of PPG signal and 2 trials withdrawn due to bad quality ECG. Totally, 1709 trials were used in further analysis.

5.2.2 Mean blood pressure analysis

Linear correlation analysis

Fig. 5.5 shows the results of linear correlation analysis among three parameters, PAT_{finger}, PAT_{ear}, PTT_{bra}, and SBP, MBP and DBP in all subjects. Table 5.3 lists the quantitative data corresponding to the qualitative description shown in Fig. 5.5. In most of the subjects, PAT_{finger}, PAT_{ear} and PTT_{bra} were negatively correlated with SBP, MBP and DBP. ANOVA with Bonferroni post hoc analyses revealed that PAT_{finger} and PAT_{ear} were superior surrogates of SBP and MBP to PTT_{bra}, and there were no significant differences on mean r between correlations of SBP and MBP with PAT_{finger} and between correlations of SBP and MBP with PAT_{ear}. From visual illustration (Fig. 5.5), the mean r between PAT_{finger} and SBP and between PAT_{finger} and MBP are higher than the corresponding mean r between PAT_{ear} and SBP and between PAT_{ear} MBP, respectively, and the 95% credit intervals are narrower. For DBP, the performances of PATs and PTT_{bra} were comparable. As shown in Table 5.3, the mean r of PAT_{finger} is the highest (mean r = -0.50), while PTT_{bra} owes the highest no. of subjects with significant correlations (n = 56).

Table 5.3 Results of linear correlation analysis between time delays and BPs in global analysis and sub-group analysis.

Time Delays	BPs	Global Analysis	Sub-Group Analysis			
			Heart Failure	Disease Control	Normal Control	Normal Healthy
PAT_{finger}	SBP	-0.90±0.09	-0.90±0.08	-0.91±0.08	-0.94±0.04	-0.86±0.12
	MBP	-0.85±0.12	-0.87±0.12	-0.86±0.13	-0.86±0.11	-0.80±0.09
	DBP	-0.50±0.34	-0.59±0.34	-0.51±0.34	-0.32±0.47	-0.51±0.17
PAT_{ear}	SBP	-0.83±0.14	-0.83±0.16	-0.81±0.13	-0.88±0.10	-0.81±0.11
	MBP	-0.75±0.19	-0.76±0.23	-0.74±0.14	-0.75±0.17	-0.74±0.13
	DBP	-0.37±0.41	-0.48±0.43	-0.36±0.28	-0.16±0.47	-0.42±0.30
PTT_{bra}	SBP	-0.61±0.35	-0.61±0.31	-0.63±0.36	-0.61±0.41	-0.61±0.23
	MBP	-0.63±0.35	-0.63±0.30	-0.62±0.40	-0.65±0.41	-0.63±0.41
	DBP	-0.46±0.37	-0.49±0.29	-0.45±0.42	-0.42±0.46	-0.45±0.26

'±' indicates mean ± SD.

ANOVA with post hoc testing revealed that the mean r between PAT_{finger} and SBP and that between PAT_{finger} and MBP were both higher than that between PAT_{finger} and DBP, and there is no difference on mean r between PAT_{finger} versus SBP and $PAT_{fingerv}$ versus MBP. ANOVA with Bonferroni post hoc analyses on mean r between PAT_{ear} and different BPs revealed the same results as those of PAT_{finger}. For PTT_{bra}, ANOVA with Bonferroni post hoc analyses only revealed significantly higher mean r of PTT_{bra} versus DBP as compared with that of PTT_{bra} versus SBP and PTT_{bra} versus MBP.

Fig. 5.6 shows the results of linear correlation analysis on different subject groups. The corresponding quantitative data are listed in Table 5.3. In each group, the main observations were

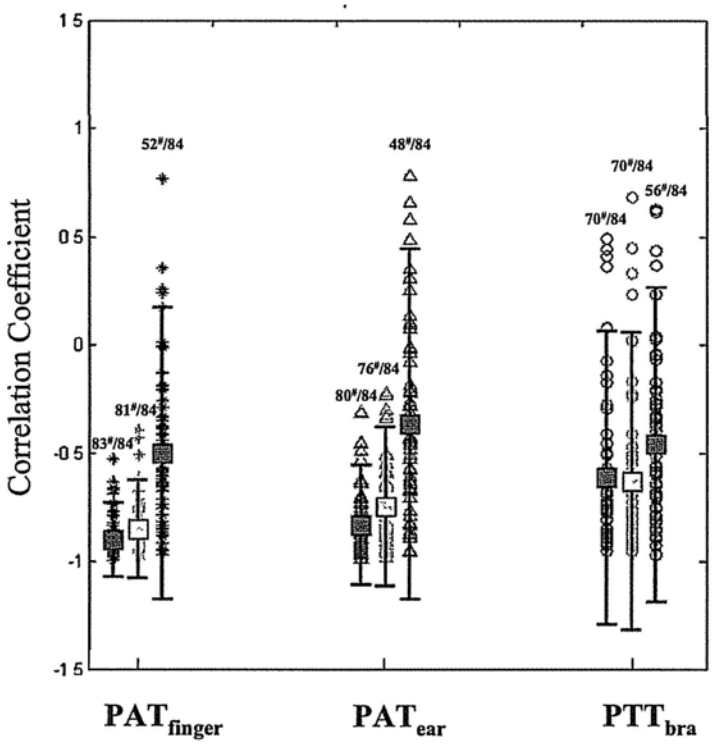

Fig. 5.5. Intra-subject correlation coefficients between measured time delays (PAT_{finger}, PAT_{ear}, PTT_{bra}) with BPs (SBP, MBP, DBP) in all subjects. Y-axis is the correlation coefficient, x-axis is time delay parameters: PAT_{finger}, PAT_{ear} and PTT_{bra} groups. Individual correlation coefficient is represented by '*' for PAT_{finger}, 'Δ' for PAT_{ear} and 'o' for PTT_{bra}. For each time delay parameter, correlation coefficients between this parameter with SBP (red), MBP (green) and DBP (blue) are separated by vertical lines with different colors. On each vertical line, the solid square represents the group mean and the vertical solid line represents the range where 95% data stay. The number "**#/**"over each vertical line indicates "the no. of significant correlations#/number of correlations".

similar to those shown in the global data: 1) PAT_{finger} and PAT_{ear} were superior surrogates of SBP and MBP to PTT_{bra}; 2) The mean r between PATs and SBP and that between PATs and MBP were significantly higher than that between PATs and DBP; 3) performances of PAT_{finger}, PAT_{ear} and PTT_{bra} on DBP were comparable. Age effect was investigated by group t-test conducted on normal healthy and normal control groups. For both PAT_{finger} and PAT_{ear}, group t-test revealed: there were no significant differences on mean r between PAT and SBP in the younger and older groups but significant differences on mean r between PAT and MBP and between PAT and DBP between the younger and older groups. The disease effect was investigated by comparing the results on normal control, disease control and heart failure groups. The ANOVA with post hoc testing indicated no significant differences among the correlations of different subject groups except for significant difference on the mean r of PAT_{ear} and DBP between heart failure and normal control groups (p = 0.0498). The gender effect was also investigated. There were totally 58 male and 26 female subjects, and the group t test revealed no significant differences on mean r of different gender groups except for the only significant difference on mean r of PAT_{ear} and SBP between gender

groups ($p = 0.0481$).

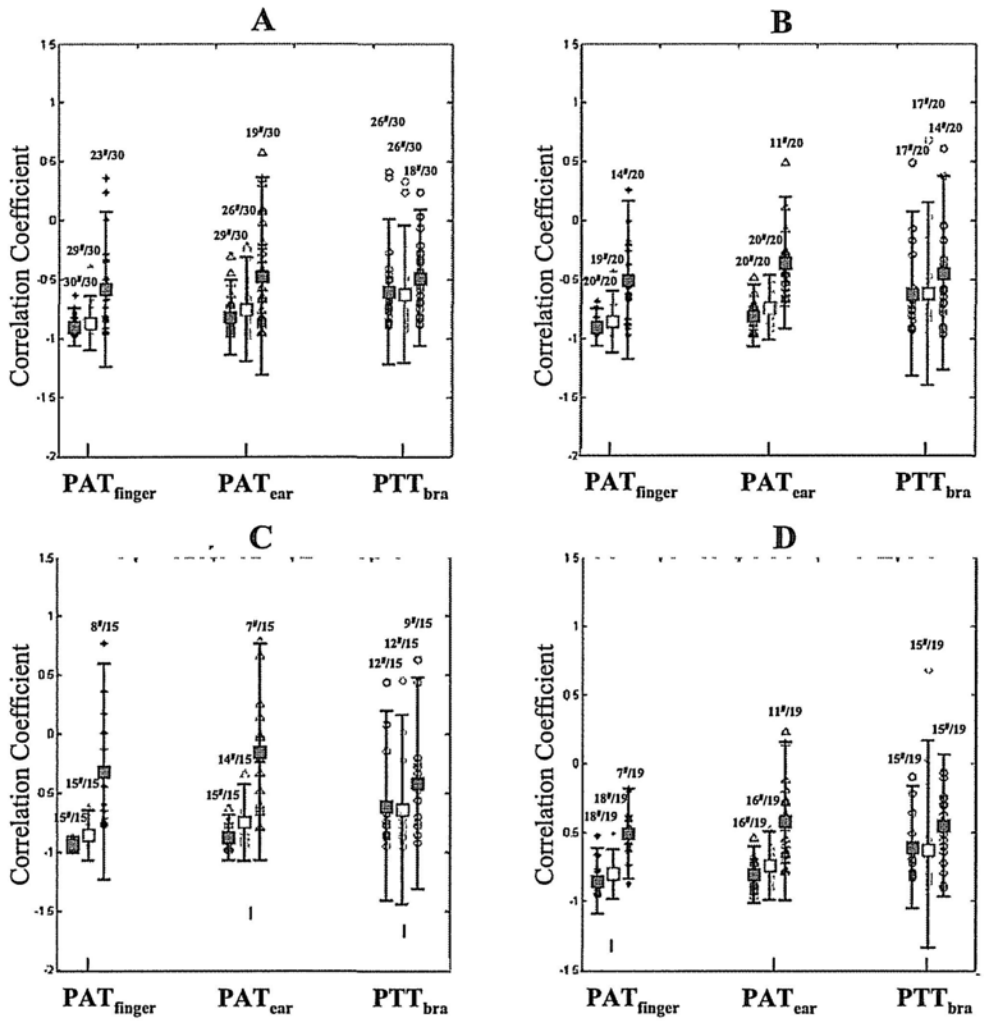

Fig. 5.6. Intra-subject correlation coefficients between measured time delays (PAT_{finger}, PAT_{ear}, PTT_{bra}) with BPs (SBP, MBP, DBP) in different subject groups: A heart failure group, B disease control group, C normal control group and D normal healthy group. For the meanings of the symbols in A-D, please refer to the legend of Fig. 5.5. The number "**$^{\#}$/**"over each vertical line indicates "the no. of significant correlations$^{\#}$/number of correlations".

Results of BP estimation

The dynamic exercise induced big changes of MBP and PAT_{finger}. The reference MBP changed from 64.0 mmHg to 157.8 mmHg (104.9 ± 17.5 mmHg) and PAT_{finger} decreased from 224 ms to 72 ms (131± 27 ms). The results of best-fit MBP estimated from PAT_{finger} for all subjects are visually illustrated in Fig. 5.7 A and B. The estimated MBP ranged from 60.6 mmHg to 156.3 mmHg (104.9 ± 16.9 mmHg) and there was a significantly high and positive correlation between the reference and estimated MBP (r = 0.96). The bias ± SD of the estimation errors was 0 ± 4.71 mmHg. The above data demonstrated the best possible MBP estimation results from a linear

model using PAT_{finger}. The results of sub-group analysis for the best-fit MBP estimation are shown in Fig. 5.8 and the quantitative data are listed in Table 5.4. The precisions of best-fit estimations are similar in the heart failure, normal control and normal healthy groups, and the precision is a bit lower in the disease control group. The close and small bias ± SDs of errors in all subject groups indicated the good performance of PAT_{finger} for MBP estimation in different subject populations.

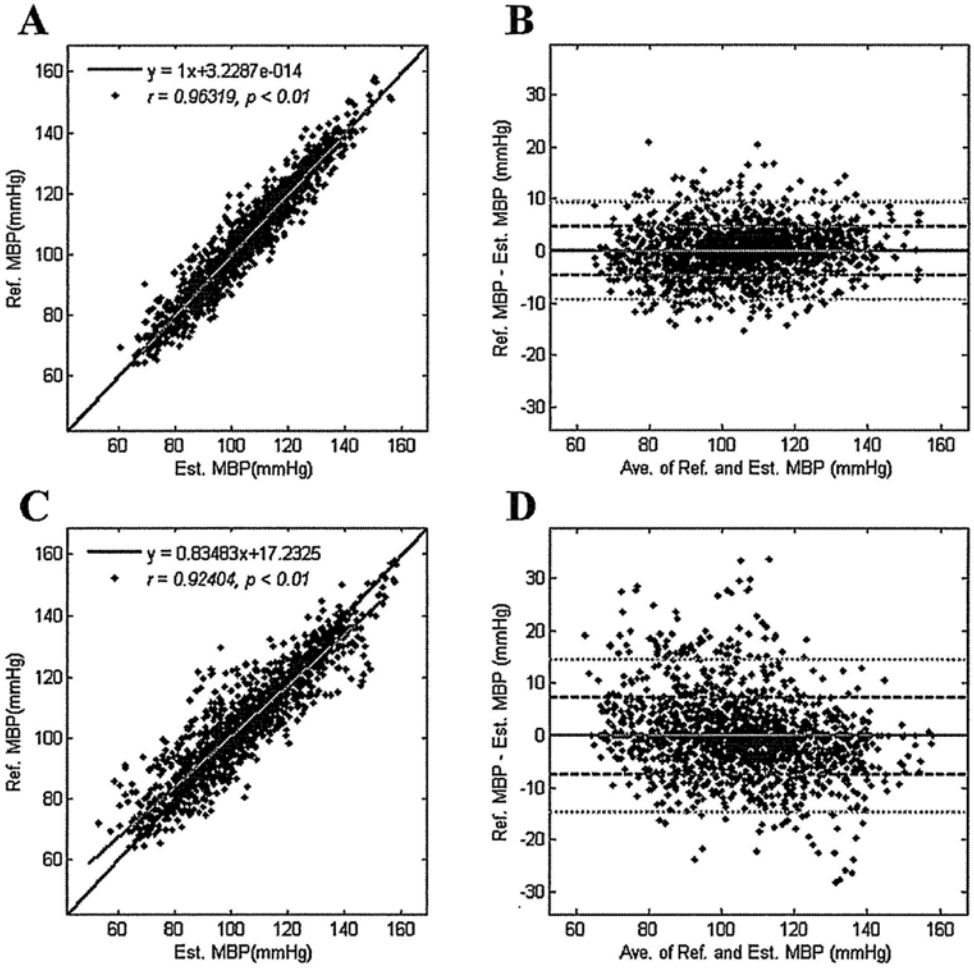

Fig. 5.7. Regression analysis plot (A) and Bland-Altman plot (B) for the best-fit estimation results of MBP and regression analysis plot (C) and Bland-Altman plot (D) for mean calibration estimation results of MBP. In the regression equation, y is reference MBP and x is estimated MBP. The black solid line is the equality line and the red solid line is the regression line of data. In the Bland-Altman plots, the red solid line is the bias; the range between two blue dash lines is bias ± SD; the range between two green lines is bias ±1.96SD, where 95% of the data stay.

Fig. 5.7 C and D show the MBP estimation results based on mean calibration method. The range of the estimated MBP was from 52.7 mmHg to 158.3 mmHg (104.9 ± 17.5 mmHg). As shown in the regression plot (Fig. 5.7 C), the estimated MBP underestimates reference MBP at lower MBP levels and overestimated MBP at higher MBP levels. The correlation coefficient between reference

and estimated MBP was high, i.e. 0.92. The SD of errors was 7.42 mmHg. Fig. 5.9 shows the sub-group results, where a trend of underestimation at lower MBP levels and overestimation at higher MBP values exists in all subject groups. The estimation results in normal control group showed the worst performance, with lowest correlation between the estimated and reference MBP. Table 5.5 lists the estimation results in different subject groups.

Table 5.4 Sub-group results of the best-fit estimation.

Results	Heart Failure	Disease Control	Normal Control	Normal Healthy
Ref. MBP (mmHg)	77.3~153.2 (111.8 ± 15.0)	66.3~145.8 (103.2 ± 15.0)	70.0~157.8 (109.7 ± 17.7)	64.0~118.0 (84.5 ± 10.7)
Est. MBP (mmHg)	73.2~156.3 (111.8 ± 14.3)	69.1~143.7 (103.2 ± 14.0)	71.2~150.9 (109.7 ± 17.1)	60.6~112.7 (84.5 ± 9.9)
Bias± SD (mmHg)	0 ± 4.52	0 ± 5.20	0 ± 4.60	0 ± 4.23

Ref.: reference value; Est. estimated value; '±': mean ± SD, '~': minimum value ~ maximum value.

Table 5.5 Sub-group results of the mean calibration.

Results	Heart Failure	Disease Control	Normal Control	Normal Healthy
Ref. MBP (mmHg)	77.3~153.2 (111.8 ± 15.0)	66.3~145.8 (103.2 ± 15.0)	70.0~157.8 (109.7 ± 17.7)	64.0~118.0 (84.5 ± 10.7)
Est. MBP (mmHg)	62.5~157.9 (111.8 ± 17.4)	60.6~149.1 (103.3 ± 18.1)	60.7~158.3 (109.7 ± 19.7)	52.7~118.0 (84.5 ± 13.1)
Bias± SD (mmHg)	0 ± 7.61	0 ± 7.70	0 ± 7.11	0 ± 6.49

Ref.: reference value; Est. estimated value; '±': mean ± SD, '~': minimum value ~ maximum value.

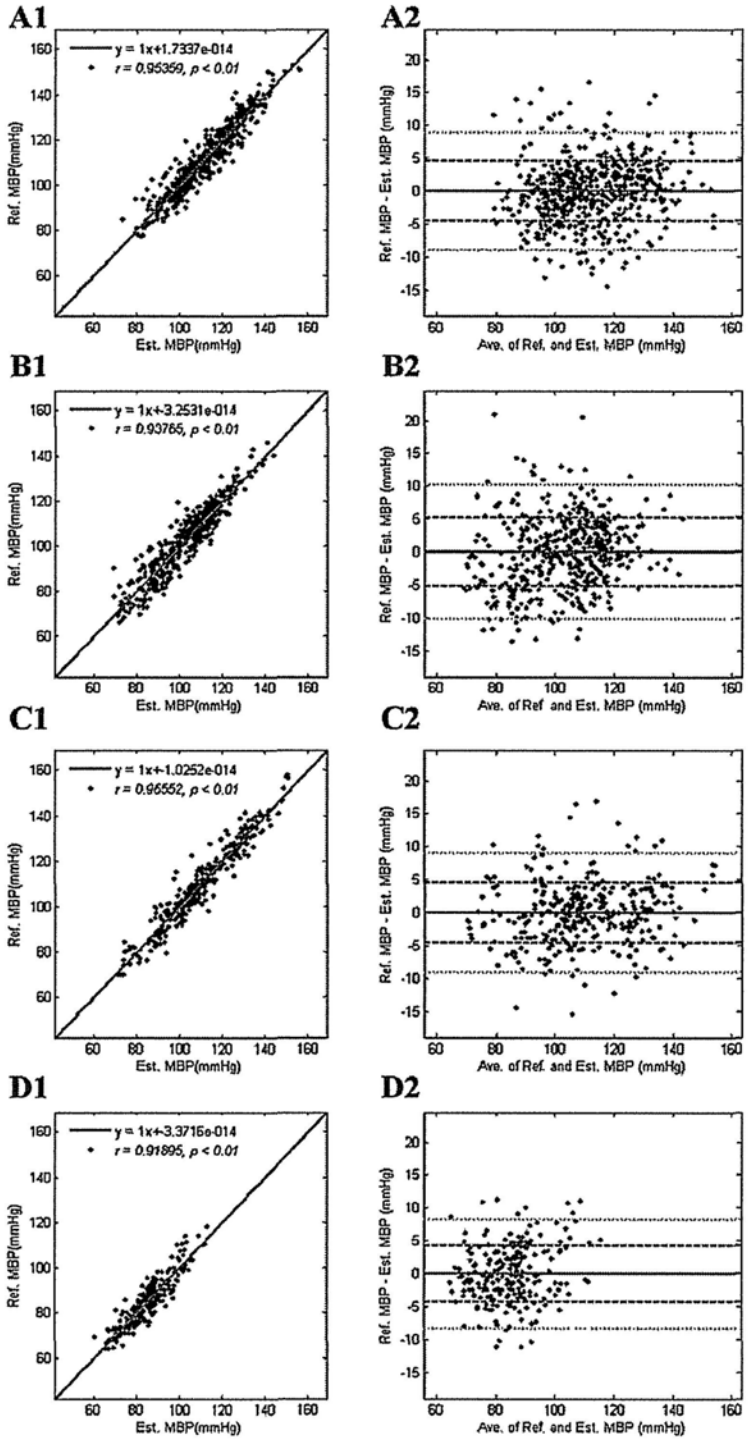

Fig. 5.8. Regression analysis plots (left figures, A1-D1) and Bland-Altman plots (right figures, A2-D2) for the best-fit MBP estimation results for heart failure group (A1 and A2), disease control group (B1 and B2), normal control group (C1 and C2) and normal healthy group (D1 and D2). In the regression equation, y is reference MBP and x is estimated MBP. The black solid line is the equality line and the red solid line is the regression line of data. In the Bland-Altman plots, the red solid line is the bias; the range between two blue dash lines is bias ± SD; the range between two green lines is bias ±1.96SD, where 95% of the data stay.

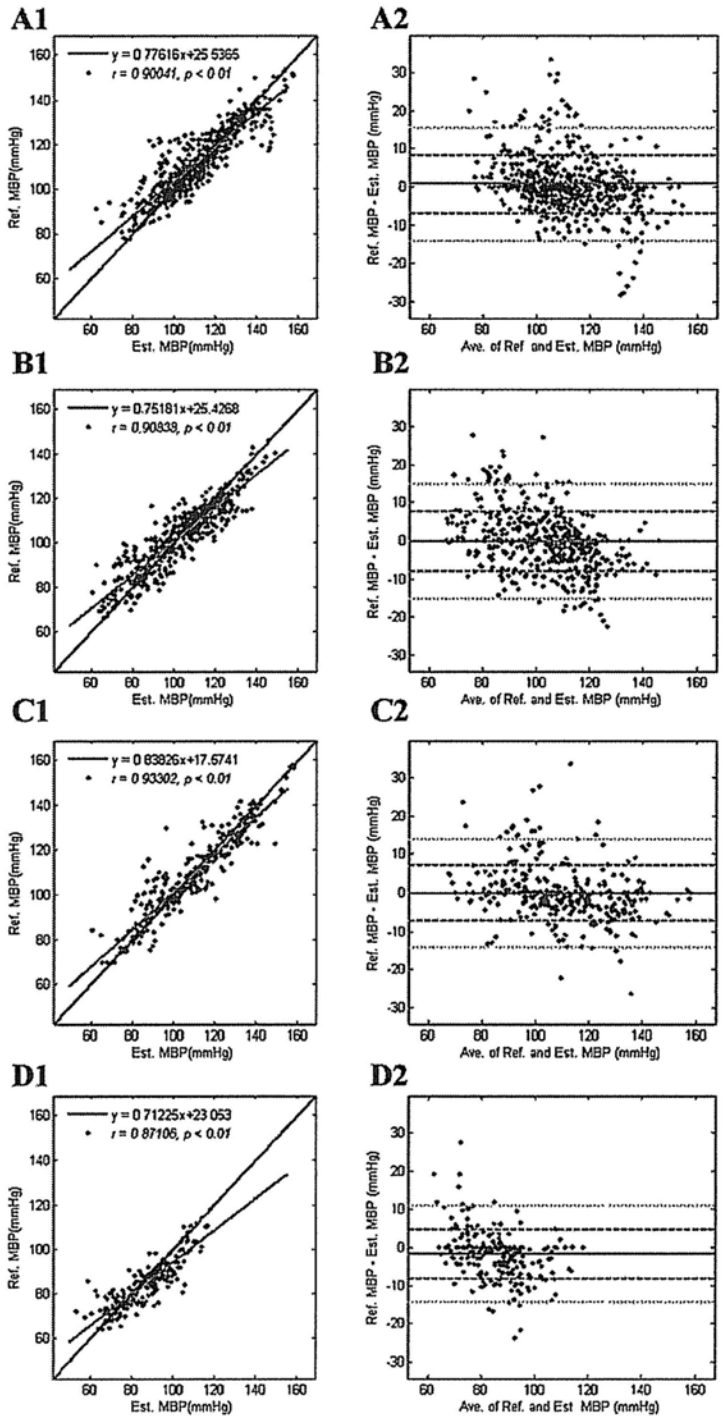

Fig. 5.9. Regression analysis plots (left figures, A1-D1) and Bland-Altman plots (right figures, A2-D2) for the mean calibration MBP estimation results for heart failure group (A1 and A2), disease control group (B1 and B2), normal control group (C1 and C2) and normal healthy group (D1 and D2). In the regression equation, y is reference MBP and x is estimated MBP. The black solid line is the equality line and the red solid line is the regression line of data. In the Bland-Altman plots, the red solid line is the bias; the range between two blue dash lines is bias ± SD; the range between two green lines is bias ±1.96SD, where 95% of the data stay.

5.2.3 Cardiac output analysis

Linear correlation analysis

Fig. 5.10 shows the results of linear correlation analysis between two CO indices, PTRR$^{\#}$ and PTRR*, and CO in all subjects and in subject groups. Table 5.6 lists the quantitative data corresponding to the visual illustration shown in Fig. 5.10. In all subjects, both PTRR$^{\#}$ and PTRR* showed positive correlations with CO, and there were significant correlations in 83 out of 84 subjects. The mean r for both PTRR$^{\#}$ versus CO and PTRR* versus CO was 0.92 and r was over 0.9 in 82% and 81% of the subjects, respectively, between PTRR$^{\#}$ and CO and between PTRR* and CO. Group t-test indicated no significant differences between the mean correlation r between PTRR$^{\#}$ versus CO and PTRR* versus CO ($p = 0.8621$).

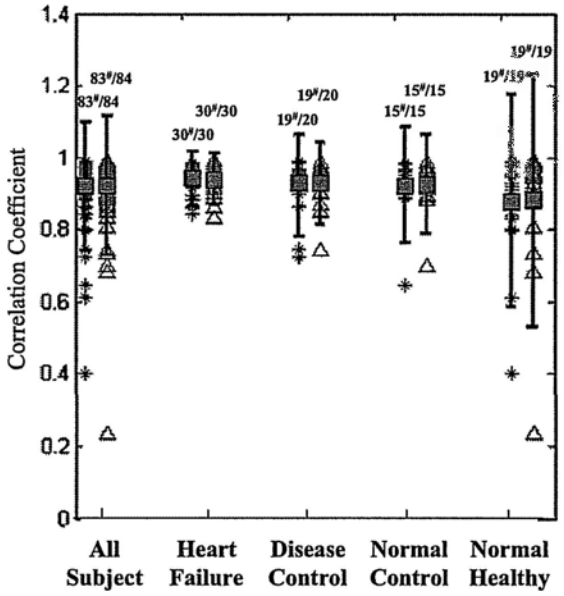

Fig. 5.10. Intra-subject correlation coefficients between PTRRs (PTRR$^{\#}$ and PTRR*) and reference CO in all subjects and subject groups. Individual correlation coefficient is represented by '*' for PTRR$^{\#}$ and 'Δ' for PTRR*. In each vertical line, the solid square represents the group mean and the vertical solid line represents the range where 95% data stay. The number "**$^{\#}$/**"over each vertical line indicates "the no. of significant correlations$^{\#}$/number of correlations".

The results of subgroup analysis are shown in Fig. 5.10 and Table 5.6. Group t-test indicated no significant differences on the mean r between PTRR$^{\#}$ and CO and between PTRR* and CO in any group (heart failure group: p=0.8435; disease control group: p=0.7788; normal control group: p=0.9254; normal healthy group: p=0.7652). The age effect and disease effect were investigated and ANOVA with Bonferroni post hoc analyses revealed no significant differences on mean r among subject groups both for correlations between PTRR$^{\#}$ and CO and correlations between PTRR* and CO. The gender effect was also investigated. The group t test revealed no significant

differences on mean r between gender groups.

Table 5.6 Results of linear correlation analysis between PTRRs and CO.

Correlation	Global Analysis	Sub-Group Analysis			
		Heart Failure	Disease Control	Normal Control	Normal Healthy
$PTRR^{\#}$ and CO	0.92±0.09	0.94±0.04	0.92±0.07	0.92±0.08	0.88±0.15
$PTRR^{*}$ and CO	0.92±0.10	0.94±0.04	0.93±0.06	0.92±0.07	0.88±0.18

'±' indicates mean ± SD.

Results of CO estimation

The increase in CO during exercise ranged from 3.02 L min^{-1} to 24.38 L min^{-1} (9.03 ± 3.14 L min^{-1}) and the ranges of estimated CO were 2.77 L min^{-1} to 24.71 L min^{-1} (9.03 ± 3.25 L min^{-1}) and 2.10 L min^{-1} to 23.55 L min^{-1} (9.03 ± 3.26 L min^{-1}) , respectively, for estimation using $PTRR^{\#}$ and estimation using $PTRR^{*}$. The corresponding relative changes of reference CO, $PTRR^{\#}$ and $PTRR^{*}$ were from 34% to 185% (100% ± 25%), from 38% to 199% (100% ± 27%), from 27% to 184% (100% ± 27%), respectively. As shown in the regression plots in Fig. 5.11 A and C, the estimated CO from both $PTRR^{\#}$ and $PTRR^{*}$ traced the reference CO closely ($r > 0.9$ for both $PTRR^{\#}$ and $PTRR^{*}$). The agreements between reference and estimated CO are shown in the Bland-Altman plots (see Fig. 5.11 B and D), where the precisions for $PTRR^{\#}$ and $PTRR^{*}$ based estimations are 2.04 L min^{-1} and 2.08 L min^{-1}, respectively. The percent errors were 22.57% and 23.05% and RMSNEs were 12.17% and 12.47% for the estimation results based on $PTRR^{\#}$ and $PTRR^{*}$, respectively.

Fig. 5.12 shows the agreements between the relative reference CO and two CO indices. There were significantly high and positive correlations between the relative changes of reference CO and $PTRR^{\#}$ ($r = 0.91$) and between those of reference CO and $PTRR^{*}$($r = 0.91$). Fig. 5.12 indicates that both relative $PTRR^{\#}$ and $PTRR^{*}$ underestimates the relative CO at lower CO level and overestimate CO at higher CO level. The precisions of relative errors between CO and $PTRR^{\#}$ and that between CO and $PTRR^{*}$ are 22.13% and 22.39%, respectively, both improved as compared to the precisions of the corresponding absolute errors.

The results of CO estimation using $PTRR^{\#}$ in different subject groups are visually compared in Fig. 5.13, and the corresponding statistical analysis results are listed in Table 5.7. In all groups, there was a significantly high and positive correlation between estimated and reference CO (r>0.9). The estimation precisions of $PTRR^{\#}$ in different subject groups were similar, at a level of 2 L min^{-1}. As shown in the regression plots (Fig. 5.13, A1-D1), the estimated CO underestimates the reference CO at lower CO level and overestimate reference CO at higher levels in the heart failure group, disease control group and normal control group, in the normal healthy group however, the condition verses.

The results of CO estimation using PTRR* in different subject groups are compared in Fig. 5.14

Table 5.7 Sub-group CO estimation results using PTRR#.

Results	Heart Failure	Disease Control	Normal Control	Normal Healthy
Ref. CO (L min^{-1})	3.35~24.38 (9.06 ± 3.43)	3.02~17.27 (8.65 ± 3.01)	4.22~20.86 (9.92 ± 3.11)	4.37~16.30 (8.39 ± 2.27)
Est. CO (L min^{-1})	3.42~24.71 (9.06 ± 3.57)	2.77~16.11 (8.65 ± 3.06)	3.16~19.37 (9.92 ± 3.40)	3.98~13.77 (8.39 ± 2.00)
Bias± 1.96SD (L min^{-1})	0 ± 2.04	0 ± 2.00	0 ± 2.19	0 ± 1.89
Percent Error (%)	22.49	23.16	22.03	22.46
RMSNE (%)	12.61	12.51	11.10	11.91

Ref.: reference value; Est. estimated value; '±': mean ± SD, '~': minimum value ~ maximum value. For definition of RMSNE, refer to the text.

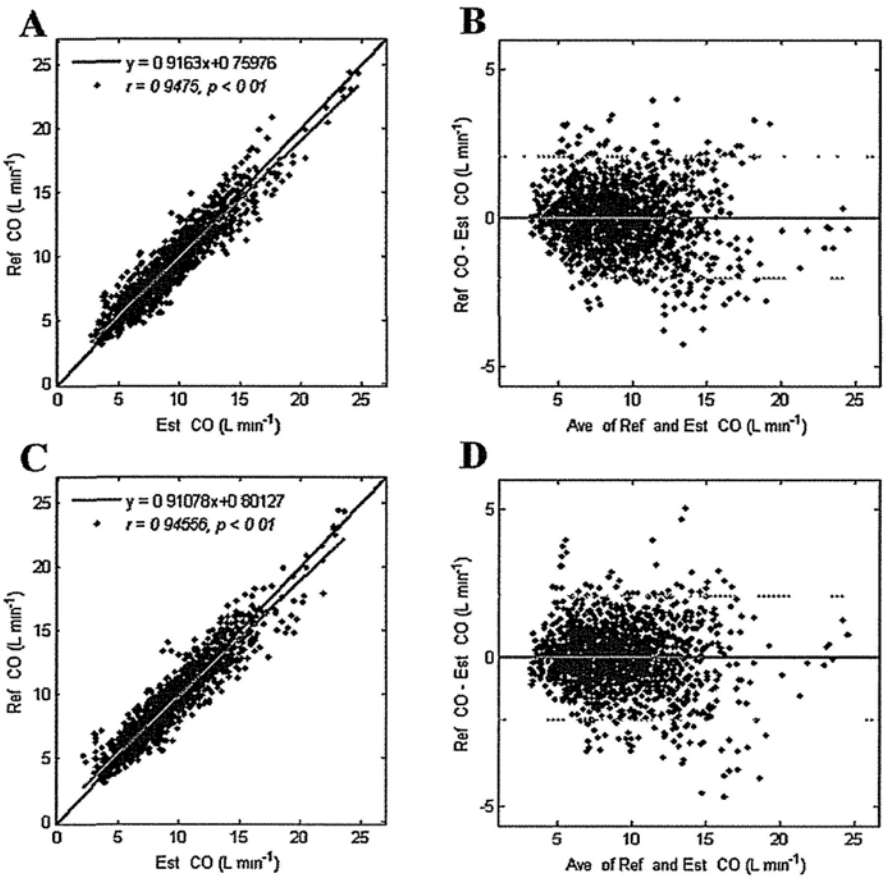

Fig. 5.11. Regression analysis plots (left figures, A and C) and Bland-Altman plots (right figures, B and D) for the absolute estimation results of PTRR# (A and B) and PTRR* (C and D). In the regression analysis plots, regression equation is shown in the legend, where 'y' is the reference CO and 'x' is estimated CO; The black solid line is the equality line and the red solid line is the regression line of data. In the Bland-Altman plots, the red solid line is the bias and the range between two green lines is bias ±1.96SD, where 95% of the data stay.

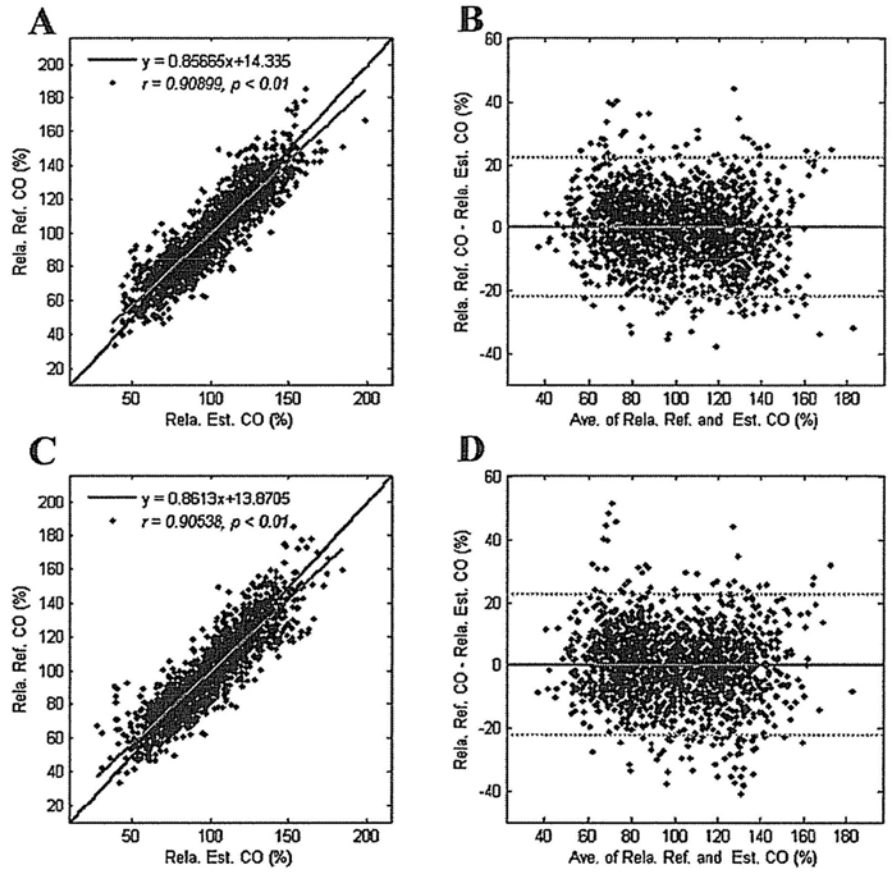

Fig. 5.12 Regression analysis plots (left figures, A and C) and Bland-Altman plots (right figures, B and D) for the relative reference CO and PTRR[#] (A and B) and for the relative reference CO and PTRR[*] (C and D). In the regression analysis plots, regression equation is shown in the legend, where 'y' is the relative reference CO and 'x' is estimated CO; The black solid line is the equality line and the red solid line is the regression line of data. In the Bland-Altman plots, the red solid line is the bias and the range between two green lines is bias ±1.96SD, where 95% of the data stay.

Table 5.8 Sub-group CO estimation results using PTRR[*].

Results	Heart Failure	Disease Control	Normal Control	Normal Healthy
Ref. CO (L min^{-1})	3.35~24.38 (9.06 ± 3.43)	3.02~17.27 (8.65 ± 3.01)	4.22~20.86 (9.92 ± 3.11)	4.37~16.30 (8.39 ± 2.27)
Est. CO (L min^{-1})	2.10~23.55 (9.06 ± 3.58)	3.05~16.00 (8.65 ± 2.97)	3.19~21.89 (9.92 ± 3.46)	3.97~16.90 (8.39 ± 2.20)
Bias ± 1.96SD (L min^{-1})	0 ± 2.10	0 ± 1.87	0 ± 2.43	0 ± 1.89
Percent Error (%)	23.18	21.56	24.52	22.48
RMSNE (%)	13.49	11.81	11.59	12.40

Ref.: reference value; Est. estimated value; '±': mean ± SD, '~': minimum value ~ maximum value. For definition of RMSNE, refer to the text.

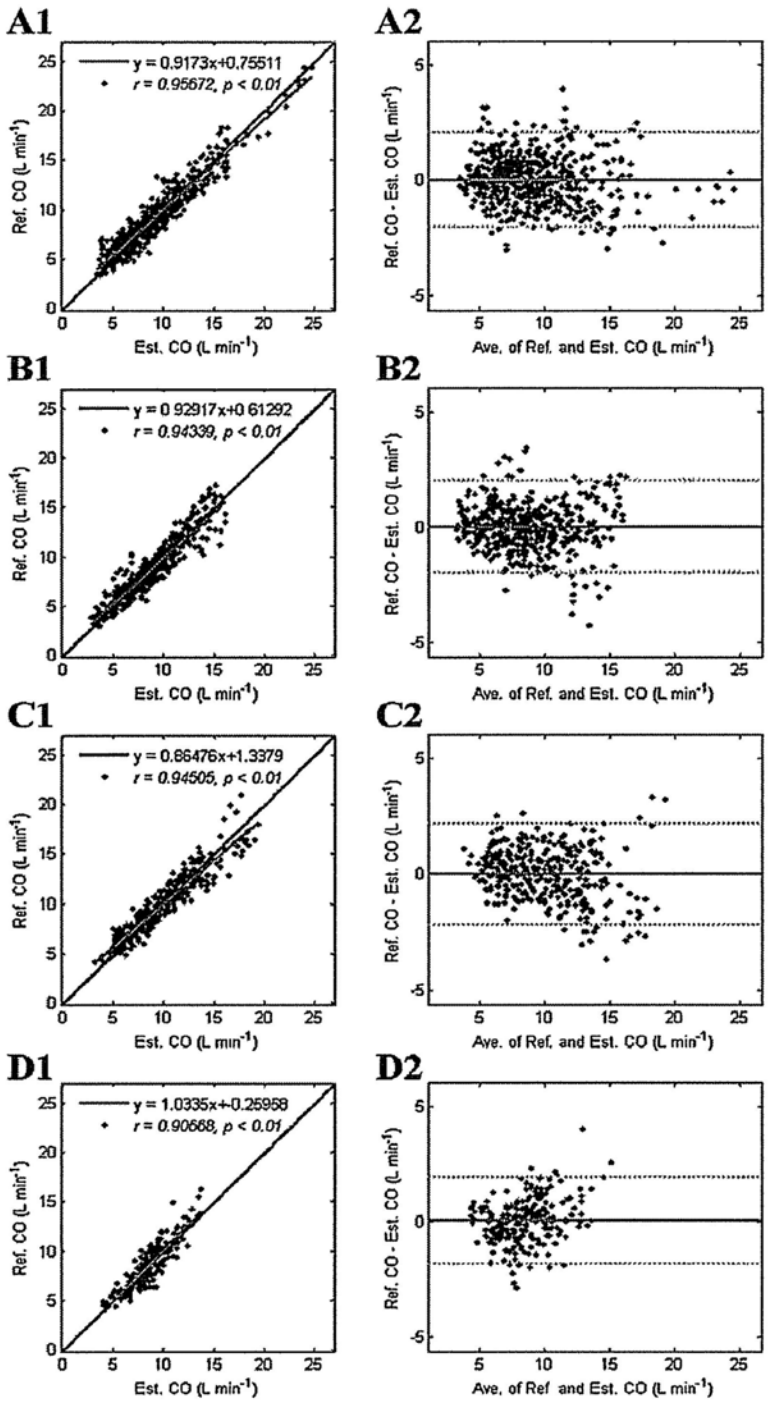

Fig. 5.13 Regression analysis plots (left figures, A1-D1) and Bland-Altman plots (right figures, A2-D2) for absolute estimation results for CO using PTRR[#] on heart failure group (A1 and A2), disease control group (B1 and B2), normal control group (C1 and C2) and normal healthy group (D1 and D2). In the regression analysis plots, regression equation is shown in the legend, where 'y' is the relative reference CO and 'x' is estimated CO; the black solid line is the equality line and the red solid line is the regression line of data. In the Bland-Altman plots, the red solid line is the bias and the range between two green lines is bias ±1.96SD, where 95% of the data stay.

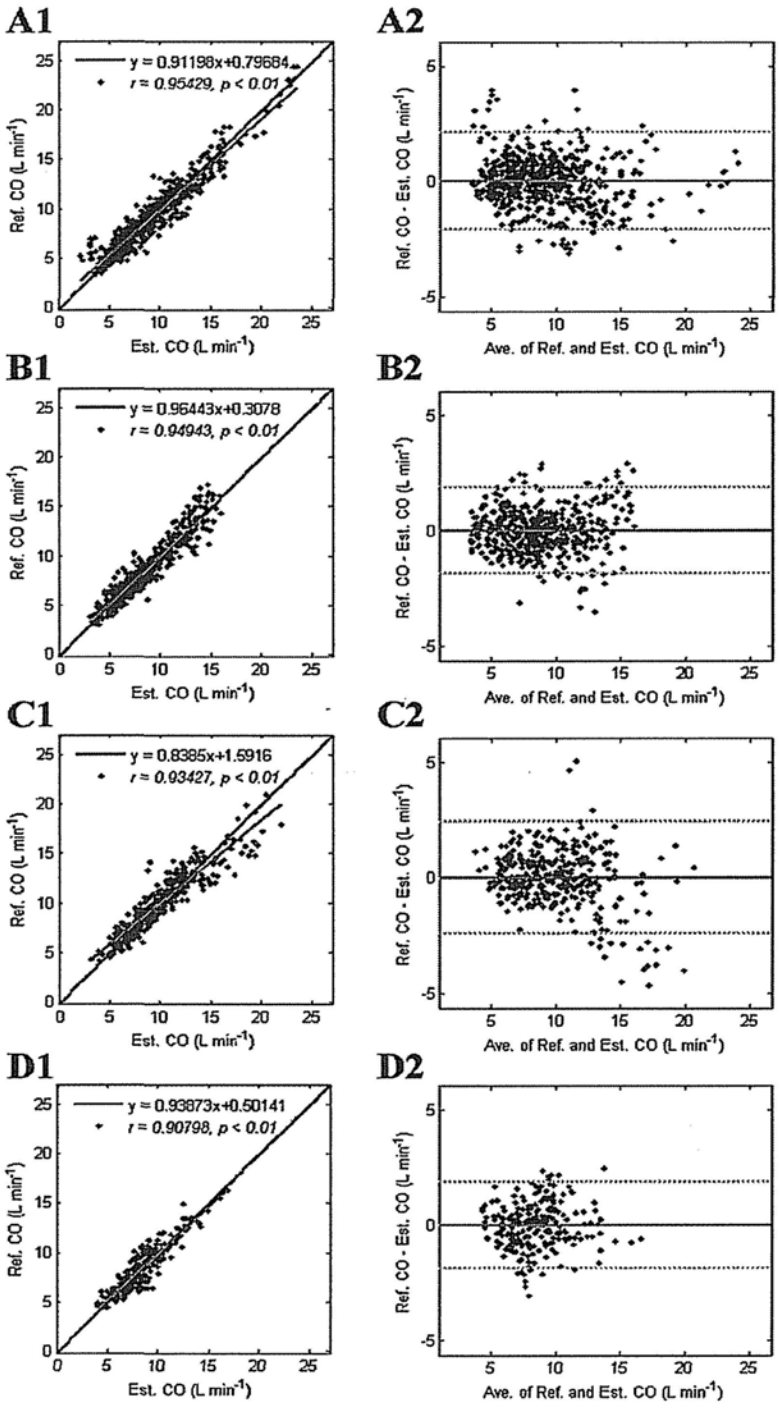

Fig. 5.14 Regression analysis plots (left figures, A1-D1) and Bland-Altman plots (right figures, A2-D2) for absolute estimation results for CO using PTRR$^{\#}$ on heart failure group (A1 and A2), disease control group (B1 and B2), normal control group (C1 and C2) and normal healthy group (D1 and D2). In the regression analysis plots, regression equation is shown in the legend, where 'y' is the relative reference CO and 'x' is estimated CO; the black solid line is the equality line and the red solid line is the regression line of data. In the Bland-Altman plots, the red solid line is the bias and the range between two green lines is bias ±1.96SD, where 95% of the data stay.

and Table 5.8. The estimation accuracies in subject groups had larger variations compared to those obtained from PTRR#. For example, the difference between the precision of disease control group and normal control group was as large as 0.5 L min^{-1}.

The subgroup analysis on the relative changes of CO and PTRR# are illustrated qualitatively in Fig. 5.15 and quantitatively in Table 5.9. The percent error and RMSNE of the relative errors were the same as those of the absolute errors, so they were not listed in Table 5.8 and 5.9. Similar as shown in Fig. 5.12 A, there is an obvious underestimating bias at lower CO levels and an overestimating bias at higher CO level between relative PTRR# and CO in heart failure, disease control and normal control groups (see Fig. 5.15, A1-C1 and A2-C2). This trend of bias was corrected in the data of the normal healthy group, where the slope of the regression equation is close to 1 and intercept close to 0. Fig. 5.16 and Table 5.10 show the results of subgroup analysis on the relative changes of CO and PTRR*.

Table 5.9 Comparison on relative changes of CO and PTRR# in subject groups.

Relative Values	Heart Failure	Disease Control	Normal Control	Normal Healthy
Ref. CO (%)	40.25~178.16 (100 ± 25.56)	33.60~185.24 (100 ± 27.50)	42.30~155.89 (100 ± 24.26)	49.60~150.05 (100 ± 22.51)
Est. CO (%)	43.55~170.89 (100 ± 27.57)	39.53~198.72 (100 ± 28.75)	38.03~165.79 (100 ± 28.04)	52.32~148.15 (100 ± 19.38)
Bias± 1.96SD (%)	0 ± 22.78	0 ± 22.34	0 ± 20.92	0 ± 21.90

Ref.: reference value; Est. estimated value; '±': mean ± SD, '~': minimum value ~ maximum value. For definition of RMSNE, refer to the text.

Table 5.10 Comparison on relative changes of CO and PTRR* in subject groups.

Relative Values	Heart Failure	Disease Control	Normal Control	Normal Healthy
Ref. CO (%)	40.25~178.16 (100 ± 25.56)	33.60~185.24 (100 ± 27.50)	42.30~155.89 (100 ± 24.26)	49.60~150.05 (100 ± 22.51)
Est. CO (%)	27.39~184.25 (100 ± 28.16)	41.51~175.01 (100 ± 26.99)	31.08~155.69 (100 ± 27.52)	56.20~148.45 (100 ± 20.90)
Bias± 1.96SD (%)	0 ± 24.13	0 ± 20.37	0 ± 21.65	0 ± 22.88

Ref.: reference value; Est. estimated value; '±': mean ± SD, '~': minimum value ~ maximum value. For definition of RMSNE, refer to the text.

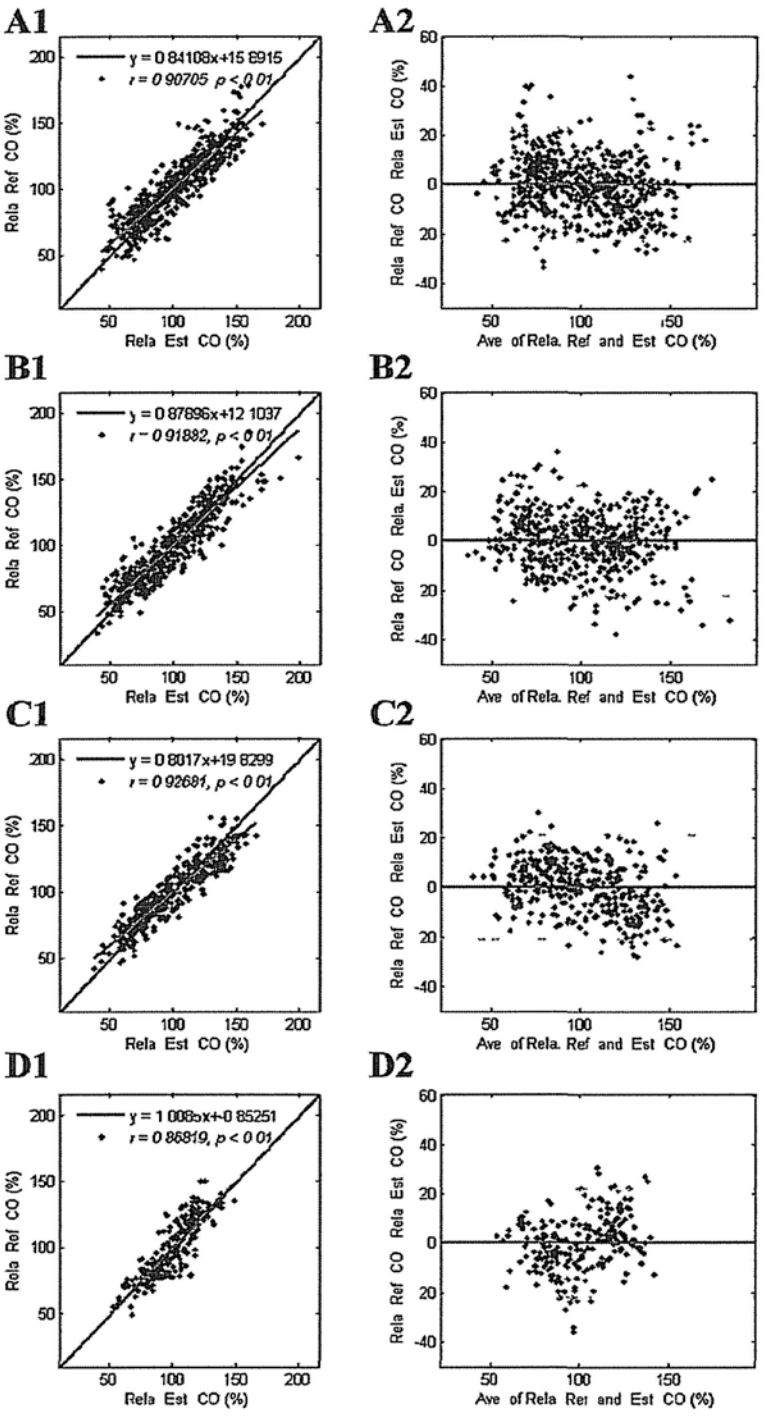

Fig 5.15 Regression analysis plots (left figures, A1-D1) and Bland-Altman plots (right figures, A2-D2) for relative CO and relative PTRR[#] on heart failure group (A1 and A2), disease control group (B1 and B2), normal control group (C1 and C2) and normal healthy group (D1 and D2). In the regression analysis plots, regression equation is shown in the legend, where 'y' is the relative reference CO and 'x' is estimated CO, the black solid line is the equality line and the red solid line is the regression line of data. In the Bland-Altman plots, the red solid line is the bias and the range between two green lines is bias ±1.96SD, where 95% of the data stay

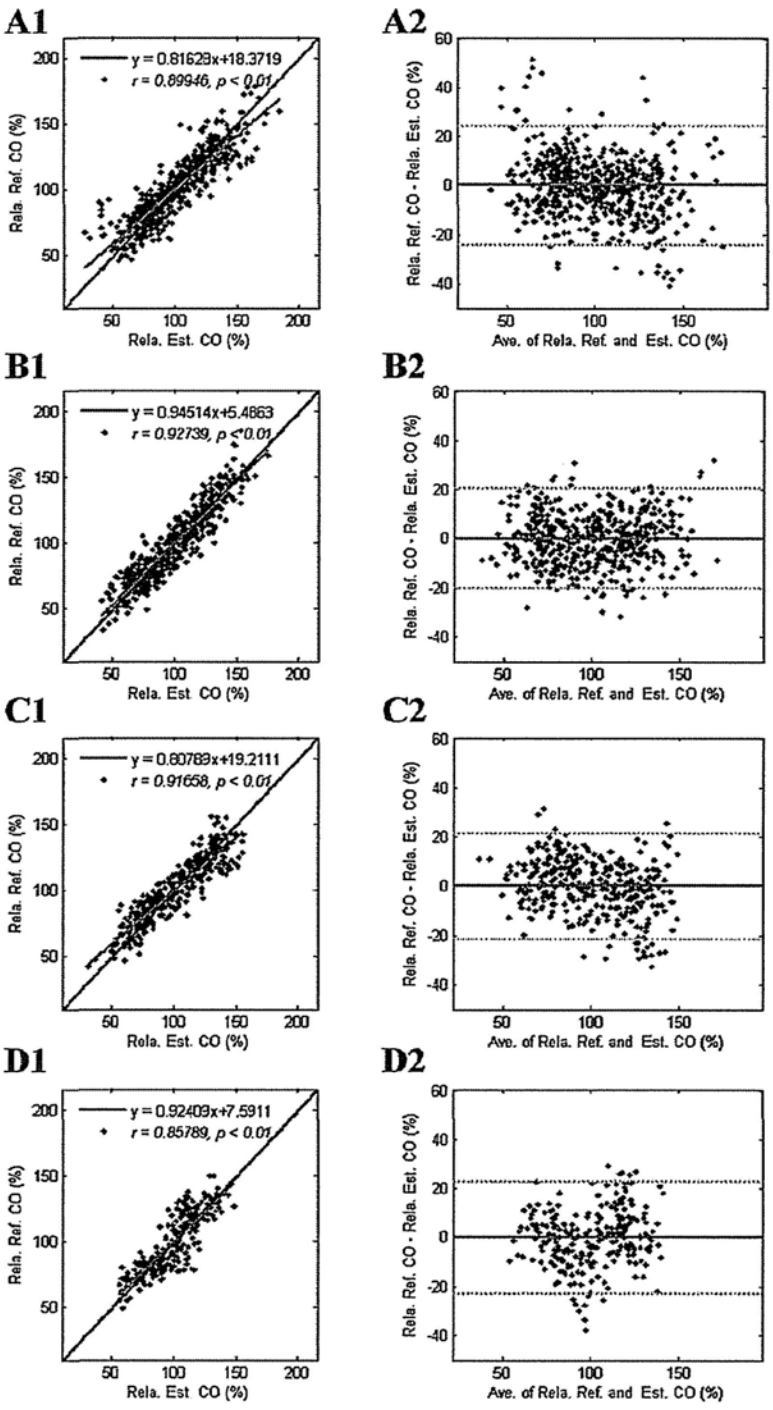

Fig. 5.16 Regression analysis plots (left figures, A1-D1) and Bland-Altman plots (right figures, A2-D2) for relative CO and relative PTRR* on heart failure group (A1 and A2), disease control group (B1 and B2), normal control group (C1 and C2) and normal healthy group (D1 and D2). In the regression analysis plots, regression equation is shown in the legend, where 'y' is the relative reference CO and 'x' is estimated CO; the black solid line is the equality line and the red solid line is the regression line of data. In the Bland-Altman plots, the red solid line is the bias and the range between two green lines is bias ±1.96SD, where 95% of the data stay.

5.3 Discussion

In order to validate the theoretical findings in chapter 3, we analyzed the correlations between BP parameters, PAT_{finger}, PAT_{ear}, PTT_{bra}, with SBP, MBP and DBP measured in the experiments. Both PAT_{finger} and PAT_{ear} showed high correlations with SBP and MBP but low correlations with DBP, which were consistently with the simulation results in chapter 3. PAT_{finger}, PAT_{ear} and PTT_{bra} showed comparable correlations with DBP, indicating that the correlation between PAT and DBP during exercise was mainly due to the contribution of PTT but not PEP. The correlation between PTT_{bra} and DBP was not high, which was different from the simulation results. This result also differs from other experiment observations where a high correlation was found between PTT and DBP [10, 11]. A possible reason is that PTT_{bra} is not true PTT measured on brachial artery but an approximation calculated from the difference between PAT_{finger} and PAT_{ear}. The common timing components of PAT_{finger} and PAT_{ear} are PEP and pulse transit time from the aortic root to the aortic arch before its branching. Besides, PAT_{ear} includes PTT through the carotid artery. The subtraction of PAT_{ear} from PAT_{finger} removed not only the common components but carotid PTT. Since carotid PTT and brachial PTT both change inversely with DBP during exercise, such a subtraction may reduce the change of PTT_{bra} with DBP, and reduce the correlation.

In MBP analysis, the precision of estimation results from two calibration methods both achieved the AMMI standard (SD< 8 mmHg), showing that PAT_{finger} is an effective MBP index during dynamic exercise. The results obtained from best-fit method implied the potential best performance of the PAT approach in this study, i.e., about 5 mmHg. However, in the practical application, when only two points were used for calibration, biases may be introduced due to random measurement errors. In order to avoid the potential big bias induced by any single reference BP measurement, mean calibration method was utilized here. However, as shown in Fig. 5.7, there is still a trend of underestimation at lower MBP levels but overestimation at higher MBP levels when MBP was estimated from PAT through a linear model. This might be mainly due to the overestimation of PAT on MBP during higher exercise level where the rising of MBP is reduced by the drop of DBP induced by sharply decreasing of peripheral resistance whereas the changing trend of PAT is little influenced by this phenomenon. If this is true, a simple linear model using a single PAT may be not accurate enough for MBP estimation during dynamic exercise, and instead, indices which trace DBP changes should be added into the model. One possible choice is to introduce PTT, since its high correlation with DBP has been proved both by previous experimental observations [10, 11] and our model simulation. However, this method requires another measurement tool to determine PEP. An alternative here is to investigate other DBP indices from the shape features of PPG. Previous studies showed that the augmentation index (AI) on PPG wave correlated with DBP [12-14]. However, this reported result has been controversial [15, 16]. Kim *et al* [17] tested the correlations between DBP and 16 parameters extracted from shape features of PPG and found that a time delay from peak of 1^{st} derivative PPG to peak of PPG second wave showed a high correlation with DBP. They then added both heart rate and this time delay, namely the arterial stiffness parameter, to the PAT equation and the estimation accuracy was significantly improved. However, it should be cautious if heart rate was introduced. As mentioned by the authors, heart rate could affect BP differently. HR increases as BP increases in some situation such as exercise, but it decreases as BP increases in other situations such as the Valsalva

maneuver intervention. A further shortcoming of the study in [17] was that the physiological meaning of the time delay parameter from PPG was unclear. Although it was named an arterial stiffness parameter, no results have been shown to indicate its relationship with arterial stiffness.

In the CO analysis, both $PTRR^{\#}$ and $PTRR^{*}$ showed high correlations with reference CO, which were consistent with the theoretical findings in Chapter 4. As shown in Fig. 5.10, $PTRR^{*}$ and $PTRR^{\#}$ show comparable correlations with CO in global data and data from all subject groups. This indicates that the MBP information included in $PTRR^{*}$ does not make it a superior CO index, demonstrating that BP measurement may not be a necessity in the CO estimation. In both Fig. 5.11 and 5.12, there is a trend of underestimation at lower CO levels but overestimation at higher CO levels when CO is estimated from both $PTRR^{*}$ and $PTRR^{\#}$ through a linear model. This is mainly due to the problem existing in the relationship between PAT and MBP, which has been extensively discussed in the previous paragraph. Although such biases were introduced, $PTRR^{\#}$ performed well in CO estimation. On both global and sub-group analyses, the percent errors of estimated results were less than 30%, at an accuracy level that was considered as clinically acceptable [1].

The mean calibration method utilized in this study was proposed in [6]. In that study, an approach was presented to estimate CO from a two-element Windkessel model whose parameters were calculated from the impulse response function of long time blood pressure intervals [6]. This research group did two experiments to verify this approach on different human subjects [7], one on 15 patients in the intensive care unit (CO range: 2.9 L/min ~ 9.5 L/min; RMSNE = 15.3%) and the other on 10 healthy subjects (CO range: 3.5 L/min ~ 8.4 L/min; RMSNE = 15.1%). In this study, the range of CO was 3.35 ~ 24.38 L/min, about three times of the CO ranges in their study, and the RMSNEs for healthy young, healthy elderly, cardiovascular and heart failure groups in this study were 11.91%, 11.10% and 12.51% and 12.61%. This better performance is probably because PTRR is derived from the asymmetric T-tube model which considers wave reflections in the arterial system. Hence, PTRR can trace the quick changes of CO altered by wave reflection, which is difficult to be obtained using the two-element Windkessel model.

The impedance cardiographic device (PF-05) used in this study has been verified in a number of previous studies. Table 5.11 lists the reported data in 8 validation studies related to PF-05, with 3 at rest and the other 5 during exercise. The studies at rest were carried out under the most difficult conditions for testing a novel CO measuring technique: patients presenting a very large variety of pathologies [24-26] and in [25] and [26] only one single measurement was conducted per patient. Despite the tough testing conditions, all studies at rest concluded that this device could provide reliable, accurate and repeatable CO measurement at a clinical acceptable accuracy [24-26]. However, the conclusions from 5 validations of PR-05 under exercise varied on the accuracy of this device. PF-05 was shown to agree well with the direct Fick [2], [4] and CO_2 rebreathing [5] methods during exercise but was reported to overestimate CO compared with direct [18] and continuous [19] Fick methods under exercises condition. As noted by the authors in [19], the poor performances of PF-05 in [18] and [19] might be due to that the autocalibratoin algorithm of Physioflow is less suited for patients with relatively low SV values. However, the poor performance may also result from the inaccuracy of direct and continuous Fick methods at severe exercise when the steady state required by the Fick method is rarely available [28]. Further, it is

Table 5.11 Summary of reported validation studies of PF-05.

Author	Population (no. of subjects; no. of trials)	Reference method	Exercise?	Ref. CO values (L/min)	r	Bias±sd or reg. equation (L/min)
Studies with positive conclusion on the accuracy of PF-05						
Shoemaker et al [24]	Trauma patients (262; 907)	Thermodilution	No	CI (L/min/m^2) 4.59 ± 1.27/ 4.09±1.37	0.91	CI (L/min/m^2) -0.07±0.47
Moreau et al [25]	ICU patients (107; 107)	Thermodilution	No	NM	0.88	Bias: -0.014; $y = 1.33x - 1.77$
Haynes et al [26]	ICU patients (112; 112)	Thermo-dilution	No	5.31±1.93	0.85	$y = 1.39x - 2.19$
Charloux et al [4]	Patients (40; 72) with SAS or COPD	Direct Fick	Yes	6.32 ± 1.42/ 10.15±2.35	0.89/ 0.85	0.07 ± 0.12 / 0.26±1.21
Richard et al [2]	Healthy subjects (7, 50)	Direct Fick	Yes	NM	0.94	-0.58±1.73
Tordi et al [5]	Healthy, young men (8; 40)	CO_2 rebreathing	Yes	17.60±2.69	0.85	0.06±1.41
Studies with negative conclusion on the accuracy of PF-05						
Bougault et al [18]	COPD (8; 157)	Direct Fick	Yes	4.7±1.2 / 4.6 ±0.5	0.85/ 0.70	3.2±2.9 / 2.5± 2.1
Kemps et al [19]	CHF patients (10; 94)	Direct and continuous Fick	Yes	3.8±0.7 / 6.2 ±1.3 / 9.0± 1.8 / 9.6±2.3	0.73	48%±26%

"+": mean +standard deviation; r: correlation coefficient between reference CO and CO measured by PF-05; Bias: mean error; sd: standard deviation of errors; CI: cardiac index, defined as CO/BSA, BSA is the body surface area (m^2); NM: not mentioned; SAS: sleep apnoea syndrome; COPD: chronic obstructive pulmonary disease; CHF: chronic heart failure; in cell on 3st row, 5th colume, "/": data of survivors/data of non-survivors; in cells on 6th row, 5th, 6th and 7th columes, "/": data at rest/data during exercise; in cells on 10th row, 5th, 6th and 7th columes, "/": data during IET/data during IWET, where IET is maximal incremental exercise test and IWET is strenuous intermittent work exercise test; in cell on last row, 5th colume, "/": data at rest/data during light exercise/data during moderate exercise/data at peak exercise.

found that although [19] and our study both conducted incremental to maximal exercise test on chronic heart failure patients, the CO data from PF-05 reported in [19] differ from our experimental observations. In current study, the peak CO measured on heart failure patients was 12.47±3.70 L min^{-1}, which is significantly lower than 15.6±5.4 L min^{-1} reported in [19] but quite similar in magnitude to 12.0±3.40 L min^{-1} , the CO data measured on 219 chronic heart failure patients in another symptom-limited exercise test using CO_2 rebreathing as CO measuring technique [27]. Therefore, we further presume that other reasons except for the accuracy of PF-05 may also contribute to the big bias between PF-05 and direct Fick's method reported in [19]. Last but not the least, it is clearly from Table 5.11 that the correlation between CO measured from

PF-05 and that from reference method is high in all studies. This indicates that this device is able to trace the changes of CO precisely on different subject populations and under a variant of physiological and pathological conditions. The conclusion that PF-05 is a device which measures true CO changes is especially important for the validation of the PTRR technique proposed in this study, since PTRR itself can only trace the relative changes of CO and it shows high correlation with CO obtained from PF-05.

However, the current study is limited by using the cardiographic device as the only reference method to measure standard values of CO, mainly due to the debate on the accuracy of this method on chronic heart failure patients during exercise. As mentioned in Chapter 1, heart failure patients are the major potential users of a wearable CPO technique used under exercise condition. Thus it is obligatory to confirm the accuracy of the proposed technique on this population. In the future, the accuracy of the proposed technique should be tested on the heart failure patients using more accurate CO measurement as reference, e.g. thermodilution. On the other hand, in this study, we aim at developing a technique which is potentially to be used under dynamic exercise condition in mobile environment, and it is thus better if the experiment set-up is mimicking such a situation. However, the subjects of the current study were doing exercise lying on bed, mainly due to the inability of the cardiographic device to be used in a mobile environment. Further, we found that a mobile design is very difficult since no currently established CO measurement techniques are available to be used as a reference in mobile environment. Therefore, in this study, we first aim at proposing a method for estimating CO from signals acquirable from wearable devices and evaluating the accuracy of the proposed method for a dynamic range of CO, which is achieved in this study by asking the subjects to perform cycling exercise. Next step, the stability and reliability of the proposed technique under mobile environment should be tested. And the potentially big problems with movement artifacts from the PPG-sensor on a mobile subject under dynamic exercise should be considered. Algorithms based on smoothed pseudo Wigner-Ville distribution [21], independent component analysis [22] and Widrow's adaptive noise cancellation [23] might be incorporated to reduce motion artifacts in the signals.

The experimental results showed that the proposed method can estimate MBP and CO at an acceptable precision for medical diagnosis, thus provides a promising wearable technique to estimate dynamic CPO. However, some potential pitfalls of using such an indirect method to measure CPO should be taken into consideration. In Chapter 3 and 4, we simulated the relationship between PAT and MBP and that between PTRR and CO by altering individual model parameter. However, in the real physiological conditions, a single model parameter does not always changes individually but with other parameters by the complex reflex control of the human body. In this study, we mimicked the exercise condition by simultaneously changing related parameters according to exercise physiology and discussed the validity of the proposed technique under dynamic exercise. In the future, the validity of the proposed technique under other physiological conditions, such as drug condition, should be discussed. Besides, novel calibration methods should be developed make the proposed technique easier to be implemented in real applications. For example, a recently developed hydrostatic approach utilized the hydrostatic BP changes to calibrate the BP linear prediction model and no extra reference BP measurement is

needed [20]. Further, in order to apply the proposed method for monitoring CPO during daily activities, algorithms might be incorporated to reduce motion artifacts in the signals.

In addition, the validation of the proposed model is limited to qualitatively compare the simulation result with some experimental data published in previous studies. Further verification of proposed model based on invasively measured ventricular-aortic hemodynamic data under different physiological condition is necessary to assure that the proposed model can represent the behavior of the real heart-arterial system with sufficient accuracy.

5.4 Conclusion

In this chapter, we presented the experiment validation for the theoretical findings in chapter 3 and 4. A supine bicycle exercise study was conducted on a wide range of subjects, including populations with different age ranges and patients with different cardiovascular diseases. The experiment results showed high consistence with the theoretical findings in:

1) During dynamic exercise, there were significantly high and negative correlations between PAT and SBP and between PAT and MBP but a low negative correlation between PAT and DBP;
2) PAT may underestimate MBP during high exercise levels due to the influence of DBP drop caused by decreasing peripheral resistance;
3) During dynamic exercise, there was a significantly high and positive correlation between $PTRR^{\#}$ and CO.

The MBP estimation results passed the requirements of the AMMI standard and CO estimation results were considered as clinically acceptable, indicating the proposed method a promising measuring technique of CPO during dynamic exercise.

Reference

[1] L. A. Critchley and J. A. Critchley, "A meta-analysis of studies using bias and precision statistics to compare cardiac output measurement techniques," *J. Clin. Monit. Comput.*, vol. 15, pp. 85-91, Feb. 1999.

[2] R. Richard, E. Lonsdorfer-Wolf, A. Charloux, S. Doutreleau, M. Buchheit, M. Oswald-Mammosser, E. Lampert, B. Mettauer, B. Geny and J. Lonsdorfer, "Non-invasive cardiac output evaluation during a maximal progressive exercise test, using a new impedance cardiograph device," *Eur. J. Appl. Physiol.*, vol. 85, pp. 202-207, Aug. 2001.

[3] K. H. Tan, F. O. Lai and N. C. Hwang, "Measurement of cardiac output using Physio Flow® with different positions of electrode placement," *Singapore Med. J.*, vol. 47, pp. 967-70, Nov. 2006.

[4] A. Charloux, E. Lonsdorfer-Wolf, R. Richard, E. Lampert, M. Oswald-Mammosser, B. Mettauer, B. Geny and J. Lonsdorfer, "A new impedance cardiograph device for the non-invasive evaluation of cardiac output at rest and during exercise: comparison with the "direct" Fick method," *Eur. J. Appl. Physiol.*, vol. 82, pp. 313-320, Jul. 2000.

[5] N. Tordi, L. Mourot, B. Matusheski and R. L. Hughson, "Measurements of cardiac output during constant exercises: comparison of two non-invasive techniques," *Int. J. Sports Med.*, vol. 25, pp. 145-149, Feb. 2004.

[6] R. Mukkamala, A. T. Reisner, H. M. Hojman, R. G. Mark and R. J. Cohen, "Continuous cardiac output monitoring by peripheral blood pressure waveform analysis," *IEEE Trans. Biomed. Eng.*, vol. 53, pp. 459-467, Mar. 2006.

[7] Z. Lu and R. Mukkamala, "Continuous cardiac output monitoring in humans by invasive and noninvasive peripheral blood pressure waveform analysis," *J. Appl. Physiol.*, vol. 101, pp. 598-608, Aug. 2006.

[8] N. W. Linton and R. A. Linton, "Is comparison of changes in cardiac output, assessed by different methods, better than only comparing cardiac output to the reference method?, " *Br. J. Anaesth.*, vol. 89, pp. 336-337, Aug. 2002.

[9] J. M. Bland and D. G. Altman, "Statistical methods for assessing agreement between two methods of clinical measurement," *Lancet*, vol. 1, 307-310, Feb. 1986.

[10]R. Ochiai, J. Takeda, H Hosaka, et al., The relationship between modified pulse wave transit time and cardiovascular changes in isoflurane anesthetized dogs, J. Clin. Monit., vol. 15, pp. 493-501, 1999.

[11]R. A. Payne, C. N. Symeonides, D. J. Webb, et al., Pulse transit time measured from the ECG: an unreliable marker of beat-to-beat blood pressure. *J. Appl. Physiol.*, vol. 100, pp. 136-141, 2006.

[12]Yasmin and M. J. Brown, Similarities and differences between augmentation index and pulse wave velocity in the assessmen of arterial stiffness, *Q. J. Med.*, vol. 92, pp. 595-600, 1999.

[13]I. B. Wilkinson, S. S. Franklin, I. R. Hall, et al., Pressure amplification explains why pulse pressure is unrelated to risk in young subjects, *Hypertension*, vol. 38, pp. 1461-1466, 2001.

[14]J. Nurnberger, S. Dammer, S. O. Opazo, et al., Diastolic blood pressure is an important determinant of augmentation index and pulse wave velocity in young, healthy males, *J. Human Hypertens.*, vol. 17, pp. 153-158, 2003.

[15]J. D. Cameron, B. P. McGrath and A. M. Dart, Use of radial artery applanation tonometry and a generalized transfer function to determine aortic pressure augmentation in subjects with treated hypertension, *J. Am. Coll. Cardiol.*, vol. 32, pp. 1214-1220, 1998.

[16]H. Tanaka, C. A. DeSouza and D. R. Seals, Absence of age related increase in central arterial stiffness in physically active women, *Arterioscler. Thromb. Vasc. Biol.*, vol. 18, pp. 127-132.

[17]J. S. Kim, K. K. Kim, H. J. Baek, et al., Effect of confounding factors on blood pressure estimation using pulse arrival time, *Physiol. Meas.*, vol. 29, pp. 615-624, 2008.

[18]V. Bougault, E. Lonsdorfer-Wolf, A. Charloux, R. Richard, B. Geny and M. Oswald-Mammosser, Does thoracic bioimpedance accurately determine cardiac output in COPD patients during maximal or intermittent exercise, *Chest*, vol. 127, pp.1122-1131, Apr. 2005.

[19]H. M. Kemps, E. J. Thijssen, G. Schep, B. T. Sleutjes, W. R. De Vries, A. R. Hoogeveen, P. F. Wijn and P. A. Doevendans, Evaluation of two methods for continuous cardiac output assessment during exercise in chronic heart failure patients, *J. Appl. Physiol.*, vol. 105, pp. 1822-1829, Oct. 2008.

[20]C. C. Y. Poon, Y. T. Zhang and Y. B. Liu, Modeling of pulse transit time under the effects of hydrostatic pressure for cuffless blood pressure measurements, *3rd IEEE/EMBS Int. Summer School on Medical Devices and Biosensors*, pp. 65-68, Sept. 2006.

[21]Y. S. Yan, C. C. Y. Poon and Y. T. Zhang, Reduction of motion artifact in pulse oximetry by smoothed pseudo Wigner-Ville distribution, *J. Neuroeng. Rehabil.*, vol.2, pp. 3, 2005.

[22]B. S. Kim and S. K. Yoo, Motion artifact reduction in photoplethysmography using independent component analysis, *IEEE Trans Biomed Eng.*, vol. 53, pp. 566-568, 2006.

[23]L. B. Wood and H. H. Asada, Low variance adaptive filter for cancelling motion artifact in wearable photoplethysmogram sensor signals, *Conf. Proc. 29th IEEE Engineering in Medicine and Biology Society (EMBS)*, pp 652-5, 2007.

[24]W. C. Shoemaker, C. C. Wo, L. C. Chien, et al., Evaluation of invasive and noninvasive hemodynamic monitoring in trauma patients, *J. Trauma*, vol. 61, pp. 844-853, 2006.

[25]X. Moreau, J. M. Rousseau, J. C. Thiranos, et al, Cardiac output measurements: comparison between a new transthoracic electrical bioimpedance method (Physioflow^{TM}) and the Swan-Ganz method (continuous cardiac output or bolus technique), *French Anaesthesiology Society*, Sept. 2001.

[26]G. R. Haynes, X. Moreau, J. M. Rousseau, et al., Cardiac output with a new bioimpedance monitor: comparison with thermodilution methods, Anesthesiology, vol. 105, pp. A470, 2006.

[27]S. G. Williams, G. A. Cooke, D. J. Wright, et al., Peak cardiac power output: a powerful prognostic indicator in chronic heart failure, vol. 22, *Eur. Heart J.*, pp 1496–1503, 2001.

[28]D. E. Warburton, M. J. Haykowsky, H. A. Quinney, et al., Reliability and validity of measures of cardiac output during incremental to maximal aerobic exercise. Part I: Conventional techniques, *Sports Med.*, vol. 27, pp. 23-41, 1999.

Chapter 6

Conclusions and Suggestions for Future Work

This thesis focuses on developing a novel measurement technique of CPO in dynamic exercise using multiple physiological signals measured on body surface, specifically, electrocardiogram (ECG) and photoplehtysmogram (PPG). The main work is composed of three parts: 1) a model-based study on the relationship between pulse arrival time and arterial blood pressure; 2) a novel approach for cardiac output estimation using ECG and PPG; 3) experimental work for estimation of cardiac power output in dynamic exercise. The originality and contribution of this thesis study from each part are summarized as follows.

6.1 Summary

6.1.1 A model-based study on the relationship between pulse arrival time and arterial blood pressure

In chapter 3, we focused on developing the mathematical relationship between PAT and BP by modeling the heart-arterial interaction. Our work started from investigating the influence factors of PEP through a pressure-source ventricular model which describes the ventricular pressure as a function of volume and time. The exponential mathematical form of this model uses separate mathematical equations for ventricular isovolumic contraction phase (non-ejection phase) and ejection phase, which provides basis for developing an explicit PEP mathematical description. Based on the experimental observations by Regen *et al* [1] and the previous theoretical investigations by Ottesen and Danielsen [2], we improved this model by introducing the arbitrary heart rate into the exponential mathematical form of ventricular pressure activation function and further deduced the explicit mathematical expression of PEP as a function of DBP and other ventricular parameters, such as heart contractility, end-diastolic volume, etc. This work firstly quantitatively clarified the ventricular and arterial effects on PEP timing.

Secondly, we described the arterial system by an asymmetric T-tube model composed of two frictionless transmission paths terminated by complex loads. The asymmetric T-tube model was adopted here since it provides a suitable compromise between a model's capacity to reproduce key features of the cardiovascular system and its simplicity for mathematical tractability. PTT and BP were both parameters in the asymmetric T-tube model, however, they were not mathematically related. We then built the relationship between PTT and BP by introducing a nonlinear pressure-volume relationship into the model. This modification quantitatively described the effect of pulsatile BP on arterial parameters in the model.

Thirdly, we proposed the mathematical equation between PAT and BP by coupling the modified ventricular and arterial models. Then, we validated the performance of the coupling model by qualitative and quantitative comparisons of the model outputs with previous in-situ experimental results. Then, the relationships between PAT with systolic blood pressure (SBP), MBP and DBP

were simulated under changing heart contractility, preload, heart rate, peripheral resistance, arterial stiffness and a mimic exercise condition. The simulation results indicated significantly high and negative correlations between PAT and SBP and between PAT and MBP whereas the correlation between DBP and PAT was low. To our knowledge, it is the first study describing the quantitative relation of PAT and BP by model of ventricular-arterial coupling.

6.1.2 A novel approach for cardiac output estimation using electrocardiogram and photoplethysmogram

A novel CO index, namely PTRR was derived from the asymmetric T-tube model and expressed in terms of MBP and mean aortic reflection coefficient ($\Gamma(0)$). PTRR was further expressed in terms of PAT and inflection point area (IPA), a surrogate of $\Gamma(0)$ from the shape feature of PPG. IPA is the ratio of the area after the inflection point on the PPG waveform to the area of the whole curve and it was proposed based on the hypothesis that the diastolic part of the PPG curve was mainly composed of reflective waves and the systolic PPG wave mainly consisted of the forward wave. The relationships between PTRR and CO and between IPA and $\Gamma(0)$ were simulated under changing heart contractility, preload, heart rate, peripheral resistance, arterial stiffness and a mimic exercise condition. Simulation results suggested that $\Gamma(0)$ was mostly sensitive to the changes of peripheral resistance and arterial stiffness and changing of these two factors induced a significantly positive and high correlation between IPA and $\Gamma(0)$ during exercise. Simulation results further indicated that PTRR was able to trace CO changes with a high precision under changing contractility, preload, peripheral resistance and during exercise. The convex effect from PAT and concave effect from IPA on estimated CO during exercise compensated each other in the calculation of PTRR, making PTRR a better surrogate of CO than introducing PAT or IPA along. In addition, a simpler form of PTRR, $PTRR^{\#}$, can be used as an acceptable surrogate of PTRR during changing heart contractility, peripheral resistance and during exercise. Finally, we addressed the feasibility of using constant characteristic impedance (Z_c) in the PTRR. The simulation results demonstrated that Z_c kept almost unchanged during exercise and CO estimated by PTRR with constant Z_c approximately achieved a similar precision level those estimated by PTRR with variant Z_c.

6.1.3 Experimental work for estimation of cardiac power output in dynamic exercise

In order to verify the theoretical findings, two experiments were carried out. One was incremental supine bicycle exercise conducted on 19 young healthy subjects and the other was incremental to maximum supine bicycle exercise conducted on 65 subjects, including 30 heart failure patients, 20 cardiovascular patients and 15 healthy elderly subjects. The data analysis was mainly composed of two parts, MBP analysis and CO analysis mainly due to the lack of standard to evaluate the accuracy of a novel CPO measuring method.

In BP analysis, two PATs, PAT_{ear} and PAT_{finger}, were calculated from PPG measured from the ear and finger, respectively. An approximate of PTT on the brachial artery, namely PTT_{bra}, was obtained by subtracting PAT_{ear} from PAT_{finger}. Results of linear correlation analysis revealed that: 1) PAT_{finger} and PAT_{ear} were superior surrogates of SBP and MBP to PTT_{bra}; 2) The mean correlation coefficient (mean r) between PATs and SBP and that between PATs and MBP were significantly

higher than that between PATs and DBP; 3) Performances of PAT_{finger}, PAT_{ear} and PTT_{bra} on DBP were comparable. These results strongly supported the theoretical findings in chapter 3. In CO analysis, since Z_c was unavailable, two surrogates of PTRR, $PTRR^{\#}$ and $PTRR^{*}$, were used to investigate the relationship between PTRR and CO. $PTRR^{*}$ was different from $PTRR^{\#}$ by including an extra calibration from PAT to MBP inside and it was introduced to test whether MBP measurement is a necessity in CO estimation using PTRR. The results revealed that both $PTRR^{\#}$ and $PTRR^{*}$ showed high correlations with reference CO, which were consistent with the theoretical findings in chapter 4. Further, the results indicated that $PTRR^{*}$ and $PTRR^{\#}$ showed comparable correlations with CO, demonstrating that BP measurement may not be a necessity in the CO estimation. To conclude, the above experiment results verified the main theoretical findings of the model.

Finally, based on the theoretical and experimental verifications, linear prediction models were proposed to estimate MBP from PAT and estimate CO from PTRR. Mean calibration method was utilized, because calibration with any single reference and estimated values would bias the subsequent evaluation results. The results showed that PAT can estimate MBP with a standard deviation of 7.42 mmHg, indicating PAT model has the potential to achieve the accuracy required by AMMI standard (mean error within ± 5 mmHg and SD less than 8 mmHg). The results also showed that PTRR can estimate CO with a percent error of 22.57%, showing an accuracy which was considered as clinically acceptable (percent error less than 30%).

To summarize, the original contributions of this thesis are:

1. An explicit mathematical description of PEP in terms of DBP was proposed, which in the first time quantitatively clarified the ventricular and arterial effects on PEP timing.

2. A nonlinear pressure-volume relationship which reflected the natural arterial wall properties was introduced into the asymmetric T-tube arterial model, which effectively and quantitatively described the effect of pulsatile BP on arterial parameters, e.g., compliance, PTT etc.

3. A mathematical relationship between PAT and BP was firstly proposed as a result of the heart-arterial interaction, which simulated a significantly strong and negative relationship between PAT and SBP and between PAT and MBP but a much weaker negative relationship between PAT and DBP during exercise. The hypothesis was supported by the experiment data. To our knowledge, it is the first study describing the quantitative relation of PAT and BP by both model-based study and experimental data.

4. A novel wearable measurable CO parameter, PTRR, was proposed and it successfully showed a significantly high and positive correlation with CO during exercise both in model simulation and in the experiments.

5. Linear prediction models using PAT to estimate MBP and using PTRR to estimate CO were proposed and evaluated in two exercise experiments conducted on 84 subjects with different ages and cardiovascular diseases. Results showed the proposed method could achieve the

accuracy required for medical diagnosis.

6. By the findings in 3, 4 and 5, this study in the first time provided both the theoretical basis and experimental verifications of developing a wearable and direct measurement technique of CPO in dynamic exercise using multiple physiological signals measured on body surface.

6.2 Suggestions for future work

6.2.1 Future study on the proposed heart-arterial coupling model

The two transmission lines in the asymmetric T-tube model are not real arterial segments but virtual branches which only functionally describe the wave transmissions in the upper and lower body terminals as seen from the heart. However, PPG is measured from a real physical site on the body surface which has a certain distance away the aorta. Hence, the PTT measured from PPG signal is not necessarily related to the PTT parameter interpreted in the model. In this study, we linked these two timings by introducing the experimental findings reported by Hahn *et al* [3] where PTT estimated from the asymmetric T-tube model only differed from PTT measured from the real physical sites by a constant bias. However, this assumption is not necessarily valid for our study. PTT in Hahn's experiment was measured from the aortic root to the radial artery of the swine, and it defers from PTT measured from PPG, since the path of the former only includes the main arteries but the latter also includes small arteries and arterioles. The wave transmission in the small arteries and arterioles are different from that of the big arteries, due to sharply increased arterial resistance and decreased arterial conductance. Hence, both experimental and theoretical investigations are suggested in the future to verify the relationship between PTT estimated from the asymmetric T-tube model and PTT measured from PPG.

In addition, the validation of the proposed model is limited to qualitatively compare the simulation result with some experimental data published in previous studies. Further verification of proposed model based on invasively measured ventricular-aortic hemodynamic data under different physiological condition is necessary to assure that the proposed model can represent the behavior of the real heart-arterial system with sufficient accuracy.

6.2.2 Future development of wearable cardiac power output measurement

This study provided both the theoretical basis and experimental verifications of developing a wearable and direct measurement technique of CPO in dynamic exercise using ECG and PPG. If a wearable device of CPO is to be developed based on this approach, several work needs to be done in the future:

Further improvement of the proposed technique

As mentioned in the discussion of chapter 5, there is a trend of underestimation at lower MBP levels but overestimation at higher MBP levels when MBP is estimated from PAT through a linear model. This may be mainly due to the overestimation of PAT on MBP during higher exercise level where the rising of MBP is reduced by the drop of DBP induced by sharply decreasing of

peripheral resistance whereas the changing trend of PAT is little influenced by this phenomenon. Hence, a simple linear model based on a single PAT may be not accurate enough for MBP estimation during dynamic exercise, and instead, indices which trace DBP changes should be added into the model. Besides, a novel calibration method should be proposed in the future to make the technique easier to be implemented in real applications. Further, in order to apply the proposed method for monitoring CPO by a wearable device, algorithms to reduce the motion artifacts interference should be developed and incorporated into the system.

Further validation of the proposed technique

The validation of the proposed technique on heart failure patients is critical since heart failure patients are the major target users of a wearable CPO measurement device. However, although the proposed technique showed a good estimation performance for both MBP and CO on the heart failure patients enrolled in our experimental study, the results may be doubted due to the potential inaccuracy of the CO measurement on chronic heart failure patients by the cardiographic device PF-05 [4]. Therefore, more invasive but accurate CO methods such as thermodilution and Fick's method should be used as reference to verify the testing technique on chronic heart failure patients in future. In addition, The wearable device based on the proposed technique should be further tested on mobile subjects during movements.

Reference

[1] D. M. Regen, W. C. Howe, L. H. Peterson, et al., Characteristics of single isovolumic left-ventricular pressure waves of dog hearts in situ, *Heart Vessels*, vol. 8, pp. 136-148, 1993.

[2] J. T. Ottesen and M. Danielsen, "Modeling ventricular contraction with heart rate changes," *J. Theor. Biol.*, vol. 222, pp. 337–346, 2003.

[3] Jin-Oh Hahn, A. T. Reisner, H. H. Asada, Estimation of pulse transit time using two diametric blood pressure waveform measurements, *Med. Eng. Phys.*, E-pub ahead of print, 2010.

[4] H. M. Kemps, E. J. Thijssen, G. Schep, B. T. Sleutjes, W. R. De Vries, A. R. Hoogeveen, P. F. Wijn and P. A. Doevendans, "Evaluation of two methods for continuous cardiac output assessment during exercise in chronic heart failure patients," *J. Appl. Physiol.*, vol. 105, pp. 1822-1829, Oct. 2008.

Appendix

List of Publications and Awards Related to This Study

Published Journal Paper:

L. Wang, C. C. Y. Poon and Y. T. Zhang, "The non-invasive and continuous estimation of cardiac output using photoplethysmogram and electrocardiogram during incremental exercise", *Physiological Measurement*, vol. 31, pp. 715-726, 2010.

Accepted Journal Paper:

Z. Zhao, **L. Wang**, C. C. Y. Poon and Y. T. Zhang, "Measurement principles and development of cardiac output monitoring," *Transactions of Biomedical Engineering in China* (中国生物医学工程学报), accepted. (Chinese)

Journal Paper in Preparation:

L. Wang, C. C. Y. Poon, Y. T. Zhang et al., "Evaluation of a method for noninvasive cardiac output assessment using photoplethysmogram and electrocardiogram on the healthy elderly, cardiovascular and heart failure patients during exercise," to be submitted to *IEEE Transactions on Biomedical Engineering*, in preparation.

Published Conference Papers:

[1] **L. Wang**, C. C. Y. Poon, Y. T. Zhang, "The age effects on the waveform of photoplethysmogram at a specific range of arterial blood pressure," 6th International School and Symposium on Medical Devices and Biosensors (MDBS 2009) in conjunction with 4th International School and Symposium on Biomedical and Health Engineering (BHE 2009), 2009, Dec., Shenzhen, China, pp. 26-28.

[2] **L. Wang**, E. Pickwell-MacPherson, Y. P. Liang, Y. T. Zhang, "Noninvasive cardiac output estimation using a novel photoplethysmogram index," 31st Annual International Conference of the IEEE Engineering in Medicine and Biology Society (EMBC 2009), 2009, Sept. 3-6, Hilton Minneapolis, USA, pp: 1746-1749.

[3] **Ling Wang** and Y. T. Zhang, "A novel photoplethysmogram index for total peripheral resistance after bicycle exercise," the 5th International Conference on Ubiquitous Healthcare, 2008, Oct. 29-31, Pusan, Korea, pp.: 175-176.

[4] **L. Wang**, E. Pickwell-MacPherson, Y. T. Zhang, "Blood pressure contour analysis after exercise by the photoplethysmogram using a transfer function method," 5th International Summer School and Symposium on Medical Devices and Biosensors, 2008, Jun 1-3, HKSAR, China, pp.: 284-287.

Scientific Awards:

- China Youth Technology Innovation Award 2008.
- The First Prize in the 10th "Challenge Cup" National College Students Competition of Extracurricular Scientific and Technological Innovations, Project Title: A body sensor network for wireless and continuous estimation and control of blood pressure.